The Global Change Research Center Atmospheric Chemistry Model

Francis Perry Moraes Jr.
B.S., Sonoma State University
M.S., Oregon Graduate Institute of Science & Technology

A dissertation submitted to the faculty of the
Oregon Graduate Institute of Science & Technology
in partial fulfillment of the
requirements for the degree
Doctor of Philosophy
in
Atmospheric Physics

January 1995

The dissertation "The Global Change Research Center Atmospheric Chemistry Model" by Francis Perry Moraes Jr. has been examined and approved by the following Examination Committee:

Dr. M. A. K. Khalil
Professor
Thesis Research Adviser

Dr. Jack Fishman
Branch Head, Chemistry and Dynamics,
NASA-Langley Research Center

Dr. Fred Holmes
Professor

Dr. Paul Quay
Associate Professor,
University of Washington

Dr. Reinhold A. Rasmussen
Professor

Dedication

I still have
that picture

of you

in your safari shoes
(the ones that say

you know

Africa)
beside the

Pacific Ocean.

That day
its name
seemed not quite so

ironic.

Acknowledgements

A few years ago a student told me to write my acknowledgments early because I wouldn't have time to write them later. How right he was. It is now five hours before I must turn in the final copy of my thesis to Admissions and Records and I am just starting my acknowledgments. I apologize, in advance, to everyone I am about to neglect.

My thesis committee was fantastic. Too often thesis committees are filled up with a bunch of people who are not very interested in the subject. Everyone on my committee had direct research interests associated with my work and showed a lot of enthusiasm which was very helpful especially at those times when I wasn't sure I had done *anything* right.

Aslam's impact on this dissertation could hardly be greater if he had sat down and typed it in himself. This is not to say that he managed the project though. Aslam and I discuss the work that is going on in the group almost every day. As a result many of the ideas that I would claim as my own in this work are really the result of our discussions. And there is more to come.

I have never met Jack Fishman and I only talked to him for the first time last summer. But he has had a profound effect on this work. After reading the first copy of this dissertation he showed that the errors in the model (or any model of its kind) were much too large to draw the conclusions that I was drawing. As a direct result of his involvement the model was changed from 2 to 2.5 dimensions and chapters 3 and 4 were written. This work and, more importantly, the model are much better thanks to his help.

Every time I'm in Seattle I stop by and see Paul Quay. His major contribution to this work has been the error analysis of the reaction rate constants which turned out to be pretty important. But more important have been the discussions which we have had related to his work on isotope measurements of CO and CH_4. They have given me tremendous creative energy and hopefully we will collaborate on some of this work in the near future.

This project has not been as closely tied to Rei as others like my Master's work. But Rei was present for the entire project, telling me I was full of it when necessary. We are likely to be collaborating in the future on a project I'm so excited about I won't even mention it here.

Fred Holmes was the radiation person on the committee. He did not have a great influence on the present work because I managed to get the radiation stuff right in the first place (I *am* a physicist after all). It was comforting to know that Fred was around to keep me straight though. Recently we have been discussing the possibility of measuring HO which is very exciting.

There are several staff members who have been a great deal of help to me. The most important is Marty Shearer. From a research stand-point Marty is the person in the group who holds it all together. If you need a global distribution of CO_2 sources, Marty has it. If you need some paper which Aslam has told you is by Crutzen and Fishman from the late 70s, Marty will find it, even if it *is* by Fishman and Crutzen. It would be impossible to list all of the help she has been. The work that I do requires a pretty varied collection of data and papers and Marty been extremely good at providing this kind of stuff for me. At Livermore they had a whole building full of people who did this, in the GCRC, we have Marty. She also proof-read my dissertation and caught many of my cryptic ramblings before anyone else saw them.

Xvgr was used for all of the two-dimensional plots used in this thesis. Paul Turner wrote this program and has distributed it freely for many years. I thank Paul and all of the writers of free software who have to a large extent made this dissertation possible. I'm very happy that the GCRC is part of this trend even if the software we create and distribute is of less general interest than xvgr.

Edie Taylor is my constant reminder that I live in a civilized world. She did the proof of this dissertation but any errors you find are my fault because it has changed quite a lot since she last saw it.

Several students have been of considerable help to me in doing this work. Tony Ye has shown himself to be extremely capable in the area of bug finding. In particular, he found a major error in the radiation code of the model. I have depended upon Bill Bagby to explain the intricacies of organic chemistry and bounding theory. When you're a physicist doing a chemist's job, you need someone like Bill around. And finally, Claude Errera has been helpful in explaining how satellites measure gases and miscellaneous other esoterica which I have found need to know over the past few years.

I'm afraid that I have gotten to a point in life where it makes the most sense to do the things that are expected. So here goes. I thank my family for thinking what I'm doing makes sense. I thank my friends for making me a little less unhappy. And, of course, I thank everyone at OGI for putting up with me these last years.

Aslam has been the best thesis advisor that I can imagine anyone having, much less, that I deserve. Working with him is a great pleasure because of the excitement that he brings to every project. But he is also an extremely decent human being who has gone far out of his way to promote my scientific career. In the final analysis I will say what I never say easily: I consider him my friend.

Contents

Dedication **iv**

Acknowledgements **v**

Abstract **xvii**

1 Introduction **1**

1.1 Purposes 1
1.2 The New Chemistry Model 1
1.2.1 Open Models 1
1.2.2 Clouds 2
1.2.3 Model Structure 3
1.3 Previous Work 3
1.4 New Work 4

2 GCRC-ACM Description **5**

2.1 Model Overview 5
2.2 Chemistry 8
2.2.1 The Base Model 8
2.2.2 The HO_x Cycle 9
2.2.3 The NO_x Cycle 10
2.2.4 The Methane Cycle 12
2.2.5 Model Shell Comparison 13
2.2.6 Atmospheric Chemistry Reactions 14
2.3 Solar Radiation 18
2.3.1 Clear Sky 18
2.3.2 Cloudy Sky 19
2.3.3 Numerical Analysis 21
2.4 Source Gases 22
2.4.1 H_2O 22

2.4.2 O_3 . . . 23
2.4.3 NO_x . . . 24
2.4.4 CH_4 . . . 24
2.4.5 CO . . . 24
2.4.6 HNO_3 . . . 25
2.4.7 H_2 . . . 25
2.5 Model Implementation . . . 25

3 Tropospheric NO_x 30
3.1 Tropospheric NO_x Measurements and Derivations . . . 31
3.1.1 Available Data . . . 31
3.1.2 Early Measurements . . . 32
3.1.3 North America and Asia . . . 32
3.1.4 Western Europe and Eastern United States . . . 35
3.1.5 Arctic . . . 41
3.1.6 Northern Hemisphere Oceans . . . 43
3.1.7 The Southern Hemisphere . . . 46
3.2 Sources and Sinks of Tropospheric NO_x . . . 49
3.2.1 Sources . . . 49
3.2.2 Sinks . . . 51
3.3 Model Inputs . . . 53

4 Tropospheric O_3 59
4.1 O_3 Distribution: Representative Data . . . 60
4.1.1 Northern High and Middle Latitudes . . . 61
4.1.2 Tropics . . . 61
4.1.3 Southern High and Middle Latitudes . . . 62
4.2 Model Inputs . . . 63
4.2.1 Distribution Comparison . . . 65

5 Model Sensitivity Analysis 68
5.1 Overview . . . 68
5.2 NO_x . . . 68
5.3 O_3 . . . 72
5.4 H_2O . . . 74
5.5 CO . . . 74
5.6 Clouds . . . 76

5.7 Rate Constants 76
5.8 Total Error 79

6 Cloud Effects on Trace Gases **81**
6.1 Introduction 81
6.2 GCRC-ACM Determined Cloud Effects 82
6.2.1 Cloud Model Accuracy 83
6.2.2 HO Results 83
6.2.3 Other Methods of HO Determination 86

7 Atmospheric Chemistry of the Past **95**
7.1 Introduction 95

8 Summary **98**

Bibliography **100**

A GCRC-ACM Source Code **114**
A.1 Makefile 114
A.2 global.c 115
A.3 mkdist.c 118
A.4 acm.c 121
A.5 acs.c 127
A.6 actinic.c 131
A.7 getacs.c 133
A.8 getact.c 135
A.9 getcons.c 148
A.10 getdata.c 160
A.11 getinit.c 165
A.12 getj.c 171
A.13 getk.c 173
A.14 getline.c 176
A.15 getstdat.c 177
A.16 j.c 182
A.17 output.c 193
A.18 qy.c 206
A.19 solvemat.c 213

A.20 terrxn.c 219
A.21 acm.h 220
A.22 acs.h 220
A.23 actinic.h 221
A.24 gases.h 221
A.25 j.h 222
A.26 kbinary.h 222
A.27 kter.h 224
A.28 rxn.h 224
A.29 solve.h 226

B GCRC-ACM Input Data **228**

B.1 albedoland.dat 228
B.2 albedosea.dat 228
B.3 ch4.dat 228
B.4 coland.dat 232
B.5 cosea.dat 236
B.6 h2.dat 240
B.7 h2coacs.dat 240
B.8 h2oland.dat 241
B.9 h2osea.dat 244
B.10 hno2acs.dat 248
B.11 hno3acs.dat 249
B.12 hno3land.dat 250
B.13 hno3sea.dat 250
B.14 hno4acs.dat 250
B.15 kz.dat 250
B.16 n2.dat 251
B.17 n2o5acs.dat 251
B.18 no2acs.dat 251
B.19 no3acs.dat 252
B.20 noxland.dat 252
B.21 noxsea.dat 256
B.22 o2.dat 260
B.23 o3acs.dat 260
B.24 o3land.dat 261

B.25 o3sea.dat 265
B.26 par.dat 269
B.27 solarflx.dat 269
B.28 stdatm.dat 271
B.29 templand.dat 271
B.30 tempsea.dat 275

C GCRC-ACM User's Guide **280**
C.1 Name 280
C.2 Syntax 280
C.3 Description 280
C.4 Conventions 281
C.5 Command-Line Arguments. 281
C.6 Parameter File 282
C.7 Availability 283

List of Tables

2.1 GCRC-ACM constant grid layer parameters. The height and thickness are given in km, the pressure is given in N·m^{-2}, and the density in molec·cm^{-3}. 6

2.2 GCRC-ACM chemical inputs and outputs. Species followed by an asterisk are inputs, the rest are outputs. 7

2.3 Binary Chemical Reactions. 16

2.4 Termolecular Chemical Reactions 17

2.5 Photochemical reactions 17

2.6 Cloud Optical Depths 20

3.1 North America and Asia NO_x. The "Air" column is 'BL' for boundary layer, 'FT' for free troposphere, and 'T' for tropopause. 36

3.2 Europe and Eastern United States NO_x. The "Air" column is 'BL' for boundary layer, 'FT' for free troposphere, and 'T' for tropopause. 40

3.3 Arctic NO_x. The "Air" column is 'BL' for boundary layer, 'FT' for free troposphere, and 'T' for tropopause. 43

3.4 Northern Hemisphere Ocean NO_x. The "Air" column is 'BL' for boundary layer, 'FT' for free troposphere, and 'T' for tropopause. 46

3.5 Southern Hemisphere NO_x. The "Air" column is 'BL' for boundary layer, 'FT' for free troposphere, and 'T' for tropopause. 48

3.6 Southern Hemisphere NO_x data from the STRATOZ III campaign. 49

3.7 Global sources of NO_x. All values are given in teragrams of nitrogen per year per hemisphere. 51

3.8 Global sources of NO_x. All values are given in teragrams of nitrogen per year per hemisphere. 52

4.1 Comparison of the tropospheric column derived from the GCRC-ACM ozone distribution with the satellite data from Fishman et al. [1990]. The numbers given are percentage different from the satellite data. 67

5.1 GCRC-ACM sensitivity to NO_x. In this test the mixing ratio of NO_x was set to a constant value (given in the first column in pptv) for the entire troposphere. The second and third columns contain the derived global HO concentrations (in 10^5 molec·cm^{-3}) with and without clouds. Methane destruction for these two cases is shown in final two columns (in Tg·yr^{-1}). 69
5.2 GCRC-ACM sensitivity to NO_x. In this test the mixing ratio of NO_x was set to a relative value based upon the NO_x values used in the model by default. 71
5.3 GCRC-ACM sensitivity to O_3. In this test the mixing ratio of O_3 was set to a relative value based upon the O_3 values used in the model by default. 72
5.4 GCRC-ACM sensitivity to H_2O. In this test the mixing ratio of H_2O was set to a relative value based upon the H_2O values used in the model by default. 74
5.5 GCRC-ACM sensitivity to CO. In this test the mixing ratio of CO was set to a relative value based upon the CO values used in the model by default. 76
5.6 GCRC-ACM sensitivity to clouds. In this test the optical depths of high, middle, and low clouds have been changed from 1, 30, 10 (the default case) to 0.5, 1, and 3. 77
5.7 Input data used to determine the ACM sensitivity to the reaction rate constant uncertainties. Temperature is given in Kelvin and all concentrations in molecules·cm^{-3} 78
5.8 GCRC-ACM sensitivity to the most important input parameters. 80

6.1 Equations for determining the fraction of sky that contains various combinations of cloud cover given the total fractions of high (H), middle (M), and low (L) clouds. 85
6.2 Comparison of the average global HO concentrations between the GCRC-ACM and other investigators. Units are given in 10^5 molec·cm^{-3}. 93

7.1 Input parameters to the Pinto model. All values are given in ppbv. 96
7.2 Calculated HO values for the modern, pre-industrial, and ice age periods. 97

List of Figures

2.1 Model Shell Comparison. Each model shell is cumulative so the HO_x shell includes the base shell and the HO_x shell and so on. 14

2.2 Direct radiation grid 19

2.3 Water Vapor Mixing Ratios 23

2.4 HNO_3 Mixing Ratios 26

2.5 GCRC-ACM Program Flow 29

3.1 Oceanic NO_x. The graphs are, bottom to top, boundary layer, free troposphere, and tropopause. Note that the seasons shown in this graph are northern hemispheric seasons. 57

3.2 Land NO_x. The graphs are, bottom to top, boundary layer, free troposphere, and tropopause. Note that the seasons shown in this graph are northern hemispheric seasons. 58

4.1 Tropospheric ozone column derived from the GCRC-ACM ozone distribution. The top graph is for oceanic areas while the bottom graph is for land areas. The seasons are northern hemisphere seasons. 66

5.1 HO sensitivity to changes in NO_x spanning pre-industrial to modern urban values. 70

5.2 HO sensitivity to changes in O_3 73

5.3 HO sensitivity to relative changes in O_3, NO_x, and H_2O 75

5.4 Model derived HO sensitivity to the reaction rate constants in the five most important reactions. 78

6.1 Comparison of above (top) and below (bottom) cloud actinic fluxes determined by delta-Eddington (solid line) and ACM (dotted line) models. . 84

6.2 Tropospheric HO concentrations for land (bottom) and oceanic (top) areas for the spring. The lines are given in units of molec·cm^{-3}. 87

6.3 Tropospheric HO concentrations for land (bottom) and oceanic (top) areas for the winter. The lines are given in units of molec·cm^{-3}. 88

6.4 Globally and seasonally averaged tropospheric HO concentrations. 89
6.5 Total tropospheric HO at 15°N latitude for the spring with a ground albedo of 0 (top) and 20% (bottom). The units are in fraction of the clear sky value. 90
6.6 Total tropospheric CH_4 removal at 15°N latitude for the spring with a ground albedo of 0. The units are in fraction of the clear sky removal. . . 91
6.7 Changes to the reaction rate constant of CH_3CCl_3 with HO between 1990 and 1992. 94

Abstract

The Global Change Research Center
Atmospheric Chemistry Model

Francis Perry Moraes Jr., Ph.D.
Oregon Graduate Institute of Science & Technology, 1995

Supervising Professor: Dr. M. A. K. Khalil

This work outlines the development of a new model of the chemistry of the natural atmosphere. The model is 2.5-dimensional, having spatial coordinates height, latitude, and, the half-dimension, land and ocean. The model spans both the troposphere and stratosphere, although the troposphere is emphasized and the stratosphere is simple and incomplete. The chemistry in the model includes the O_x, HO_x, NO_x, and methane cycles in a highly modular fashion which allows model users great flexibility in selecting simulation parameters. A detailed modeled sensitivity analysis is also presented.

A key aspect of the model is its inclusion of clouds. The model uses current understanding of the distribution and optical thickness of clouds to determine the true radiation distribution in the atmosphere. As a result, detailed studies of the radiative effects of clouds on the distribution of both oxidant concentrations and trace gas removal are possible. This work presents a beginning of this study with model results and discussion of cloud effects on the hydroxyl radical.

Chapter 1

Introduction

1.1 Purposes

In this work I present two pieces of research: the development of a new model of the chemistry of the natural atmosphere, the Global Change Research Center Atmospheric Chemistry Model (GCRC-ACM), and the use of this model to study the tropospheric abundance and distribution of the hydroxyl radical (HO), the most important oxidizing agent in the troposphere. The effect of clouds on the distribution of HO are stressed and the net effect of clouds on the removal of trace gases in the troposphere is discussed.

1.2 The New Chemistry Model

The atmospheric chemistry model, while new, is part of a relatively long tradition of such models. Most atmospheric chemistry models have been developed to study local air pollution, but a number of "natural" chemistry models have been developed over the years and these models have greatly improved our understanding of the natural atmosphere.

1.2.1 Open Models

The GCRC-ACM is different in a few important respects from other atmospheric chemistry models. The most important is that it is an "open" model. By "open" I mean that the model, its source code and input data are all freely available to the scientific community. There are a number of advantages to having an open model: it improves and expedites the scientific process, it lays bare the meaning of the results presented in this work or any work that uses the model, and it is hoped that, in the long run, having the model used by other scientists will uncover bugs in the program and increase development on it.

Understandably, given the enormous effort required to construct most atmospheric models, research groups tend to consider their models proprietary. This is an unfortunate state for our science to be in, however. Because of the large amount of data required as inputs, it is very hard to reproduce results obtained by other scientists. Atmospheric chemistry models are generally quite sensitive to input parameters, particularly trace gases such as NO_x and O_3. In addition to this the data available are often poor and sparse, requiring many assumptions in order to create global databases. At this time, no one has produced set distributions of these gases that could be used to compare models. This leads to a slowing of progress in the field.

The GCRC-ACM makes a small step in correcting this problem by providing everything used in the model. Unfortunately, some of the input parameters are not as good as one would wish, but it does begin a process that will eventually lead to better datasets.

1.2.2 Clouds

Clouds are particularly important to the chemistry of the atmosphere. They not only affect important gases, such as HO, directly but affect gases indirectly as well. Gases such as the hydrocarbons are removed primarily in the lower atmosphere where cloud effects on HO and other atmospheric oxidizers are the greatest.

One aspect of the GCRC-ACM which is particularly important is the manner in which clouds are included in the model. A new cloud parameterization has been developed which builds on the work of earlier models. This parameterization is quite fast; its radiation code is nearly as fast with clouds as without.

In addition to the cloud model, the most thorough cloud climatology of the world which includes high, middle and low clouds is used by the ACM. No other chemistry model is using this database and it provides a substantial advance in the state of the art.

1.2.3 Model Structure

The GCRC-ACM has been built from the ground up; that is to say, it was constructed so that only the most essential chemicals were included in the model at the beginning and that this serves as a kind of foundation upon which other chemical cycles are built. In the ACM, the user may select to include or exclude *any* of the chemicals in the model, including the intermediate species. This is very helpful in understanding how the various cycles and individual species interact in the atmosphere. It also allows investigators to use a small subset of chemicals to reduce computational time.

1.3 Previous Work

The GCRC-ACM is described in detail in Chapter 2. Other than the cloud model, which is an important improvement of an older model, the ACM is fundamentally the same as earlier chemistry models [Fishman and Crutzen, 1978; Logan et al., 1981; Thompson, 1984; Spivakovsky et al., 1990; Pinto and Khalil, 1991]. In this way, the ACM is firmly rooted in the tradition of atmospheric chemistry studies.

Other investigators have looked at the effects of clouds on the chemistry of the atmosphere. Early investigators included cloud effects implicitly in their models but did not assess the effect that the clouds have on the model output nor did they provide sufficient details on the cloud parameterizations used to assess their accuracy [see e.g., Logan et al., 1981]. In the mid- to late-eighties, thorough cloud databases became available [Warren et al., 1986a; Warren et al., 1986b] that indicated that clouds were even more abundant than previously thought [London, 1952]. This spurred some work on the effects of clouds on atmospheric chemistry [Thompson, 1984; Grant et al., 1992; Lu, 1993]. These investigators looked only at local effects, however and of these, only Thompson [1984] looked at indirect effects (the effects of clouds on a gas because of the radiative effects on a different gas).

1.4 New Work

In this work I show that the primary sink of many atmospheric trace gases, reaction with the HO radical, is greatly affected by clouds and that the effect on the removal of the trace gases is highly non-linear. On a global scale the effect is small but on local scales it can be extremely important. The GCRC-ACM is used to look at this effect. Locally, when clouds are present in the sky, the actinic flux of shortwave radiation decreases beneath the cloud and increases above. As a result, HO concentrations are generally lower below a cloud layer and higher above.

Chapter 2

GCRC-ACM Description

2.1 Model Overview

The Global Change Research Center Atmospheric Chemistry Model (GCRC-ACM) is a 2.5-dimensional model of the chemistry of the remote atmosphere. Its dimensions are latitude and height along with the half-dimension of land and ocean. The model includes vertical transport but no horizontal transport at this time. This is not a limitation, however, because all of the gases that are long-lived (and thus transported appreciably in the horizontal directions) are input into the model from global datasets. The model spans the distance from the surface of the earth up to the stratopause (52 km). The chemistry of the stratosphere is not complete in the ACM, however, and stratospheric outputs from the model, particularly the Nitrogen compounds, should be approached with suspicion. In the coming year the troposphere of the ACM will be combined with the stratospheric model currently under development in the GCRC.

The model grid layers and their parameters are shown in Table 2.1. The sizes of the grids were chosen so that the model would have the highest resolution for the lower atmosphere. The grid is model-independent, however; the ACM inputs all of the data in Table 2.1. Thus the user may change the grid as long as the number of grid elements (21) remains the same (and even the number of grid elements may be changed simply by changing a single line in the program). The other input data (see Appendix B) depend upon the grid layer, however, and so would need to be changed as well, should the grid change.

Table 2.1: GCRC-ACM constant grid layer parameters. The height and thickness are given in km, the pressure is given in N·m^{-2}, and the density in molec·cm^{-3}.

Grid	Height	Thickness	Pressure	Density
0	0.500	1	$9.55 \cdot 10^{4}$	$2.45 \cdot 10^{19}$
1	1.500	1	$8.46 \cdot 10^{4}$	$2.20 \cdot 10^{19}$
2	2.500	1	$7.47 \cdot 10^{4}$	$1.99 \cdot 10^{19}$
3	3.500	1	$6.58 \cdot 10^{4}$	$1.79 \cdot 10^{19}$
4	4.500	1	$5.77 \cdot 10^{4}$	$1.62 \cdot 10^{19}$
5	5.500	1	$5.05 \cdot 10^{4}$	$1.45 \cdot 10^{19}$
6	6.500	1	$4.40 \cdot 10^{4}$	$1.30 \cdot 10^{19}$
7	7.500	1	$3.83 \cdot 10^{4}$	$1.16 \cdot 10^{19}$
8	8.500	1	$3.31 \cdot 10^{4}$	$1.03 \cdot 10^{19}$
9	9.500	1	$2.85 \cdot 10^{4}$	$9.13 \cdot 10^{18}$
10	10.500	1	$2.45 \cdot 10^{4}$	$8.06 \cdot 10^{18}$
11	11.500	1	$2.26 \cdot 10^{4}$	$7.01 \cdot 10^{18}$
12	12.500	1	$1.66 \cdot 10^{4}$	$5.28 \cdot 10^{18}$
13	13.500	1	$1.44 \cdot 10^{4}$	$4.57 \cdot 10^{18}$
14	14.500	1	$1.21 \cdot 10^{4}$	$4.05 \cdot 10^{18}$
15	18.500	7	$5.53 \cdot 10^{3}$	$1.85 \cdot 10^{18}$
16	24.500	5	$2.55 \cdot 10^{3}$	$8.37 \cdot 10^{17}$
17	29.500	5	$1.20 \cdot 10^{3}$	$3.84 \cdot 10^{17}$
18	34.500	5	$5.75 \cdot 10^{2}$	$1.77 \cdot 10^{17}$
19	39.500	5	$2.87 \cdot 10^{2}$	$8.37 \cdot 10^{16}$
20	44.500	5	$1.49 \cdot 10^{2}$	$4.12 \cdot 10^{16}$
21	49.500	5	$7.98 \cdot 10^{1}$	$2.15 \cdot 10^{16}$

The ACM inputs trace gas concentrations of long-lived and "source" gases, most notably, CH_4, carbon monoxide (CO), water vapor (H_2O), ozone (O_3), and the total nitrogen oxide level (NO_x). The model is a work in progress, however, and in time these gases will be outputs of the model. For the time, holding these gases constant assures a high level of accuracy and robustness in the ACM.

The outputs of the ACM are mostly short-lived, but important, trace gases such as HO, HO_2, NO_2, and excited-state oxygen, $O(^1D)$. For each species, the continuity equation is solved.

$$\frac{\partial c(z,t)}{\partial t} = \frac{\partial}{\partial z}\left[K(z)N(z)\frac{d}{dz}\left(\frac{c(z,t)}{N(z)}\right)\right]+P-L \tag{2.1}$$

In this equation z is the height, t is the time, c is the gas concentration, K is the eddy diffusion coefficient, N is the atmospheric density, P is the total source strength, and L is the total loss rate.

The model, when run with its full chemistry, has eight inputs and eighteen outputs. These species are listed in Table 2.2. In the following sections I present detailed descriptions of the chemistry, radiation, inputs, and numerical elements of the GCRC-ACM.

Table 2.2: GCRC-ACM chemical inputs and outputs. Species followed by an asterisk are inputs, the rest are outputs.

Base	HO_x	NO_x	Methane
CH_4*	H	HNO_2	CH_3
CO*	H_2*	HNO_3	CH_3O
H_2O*	H_2O_2	HO_2NO_2	CH_3O_2
HO	HO_2	N_2O_5	CH_3OOH
N_2*		NO	HCO
$O(^1D)$		NO_2	H_2CO
O_2*		NO_3	
O_3*		NO_x*	

2.2 Chemistry

The chemistry in the ACM is structured in shells. The first shell contains the fundamental chemical species and reactions. Although it is not a very accurate representation of the atmosphere (it under estimates tropospheric HO concentrations by up to an order of magnitude), it is accurate enough for many purposes [e.g. Prather, 1994] and is very useful from a pedagogical perspective. On top of this model shell is built the HO_x cycle, which adds many important chemical feedbacks to the model and greatly increases its accuracy. The NO_x and methane cycles are added next, each of which adds reaction pathways, increasing the accuracy of the representation of the atmosphere. A comparison of the various model shells is discussed in Section 2.2.5.

2.2.1 The Base Model

The simplest model of the chemistry of the troposphere consists of O_3, $O(^1D)$, HO, H_2O, CH_4, CO, and air. This reaction cycle was first proposed by Levy [1971] to explain the oxidation of CO. In the ACM, O_3, H_2O, CH_4, and CO are held constant so only two chemicals, $O(^1D)$ and HO, are allowed to vary. The production of HO is started by the photodissociation of O_3 to form $O(^1D)$.

$$O_3 \xrightarrow{h\nu} O(^1D) + O_2 \tag{2.2}$$

$O(^1D)$ is very short-lived; at the surface of the earth its residence time is roughly a nanosecond. The majority of the $O(^1D)$ produced (roughly 95%) is catalytically removed by air molecules.

$$\begin{aligned} O(^1D) + N_2 &\rightarrow O + N_2 \quad (2.3)\\ O(^1D) + O_2 &\rightarrow O + O_2 \quad (2.4) \end{aligned}$$

The $O(^1D)$ not destroyed by reaction with air molecules reacts with water vapor to form HO.

$$O(^1D) + H_2O \rightarrow HO + HO \tag{2.5}$$

This is the primary source of HO in the atmosphere.

HO is destroyed primarily by reaction with CO and CH_4.

$$HO + CO \rightarrow H + CO_2 \tag{2.6}$$

$$HO + CH_4 \rightarrow H_2O + CH_3 \tag{2.7}$$

Due only to direct chemical effects, CO removes twice as much HO as does CH_4. By taking chemical feedbacks into account, however, CH_4 may be more important [Lu and Khalil, 1993]. This theory is controversial because it has not been shown how different assumptions about NO_x concentrations affect the feedbacks. Regardless, in this simple model, these feedbacks do not exist and so CO does destroy more HO than CH_4.

This model does a reasonably good job of determining the concentration of HO in the atmosphere. Generally the concentration is lower than is predicted when the HO_x cycle is included in the model because of the feedbacks in the HO_x cycle which tend to create HO.

2.2.2 The HO$_x$ Cycle

The chemicals involved in the HO_x cycle are the hydrogen molecule (H_2), hydrogen atom (H), peroxy radical (HO_2), hydrogen peroxide (H_2O_2), and HO. In the ACM, H_2 is an input because it is created primarily by biospheric processes rather than chemical processes (see section 2.4). The other species are determined from within the model.

The HO_x cycle begins with equation 2.6. The H atom that it produces is destroyed entirely by a three-body reaction with molecular oxygen.

$$H + O_2 \overset{h\nu}{\rightarrow} HO_2 \tag{2.8}$$

An implicit assumption of this model shell is that the atmosphere is clean, meaning there is little NO_x. With the current implementation of the model we approximate a clean atmosphere with no NO_x whatsoever. This approximation means that only about 10% of the HO_2 produced generates HO as opposed to 25% with low-level NO_x and

40% with high-level NO_x. In a no-NO_x atmosphere the only HO-producing reaction involving HO_2 is the reaction with O_3.

$$HO_2 + O_3 \rightarrow HO + 2\ O_2 \tag{2.9}$$

The cycle continues as the majority of the HO_2 produced reacts with itself to produce hydrogen-peroxide. This is the only means of H_2O_2 production.

$$HO_2 + HO_2 \rightarrow H_2O_2 + O_2 \tag{2.10}$$

Three major pathways exist for the destruction of H_2O_2. The first is photodissociation into two HO radicals. This is the dominant reaction responsible for roughly 50% of the H_2O_2 destruction.

$$H_2O_2 \xrightarrow{h\nu} HO + HO \tag{2.11}$$

The second most important destruction mechanism for H_2O_2 is heterogeneous removal. It is important to note, however, that heterogeneous processes are handled in a very simplistic manner in this model (see Section 2.2.6) and the entire issue of heterogeneous processes in chemistry models are not well understood. However, an upper bound on the effect can be determined. Warneck [1974] estimated the time constant associated with aerosol collisions were in the range 16 to 1150 seconds [Warneck, 1974]. The final removal mechanism is reaction with HO.

$$H_2O_2 + HO \rightarrow H_2O + HO_2 \tag{2.12}$$

This completes the description of the HO_x cycle. Some parts of the cycle will be expanded upon in the next two sections because they interact with the NO_x and methane cycles.

2.2.3 The NO$_x$ Cycle

The compounds involved in the NO_x cycle are NO, NO_2, NO_3, N_2O_5, HNO_3, and HO_2NO_2. NO and NO_2 are by far the most important Nitrogen-containing gases to the NO_x cycle, but other chemicals such as nitrous acid, in addition to being important reservoirs for NO_2, are environmentally important and of general interest in a model of the chemistry of the atmosphere.

NO_x is primarily a source gas produced by anthropogenic activities with roughly 20% created in the atmosphere, mostly by lightning and NH_3 oxidation [Ehhalt and Drummond, 1988] (see Section 2.4). The majority of NO_x emitted directly into the atmosphere comes in the form of NO. In the atmosphere, however, most of the NO reacts to form NO_2, yielding roughly a 3:1 NO_2:NO ratio. There are four reactions that are important in producing NO_2 from NO.

$$NO + NO_3 \rightarrow 2\ NO_2 \tag{2.13}$$

$$NO + O_3 \rightarrow NO_2 + O_2 \tag{2.14}$$

$$RO_2 + NO \rightarrow RO + NO_2 \tag{2.15}$$

$$HO_2 + NO \rightarrow HO + NO_2 \tag{2.16}$$

The R in Equation 2.15 refers to an organic group such as CH_3 or C_2H_5. In the GCRC-ACM, only the CH_3 group is used.

Two reactions are primarily responsible for the removal of NO_2.

$$NO_2 + NO_3 \rightarrow N_2O_5 \tag{2.17}$$

$$NO_2 \xrightarrow{h\nu} NO + O \tag{2.18}$$

Equation 2.17 is the only source of atmospheric N_2O_5, which is linked to the NO_x cycle only by this reaction and heterogeneous reactions with water vapor to form HNO_3. These reactions act as reservoirs of NO_x but are of more interest with regards to the role of the Cl cycle which is a frontier in atmospheric chemistry.

The reaction of NO_2 and O_3, while not important for the destruction of NO_2, is the sole creation mechanism for the nitrate radical. NO_3 is destroyed by two processes, Equation 2.13 and the direct photolysis of NO_3.

$$\begin{aligned} NO_3 &\xrightarrow{h\nu} NO + O_2 \\ &\xrightarrow{h\nu} NO_2 + O \end{aligned} \tag{2.19}$$

NO_3 also provides a source of nitric acid, but this is not included in the model, currently. HO_2NO_2 is created by the oxidation of NO_2 and destroyed by its photolysis back into HO_2.

2.2.4 The Methane Cycle

As discussed in Section 2.2.1, methane is quite important in atmospheric chemistry, particularly regarding its role in the destruction of HO. Equation 2.7 is much more important than it first appears, however, because it starts a cycle which has a number of feedbacks that are important to all of the model shells discussed previously. The methyl radical liberated by the oxidation of CH_4 reacts with molecular oxygen.

$$CH_3 + O_2 \xrightarrow{M} CH_3O_2 \tag{2.20}$$

At this point in the cycle, two paths diverge, one for low NO_x regions and one for high. Low NO_x conditions are defined by Fishman et al. [1979] by concentrations below roughly 10 pptv. NO_x this low and extremely rare in the modern atmosphere, limited almost exclusively to Antarctica. Wuebbles and Tamaresis [1993] have model results indicating that this limit may be substantially higher under warm and humid conditions. Low NO_x chemistry is also important when looking at old atmospheres. I will discuss each pathway in turn.

High NO$_x$ Chemistry

Reaction 2.20 is followed by 2.15 as described in Section 2.2.3. The CH_3O so produced is then oxidized to form formaldehyde, which has three major pathways to oxidation, each of which results in the creation of a CO molecule [Wuebbles and Tamaresis, 1993].

H_2CO is photodissociated along two paths. The first, and most important, is the oxidation directly to CO.

$$H_2CO \xrightarrow{h\nu} CO + H_2 \tag{2.21}$$

This reaction pathway is followed roughly half of the time [Crutzen, 1988]. The second photochemical pathway creates HCO, which reacts with O_2 to form CO.

$$H_2CO \overset{h\nu}{\rightarrow} H + HCO \tag{2.22}$$

$$HCO + O_2 \rightarrow CO + HO_2 \tag{2.23}$$

The final pathway, which is about as important as the second, is initiated by the oxidation of H_2CO with HO followed by Equation 2.23 above.

$$H_2CO + HO \rightarrow H_2O + HCO \tag{2.24}$$

Low $\mathbf{NO}_x$ Chemistry

The CH_3O_2 produced by the destruction of the methyl radical next reacts with HO_2 to form CH_3O_2H which in turn reacts with the HO radical, catalytically to form H_2CO and water vapor. This series of reactions has been summarized by Wuebbles and Tamaresis [1993].

$$CH_4 + HO + HO_2 \rightarrow H_2CO + 2\ H_2O \tag{2.25}$$

The H_2CO produced has three possible reaction pathways. The first is the simple photodissociation to form H_2 and CO. The second is the reaction of H_2CO with two ozone molecules to form a CO molecule and two HO radicals. And the last is the reaction of H_2CO with a single ozone molecule to form CO and water vapor. The branching ratios of each of these pathways are roughly 50%, 25%, and 25% [Wuebbles and Tamaresis, 1993].

2.2.5 Model Shell Comparison

A comparison of the various model shells is shown in Figure 2.1 where the tropospheric average of each latitudinal band is shown for land areas. The "Base" line indicates the base model described in Section 2.2.1. The "HO$_x$" line uses the base model plus the HO_x cycle. The "NO$_x$" line is the base model including both HO_x and NO_x cycles. Finally, the "All" line includes the entire model chemistry including the methane cycle.

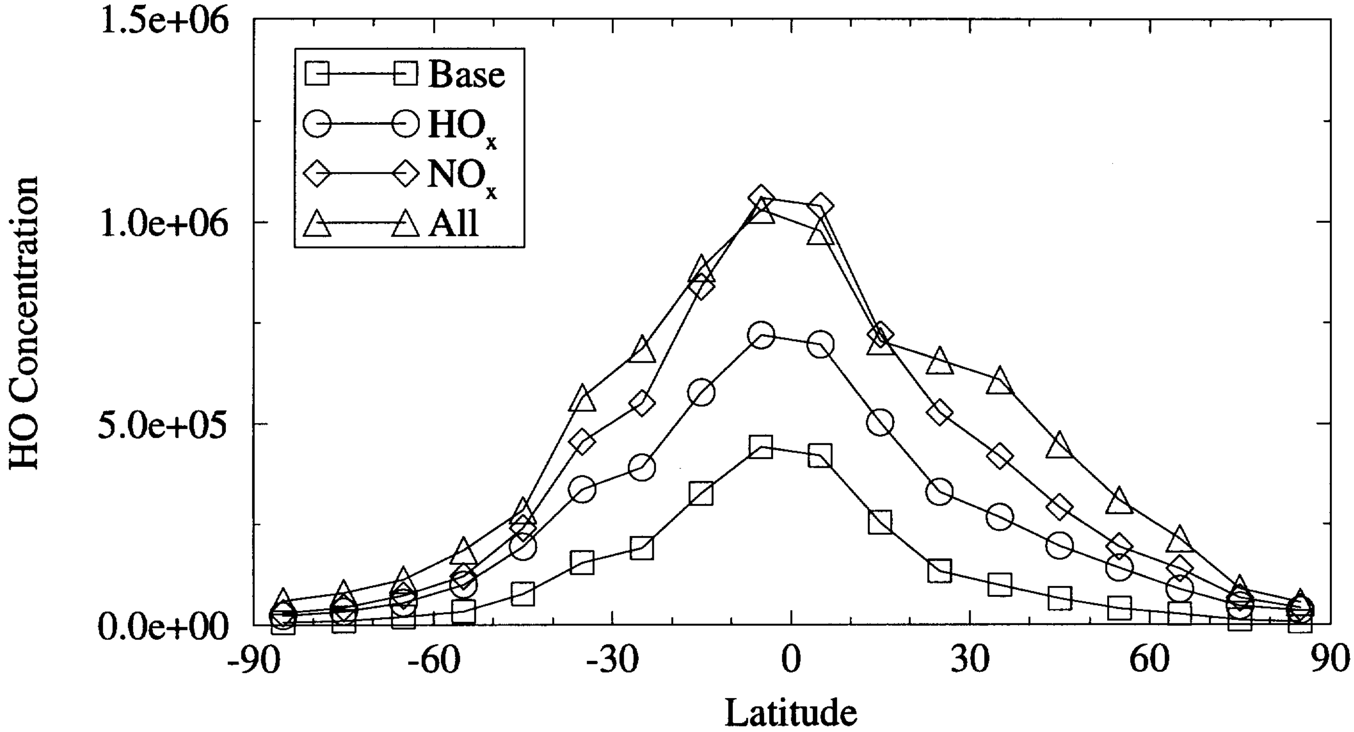

Figure 2.1: Model Shell Comparison. Each model shell is cumulative so the HO_x shell includes the base shell and the HO_x shell and so on.

Figure 2.1 shows clearly how the lack of chemical feedbacks, most notably the HO_x and NO_x cycles, causes the HO concentrations to be anywhere from a factor of two to an order of magnitude too low.

2.2.6 Atmospheric Chemistry Reactions

Three distinct types of chemical reactions take place in the atmosphere: thermal, photochemical, and heterogeneous. Thermal reactions are generally subdivided into binary (or two-molecule) and termolecular (or three-molecule) reactions. The main distinction between these reactions is the manner in which the reaction rate constants are determined. Binary reactions generally follow the Arrhenius equation,

$$K = Ae^{(E/R)/T} \tag{2.26}$$

where K is the reaction rate constant (generally given in $cm^{-3}molec^{-1}s^{-1}$), A is the Arrhenius constant, E/R is the activation temperature, and T is the air temperature. One reaction, Equation 2.6, depends upon pressure instead of temperature. The parameters used in the ACM are given in Table 2.3 [DeMore et al., 1992].

Termolecular reactions are those that involve a third gas, usually air, as a catalyst. The reader will note that two termolecular reaction was listed with the binary reactions in Table 2.3. This is done for convenience only because these reactions follow the Arrhenius equation. The other termolecular reactions, which are listed in Table 2.4 [DeMore et al., 1992], take on the following form.

$$K = \frac{K_o[M]}{1 + K_o[M]/K_\infty} 0.6^{\frac{1}{1+log_{10}(K_o[M]overk_\infty)^2}} \tag{2.27}$$

Photochemical reactions are the most important for atmospheric chemistry, especially for the production of HO. Reaction rate constants for photochemical reactions are generally denoted by J (having units of s^{-1}) and are dependent upon three variables: Φ, the quantum yield, σ, absorption cross section, and F, the actinic flux.

$$J = \int_\lambda \Phi \sigma F d\lambda \tag{2.28}$$

The absorption cross section is a measure of the fraction of incident light that a molecule absorbs. The quantum yield is the fraction of photodissociations along a particular path (some molecules dissociate in more than one way) that occurs for every photon absorbed. The actinic flux is the integrated radiation from all directions given by the equation below [Madronich, 1987].

$$F = \int_\phi \int_\theta L(\theta, \phi) sin\theta d\theta d\phi \tag{2.29}$$

It is not possible to list values for the photochemical reaction rate constants because of the complexity of the process of calculating them and their dependence upon altitude, solar zenith angle, and wavelength. As a result, the J values are calculated within the model given input data for σ and Φ. These data are given in Appendix B [DeMore et al., 1992]. The reactions are listed in Table 2.5.

Table 2.3: Binary Chemical Reactions.

Chemical Reaction			Rate Expression
$CH_3O + O_2$	$\rightarrow$	$H_2CO + HO_2$	$3.9 \cdot 10^{-14}\ e^{-900/T}$
$2\ CH_3O_2$	$\rightarrow$	$2\ CH_3O + O_2$	$8.3 \cdot 10^{-12}\ e^{190/T}$
$2\ CH_3O_2$	$\rightarrow$	$CH_3OH + H_2CO + O_2$	$8.3 \cdot 10^{-12}\ e^{190/T}$
$2\ CH_3O_2$	$\rightarrow$	$CH_3OOH_3 + O_2$	$8.3 \cdot 10^{-12}\ e^{190/T}$
$CH_3O_2 + HO_2$	$\rightarrow$	$CH_3OOH + O_2$	$3.8 \cdot 10^{-13}\ e^{800/T}$
$CH_3O_2 + NO$	$\rightarrow$	$CH_3O + NO_2$	$4.2 \cdot 10^{-12}\ e^{180/T}$
$CH_3OOH + HO$	$\rightarrow$	$CH_3O_2 + H_2O$	$1.0 \cdot 10^{-11}$
$CH_4 + HO$	$\rightarrow$	$H_2O + CH_3$	$2.9 \cdot 10^{-12}\ e^{-1820/T}$
$CH_4 + O(^1D)$	$\rightarrow$	$CH_3 + HO$	$1.4 \cdot 10^{-10}$
$CH_4 + O(^1D)$	$\rightarrow$	$H_2 + H_2CO$	$1.4 \cdot 10^{-11}$
$CO + HO$	$\rightarrow$	$CO_2 + H$	$1.5 \cdot 10^{-13}\ (1 + 0.6 \cdot P_{atm})$
$H_2 + HO$	$\rightarrow$	$H_2O + H$	$5.5 \cdot 10^{-12}\ e^{-2000/T}$
$H_2 + O(^1D)$	$\rightarrow$	$H + HO$	$1.0 \cdot 10^{-10}$
$H_2CO + HO$	$\rightarrow$	$H_2O + HCO$	$1.0 \cdot 10^{-11}$
$H_2O + O(^1D)$	$\rightarrow$	$2\ HO$	$2.2 \cdot 10^{-10}$
$H_2O_2 + HO$	$\rightarrow$	$H_2O + HO_2$	$2.9 \cdot 10^{-12}\ e^{-160/T}$
$HCO + O_2$	$\rightarrow$	$CO + HO_2$	$3.5 \cdot 10^{-12}\ e^{140/T}$
$HO + HO_2$	$\rightarrow$	$H_2O + O_2$	$4.8 \cdot 10^{-11}\ e^{250/T}$
$HO + O_3$	$\rightarrow$	$HO_2 + O_2$	$1.6 \cdot 10^{-12}\ e^{-940/T}$
$2\ HO_2$	$\rightarrow$	$H_2O_2 + O_2$	$2.3 \cdot 10^{-13}\ e^{600/T}$
$HO_2 + O_3$	$\rightarrow$	$HO + 2\ O_2$	$1.1 \cdot 10^{-14}\ e^{-500/T}$
$HO_2 + HO_2$	$\xrightarrow{M}$	$H_2O_2 + O_2$	$1.7 \cdot 10^{-33}\ [M]\ e^{1000/T}$
$HO_2 + NO$	$\rightarrow$	$HO + NO_2$	$3.7 \cdot 10^{-12}\ e^{250/T}$
HO_2NO_2	$\xrightarrow{M}$	$HO_2 + NO_2$	$1.3 \cdot 10^{-14}\ e^{-10418/T}$
$N_2 + O(^1D)$	$\rightarrow$	$O + N_2$	$1.8 \cdot 10^{-11}\ e^{110/T}$
N_2O_5	$\rightarrow$	$NO_2 + NO_3$	$\mathrm{K}_{NO_2+NO_3} \cdot 5.7 \cdot 10^{26} \mathrm{e}^{-11000/T}$
$NO + NO_3$	$\rightarrow$	$2\ NO_2$	$1.5 \cdot 10^{-11}\ e^{250/T}$
$NO + O_3$	$\rightarrow$	$O_2 + NO_2$	$2.0 \cdot 10^{-12}\ e^{-1400/T}$
$NO_2 + O_3$	$\rightarrow$	$NO_3 + O_2$	$1.2 \cdot 10^{-13}\ e^{-2450/T}$
$O(^1D) + O_2$	$\rightarrow$	$O + O_2$	$3.2 \cdot 10^{-11}\ e^{70/T}$

Table 2.4: Termolecular Chemical Reactions

Chemical Reaction			K_o^{300}	n	K_∞^{300}	m
$CH_3 + O_2$	$\rightarrow$	CH_3O_2	$4.5 \cdot 10^{-31}$	3.0	$1.8 \cdot 10^{-12}$	1.7
$CH_3O_2 + NO_2$	$\rightarrow$	$CH_3O_2NO_2$	$1.5 \cdot 10^{-30}$	4.0	$6.5 \cdot 10^{-12}$	2.0
$H + O_2$	$\rightarrow$	HO_2	$5.7 \cdot 10^{-32}$	1.6	$7.5 \cdot 10^{-11}$	0.0
$HO + NO$	$\rightarrow$	HNO_2	$7.0 \cdot 10^{-31}$	2.6	$1.5 \cdot 10^{-11}$	0.5
$HO + NO_2$	$\rightarrow$	HNO_3	$2.6 \cdot 10^{-30}$	3.2	$2.4 \cdot 10^{-11}$	1.3
$HO_2 + NO_2$	$\rightarrow$	HO_2NO_2	$1.8 \cdot 10^{-31}$	3.2	$4.7 \cdot 10^{-12}$	1.4
$NO_2 + NO_3$	$\rightarrow$	N_2O_5	$2.2 \cdot 10^{-30}$	3.9	$1.5 \cdot 10^{-12}$	0.7

Table 2.5: Photochemical reactions

Chemical Reaction		
CH_3OOH	$\xrightarrow{h\nu}$	$CH_3O + HO$
O_3	$\xrightarrow{h\nu}$	$O(^1D) + O_2$
H_2O_2	$\xrightarrow{h\nu}$	$HO + HO$
H_2CO	$\xrightarrow{h\nu}$	$H + HCO$
H_2CO	$\xrightarrow{h\nu}$	$H_2 + CO$
HNO_2	$\xrightarrow{h\nu}$	$NO + HO$
HNO_3	$\xrightarrow{h\nu}$	$NO_2 + HO$
HO_2NO_2	$\xrightarrow{h\nu}$	$NO_3 + HO$
N_2O_5	$\xrightarrow{h\nu}$	$NO_3 + NO_2$
NO_2	$\xrightarrow{h\nu}$	$NO + O$
NO_3	$\xrightarrow{h\nu}$	$NO + O_2$
NO_3	$\xrightarrow{h\nu}$	$NO_2 + O$

Heterogeneous reactions are parameterized using the simple procedure of Logan et al. [1981], which attempts to take into account the altitudinal dependence of rain. The total removal was chosen to be consistent with ^{210}Pb and ^{210}Po observations, which are created by the radioactive decay of ^{222}Rn. Up to four km, the removal is constant at $2.31 \cdot 10^{-6}\ s^{-1}$. Above this altitude, the removal decreases exponentially.

$$K = 2.31 \cdot 10^{-6} e^{1.6 \cdot (4-z)} \tag{2.30}$$

2.3 Solar Radiation

2.3.1 Clear Sky

A two-stream algorithm is used to determine the actinic flux throughout the atmosphere. The basic idea of the algorithm is that, instead of taking into account all directions of diffuse radiation, only the net upward and downward diffuse fluxes are used. Although this method is extremely simple, it has been shown to yield results within 11% of methods that solve the the radiative transfer equations explicitly [Luther and Gelinas, 1976].

The direct radiation at a given model layer is equal to the direct radiation in the model layer just above, multiplied by the fraction of light that is transmitted through the air between the layer above and the given layer. In a clean atmosphere this is given by

$$F_{dir}^{i} = F_{dir}^{i+1} e^{\sigma_{O_3} + \sigma_{Ray}}. \tag{2.31}$$

In this equation F_{dir}^{i} is the direct sunlight at the ith model grid layer, which runs from 0 at the surface of the earth up to N at the stratopause, and σ_{O_3} and σ_{ray} are the optical depths due to O_3 absorption and Rayleigh scattering. This is illustrated in Figure 2.2 below.

The diffuse radiation parameterization is more complex than that of the direct radiation. The diffuse radiation traveling upwards at a given model grid layer is the sum of the transmitted diffuse light traveling upwards from below, the diffuse light traveling

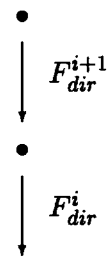

Figure 2.2: Direct radiation grid

downward from above, and the direct light that is scattered. This is given by

$$F_{\uparrow}^{i+1} = \left(f_t^{i+1/2} + \frac{1}{2}f_s^{i+1/2}\right)F_{\uparrow}^{i} + \frac{1}{2}f_s^{i+1/2}F_{\downarrow}^{i+1} + f_{s,dir}^{i+1/2}\cos\theta F_{dir}^{i+1}. \tag{2.32}$$

Here, F_{dir}^{i} is the direct radiation and $F_{\uparrow}^{i}$ and $F_{\downarrow}^{i}$ are the upward and downward diffuse radiation at the ith model grid layer, $f_t^{i+1/2}$ and $f_s^{i+1/2}$ are the diffuse light transmitted and scattered through the atmosphere between the ith and $i+1$th model grid layers, $f_{s,dir}^{i+1/2}$ is the direct light scattered through the same layers, and θ is the angle of incidence of the direct radiation.

The diffuse radiation traveling downwards at an atmospheric layer is the sum of the diffuse light traveling upwards from below, which is scattered, the downward diffuse light from above, which is transmitted and scattered, and the direct sunlight which is scattered through the grid layer. This is given by

$$F_{\downarrow}^{i} = \left(f_t^{i+1/2} + \frac{1}{2}f_s^{i+1/2}\right)F_{\downarrow}^{i+1} + \frac{1}{2}f_s^{i+1/2}F_{\uparrow}^{i} + f_{s,dir}^{i+1/2}\cos\theta F_{dir}^{i+1}. \tag{2.33}$$

The variables in this equation are the same as those above.

2.3.2 Cloudy Sky

Clouds are parameterized in the GCRC-ACM using a modification of the two-stream approximation discussed in Section 2.3.1 combined with a modification of the simple cloud radiation models of Thompson [1984] and Madronich [1987]. Without clouds, the direct radiation at a given model layer is equal to the direct radiation in the model layer just above multiplied by the fraction of light that is transmitted through the air between the layer above and the given layer. In a clean atmosphere this is given by Equation 2.31. For atmospheric layers just below clouds an extra factor must be taken into account when calculating the transmission of direct sunlight. The direct radiation at these grid points is given as

$$F_{dir}^{c-1} = F_{dir}^{c} e^{\sigma_{O_3} + \sigma_{ray} + \sigma_{cloud}}. \tag{2.34}$$

Here the extra term, σ_{cloud}, is the optical depth of the cloud in the space between layers c and $c-1$. The following list of cloud optical depths, taken from London [1952], are used in this model.

Table 2.6: Cloud Optical Depths

Cloud Type	Optical Depth
Cirrus	1
Altostratus	30
Nimbostratus	250
Stratus	10
Cumulus	100
Cumulonimbus	500

The diffuse radiation parameterization for clouds is more complex than that of the direct radiation, but it too is only a modification of the two-stream approximation. The diffuse radiation traveling upwards at the atmospheric layer just above a cloud is the sum of the transmitted diffuse light traveling upwards from below the cloud, the reflected diffuse light traveling downward just above the cloud, and the direct light that is reflected by the cloud. This is given by

$$\begin{aligned} F_{\uparrow}^{c} = (1 - A_{diff})\left(f_t^{c-1/2} + \tfrac{1}{2} f_s^{c-1/2}\right) F_{\uparrow}^{c-1} + \left(A_{diff} + \tfrac{1}{2} f_s^{c-1/2}\right) F_{\downarrow}^{c} + \\ (2A_{dir} + f_{s,dir}^{c-1/2}) \cos\theta F_{dir}^{i+1}. \end{aligned} \tag{2.35}$$

A_{dir} and A_{diff} are the direct and diffuse albedos of the cloud.

The diffuse radiation traveling downwards at the atmospheric layer just below a cloud is the sum of the diffuse light traveling upwards from below, which is reflected by the cloud, the downward diffuse light from above the cloud, which is transmitted and scattered through the cloud, and the direct sunlight which is scattered through the cloud. This is given by

$$F_{\downarrow}^{c-1} = (1 - A_{diff})\left(f_t^{c-1/2} + \tfrac{1}{2}f_s^{c-1/2}\right)F_{\downarrow}^{c} + \left(A_{diff} + \tfrac{1}{2}f_s^{c-1/2}\right)F_{\uparrow}^{c-1} + \\ f_{s,dir}^{c-1/2}(1 - A_{dir})F_{dir}^{c}\cos\theta. \tag{2.36}$$

The variables in this equation are the same as those above except for the addition of $f_{s,dir}^{c-1/2}$, which is the percentage of the direct radiation which is scattered between model grid layers c and $c+1$.

2.3.3 Numerical Analysis

In the model, the upward and downward diffuse flux values are determined simultaneously and stored in a single array that alternates downward and upward fluxes (the downward fluxes are in the even array elements and the upward are in the odd array elements). This procedure yields a penta-diagonal matrix. By rearranging terms, however, a tridiagonal matrix may be constructed, which is easily and efficiently solved [Press et al., 1988]. This is done by first reversing the ordering of the array elements (putting the upward fluxes first). Next Equations 2.32 and 2.33 are combined as follows.

$$(2.32) - \frac{\left(f_t^{i+1/2} + \frac{1}{2}f_s^{i+1/2}\right)}{\frac{1}{2}f_s^{i+1/2}}(2.33) \tag{2.37}$$

This equation yields a matrix function, which depends only on the elements above and below it.

$$F_{\uparrow}^{i+1} = \left[\tfrac{1}{2}f_s^{i+1/2} - \left(f_t^{i+1/2} + \tfrac{1}{2}f_s^{i+1/2}\right)\frac{\left(f_t^{i+1/2}+\frac{1}{2}f_s^{i+1/2}\right)}{\frac{1}{2}f_s^{i+1/2}}\right]F_{\downarrow}^{i+1} + \\ \frac{\left(f_t^{i+1/2}+\frac{1}{2}f_s^{i+1/2}\right)}{\frac{1}{2}f_s^{i+1/2}}F_{\downarrow}^{i} + f_{s,dir}^{i+1/2}\cos\theta F_{dir}^{i+1} - \frac{\left(f_t^{i+1/2}+\frac{1}{2}f_s^{i+1/2}\right)}{\frac{1}{2}f_s^{i+1/2}}f_{s,dir}^{i+1/2}\cos\theta F_{dir}^{i+1} \tag{2.38}$$

The downward flux is rearranged similarly.

$$(2.33) - \frac{\frac{1}{2}f_s^{i+1/2}}{\left(f_t^{i+1/2} + \frac{1}{2}f_s^{i+1/2}\right)}(2.32) \tag{2.39}$$

This equation leads to a tridiagonal formulation for the downward flux.

$$F_{\downarrow}^{i} = \frac{\frac{1}{2}f_s^{i+1/2}}{\left(f_t^{i+1/2}+\frac{1}{2}f_s^{i+1/2}\right)}F_{\uparrow}^{i+1} +$$
$$\left[\frac{1}{2}f_s^{i+1/2} - \left(f_t^{i+1/2} + \frac{1}{2}f_s^{i+1/2}\right)F_{\uparrow}^{i} + \frac{1}{2}f_s^{i+1/2}\frac{\frac{1}{2}f_s^{i+1/2}}{\left(f_t^{i+1/2}+\frac{1}{2}f_s^{i+1/2}\right)}F_{\uparrow}^{i}\right] + \tag{2.40}$$
$$f_{s,dir}^{i+1/2}\cos\theta F_{dir}^{i+1} - \frac{\frac{1}{2}f_s^{i+1/2}}{\left(f_t^{i+1/2}+\frac{1}{2}f_s^{i+1/2}\right)}f_{s,dir}^{i+1/2}\cos\theta F_{dir}^{i+1}$$

This implementation is numerically identical to the more complex procedure developed in Section 2.3.1.

2.4 Source Gases

2.4.1 H_2O

Water vapor in the atmosphere is the result of evaporation, primarily from oceans, and transport by atmospheric motions. Because of this, H_2O, which has highly variable sources spatially and a short lifetime (about 9 days [Warneck, 1988]), cannot be modeled effectively in the ACM. Some effort has been made in this capacity by Manabe and Wetherald [1967], but such models are not acceptably accurate given the importance of H_2O concentrations to atmospheric chemistry, particularly HO production. As a result, the GCRC-ACM inputs H_2O concentrations.

Figure 2.3 shows the annual average water vapor mixing ratios used in the GCRC-ACM.

The 2.5-D distribution for H_2O was constructed by interpolating and averaging the NCAR seven-layer and ten-year monthly data set of temperature and relative humidity [Mulder, 1986]. The data are given in 2.5° by 2.5° cells. The data set was averaged to give 10° cells for each season. The data sets for temperature and relative humidity were then combined with the "Fraction of Area Which Is Land (Map 0)" from Warren et al. [1986a] to construct global two-dimensional fields for land and sea areas. Finally, the relative humidities were converted to mixing ratios using the Clausius-Clapeyron

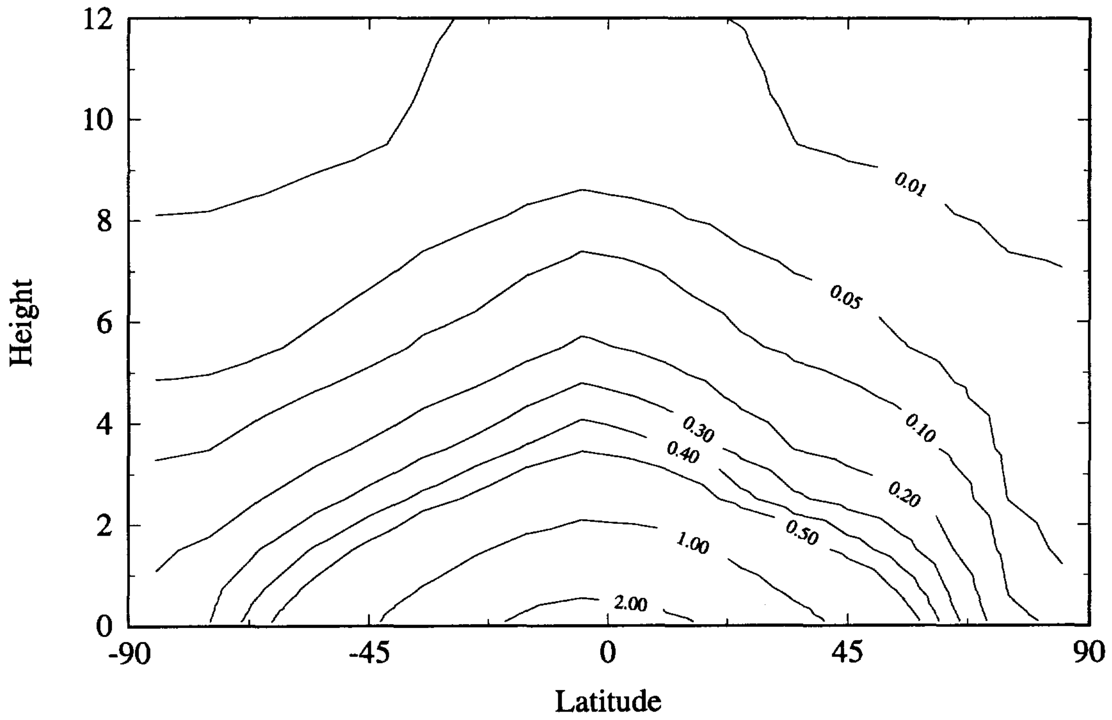

Figure 2.3: Water Vapor Mixing Ratios

relation.

2.4.2 O_3

The lifetime of O_3 in the troposphere is roughly 3 to 5 months [Warneck, 1988]. As a result of this long lifetime and the incomplete inclusion of stratospheric chemistry in the ACM, O_3 is input directly. It is possible, however, to parameterize tropospheric chemistry. Thompson [1984] has done this by adding a flux at the top of the troposphere of $5{\cdot}10^{10}$molec$\cdot$cm$^{-2}\cdot$s^{-1} and a deposition velocity at the surface of the earth of 0.05

$cm \cdot s^{-1}$. The main problem with this approach is that most O_3 entering the troposphere from the stratosphere does so as a result of seasonal adjustments of the tropopause. This problem is certainly not insurmountable, however, and ozone will be created by the model after the stratospheric ozone model, which is currently being developed in the GCRC, is complete.

The ozone data used in the ACM were derived from current literature sources. See Chapter 4 for details. The ACM data are listed in Appendix B.

2.4.3 NO_x

NO_x is highly variable in the atmosphere, but its sources are reasonably well known [Ehhalt and Drummond, 1988; Dignon and Penner, 1991; Dignon, 1992]. A combined NO_x source and chemistry model is an obvious extension to the ACM. Currently, however, the ACM uses data derived from current literature sources. See Chapter 3 for details.

2.4.4 CH_4

CH_4 has the longest lifetime of any gas in the ACM. This makes it particularly difficult to model even though it is produced solely at the surface of the earth and removed predominately by reaction with HO in the troposphere.

The methane data used were derived from surface measurements [Khalil and Rasmussen, 1990a] and vertical distributions [Fabian et al., 1981; Schmidt et al., 1984; Taylor et al., 1989] assuming a seasonal cycle of ± 20 ppbv with a trough in the hemispheric summer and peak in the winter [see Figure 3b of Khalil et al., 1993]. The data are listed in Appendix B.

2.4.5 CO

CO has a tropospheric lifetime similar to that of O_3, but its sources are much more complex. Atmospheric CO is produced by primary injection from anthropogenic and biogenic activities, particularly from inefficient combustion, as well as in the atmosphere through the oxidation of CH_4 and other hydrocarbons as discussed in Section 2.2.4.

The CO data used by the ACM were derived in much the same way as the CH_4 data. The surface data of Khalil [1993] were interpolated and assumed constant in the troposphere and lower stratosphere. Data from Warneck [1988] were used for the upper stratosphere. A seasonal cycle of ± 40 ppbv was assumed for the northern hemisphere and no seasonal cycle was used for the southern hemisphere [Khalil and Rasmussen, 1990c]. Land areas were scaled relative to this data as shown in Spivakovsky et al. [1990]. The data are listed in Appendix B.

2.4.6 HNO$_3$

HNO_3 is taken from the model results of Penner et al. [1991]. It is assumed that HNO_3 is well-mixed vertically. The mixing ratios are shown in Figure 2.4 and listed in Appendix B.

2.4.7 H$_2$

H_2 is similar to CO in that it is produced both in the biosphere and in the atmosphere. Its lifetime is longer, however, generally about 2 years. Roughly 10% is removed by reaction with HO, the rest removed by soil uptake. Because of its relatively long lifetime, its concentration is fairly constant throughout the troposphere. As a result, a single vertical distribution for the entire atmosphere is used in the ACM [Warneck, 1988]. The data are listed in Appendix B.

2.5 Model Implementation

The source code of the GCRC-ACM is listed in Appendix A. This section is a brief overview of its design and implementation. For instructions on getting and using the model see Appendix C. The flow of the model is shown in Figure 2.5.

The ACM begins by processing user input, which comes in two forms: command line

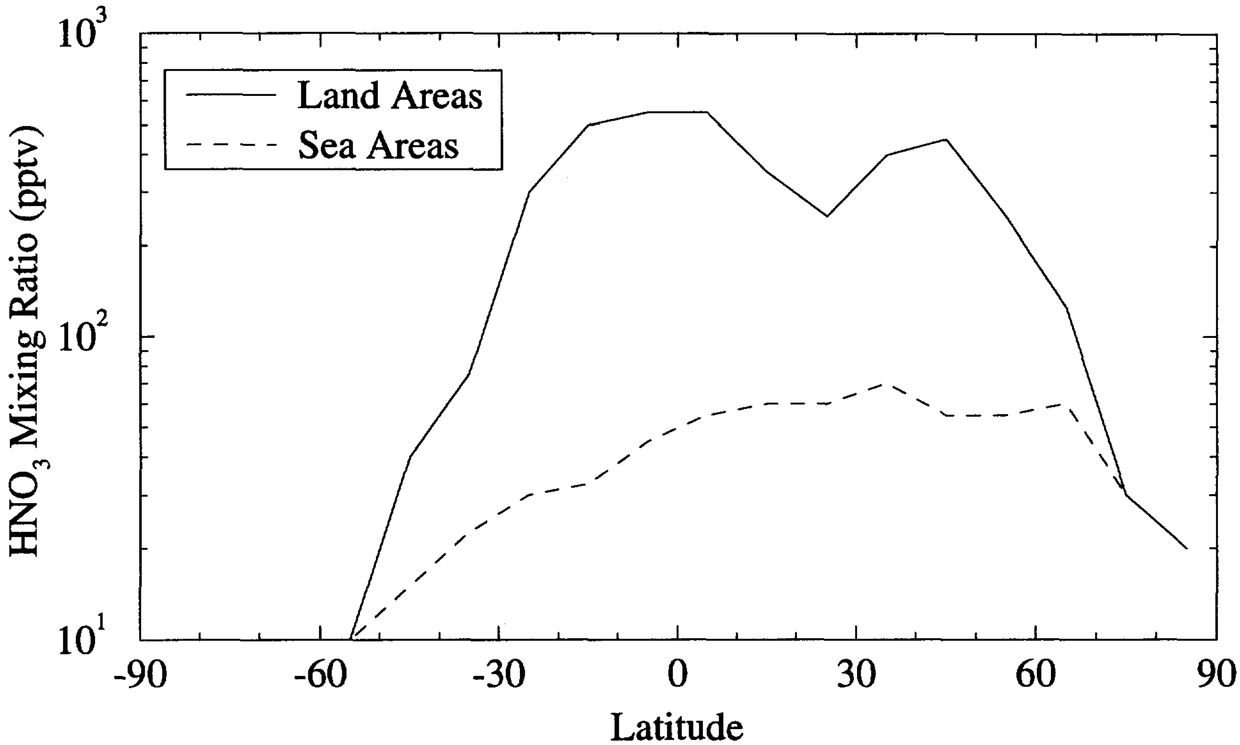

Figure 2.4: HNO_3 Mixing Ratios

arguments and a parameter file. The two input forms tell the model what latitude and season to use, which chemicals to solve and output data for, the location and optical depth of clouds in the atmosphere, and the convergence criterion. The model has a fair degree of flexibility in these parameters, but any other changes in the model require a rewrite of the code.

The model next constructs the atmosphere. It does this by reading various files for gas concentrations (N_2, O_2, H_2, O_3, CO, CH_4, NO_x, and H_2O) and physical parameters (eddy diffusion coefficient [Liu et al., 1984], temperature [Mulder, 1986], pressure, density [National Oceanic and Atmospheric Administration, 1976], and ground albedo), and model parameters (spatial grid). One physical parameter, the ground albedo, needs explanation. To derive this quantity, the zonal fraction of ocean and land [National Center for Atmospheric Research, 1983] were combined with snow-free land surface albedos for each latitude [Hansen et al., 1983] and ocean albedo of 0.2 [Dickerson et al., 1982]. All of these data are listed in Appendix B.

The model then calculates the thermal reaction rate constants for each reaction in the model at each vertical layer. [1] This is done all at once to improve the model running time. The same is done for the photochemical rate constants, which depend upon the vertical layer and the time of day. This does, however, mean that the model must store a large amount of data, roughly two megabytes depending upon the machine it is running on.

Following the thermal reaction rate constants, the photochemical constants are determined first by calculating the actinic flux in the atmosphere. This is done for wavelengths from 200 to 800 nm at every atmospheric layer for solar zenith angle of 0, 10, 20, 30, 40, 50, 60, 70, 78, and 86 degrees. When a zenith angle other than these is needed, it is linearly interpolated. Next, the absorption cross sections and quantum yields are input or calculated, and finally it is all put together to determine the photochemical rate constants at each atmospheric layer for every hour of the day.

Because the differential equations being solved are initial value problems, initial values must be picked for the concentrations. The equations used are taken from the work of Lu [1990]. The concentrations are then solved for using a finite difference scheme for Equation 2.1. This equation may be decomposed in two steps. First, the inside of the spatial term is changed.

$$\frac{\partial c}{\partial t} = \frac{\partial}{\partial z}\left(K(z)N(z)\frac{c_{i+1/2}^{j+1}/N_{i+1/2}^{j+1} - c_{i-1/2}^{j+1}/N_{i-1/2}^{j+1}}{z_{i+1/2} - z_{i-1/2}}\right) + P + L \tag{2.41}$$

In this equation, i represents the spatial step and j represents the temporal step. Further decomposing Equation 2.1 yields the complete finite difference.

$$\begin{aligned}\frac{c_i^{j+1} - c_i^j}{\delta t} &= K_{i+1/2}N_{i+1/2}\frac{c_{i+1}^{j+1}/N_{i+1}^{j+1} - c_i^{j+1}/N_i^{j+1}}{(z_{i+1/2} - z_{i-1/2})(z_{i+1} - z_i)} - \\ K_{i-1/2}N_{i-1/2}&\frac{c_i^{j+1}/N_i^{j+1} - c_{i-1}^{j+1}/N_{i-1}^{j+1}}{(z_{i+1/2} - z_{i-1/2})(z_i - z_{i-1})} + P_i^{j+1} - L_i^{j+1}\end{aligned} \tag{2.42}$$

[1]The thermal reaction rate constants are not time-dependent because the model does not include diurnal temperature changes.

The main point of interest in this equation, is that the δz terms are different for the two spatial derivatives. When done incorrectly, this can change the transport term by a large amount in areas where the model does not have constant spatial grids (the boundary layer and at the tropopause).

This equation is iterated throughout consecutive days until the concentrations do not change more than the convergence criterion between days. This is a highly inefficient method of solution because it does not take the sparseness of the matrix into account. For most simulations, this scheme takes between 100 and 1000 model days to converge. Hindmarsh [1972] has developed a system specifically suited to atmospheric chemistry models, which will converge roughly 100 times faster than the current system. The source code for this system will be available in the C programming language by the end of the summer [Hindmarsh, n.d.] and will be added to the GCRC-ACM at that time.

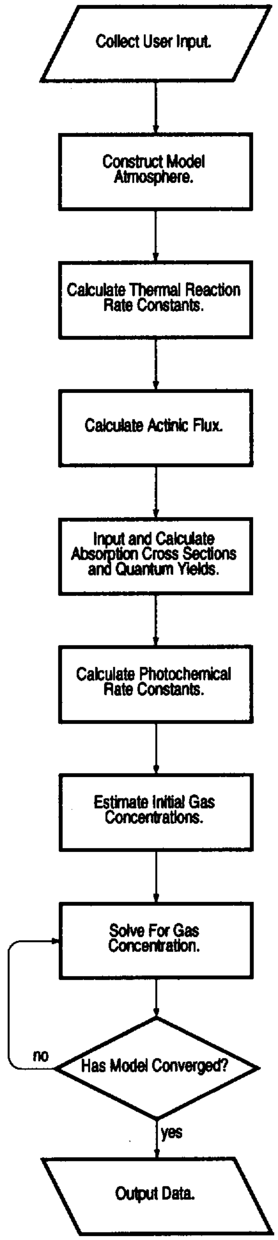

Figure 2.5: GCRC-ACM Program Flow

Chapter 3

Tropospheric NO_x

The majority of tropospheric NO_x is injected from the surface of the earth [see e.g., Logan, 1983]. There is also a small stratospheric source. The combination of these two sources and the short chemical lifetime of NO_x causes its mixing ratios to have the same fundamental vertical distribution: for land areas two maxima exist, one at the tropopause and another at the surface. For oceanic areas, a single maximum is present at the tropopause; a minimum is observed at the surface.

There are thus three distinct areas of the NO_x distribution: the boundary layer (BL), free troposphere (FT), and tropopause (T). In the boundary layer of polluted areas the NO_x mixing ratio decreases exponentially with height to the free troposphere. From the free troposphere, the mixing ratio rises exponentially to the tropopause. In non-polluted areas the NO_x mixing ratio rises exponentially to the tropopause. This behavior can be seen in most data sets [see e.g. Ehhalt and Drummond, 1988] and model results [see e.g. Law and Pyle, 1993].

This chapter provides an overview of the experimental data available for tropospheric NO_x for these three key regions and discusses how the model inputs were derived based upon them.

3.1 Tropospheric NO$_x$ Measurements and Derivations

3.1.1 Available Data

Because of its importance to tropospheric chemistry, NO_x has been measured by various investigators since the late 1970s. Most of these are direct measurements but many are derived. There are two fundamental ways to measure NO_x: (1) measure NO_2 and NO at the same time and (2) convert all of the NO_2 in an air sample to NO and measure the NO. There have been two standard means of converting NO_2 to NO: photolysis of NO_2 and reduction of NO_2 by solid ferrous sulfate. The ferrous sulfate reduction has been found to measure something called $NO\prime_x$ which is NO, NO_2, and some fraction of PAN (peroxyacetyl nitrate) and NPN (n-propyl nitrate). Generally, at high NO_x concentrations (> 1 ppbv) $NO\prime_x$ is equivalent to NO_x [Fehsenfeld et al., 1987]. This issue is discussed below where relevant.

Much of the available NO_x data are not measured at all, however; they are derived from measurements of NO (or in a few cases NO_2) and O_3. If one assumes that NO_2 is in photo-steady-state then NO_x can be calculated simply.

$$NO_x \;=\; NO\left(1 \;+\; \frac{K_{O_3}\cdot O_3 \;+\; K_{HO_2}\cdot HO_2 \;+\; K_{CH_3O_2}\cdot CH_3O_2}{J_{NO_2}}\right) \tag{3.1}$$

Similarly, NO_x can be determined when NO_2 is known.

$$NO_x \;=\; NO_2\left(1 \;+\; \frac{J_{NO_2}}{K_{O_3}\cdot O_3 \;+\; K_{HO_2}\cdot HO_2 \;+\; K_{CH_3O_2}\cdot CH_3O_2}\right) \tag{3.2}$$

Under most circumstances the O_3 term will dominate. It is only in unpolluted air masses that the other terms can be important.

Because the J_{NO_2} term is zero at night Equation 3.2 is always mathematically stable. But in order for Equation 3.1 hold with any degree of accuracy it is necessary to have near-noon values for NO and O_3. Clearly, at night the equation is unstable. As a result, many NO measurements cannot be used to determine NO_x.

Some of the derived data have been obtained from the literature and some has been found using the ACM. Details are provided when necessary.

Because of the reactivity of NO_x in the troposphere, the concentrations that have been measured are quite variable. In this section I will discuss the measurements taken in particular regions: North America and Asia, Eastern United States and Europe, the Arctic, the Pacific and Atlantic Oceans, and the southern hemisphere. Each of these regions is fairly coherent with the possible exception of the southern hemisphere where, unfortunately, there are very few data available.

3.1.2 Early Measurements

The earliest data obtained on NO_x concentrations tend to contradict what is currently believed about the global distribution of NO_x. Robinson and Robbins [1970], synthesizing the early data found that for land areas between 65°N and 65°S NO_x mixing ratios were roughly 6 ppbv and for all other areas it was 0.7 ppbv.

These high values appear to be due to the experimental techniques used, mostly wet chemical reaction, which is not sensitive enough in the sub-ppb range of mixing ratios [Warneck, 1988]. The measured values of NO_x became much smaller with the development of the chemiluminescent reaction of NO with O_3 [Ridley and Howlett, 1974]. An good example of the differences in the measured mixing ratios is the measurement of background NO_2 in the U.S. Using the wet chemical method a value of roughly 2 ppbv was found [Breeding et al., 1973] verses roughly 0.25 ppbv with the chemiluminescent method. Part of this difference may be due to meteorological differences but subsequent measurements have generally found NO_x mixing ratios to be much less than 1 ppbv.

3.1.3 North America and Asia

Bloxam et al. [1975] measured NO_2 at sunrise and sunset over northern Canada near Hudson Bay during the summer. These data, along with additional work by Kerr and McElroy [1976] were converted to NO_x concentrations by Kley et al. [1981]. The mixing ratio in the free troposphere was found to be roughly 200 pptv at 6 km altitude and the mixing ratio at the tropopause was 400 pptv.

The total tropospheric column of NO_2 at Fritz Peak Observatory in New Mexico year round ranged from roughly 0.5 to $5 \cdot 10^{15} cm^{-2}$ [Noxon, 1978; Noxon, 1980]. Assuming a two kilometer mixed layer and negligible free tropospheric NO_x, this represents a boundary layer mixing ratio of 0.1 to 1 ppbv. Assuming a constant tropospheric mixing ratio, this implies 25 to 250 pptv [Logan, 1983]. These two ways of interpreting the data are equivalent to upper and lower bounds. The average value is roughly $2 \cdot 10^{15} cm^{-2}$, which means boundary value mixing ratio is between 100 and 400 pptv.

Noxon [1978] also measured total column NO_2 at various other sites. He found that at locations over 50 km from urban centers, NO_2 values were seldom above $10^{15} cm^{-2}$ or roughly 200 pptv and were generally much less. These results were found for areas throughout the U.S., Canada, and even Peru.

NO was measured during a flight across western Canada in late spring by Schiff et al. [1979]. They found mixing ratios of 50 pptv, independent of altitude. The concentrations generally increased from 40 pptv in northern U.S. to 60 pptv at the arctic circle. Kley et al. [1981] converted this value to 150 pptv for NO_x. These values are generally consistent with the measured values they obtained for the free troposphere in Wyoming [Drummond, 1977] where boundary layer mixing ratios ranging from 100 to 400 pptv were also measured.

NO_x was measured at Niwot Ridge in the Rocky Mountains near Boulder, Colorado by Kelly et al. [1980]. They found a surface (3 km altitude) mixing ratio of roughly 200 pptv year round. Their use of a solid $FeSO_4$ converter means that this value is likely too high by roughly a factor of two, however [Fehsenfeld et al., 1987].

The Niwot Ridge sampling site has been used for several other studies of atmospheric nitrogen [for a review, see Ridley, 1991]. Its usefulness as an indicator of land area NO_x concentrations is unclear, however, because of its proximity to Denver. The NO_x mixing ratios are highly variable ranging from 20 to over 1000 pptv. The average concentration is fairly stable throughout the year with the exception of winter. During this season concentrations tend to be lower than during the other seasons because of the prevailing meteorology brings air which is isolated from contamination [Bollinger et al., 1984]. The results of Fahey et al. [1986] are consistent with the earlier the studies.

Free tropospheric NO_2 values over the south western U.S. were collected by Ridley et al. [1989] as part of the NASA GTE aircraft program. The values averaged 50 pptv. Several flights were made during tropopause folding events. Stratospheric air was very clearly defined by high O_3 and low CO mixing ratios. The NO_x measurements are thus indicative of tropopause air.

An extension of this work was done as part of the GTE/CITE 2 program by Carroll et al. [1990] in the fall of 1986. This expedition was much more extensive than the previous, consisting of 13 aircraft flights, nine over the eastern Pacific Ocean and four across the central United States. In this study continental air masses averaged 120±100 and 55 +100,-35 pptv (these error bars are one sigma) for the upper boundary layer and free troposphere.

The Arctic Boundary Layer Experiment (ABLE 3B) concentrated on eastern Canada from 37°N to 65°N. This expedition was conducted during the summer of 1990. Talbot et al. [1994] have presented data on the vertical distribution of NO_x during ABLE 3B. The data are organized into four air mass types: regional background, biomass burning influence, tropical outflow, and *stratospheric influence.* The first three of these air mass types were defined by the CO mixing ratio with high CO indicating biomass burning and low CO indicating a tropical influence. The stratospheric influence was determined by a combination of high CO and low dew point temperature. The measurements made over Quebec were a mixture of high and low CO air; the middle or "background" air samples were thus taken as indicative of this region. For the samples taken over northern Ontario, however, the air contained high CO values. Thus, the average of middle and biomass burning air samples was taken as indicative of the region. The free tropospheric NO_x values from this experiment agree very well with those of Ehhalt and Drummond [1988] which will be discussed later in this section.

As part of the same experiment, Bakwin et al. [1994] measured NO_x above a taiga woodland in northern Quebec. These results were higher but generally consistent with the boundary layer measurements of Talbot et al. [1994].

The only available measurements of NO in Asia were made by Kondo et al. [1987].

In order for Equation 3.1 to be used to determine NO_x from these data it is necessary to have near-noon values for NO and O_3. As a result, only one flight of Kondo et al. [1987], February 14 from Yao to Akita, provided NO_x concentrations for the free troposphere. A NO_x concentration of 36 pptv was determined. This value is probably more indicative of marine air than it is continental air, however, and is discussed later with other data from the Pacific Ocean.

Summary

The available NO_x data from North America are presented in Table 3.1. The data seem to suggest mixing ratios of roughly 200 (BL), 100 (FT), and 300 pptv (T). The values for the free troposphere and tropopause seem to be lowest near the tropics and highest near the pole but the data are inconclusive.

Two recent modeling studies have predicted NO_x in this area. Penner et al. [1991] find surface concentrations to be always above 500 pptv. These surface values may be too high, however. Ehhalt et al. [1992] have suggested that the vertical transport in this model is too slow. Their model, which was unfortunately only developed to model the latitude band from 40°N to 50°N, finds NO_x mixing ratios of roughly 150 (BL), 40 (FT), and 120 pptv (T). These results, while low, are much more consistent with the available data for the region. They also indicate that the data in Table 3.1 represent the region at least as it is understood theoretically.

3.1.4 Western Europe and Eastern United States

The eastern United States and western Europe share two qualities that cause their NO_x distributions to be quite similar: dense populations and high temperature coal burning. As a result, even in rural areas, NO_x concentrations in the ppb range are common.

As part of the experiment discussed above, Noxon [1978] measured total tropospheric NO_2 on the east coast of the U.S. in New Hampshire, Florida, and Massachusetts all in the winter. These values are in the 500 pptv range. The site in Massachusetts showed great variability; westerly winds brought NO_2 concentrations of less than 160 pptv

Table 3.1: North America and Asia NO_x. The "Air" column is 'BL' for boundary layer, 'FT' for free troposphere, and 'T' for tropopause.

Season	Location	Air	NO_x	Reference
Winter	Wyoming (43°)	BL	250	[Drummond, 1977]
Year	New Mexico (34°)	BL	<400	[Noxon, 1978]
Winter	Wyoming (43°)	BL	<140	[Noxon, 1978]
Winter	Montana (47°)	BL	<120	[Noxon, 1978]
Winter	Alberta (55°)	BL	<100	[Noxon, 1978]
Winter	Saskatchewan (55°)	BL	<60	[Noxon, 1978]
Winter	Goose Bay (54°)	BL	<220	[Noxon, 1978]
Spring	Colorado (40°)	BL	200	[Kelly et al., 1980]
Winter	Colorado (40°)	BL	300	[Bollinger et al., 1984]
Summer	Colorado (40°)	BL	500	[Fahey et al., 1986]
Fall	Southwest U.S. (35-45°)	BL	120	[Carroll et al., 1990]
Summer	Quebec (55°)	BL	30	[Talbot et al., 1994]
Summer	Ontario (52°)	BL	35	[Talbot et al., 1994]
Summer	Quebec (55°)	BL	49	[Bakwin et al., 1994]
Summer	Central Canada (59°)	FT	200	[Bloxam et al., 1975]
Spring	Western Canada (50-60°)	FT	150	[Schiff et al., 1979]
Winter	Wyoming (43°)	FT	150	[Kley et al., 1981]
Spring	Southwest U.S. (33°)	FT	50	[Ridley et al., 1989]
Fall	Southwest U.S. (35-45°)	FT	55	[Carroll et al., 1990]
Summer	Quebec (55°)	FT	34	[Talbot et al., 1994]
Summer	Ontario (52°)	FT	28	[Talbot et al., 1994]
Summer	Central Canada (59°)	T	400	[Bloxam et al., 1975]
Spring	Southwest U.S. (33°)	T	110	[Ridley et al., 1989]

whereas easterlies brought 1 ppb.

Ritter et al. [1979] have measured the mixing ratio of NO_x in Michigan and found roughly the same range as Noxon [1978]. These measurements were done using $FeSO_4$ to convert NO_2 to NO and so again they may err on the high side.

Drummond and Volz [1982] measured NO and NO_2 in the free troposphere over West Germany in the spring of 1981. In the free troposphere NO_2 measurements done with a $FeSO_4$ converter compared very well with the matrix isolation ESR technique. In the boundary layer, the $FeSO_4$ converter over estimated NO_2 noticeably and so the ESR data are used for the boundary layer measurements. In the free troposphere NO_x ranged from 300 to 600 pptv and in the boundary layer (at 1 km) it ranged from 2 to 5 ppbv.

A study of three sites in the Ohio River Valley was carried out by Shaw Jr. and Paur [1983]. Their measurements over the course of sixteen months showed all of the sites to agree quite well. The only clear seasonal effect was a peak in the winter when NO_x levels averaged roughly 9 ppbv. In the other seasons the mixing ratios stayed relatively constant at 4.5 ppbv [1].

A similar study was done at three sites in Hungary [Mészáros and Horváth, 1984]. Only NO_2 was measured but NO values can be inferred for an upper limit on NO_x of 7 and 3 ppbv for winter and summer.

NO_x (defined by the authors as NO + NO_2+PAN) was measured at Whiteface Mountain, New York by [Kelly et al., 1984]. Their results present a couple of difficulties. Firstly, they represent an upper limit on actual NO_x because of the PAN contamination. In addition, the altitude of the site is quite high, 1.5 km so it is at the edge of the boundary layer. Overall, however, the concentration was stable at roughly 1 ppbv.

Carroll et al. [1985] measured NO values at Wallops Island, Virginia as part of an inter-comparison. Combining these data with the O_3 measurements of Gregory et al. [1985] yield an NO to NO_x conversion factor of 3. This gives typical NO_x mixing ratios

[1]The mixing ratios presented by the authors *appear* to be mass mixing ratios but it is not clear from the paper. The results presented here have been converted to volumetric mixing ratios.

of 1000 pptv for continental air and 200 pptv for Atlantic air. Torres [1985] found similar results.

As part of the Western Atlantic Ocean Experiment (WATOX), Misanchuk et al. [1987] measured NO'_x off the east coast of North America during the winter of 1986. NO'_x is defined rather vaguely as, "NO_x + a fraction of organic nitrates." Using the same measuring technique (a chemiluminescent analyzer with a $FeSO_4$ converter), Luke and Dickerson [1987], who were also part of WATOX, found that NO'_x was roughly equal to $NO + NO_2 + 0.7 \cdot$PAN. PAN concentrations can be quite high in areas affected by pollution and so the general validity of using NO'_x in place of NO_x is called into question.

The free tropospheric mixing ratios of NO'_x and NO are 0.55 and 0.18 ppbv [Misanchuk et al., 1987] and 0.24 and 0.02 ppbv [Luke and Dickerson, 1987]. This implies NO:NO_2 ratios of 0.49 and 0.09. This tends to imply that the NO'_x determined by Misanchuk et al. [1987] is approximately equal to NO_x because this ratio is roughly what one would expect in the winter atmosphere. The other data set probably greatly over-estimates the NO_x mixing ratio. This is in general agreement with the NO_x intercomparison of Fehsenfeld et al. [1987] who found that the use of solid ferrous sulfate to reduce NO_2 resulted in a much higher derived NO_x mixing ratio for low NO_x ($<$ 400 pptv) conditions. As a result it is not reasonable to use the data of Luke and Dickerson [1987] in a NO_x inventory.

Simpson et al. [1990] measured NO_2 at 44 sites in the United Kingdom over the course of a year. Most of the measurements were made in the south where direct pollution sources are dense. For all of the sites an average mixing ratio of 9 ppbv existed. For the northern sites the mixing ratio was much smaller, 3 ppbv. For the entire region a mixing ratio of roughly 6 ppbv for NO_x is probably indicative.

A coastal location in southwest Ireland was studied by Cox [1977]. The surface mixing ratio averaged roughly 500 pptv with an upper limit of 600 pptv because of the detection limit of the NO measured. These results are a stark contrast to those taken in in the United Kingdom and tend to indicate that the U.K. results represent a very limited area.

Platt and Perner [1980] measured NO_2 at four sites in western Europe. At the marine sites the NO_2 concentrations were generally low (less than 1 ppbv). The unpolluted continental site averaged roughly 3 ppbv and the urban site had mixing ratios up to 75 ppbv. These results are generally in agreement with other European data.

NO_x was measured near the tropopause over Europe as part of a much longer trip from Frankfurt, West Germany to Sao Paulo, Brazil and the return [Dickerson, 1984]. The average NO_x mixing ratio of both flights over Europe was 190±40 pptv (this value should be thought of as an upper limit, however, because it was measured with a $FeSO_4$ converter). Another flight also across Europe during a lightning storm showed very high NO_y (defined as total reactive nitrogen, NO + NO_2 + NO_3 + HNO_3 + HNO_4 + $2N_2O_5$) mixing ratios (NO_x was not measured). These data indicate that NO_x concentrations are highly variable, especially on continental sites where high boundary layer concentrations can be quickly mixed into the free troposphere, creating high NO_x concentrations there.

An extensive measurement campaign was carried out in the eastern U.S. by Parrish et al. [1993]. Three sites provided NO_x data: Egbert, near Toronto, Canada; Bondville in Illinois; and Scotia in Pennsylvania.

Summary

As with the data from North America the boundary layer concentrations are lower than predicted by Penner et al. [1991]. In central Europe, Ehhalt et al. [1992] model NO_x mixing ratios of roughly 1.5 ppbv which is somewhat smaller than *some* of the data would suggest but is definitely within the variability of the data. It appears that some of the boundary layer data is more urban than the locales would suggest. This is particularly true of the studies in the Ohio River Valley [Shaw Jr. and Paur, 1983] and Hungary [Mészáros and Horváth, 1984]. By excluding these data, a very good match is found between the model result and the remaining data.

In the free troposphere rather large differences are found between the data and model results. Ehhalt et al. [1992] find free tropospheric mixing ratios over Europe and the eastern U.S. to be 150 and 100 pptv. These are factors of 3 and 5 lower than the two experimental measurements available. These two sites are rather urban and boundary layer air can mix rapidly throughout the troposphere due to convective mixing. This is to say that these free tropospheric mixing ratios are high because the ground level mixing ratios are high. The boundary layer to free troposphere ratios are 8 and 5 for West Germany and Massachusetts. For a boundary layer mixing ratio of 1500 pptv this would imply at mixing ratio of between 200 and 300 pptv for the free troposphere. This value is reasonably consistent with the results of Ehhalt et al. [1992].

Table 3.2: Europe and Eastern United States NO_x. The "Air" column is 'BL' for boundary layer, 'FT' for free troposphere, and 'T' for tropopause.

Season	Location	Air	NO_x	Reference
Winter	New Hampshire (43°)	BL	360	[Noxon, 1978]
Winter	Massachusetts (42°)	BL	500	[Noxon, 1978]
Winter	Florida (28°)	BL	600	[Noxon, 1978]
Spring	West Germany (51°)	BL	3500	[Drummond and Volz, 1982]
Winter	Ohio (40°)	BL	9000	[Shaw Jr. and Paur, 1983]
Summer	Ohio (40°)	BL	4500	[Shaw Jr. and Paur, 1983]
Winter	Hungary (47°)	BL	7000	[Mészáros and Horváth, 1984]
Summer	Hungary (47°)	BL	3000	[Mészáros and Horváth, 1984]
Summer	New York (44°)	BL	<1000	[Kelly et al., 1984]
Summer	Virginia (38°)	BL	600	[Carroll et al., 1985]
Winter	Massachusetts (42°)	BL	2900	[Misanchuk et al., 1987]
Year	United Kingdom (54°)	BL	6000	[Simpson et al., 1990]
Fall	United Kingdom (52°)	BL	500	[Cox, 1977]
Fall	Bondville (40°)	BL	1500	[Parrish et al., 1993]
Fall	Bondville (40°)	BL	1800	[Parrish et al., 1993]
Fall	Scotia (41°)	BL	1800	[Parrish et al., 1993]
Fall	Egbert (44°)	BL	2000	[Parrish et al., 1993]
Fall	Scotia (44°)	BL	2000	[Parrish et al., 1993]
Spring	West Germany (51°)	FT	450	[Drummond and Volz, 1982]
Winter	Massachusetts (42°)	FT	550	[Misanchuk et al., 1987]
Summer	Europe (40°)	T	<190	[Dickerson, 1984]

3.1.5 Arctic

Much work has been done in the Arctic to try to determine the sources of pollution in the region. There is not a clear distinction between land and oceanic areas.

Dickerson [1985] did some of the earliest NO_x measurements in the Arctic near Europe. Mixing ratios for the free troposphere ranged from roughly 100 to 400 pptv with an average of roughly 200 pptv. In the boundary layer they were higher, about 500 pptv. NO was also below the detection limits of the system, 10 pptv, which adds support to the assumption that NO_2 is equal to NO_x in the arctic region. The measurements of NO_x used a $FeSO_4$ column to convert NO_2 to NO so these values are likely high. The author states that PAN is converted to NO with 10% efficiency. The free tropospheric NO_y mixing ratios were roughly 500 pptv. If one assumes that all of the NO_y that is not NO_x is PAN then at most 30 pptv of the NO_x measured is neither NO nor NO_2. Of course this assumes that the conversion efficiency of other organic nitrates and nitrites is only 10%.

In the spring of 1985, Bottenheim et al. [1986] took measurements of several nitrogen species over northern Canada. In the boundary layer they found NO_2 mixing ratios of 43±9 pptv which is much smaller than the NO_2 levels found in the Arctic near Europe. There are several reasons why this may be so. The first is that Europe is generally more polluted than North America and so the Arctic above Europe may have more NO_x. The second reason may be that the NO_2 measured in this work is a lower limit; the authors state that the mixing ratios reported could be as much as four to five times too small. They also state, based upon NO_x/PAN ratios that the error is likely much smaller. The third possibility is that the measurements of Dickerson [1985] are much more compromised by PAN than thought. Bottenheim et al. [1986] found PAN mixing ratios to be quite constant and high in the Arctic, 210±6 pptv. This is certainly a possibility given the latter work of Fehsenfeld et al. [1987] but nothing can be said for certain. The two measurement sets do provide upper and lower limits for NO_x mixing ratios in the Arctic spring. For the boundary layer, NO_x ranges from 40 to 500 pptv.

As part of the Polar Sunrise Experiment in 1988, Bottenheim et al. [1990] measured temperature, ozone, and NO_2 concentrations for March and April at a surface site near Alert, Canada. The NO_2 values varied from 40 to 140 pptv with a mean of roughly 90 pptv. Very similar results were obtained by Bottenheim et al. [1993] at the same location.

NO measurements made at Barrow, Alaska agree reasonably well with this work [Jaffe et al., 1991]. During periods of time when local NO_x sources did not affect the concentrations of NO_y species, the investigators found that NO was below the detection limit of their instrument, 75 pptv. This implied, based upon modeling results, that NO_x must be below 150 pptv.

The NO_y mixing ratios found for these periods were in in the range 300-800 pptv which is very similar to the results of Dickerson [1985]. This suggests that the NO_x measured was highly contaminated by other reactive nitrogen species. This agrees with the supposition of Barrie and Bottenheim [1991] that NO_x injected into the arctic is converted to organic nitrates during the winter because they are less likely to to be removed by wet or dry deposition.

Bakwin et al. [1992] measured NO_x mixing ratios at a remote site near Bethel, Alaska. The site has very little anthropogenic influence and notably low NO_x mixing ratios of roughly 15 pptv.

As part of the Arctic Boundary Layer Expedition (ABLE 3A), Sandholm et al. [1992] have measured NO_x concentrations from the surface up to 6 km in the summer of 1988. A surprising finding of this work was that while NO_y varied widely, the concentration of NO_x was nearly constant with height.

Summary

The reason for the very different NO_x mixing ratios between summer and spring is that the main removal mechanisms for NO_x, wet deposition and photodissociation, are shut off in the winter. It would seem from the available data, sparse as it is, that the winter and spring mixing ratios are roughly 100 pptv and the summer and fall mixing ratios roughly 20 pptv. Since the majority of the NO_x in the arctic is transported from the mid-latitudes, there should not, in general be much of an altitudinal change.

These results are generally consistent with model results for the Arctic. Penner et al. [1991] find surface mixing ratios of roughly 200 and 50 pptv for the winter and summer. These mixing ratios are lower than the model predicts but this is consistent with the fact that the model apparently over-predicts surface NO_x in the mid-latitudes which is the source of most of the Arctic NO_x. One important qualitative feature of these model results is that the mixing ratio is substantially higher in the Arctic near western Europe. This is likely seen in the data but the uncertainties are high as discussed previously.

The 2-D modeling results of Isaksen and Hov [1987] are also in agreement with the data. They find a spring Arctic NO_x mixing ratio of roughly 100 pptv. Law and Pyle [1993], in comparison, finds very large Arctic mixing ratios. The authors have stated that their northern hemispheric NO_x results are indicative of polluted areas and so are not truly 2-D fields.

Table 3.3: Arctic NO_x. The "Air" column is 'BL' for boundary layer, 'FT' for free troposphere, and 'T' for tropopause.

Season	Location	Air	NO_x	Reference
Spring	North Europe (80°)	BL	<500	[Dickerson, 1985]
Spring	North Canada (82°)	BL	43	[Bottenheim et al., 1986]
Spring	North Canada (82°)	BL	90	[Bottenheim et al., 1990]
Spring	Barrow, Alaska (71°)	BL	90	[Bottenheim et al., 1990]
Summer	Bethel, Alaska (71°)	BL	15	[Bakwin et al., 1992]
Summer	Barrow, Alaska (71°)	BL	25	[Sandholm et al., 1992]
Spring	North Europe (80°)	FT	<200	[Dickerson, 1985]
Summer	Barrow, Alaska (71°)	FT	25	[Sandholm et al., 1992]

3.1.6 Northern Hemisphere Oceans

During flights between Hawaii and San Francisco as part of the Gametag program, Schiff et al. [1979] measured NO mixing ratios. Most of the measurements were taken at 6 km but several descents and ascents were taken as well. The data show no discernible altitudinal dependence of NO. The NO mixing ratios were to found have an upper limit of 40 pptv which is equivalent to a NO_x mixing ratio of 80 pptv [Kley et al., 1981].

Starr et al. [1979] measured stratospheric NO at 10°S in the summer. These measurements were converted to NO_x to give a tropopause mixing ratio of roughly 300 pptv [Kley et al., 1981].

Nitric oxide and ozone were measured over the Pacific Ocean at various altitudes and under varying meteorological conditions [Ridley et al., 1987]. Using the ACM with average ozone mixing ratios of 25 (BL), 30 (FT), and 30 ppbv (T) yields NO_x:NO ratios of roughly 2.2, 1.3, and 1.0. The NO mixing ratios for these regions were very roughly 5, 10, and 20 pptv which correspond to 11, 13, and 21 pptv. These results exclude measurements taken during electrical activity (where mixing ratios approaching 1 ppbv where measured), near the Hawaiian Islands (with mixing ratios up to 50 pptv), and during what appears to be a tropopause folding event (where NO_x rose suddenly to 700 pptv and O_3 rose to 45 ppbv).

And extension of this work was done in the spring of the following year by Ridley et al. [1989]. The flights of this campaign were close to the west coast of the United States and so the NO_x mixing ratios were higher than the central Pacific flights, 36±22 pptv.

In the fall of 1986 NO_x was measured on nine Pacific flights as part of the GTE/CITE 2 program [Carroll et al., 1990]. NO_x mixing ratios of 15 and 30 pptv were found for the boundary layer and free troposphere.

The measurements of Kondo et al. [1987], discussed above, are probably more indicative of marine air than continental air. They are listed in Table 3.4 because they are the only data from the Western Pacific Ocean.

The best NO data available from this region were taken during the STRATOZ III experiment from the leg from Halifax to Bermuda on 7 June 1984 [Drummond et al., 1988]. Ehhalt and Drummond [1988] converted these data to NO_x mixing ratios. They found values of roughly 60 (BL), 30 (FT), and 150 pptv (T). Most of the data collected in this region was taken from air which was originating over North America. Winds from over the ocean generally brought NO_x mixing ratios of roughly 20 pptv.

A flight in the same region was part of the Chemical Instrumentation Test and Evaluation experiment (CITE 3). The NO_x value for the leg in the mid-latitudes (11-1) was 66 pptv [Davis et al., 1993].

NO and NO_2 were measured as part of the Mauna Loa Observatory Photochemistry Experiment (MLOPEX) in the late fall and early summer of 1988 [Carroll et al., 1992]. Two types of air masses are indicative of this region: daytime upslope which is marine boundary layer air and some island influence and downslope which is free tropospheric air. The NO_x mixing ratios for each of these cases were quite similar: 37 and 31 pptv. Other measurements during the summer at this site found very similar results [Noxon, 1981; Noxon, 1983].

Helas and Warneck [1981] measured NO_x at a site on the west coast of Ireland. They used trajectory calculations to filter the data so that only marine air NO_x mixing ratios were reported. The NO_2 and NO mixing ratios were 87 ± 47 and <10 pptv.

Summary

The data tend to show that boundary layer concentrations of NO_x are higher over the Atlantic than the Pacific. This may be simply a sampling artifact however, since the two Atlantic measurements were made near the continents. Modeling results indicate that concentrations should be higher over the Atlantic [Penner et al., 1991; Ehhalt et al., 1992]. There are, unfortunately, no winter measurements of NO_x in the boundary layer. Penner et al. [1991] have suggested that the mixing ratios of NO_x around the perimeters of both oceans are 500 pptv. This is likely due to the slow vertical mixing in this model as discussed above. Still, it is likely that boundary value concentrations in the winter will be higher overall.

The measurements in the free troposphere are surprisingly consistent. Averaged together without regard to latitude or season they are 43 ± 12 pptv. This exactly matches the modeling results of Ehhalt et al. [1992]. At the tropopause the results are also quite close. The Ridley et al. [1987] data from 9.5 km is perhaps not at a high enough altitude to be truly indicative of the tropopause. At that altitude, Ehhalt et al. [1992] predict 50 pptv.

Table 3.4: Northern Hemisphere Ocean NO_x. The "Air" column is 'BL' for boundary layer, 'FT' for free troposphere, and 'T' for tropopause.

Season	Location	Air	NO_x	Reference
Spring	Eastern Pacific (30°)	BL	80	[Schiff et al., 1979]
Fall	Eastern Pacific (30°)	BL	10	[Ridley et al., 1987]
Fall	Eastern Pacific (30°)	BL	15	[Ridley et al., 1987]
Spring	Hawaii (20°)	BL	37	[Carroll et al., 1992]
Summer	Eastern Atlantic (53°)	BL	90	[Helas and Warneck, 1981]
Summer	Western Atlantic (40°)	BL	60	[Ehhalt and Drummond, 1988]
Spring	Eastern Pacific (30°)	FT	80	[Schiff et al., 1979]
Fall	Eastern Pacific (30°)	FT	10	[Ridley et al., 1987]
Spring	Eastern Pacific (30°)	FT	36	[Ridley et al., 1989]
Fall	Eastern Pacific (30°)	FT	30	[Ridley et al., 1989]
Spring	Pacific (30°)	FT	80	[Schiff et al., 1979]
Spring	Hawaii (20°)	FT	31	[Carroll et al., 1992]
Winter	Western Pacific (35°)	FT	36	[Kondo et al., 1987]
Summer	Western Atlantic (40°)	FT	30	[Ehhalt and Drummond, 1988]
Summer	Western Atlantic (40°)	FT	30	[Ehhalt and Drummond, 1988]
Fall	Western Atlantic (40°)	FT	66	[Davis et al., 1993]
Fall	Eastern Pacific (30°)	T	20	[Ridley et al., 1987]
Summer	Western Atlantic (40°)	T	150	[Ehhalt and Drummond, 1988]
Summer	(10°)	T	300	[Starr et al., 1979]

3.1.7 The Southern Hemisphere

As part of the experiments to measure total tropospheric NO_2, Noxon [1978] measured NO_2 at Cusco, Peru. The boundary layer concentration there was less than 200 pptv. Unfortunately, no details about the measurement site were given.

Using the NO data of Roy et al. [1980], Kley et al. [1981] determined the near-tropopause mixing ratio of this mid-latitude site to be roughly 200 pptv. Galbally and Roy [1981] measured NO and NO_2 at a rural site of Australia in the winter. The mixing ratios are rather high at this site which is somewhat influenced by anthropogenic emissions. The average NO_x mixing ratio was 150 pptv.

McFarland et al. [1979] have measured NO in the equatorial Pacific Ocean. I have combined this data with available temperature and ozone data [Liu et al., 1983] and the ACM derived J_{NO_2}, HO_2, and CH_3O_2 values to determine the NO_x concentration from Equation 3.1. NO concentrations in the southern hemisphere were roughly 5 pptv. This is equivalent to a NO_x mixing ratio of 9 pptv.

The mixing ratio of NO_2 at night (and therefore NO_x is being measured) during the summer, fall, and winter were measured at a remote site in New Zealand [Johnston and McKenzie, 1984]. The mixing ratios show no apparent seasonality. They range from the detection limit of the detector (20 pptv) up to a ppbv. The average is roughly 300 pptv.

NO_y was measured at Mt. John in New Zealand [Stedman and McEwan, 1983]. There is no clear way to deduce the NO_x concentration from this data but the NO_y values do provide an upper limit and given how low the values are, 190 pptv, this is significant.

Dickerson [1984] measured NO_x across the Atlantic from northern Africa to middle South America and over the continent to Sao Paulo, Brazil. All of the remote measurements taken in the southern hemisphere were at the tropopause where the mixing ratio was 387±62.

The most extensive measurement set available of NO_x in the southern hemisphere was derived from the STRATOZ III campaign [Ehhalt and Drummond, 1988]. The NO measurements were taken around the perimeter of South America but they are subdivided into two categories: land and oceanic air masses. The southbound leg of the trip entailed traveling down the west coast of South America and the northbound leg up the east coast. Generally, the air coming off the Pacific had less NO_x than the air from the Atlantic. This is particularly true of the tropical boundary layer where the measurements were made near the continent and therefore may not be indicative of pure marine air. In the free troposphere they are quite similar: roughly 50 pptv in the tropics and 10 pptv elsewhere. There is similar agreement near the tropopause: roughly

Table 3.5: Southern Hemisphere NO_x. The "Air" column is 'BL' for boundary layer, 'FT' for free troposphere, and 'T' for tropopause.

Season	Location	Air	NO_x	Reference
Summer	Peru (10°)	BL	<200	[Noxon, 1978]
Summer	Australia (41°)	BL	150	[Galbally and Roy, 1981]
Winter	Pacific (3°)	BL	9	[McFarland et al., 1979]
Winter	Pacific (3°)	BL	9	[McFarland et al., 1979]
Year	New Zealand (45°)	BL	300	[Johnston and McKenzie, 1984]
Year	New Zealand (44°)	BL	<190	[Stedman and McEwan, 1983]
Summer	(34°)	T	200	[Roy et al., 1980]
Summer	Europe (40°)	T	<390	[Dickerson, 1984]

100 pptv in the tropics and 25 pptv elsewhere.

The land air masses had upper boundary layer NO_x mixing ratios in the 100 pptv range. In the free troposphere the values were much less, generally around 20 pptv. Values of roughly 100 and 50 pptv were found for tropopause mixing ratios of the tropics and mid-latitudes. The mixing ratios for the main regions of the experiment are listed in Table 3.6.

Summary

The southern hemisphere data agree very well with three-dimensional model results [Penner et al., 1991]: the Penner et al. [1991] model shows a clear and constant surface level 100 pptv NO_x iso-line around South America with concentrations rising to as high as 1 ppbv in central Amazonia; Australia and Africa have similar features; The oceans generally have less than 10 pptv NO_x. Two-dimensional model results agree reasonably well although it is hard to compare them to data from individual sites [Isaksen and Hov, 1987; Law and Pyle, 1993].

Table 3.6: Southern Hemisphere NO_x data from the STRATOZ III campaign.

Air Mass	Boundary Layer	Free Troposphere	Tropopause
Tropical Marine		50	100
Tropical Continental	100	20	100
Mid-Latitude Marine	10	10	25
Mid-Latitude Continental	100	20	50

3.2 Sources and Sinks of Tropospheric NO$_x$

3.2.1 Sources

The main reason for looking at the sources of NO_x here is that it provides insight into the seasonal cycle of the global NO_x distribution. This is particularly important because the NO_x measurements are far too few to provide a good picture of how it changes over the course of a year. Most of the sources of NO_x vary seasonally and so by understanding these cycles a greater understanding of the seasonal change in the NO_x distribution is found.

The global sources of tropospheric NO_x have not changed much in the last 10 years. Table 3.7 presents current source estimates subdivided into the north and south hemispheres for winter and summer. Each of the seasons are given relative to the hemisphere in which they occur. So summer, for example, is always the warm season.

The stratospheric source is pretty much evenly distributed between the hemispheres [Ehhalt and Drummond, 1982]. The stratospheric source is due to the reaction of $O(^1D)$ with N_2O. There is clearly some seasonality to this reaction but given the size of the source it can be neglected.

Lightning is more predominate in the northern hemisphere and in the summer of each hemisphere [Turman and Edgar, 1982]. Using the global NO_x source due to lighting from Ehhalt and Drummond [1982] of 5 Tg·yr^{-1} and the relative importance of each season to lightning activity I arrive at the values in table 3.7.

Fossil fuel burning is the single largest source of NO_x, comprising almost half of the entire budget. Luckily, the great interest in global CO_2 production provides much information about the distribution of fossil fuel burning. Rotty [1987] studied the 21 countries which consume the largest amount of fossil fuels. The fuels are subdivided into gases, liquids, and solids. These countries constitute 86% of the total fuel burned. Because there is a slight bias in selecting the data from just twenty-one countries[2] I have scaled the data by the results of Marland et al. [1985] which contains complete total consumption data (it does not subdivide the fuel types however). I have used this data set to separate the northern and southern hemisphere components of the fossil fuel burning source.

The global NO_x budget due to fossil fuel burning is subdivided into five parts: coal, oil, gas, transportation, and industrial sources [Ehhalt and Drummond, 1982]. The first three items clearly map to the fossil fuel database but the last two require assumptions. The vast majority of the transportation source is due to cars and so I have assumed that this source is all liquid. Similarly, industrial energy usage is mostly in the form of coal burning and so I have assumed that all of this source is coal.

In the northern hemisphere fossil fuel combustion is highest in the winter and lowest in the summer. Winter is responsible for 28% of the combustion and summer is responsible for 23% with spring and fall being roughly equal. The southern hemisphere has a smaller seasonal cycle with winter and summer responsible for 26% and 24%. Combining all of these data, leads to the values listed in Table 3.7.

The soil source has been divided between the hemispheres solely on the basis of non-glacier land areas; the southern hemisphere has 35% of this land area [Matthews, 1983]. Parrish and Fehsenfeld [1987] have found a clear exponential temperature dependence of NO_x emissions from soils. Other investigations have agreed surprisingly well with these findings [Kaplan et al., 1988]. The ACM temperature database [Mulder, 1986] provides ten year average southern hemispheric summer and winter temperatures of 17 and 1°C; the northern hemisphere temperatures are 9 and 0°C.

[2]Using the 21 countries alone causes the total fossil fuel consumption of the southern hemisphere to be 4% instead of the correct 5%.

Biomass burning is primarily the result of anthropogenic activity. Dignon and Penner [1991] estimate that the total source is 9 Tg·yr^{-1}. 54% is in the northern hemisphere and 46% in the south. The southern hemisphere has twice the emissions on a per land area basis, however. The winter sources are larger than the summer sources. In the northern hemisphere the difference is a factor of 1.6 but in the south it is 4.0.

The largest sources of tropospheric ammonia (NH_3) are domestic animals and soils. As a result, roughly 90% of the the NH_3 in the troposphere is over land areas [Warneck, 1988]. A crude but reasonable assumption regarding the NO_x source due to NH_3 is that NO_x is *only* produced on the continents. Thus 25% of the source is emitted into the southern hemisphere. Because roughly half of the emissions are due to soils I assume that half of the source has the same seasonal dependence as the direct NO_x emissions from soils.

Table 3.7: Global sources of NO_x. All values are given in teragrams of nitrogen per year per hemisphere.

Source	North Winter	North Summer	South Winter	South Summer
Fossil Fuel	22.0	18.0	1.0	0.9
Soils	1.3	5.1	0.4	4.2
Biomass Burn	5.9	3.8	6.6	1.7
NH3 Oxidation	0.6	2.2	0.3	3.1
Lightning	1.3	4.6	1.7	2.5
Aircraft	0.3	0.3	0.0	0.0
Stratosphere	0.3	0.3	0.3	0.3
Total	31.6	34.3	10.3	12.8

3.2.2 Sinks

NO_x is removed from the atmosphere by its chemical conversion to HNO_3 or nitrate aerosol which is in turn removed by precipitation and dry deposition. The exact amount removed by these processes is extremely uncertain, however. Logan [1983], for example, estimated that wet and dry deposition are responsible for removing 12-42 and 12-22 Tg·yr^{-1} of nitrogen. In this analysis I am only interested in the seasonal cycle of the deposition. Dry deposition should be fairly constant throughout the year although clearly more nitrogen is deposited in the northern hemisphere due to its larger land area. Wet deposition should be proportional to rainfall.

Knapp et al. [1988] have measured NO_3^- over a five year period at three locations: Alaska, Hawaii, and American Samoa. They found very little seasonal variation of wet deposition in either hemisphere. Penner et al. [1991] have reported on unpublished data of W. C. Keen from Ireland and the Indian Ocean which indicate that the wet deposition in the summer in the northern hemisphere is about twice what it is in the winter. There is little variation in the southern hemisphere.

These results agree well with global precipitation data [Spencer, 1993]. For the northern hemisphere, the rain fall is substantially larger during the summer months particularly in the mid-latitudes where the NO_x concentrations are highest. The southern hemisphere summer is similarly higher but not by as much. Based upon the deposition and precipitation data the northern and southern hemispheres each have more wet deposition in the summer by a factor of 2 and 1.5.

Using middle values of 27 and 17 Tg·yr^{-1} for the NO_x removal due to wet and dry deposition [Logan, 1983] along with the rough estimate that wet deposition is twice as efficient on land as on oceanic areas yields the removal data in Table 3.8.

Table 3.8: Global sources of NO_x. All values are given in teragrams of nitrogen per year per hemisphere.

Sink	North Winter	North Summer	South Winter	South Summer
Precipitation	11	22	9	13
Dry Deposition	24	24	10	10
Total	35	46	19	23

3.3 Model Inputs

Combining the information from the measurements of NO_x collected over the last 15 years and the current understanding of sources and sinks of NO_x, it is possible to construct a NO_x distribution which is reasonable for global atmospheric modeling studies. In this section I describe the process of developing this distribution and the problems associated with the assumptions made.

70°N - 90°N

As the data suggest, there is no clear distinction between air masses of the land and sea. In addition, the NO_x of this region should not general have much altitudinal dependence because most pollutants are transported in and are not created in situ. As a result, I am assuming that this region is homogeneous, both latitudinally and altitudinally.

I separate the seasonal cycle into two parts: the winter and spring when concentrations are high because of the low NO_x sink strength and high emissions in the winter; the summer and fall when emissions are low and destruction is high. The average concentrations assumed for these two periods are 100 and 20 pptv. These concentrations agree quite well with the available data.

30°N - 70°N

This region creates perhaps the biggest problems for the land-sea dichotomy of the 2.5-dimensional model. This is so because the mid-latitudes really have three distinct air mass types: oceanic, unpolluted land such as western Canada, and polluted land such as the east coast of the United States. It is necessary to average the land data types but this an implicit error to model results of this region.

The oceanic data is quite consistent although the Atlantic data seems to be slightly more polluted. The seasonal variation, based both on the data and knowledge of the sources, is negligible. I am assuming concentrations of 40, 50, and 150 pptv for the boundary layer, free troposphere, and tropopause.

The largest land area of this region is unpolluted; this would include most of North America and Asia. The sources of NO_x are slightly larger in the summer due mostly to the soil related sources. But the summer removes about 50% more NO_x than the winter. So generally, the winter concentrations should be higher. The data tend to indicate the same thing, at least in the boundary layer. In Canada, for example, NO_x in remote sites of Quebec in the summer are roughly 40 pptv but at Alberta in the winter they are roughly 100 pptv. The data tend to indicate winter NO_x mixing ratios of 100 (BL), 50 (FT) , and 100 pptv (T). In the summer the values are 50, 50, and 100 pptv.

The polluted air masses are indicative of about a third of the land area of this region. Although peak NO_x concentrations as high as 100 ppbv are observed in urban areas the average for these industrialized regions is generally only about 1.5 ppbv. The Ohio River Valley study found that summer concentrations were roughly half of winter concentrations in the boundary layer. I assume a mixing ratio of 1 and 2 ppbv for the summer and winter. The free troposphere generally has concentrations which are 20% the boundary layer values. The tropopause concentrations are generally in the 150 pptv range.

30°N - 20°S

The tropics were not considered in the data section above because there is very little data published on this region and most of it fits into other categories. The main tropical measurement site is in the Mauna Loa Observatory on Hawaii. The concentrations at this site, which are indicative of oceanic regions, are in the 30-40 pptv range for the boundary layer and free troposphere. The STRATOZ III data are in general agreement. These concentrations should be relatively immune to seasonal changes in NO_x as discussed above. I have assumed mixing ratios of 40 (BL), 50 (FT), and 100 pptv (T).

The land areas of this region are responsible for the majority of biomass burning. In addition, the fossil fuel source is greatly reduced and so the winter source of NO_x is larger than the summer source. This is seen clearly in the STRATOZ III data. The tropical NO_x concentrations are as much as ten times higher in the southern hemisphere (winter) than in the northern hemisphere (summer). I thus take boundary layer concentrations to be 100 and 50 pptv for the winter and summer seasons. The concentrations in the free troposphere seem to be insensitive to season at roughly 50 pptv and the tropopause concentrations are the same as for the marine air.

20°S - 90°S

The only oceanic data from this region is from the STRATOZ III mission. The data compares very well to model results, however, and so I use it as being indicative of the region overall. The mixing ratios are 10 pptv for the entire troposphere with a slight increase up to 25 pptv at the tropopause.

The main land areas in this region are Australia and the southern ends of Africa and South America (and Antarctica, which I ignore). The concentrations over the latter continents is roughly 100 (BL), 20 (FT), and 50 pptv (T) for winter conditions. The concentrations seem to be slightly higher over Australia (roughly 200 pptv). I assume mixing ratios of 150 (BL), 30 (FT), and 50 pptv (T) for the winter and 75, 15, and 50 pptv for the summer.

NO_x Distribution

The transition season NO_x values are assumed to be two-thirds of the value of the season immediately preceding them and one-third of the value of the season immediately following them. I make this assumption for two different reasons. In the case of spring it takes most of the season for the climate to get to a point where the excess pollutants have been removed. In the case of fall it is only towards the end of the season that the fossil fuel source is substantially increased over the summer value.

Figures 3.1 and 3.2 contain the data used by the ACM to construct the global distribution. The model assumes that the free troposphere has a constant mixing ratio. For this purpose I define the free troposphere as the troposphere above two kilometers from the surface and below two kilometers from the tropopause. For the top and bottom of the troposphere a exponential is fit such that

$$\begin{aligned} NO_x(0\ km) &= \text{boundary layer } NO_x \\ NO_x(2\ km) &= \text{free tropospheric } NO_x \\ NO_x(z_t - 2\ km) &= \text{free tropospheric } NO_x \\ NO_x(z_t\ km) &= \text{tropopause } NO_x \end{aligned} \tag{3.3}$$

where z_t is the tropopause height.

The distribution so constructed is not ideal. The problem of developing a global NO_x distribution is so complex and data so few, however, that this is the best that can be done without a complete modeling study. And most of the modeling studies that exist, as I have shown above, do not match the available data very well. The distribution presented here is consistent with both the available data and the current understanding of the NO_x cycle.

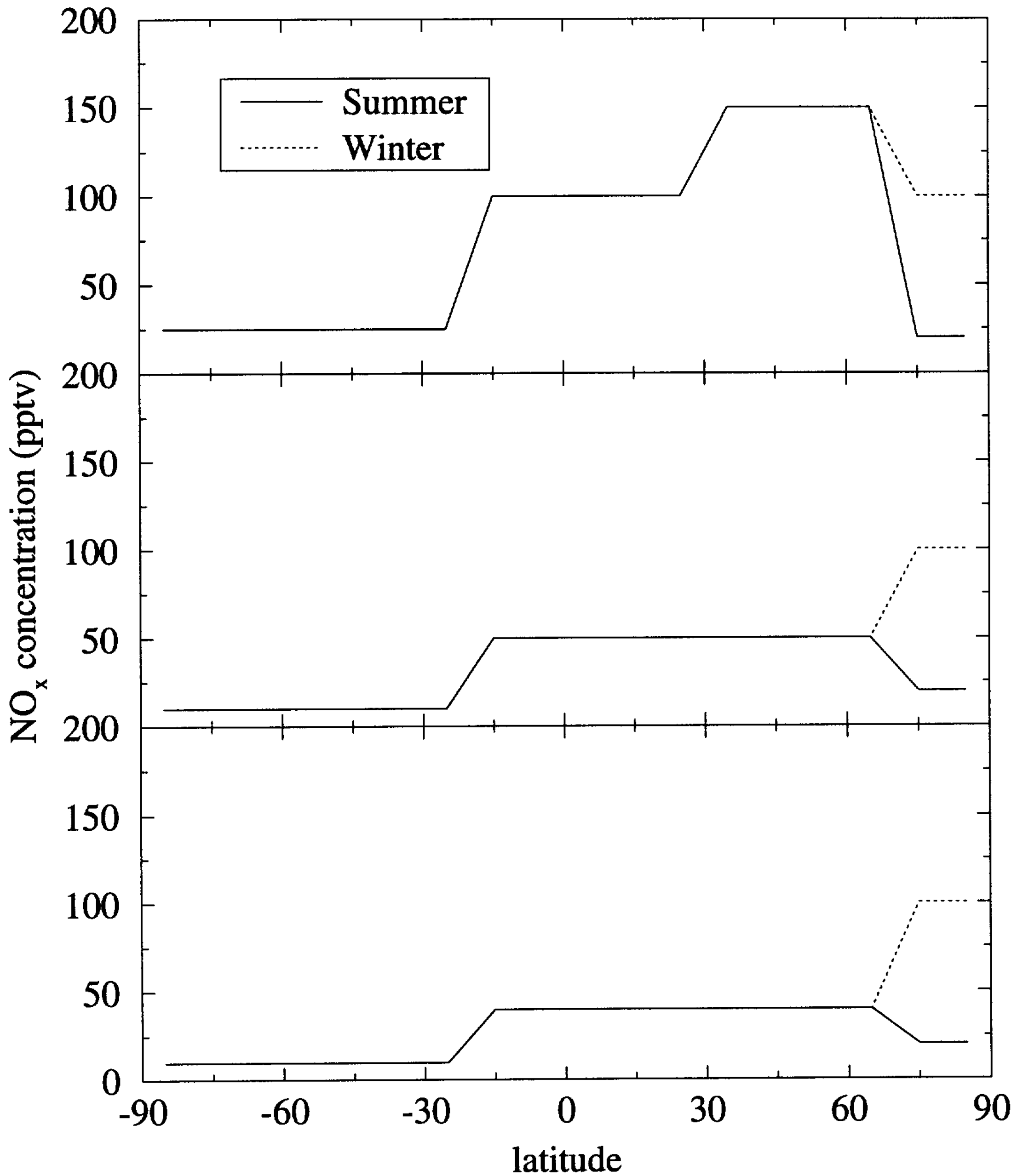

Figure 3.1: Oceanic NO_x. The graphs are, bottom to top, boundary layer, free troposphere, and tropopause. Note that the seasons shown in this graph are northern hemispheric seasons.

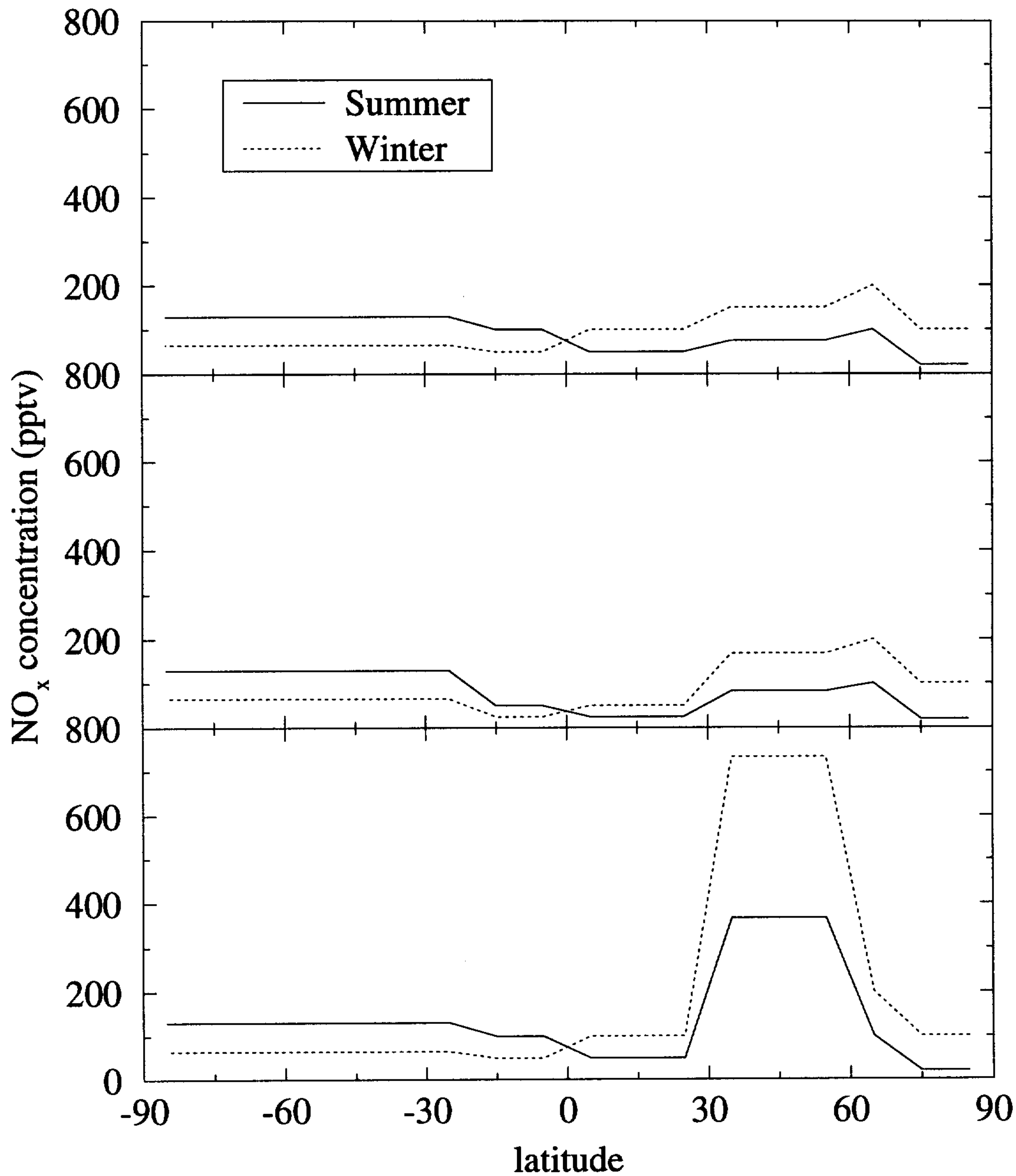

Figure 3.2: Land NO_x. The graphs are, bottom to top, boundary layer, free troposphere, and tropopause. Note that the seasons shown in this graph are northern hemispheric seasons.

Chapter 4

Tropospheric O_3

There are two main sources of ozone in the troposphere: in situ production in areas influenced by urban pollution and transport from the stratosphere. In situ O_3 production in the troposphere is dependent upon NO_x concentrations. The cycle that produces O_3 begins with the reaction of CO, CH_4, or heavier hydrocarbons with HO to produce HO_2, CH_3O_2, or RO_2. Defining these compounds as XO_2, the cycle continues:

$$XO_2 + NO \rightarrow NO_2 + XO \tag{4.1}$$

$$NO_2 + h\nu \rightarrow NO + O \tag{4.2}$$

$$O + O_2 + M \rightarrow O_3 + M \tag{4.3}$$

O_3 destruction is mostly independent of NO_x. There are three primary destruction pathways in addition to surface deposition.

$$O_3 + h\nu \rightarrow O(^1D) + O_2 \tag{4.4}$$

$$HO_2 + O_3 \rightarrow HO + 2O_2 \tag{4.5}$$

$$HO + O_3 \rightarrow HO_2 + O_2 \tag{4.6}$$

Fishman et al. [1979] found that for NO_x mixing ratios above roughly 200 pptv, O_3 removal due to NO_x becomes significant.

$$NO + O_3 \rightarrow NO_2 + O_2 \tag{4.7}$$

$$NO_2 + h\nu \rightarrow O + NO \tag{4.8}$$

It is important to note however, that NO_x concentrations this high are really only present over northern mid-latitudes as discussed in Chapter 3. This means that most oceanic areas are net photochemical sinks of O_3 whereas most land areas are sources.

Without in situ ozone production these regions have two sources of ozone: transport from the stratosphere and transport from land areas. Generally, ozone in remote areas (which are not necessarily oceanic areas) have a very slightly increasing mixing ratio profile with height [e.g., Fishman et al., 1987]. It is only near the tropopause the the concentrations increase substantially.

4.1 O$_3$ Distribution: Representative Data

The two primary sources of tropospheric ozone (in situ photochemical production and transport from the stratosphere) control its seasonal cycle. In areas without significant anthropogenic influence surface ozone concentrations peak in the spring because this is when troposphere-stratosphere exchange is most efficient. In polluted regions surface ozone concentrations exhibit a broad summer maximum owing to the increased removal of CH_4, CO, and NMHCs and the photodissociation of NO_2 which produce ozone in the troposphere. At higher altitudes, however, the cycle changes. Air masses near the tropopause exhibit a cycle more characteristic of non-urban areas (narrow peak in the spring). This behavior is also seen in satellite measurements of total tropospheric ozone [Fishman et al., 1990].

Sites which are significantly influenced by urban pollution have shown a statistically significant trend of roughly 1% per year up to the mid-1980s [Logan, 1985]. It is likely that this trend continued up to 1990 but not beyond because the CH_4 trend was decreasing by that time [Khalil and Rasmussen, 1990b], the CO trend had stopped [Khalil and Rasmussen, 1994], and NO_x does not have an established trend (either experimentally or theoretically) [Ehhalt and Drummond, 1988]. As a result, the measurements taken from the middle 1980s onward are probably fairly indicative of current concentrations.

4.1.1 Northern High and Middle Latitudes

Remote locations have surface ozone mixing ratios which oscillate between roughly 20 and 40 ppbv in the winter and late spring. Angle and Sandhu [1986] found this at three distinctly different sites in Alberta, Canada. Measurements taken in and about California in the fall were similar, in the 30 ppbv range [Fishman et al., 1987]. Generally, the data are fairly insensitive to altitude except very close to the tropopause.

Surface ozone mixing ratios over urban influenced areas in the northern mid-latitudes range from roughly 25 ppbv in the winter to 45 ppbv in the summer. At higher latitudes ozone exhibits a similar seasonal cycle [Oltmans, 1981; Oltmans and Komhyr, 1986].

In the middle troposphere, ozone mixing ratios are higher. In the middle and high-latitudes the seasonal cycle moves from 40 ppbv in the winter to roughly 60 ppbv in the late spring. At the lower elevations (roughly 3 km) the cycle is more like the surface cycle [Logan, 1985]. Near the tropopause the mixing ratios can be extremely high. At these latitudes values of 150 ppbv are typical for the spring. In the winter they fall to the 60 ppbv range [Chatfield and Harrison, 1977; Marenco and Said, 1989].

4.1.2 Tropics

The ozone mixing ratios measured in the tropics are quite variable. Logan and Kirchhoff [1986] have noted that concentrations at Natal, Brazil are substantially larger than at other tropical and southern hemisphere sites. This is likely due to the biomass burning of the region which is a large source of NO_x (see Chapter 3). Other measurements tend to indicate that the Natal data are indicative of polluted tropical areas [Marenco and Said, 1989]. Generally, ozone in the northern tropics are roughly 150% of the levels in the southern tropics [Winkler, 1989].

Oltmans and Komhyr [1986] have analyzed surface ozone data from four NOAA-GMCC stations. Two of the sites, Mauna Loa and Samoa, are in the tropics. The Mauna Loa data are subdivided into two sets depending upon whether the air mass had come from the upper atmosphere or from the surface. The surface data peak in the spring at roughly 30 ppbv and exhibit a minimum in the early fall of roughly 20 ppbv. The data from the upper atmosphere are a little higher, 35 and 23 ppbv. Vertical profiles measured in the fall are in general agreement with these values [Fishman et al., 1987]. The mixing ratios are much smaller in Samoa ranging from less than 10 ppbv in the summer and fall to almost 20 ppbv in the later winter.

4.1.3 Southern High and Middle Latitudes

Based upon 32 cruises spanning 83°N to 78°S of the Atlantic Ocean, Winkler [1989] has constructed a latitudinal and seasonal distribution of ozone. The data in the northern hemisphere agree with data presented above. The southern hemispheric data are surprisingly consistent: ozone mixing ratios peak at about 20 ppbv in the hemispheric winter and spring followed by values of 10 ppbv in the summer.

STRATOZ III measured ozone in the southern hemisphere during the hemispheric winter [Marenco and Said, 1989]. Outside of the tropics, most of the data were collected from continental air masses [Gerhardt et al., 1989]. Surface values of 25 ppbv were found which are slightly higher than those of Winkler [1989] as would be expected. The mixing ratios are quite constant up to about 10 km where they rise sharply up to around 100 ppbv at the tropopause.

Oltmans et al. [1989] have reported measurements taken at three locations of the southern high and middle latitudes. The surface concentrations agree extremely well with the data of Winkler [1989]. In the middle troposphere the concentrations agree well with the Marenco and Said [1989] data in the middle latitudes. Concentrations at the Lauder, New Zealand site higher with mixing ratios are roughly 35 pptv in the summer and fall and 50 pptv in the spring. The authors suggest these larger ozone concentrations are due to the more efficient troposphere-stratosphere exchange in the middle latitudes of the southern hemisphere.

4.2 Model Inputs

70°N - 90°N

As discussed in Chapter 3, there is no clear distinction between oceanic and continental air masses in the arctic. Thus, both land and sea areas are assumed to have the same ozone distribution here. Surface ozone in this region is driven primarily by horizontal transport [Oltmans and Komhyr, 1986] and as a result the mixing ratios are highest in the fall and lowest in the spring and summer, 35 and 20 ppbv. In the free troposphere the concentrations are controlled by stratospheric exchange and so the fall and spring values are equal at 50 ppbv. At the tropopause the spring substantially higher; the values are roughly 75 and 100 ppbv [Oltmans et al., 1989].

30°N - 70°N

The satellite data of total tropospheric ozone for this region indicate that ozone is higher over the oceans than over the land areas. This is due primarily to the production of ozone over the east coasts of North America and Asia and its transport over the oceans [Fishman et al., 1990]. In the spring over the Atlantic Ocean, Smit et al. [1989] found ozone concentrations to range from 50 ppbv at the surface, up to 75 in the middle troposphere, to 100 at the tropopause. This is consistent with the data summarized by Logan [1985]. Using the seasonal cycle from the latter work, the summer values should be roughly the same while the fall and winter values should be roughly 30, 50, and 60 ppbv.

Fishman et al. [1987] have reported ozone measurements taken during the fall of un-polluted areas in California. The profiles vary somewhat but have a characteristic constant mixing ratio of 30 ppbv. This value is likely somewhat low as compared to land areas at this latitude and I have thus chosen a constant 40 ppbv mixing ratio for the winter and fall seasons with a tropopause mixing ratio of 60 ppbv from the oceanic data. The STRATOZ III data from Europe is higher (as is expected due to the larger in situ source), 50, 70, and 100 ppbv. I have used these data as indicative of the summer concentrations.

30°N - 0°

There are two primary ozone measurement sites in the northern tropics: Hawaii and Panama. Both of these sites are most indicative of oceanic areas. Surface values at Mauna Loa exhibit a clear seasonal cycle from 20 to 35 ppbv in the fall and spring. The Panama site has little seasonal cycle, however – oscillating about 15 ppbv [Chatfield and Harrison, 1977]. Data from Venezuela [Sanhueza et al., 1985] is in general agreement although it has a clear peak in the early spring. I use 20 and 35 ppbv for the fall and spring surface concentrations.

The data of this region indicates that there is little vertical dependence of the ozone concentration [Chatfield and Harrison, 1977; Oltmans and Komhyr, 1986; Fishman et al., 1987]. The tropopause concentrations are taken to be roughly 50 ppbv in the winter and spring, rising to a maximum of 75 ppbv in the fall [Chatfield and Harrison, 1977].

For land areas I again use the STRATOZ III data as a base. The surface concentrations seem to be roughly equivalent to those of oceanic areas but the middle tropospheric and tropopause values are about 30% higher [Gerhardt et al., 1989].

The latitude band from 20 to 30°N is taken to be the average of the latitudes directly above and below it.

0° - 30°S

The Natal, Brazil site is indicative of polluted land areas and the Samoa site of oceanic areas. The Samoa site does not exhibit a great deal of seasonality. At the surface it runs from 15 ppbv in the fall to 20 ppbv in the winter and spring. In the free troposphere the concentration is roughly 30 ppbv in the fall and peaks in the spring at roughly 45 ppbv. The tropopause concentration is a maximum in the winter and spring at around 50 ppbv with a minimum in the summer of 35 ppbv.

Since only about have of the tropical land areas are directly influenced by local pollution (particularly biomass burning) I have used the average of the Samoa and Natal data for the tropical land areas. The surface, free troposphere, and near-tropopause mixing ratios are thus 20, 30, and 50 ppbv in the fall and 25, 60, and 70 ppbv in the spring.

30°S - 90°S

Surface ozone for this entire region is about 10 ppbv in the summer and 20 ppbv in the winter and spring [Winkler, 1989]. In the middle troposphere the concentrations diverge between the high and middle latitudes. In the middle-latitudes the mixing ratios are larger, generally around 40 ppbv except in the spring when they are 50 ppbv. The high-latitude values are 25 ppbv in the winter and 35 ppbv in the summer. At the tropopause the regions are even more dis-similar. Middle latitude values of 100 in the winter up to 200 in the spring are common verses high latitude values of 25 and 50.

4.2.1 Distribution Comparison

Figure 4.1 shows the derived ozone column developed in this chapter. As a check to the validity of the ozone distribution I have compared the derived tropospheric ozone column with the satellite measurements of Fishman et al. [1990]. The agreement is surprisingly good. In the tropics at specific locations the data have been found to be in agreement with ozonesonde measurements to only about 10% (where the agreement is the highest). Thus, overall agreement is probably as good as possible.

The worst area is the tropics. Overall, the distribution has too little ozone in this region. It is possible that the assumed tropopause height for this region (15 km) is incorrect. Of course, an increase in the tropopause would cause the hemispheric fall values to be much too high since the tropopause height does not change very much in the tropics. Another possibility is that the near-tropopause data used is in error. This is due mostly to the fact that I have used very few measurements for this area.

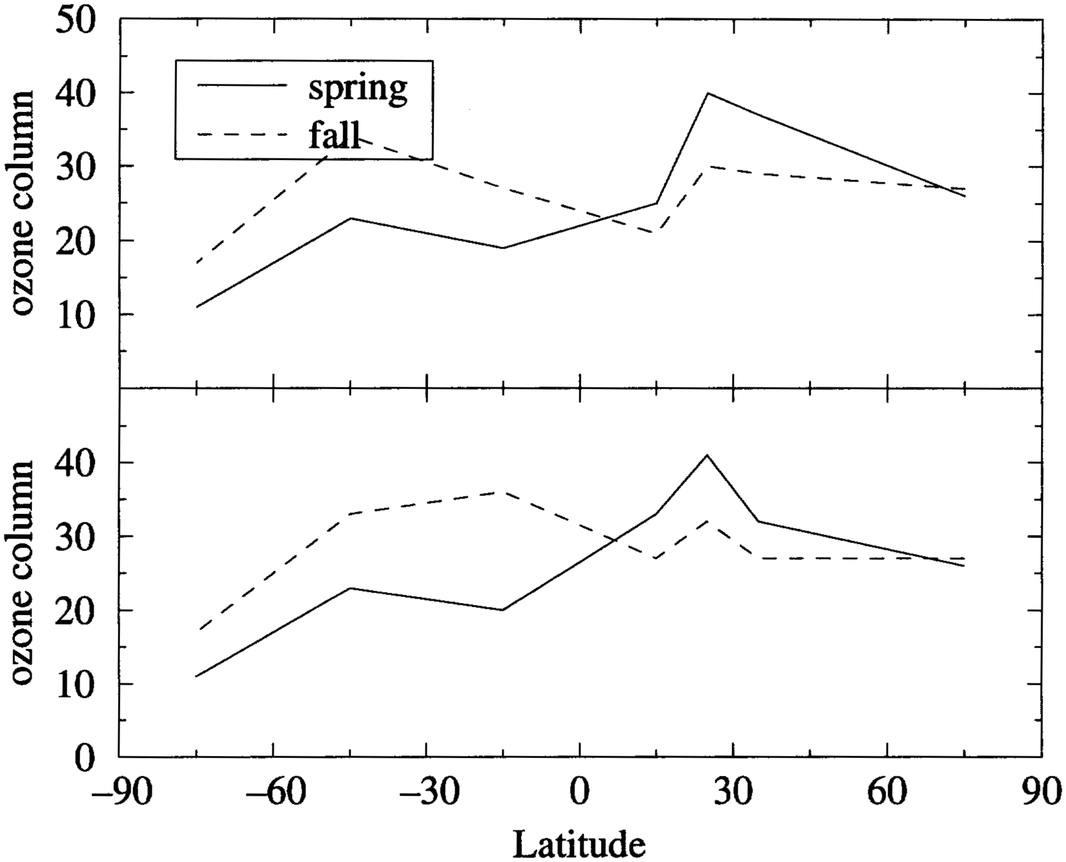

Figure 4.1: Tropospheric ozone column derived from the GCRC-ACM ozone distribution. The top graph is for oceanic areas while the bottom graph is for land areas. The seasons are northern hemisphere seasons.

Table 4.1: Comparison of the tropospheric column derived from the GCRC-ACM ozone distribution with the satellite data from Fishman et al. [1990]. The numbers given are percentage different from the satellite data.

Region	DJF	MAM	JJA	SON
	Land Areas			
Northern Mid-Latitudes	-1%	3%	13%	-5%
Northern Tropics	8%	9%	-7%	-10%
Southern Tropics	-16%	-8%	5%	10%
Southern Mid-Latitudes	-12%	5%	13%	0%
Global	-4%	2%	4%	-1%
	Ocean Areas			
Northern Mid-Latitudes	-2%	3%	10%	-2%
Northern Tropics	-6%	-0%	-5%	-10%
Southern Tropics	-9%	13%	-14%	0%
Southern Mid-Latitudes	4%	0%	6%	3%
Global	-3%	3%	-1%	-2%

Chapter 5

Model Sensitivity Analysis

5.1 Overview

Atmospheric chemistry models are quite sensitive various input parameters which are not extremely well constrained by observation, in particular NO_x, O_3, CO, and H_2O. In this chapter detailed sensitivity analyses are conducted for each of these gases. In addition a qualitative analysis of the effect of cloud optical depths and rate constant uncertainties is presented. The chapter ends with a rough calculation of the total error in the ACM.

5.2 NO$_x$

The total NO_x level affects HO through the reaction of NO and HO_2.

$$NO + HO_2 \rightarrow NO_2 + HO \tag{5.1}$$

This equation would indicate that, all else being equal, higher NO_x values produce higher HO values. All else is not equal however because this equation is also a major sink of HO_2. The reaction of NO_2 with HO_2 is also a sink.

$$NO_2 + HO_2 \rightarrow HO_2NO_2 \tag{5.2}$$

Further complicating matters is that both NO and NO_2 are sinks of HO. At low NO_x concentrations these sinks are quite small but at high levels (1000 pptv) they are significant.

As the total NO_x concentration increases the HO concentration increases because of the increased source strength from the reactions of NO_x with HO_2. At higher NO_x values, however, the destruction of HO_2 becomes so high that this source of HO slows causing larger NO_x values to cause the concentration of HO to fall. This process has been studied with a simple zero-dimensional tropospheric chemistry model by Hameed et al. [1979]. They found that HO concentrations were maximized for NO_2 mixing ratios of 230 pptv which is roughly equivalent to 300 pptv of NO_x.

The sensitivity of the ACM to NO_x was studied in two ways: by calculating the total HO with constant values of NO_x in the troposphere and with percentage changes from the regular input NO_x values. In the first test the NO_x mixing-ratio is set equal to values ranging from 10 pptv to 3 ppbv. The results are shown in Table 5.1 and Figure 5.2. The ACM maximizes HO at NO_x concentrations of roughly 500 pptv, globally. This value is consistent with the results of Hameed et al. [1979] although shows that the ACM is somewhat more sensitive to NO_x.

Table 5.1: GCRC-ACM sensitivity to NO_x. In this test the mixing ratio of NO_x was set to a constant value (given in the first column in pptv) for the entire troposphere. The second and third columns contain the derived global HO concentrations (in 10^5 molec·cm^{-3}) with and without clouds. Methane destruction for these two cases is shown in final two columns (in Tg·yr^{-1}).

NO_x	HO (clouds)	HO	CH_4 (clouds)	CH_4
10	3.5	3.7	192	208
50	5.3	6.3	254	376
100	7.1	8.5	351	516
200	9.1	11.0	479	717
400	10.1	12.4	577	904
600	10.1	12.2	672	862
800	8.8	10.9	526	861
1600	5.6	7.0	339	527
3200	3.0	3.8	180	281

The model sensitivity to NO_x is significantly greater for clear sky than from cloudy sky conditions. The decreased sunlight due to clouds causes the photodissociation of

NO_2 to be decreased.

$$NO_2 + h\nu \rightarrow NO + O \tag{5.3}$$

This means that there will be less NO in a cloudy sky. As a result, less HO_2 will be converted to HO (via Equation 5.1) and thus the total effect of NO_x on HO concentrations will be reduced. Generally, clouds cause the NO_x sensitivity to be 20% less than it would normally be.

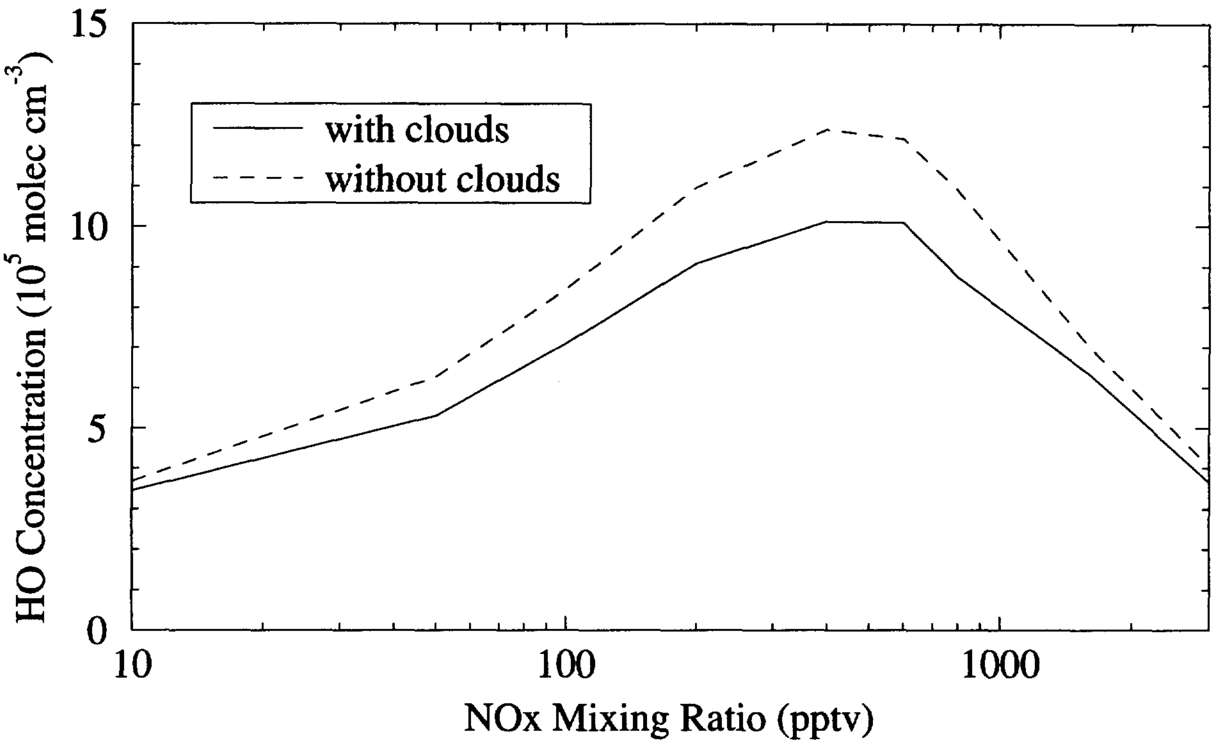

Figure 5.1: HO sensitivity to changes in NO_x spanning pre-industrial to modern urban values.

A different way to look at this problem (and perhaps a more important and insightful way) is to consider the change in atmospheric removal of a trace gas due to HO. For this purpose I look at CH_4 because its concentration is known extremely well and because it is removed primarily by HO, the results obtained are of some interest beyond demonstrating the sensitivity of the ACM.

The last two columns of Table 5.1 show the total destruction of atmospheric methane given the various NO_x values. As expected clouds have a much greater impact on the NO_x sensitivity. Whereas for HO the overall effect was 20%, for CH_4 removal it is roughly 40%. This is so for precisely the same reasons that clouds have a greater effect on CH_4 removal than they do on the concentration of HO, namely, that most removal takes place under the cloud layer. Thus, the effect described above for why the NO_x sensitivity is greater in a clear sky than a cloudy sky is even more important for CH_4 removal.

The sensitivity analysis that has been discussed thus far could be misleading because it assumes a constant NO_x mixing ratio throughout the atmosphere. To remedy this situation a second analysis has been performed which demonstrates how the model responds to relative changes in NO_x concentration in the model. The results are shown in Table 5.2. They illustrate the previous discussion is valid for the model generally.

These data also give some idea of the amount of error that is introduced into the model results because of uncertainties in the input NO_x concentrations. This is particularly important in the case of NO_x because of it variability in the atmosphere. A conservative although rough estimate of errors caused by NO_x may be made by assuming that the NO_x values are known to +100% and -75%. From Table 5.2 the errors for oceanic HO are 1.6 and 1.7 10^5molec·cm^{-3}. For land areas the errors are slightly higher: 1.5 and 2.2 10^5molec·cm^{-3}.

Table 5.2: GCRC-ACM sensitivity to NO_x. In this test the mixing ratio of NO_x was set to a relative value based upon the NO_x values used in the model by default.

NO_x (%)	Oceanic HO	Land HO
1	2.5	2.6
25	3.3	3.7
50	3.9	4.6
75	4.5	5.3
100	5.0	5.9
125	5.5	6.3
150	5.9	6.8
200	6.6	7.4

5.3 O_3

The primary mechanism by which HO is created is the reaction of water vapor and excited state oxygen atoms which are created in the troposphere exclusively by the photodissociation of ozone.

$$O_3 + h\nu \rightarrow \quad O(^1D) + O_2 \tag{5.4}$$

$$O(^1D) + H_2O \rightarrow \quad 2\ HO \tag{5.5}$$

Without these reactions, the only HO of consequence in the atmosphere would be that of the nitrogen cycle discussed in the previous section. As a result, as ozone concentrations increase so does HO. In fact, HO concentrations increase at roughly the square-root of ozone concentrations, apparently without bound. This is shown in Figure 5.3.

Table 5.3 presents the model sensitivity to relative changes in the input ozone fields. Although the overall model sensitivity to O_3 is quite different from the sensitivity to NO_x, the sensitivity in this region (current atmospheric conditions) is quite similar. Because the ozone values are more certain than they are for NO_x, I am defining the errors based upon the ozone concentrations being good to ±50% which yields upper and lower errors of 0.8 (0.8) and 1.0 (1.1) 10^5 molec·cm^{-3}for oceanic (land) areas.

Table 5.3: GCRC-ACM sensitivity to O_3. In this test the mixing ratio of O_3 was set to a relative value based upon the O_3 values used in the model by default.

O_3	Oceanic HO	Land HO
1	2.0	2.7
25	3.3	4.1
50	4.0	4.8
75	4.6	5.4
100	5.0	5.9
125	5.4	6.3
150	5.8	6.7
175	6.2	7.0

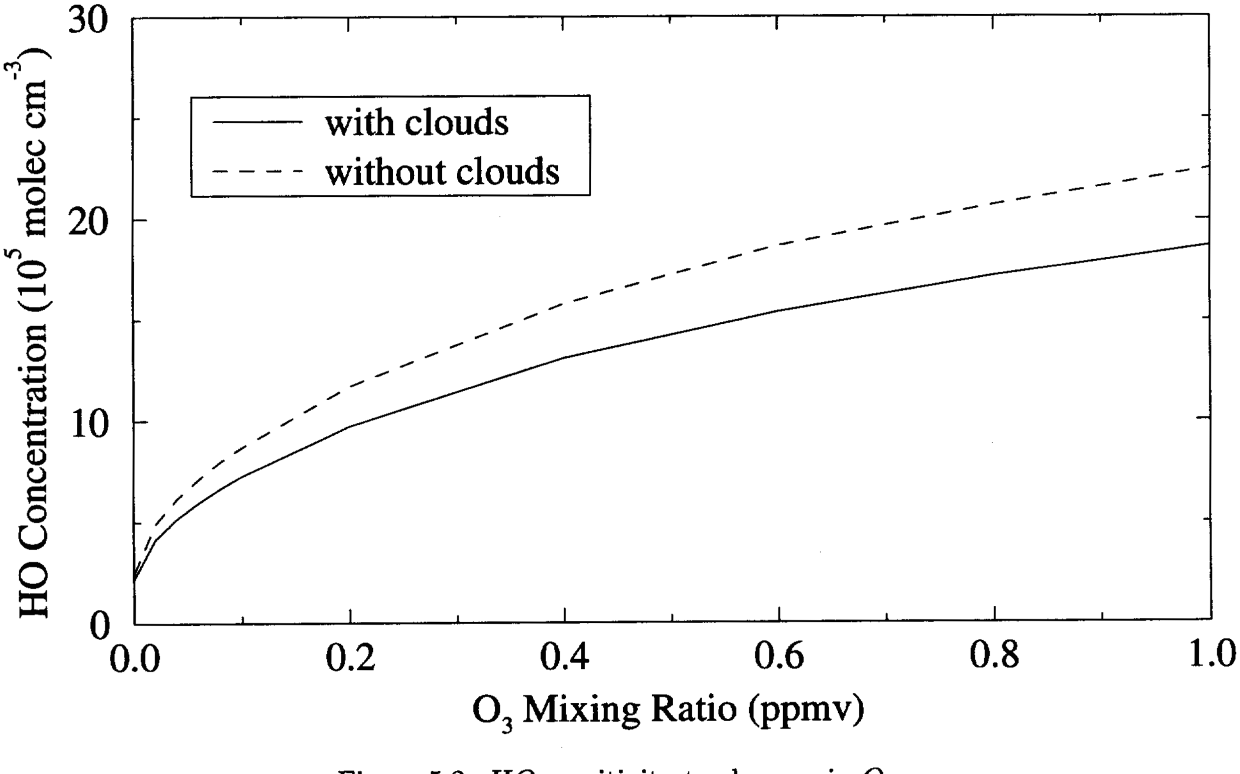

Figure 5.2: HO sensitivity to changes in O_3

5.4 H_2O

Water vapor takes part in the production of HO directly.

$$H_2O + O(^1D) \rightarrow 2\ HO \tag{5.6}$$

As a result, HO should be more sensitive to changes in H_2O than either O_3 or NO_x. This can be seen in Figure 5.4. Luckily, water vapor concentrations are known much more accurately than either of these gases. Table 5.4 shows the H_2O sensitivity in more detail for land areas. I assume an error of ±10% for this data which yields an error of 0.3 (0.2) and 0.2 (0.3) 10^5molec·cm^{-3} for HO in oceanic (land) areas.

Table 5.4: GCRC-ACM sensitivity to H_2O. In this test the mixing ratio of H_2O was set to a relative value based upon the H_2O values used in the model by default.

NO_x	Oceanic HO	Land HO
10	2.3	2.5
50	3.8	4.3
60		4.7
70		5.0
80		5.3
90	4.8	5.6
100	5.0	5.9
110	5.3	6.1
120		6.4
130		6.6
140		6.8
150	6.0	7.0
200	6.9	8.1

5.5 CO

Directly, CO removes about two-thirds of all of the HO in the atmosphere. As a result, decreases in CO will cause the concentration of HO to go up. This can be seen in Table 5.5. Generally the concentrations of CO are known fairly well for the world. I assume that the CO field is in error by upwards of 10% which yields an upper error of

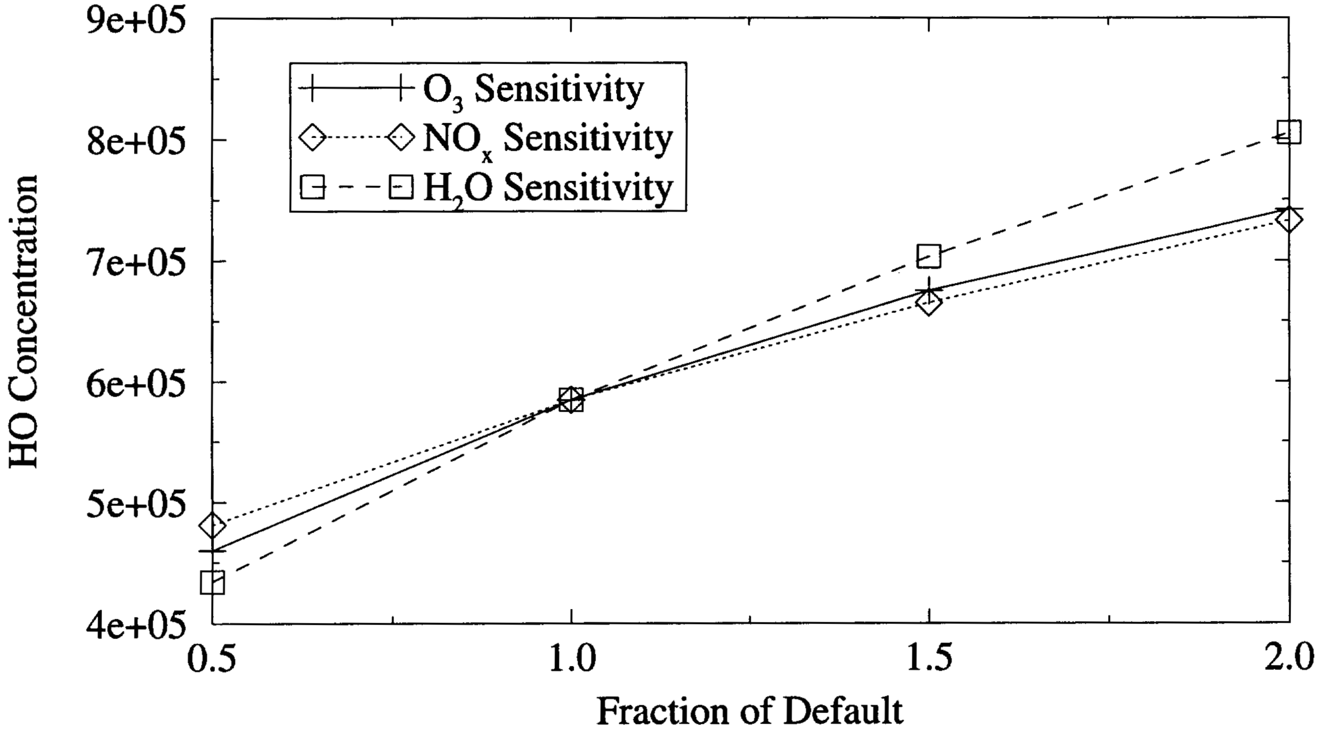

Figure 5.3: HO sensitivity to relative changes in O_3, NO_x, and H_2O

roughly 0.1 and lower error of 0.2 10^5·molec·cm^{-3}.

Table 5.5: GCRC-ACM sensitivity to CO. In this test the mixing ratio of CO was set to a relative value based upon the CO values used in the model by default.

CO	Oceanic HO	Land HO
10	8.2	8.2
50	6.0	6.8
80	5.4	
90	5.2	6.0
100	5.0	5.9
110	5.0	5.7
120	4.9	
150	4.6	5.2
200	4.1	4.7

5.6 Clouds

It is much more difficult to quantify the error associated with clouds because of the large number of variable and cloud types. In order to approach this problem correctly it would be necessary to do a Monte Carlo simulation (this would be the proper way to access errors in the model overall). Unfortunately, the computing resources for this endeavor are not currently available. As a result, I present a single test which I believe can be considered a lower bound on the effect of clouds on the global HO field.

The optical depths of high, middle and low clouds have been changed to be 0.5, 1, and 3. The results are shown in Table 5.6.

5.7 Rate Constants

In this section a simple approach is used to determine the error which the reaction rate constants added to the model. I take the five most important equations for determining HO concentrations and determine the error based upon them. The equations are given

Table 5.6: GCRC-ACM sensitivity to clouds. In this test the optical depths of high, middle, and low clouds have been changed from 1, 30, 10 (the default case) to 0.5, 1, and 3.

Season	Low Clouds	Default Clouds	No Clouds
Spring	5.16	5.30	6.01
Summer	7.30	7.44	8.57
Fall	5.41	5.53	6.31
Winter	3.23	3.39	3.67
Year	5.28	5.39	6.14

below.

$$O(^1D) + H_2O \rightarrow HO + HO \tag{5.7}$$

$$O_3 + HO_2 \rightarrow HO + 2\,O_2 \tag{5.8}$$

$$NO + HO_2 \rightarrow HO + NO_2 \tag{5.9}$$

$$CH_4 + HO \rightarrow H_2O + CH_3 \tag{5.10}$$

$$CO + HO \rightarrow CO_2 + H \tag{5.11}$$

$$\tag{5.12}$$

Assuming steady state, HO may be written rather simply.

$$[HO] = \frac{2K_1[O(^1D)][H_2O] + K_2[O_3][HO_2] + K_3[NO][HO_2]}{K_4[CH_4] + K_5[CO]} \tag{5.13}$$

Assuming that this function has normally distributed errors, the total error on HO due to rate constants can be written as follows.

$$\sigma_{HO}^2 = \sigma_{K1}^2 \cdot \frac{\partial HO}{\partial K1} + \sigma_{K2}^2 \cdot \frac{\partial HO}{\partial K2} + \sigma_{K3}^2 \cdot \frac{\partial HO}{\partial K3} + \sigma_{K4}^2 \cdot \frac{\partial HO}{\partial K4} + \sigma_{K5}^2 \cdot \frac{\partial HO}{\partial K5} \tag{5.14}$$

Assuming the reaction errors in DeMore et al. [1992] and the concentrations and other data in Table 5.7, the total error is determined to be 25% in the negative direction and 45% in the positive direction. The majority of the error comes from the CH_4 and CO reactions. This can be seen in figure 5.7. The cause is that generally the longer the gas's atmospheric lifetime, the harder it is to determine its reaction rate; CH_4 and CO are the longest lived gases in this group.

Table 5.7: Input data used to determine the ACM sensitivity to the reaction rate constant uncertainties. Temperature is given in Kelvin and all concentrations in molecules·cm^{-3}

Parameter	Value
Temperature	259
Pressure	$1.45 \cdot 10^{19}$
$O(^1D)$	$2.0 \cdot 10^{-3}$
H_2O	$2.9 \cdot 10^{17}$
O_3	$8.0 \cdot 10^{11}$
HO_2	$1.0 \cdot 10^{7}$
NO	$2.9 \cdot 10^{8}$
CH_4	$2.5 \cdot 10^{13}$
CO	$1.5 \cdot 10^{12}$

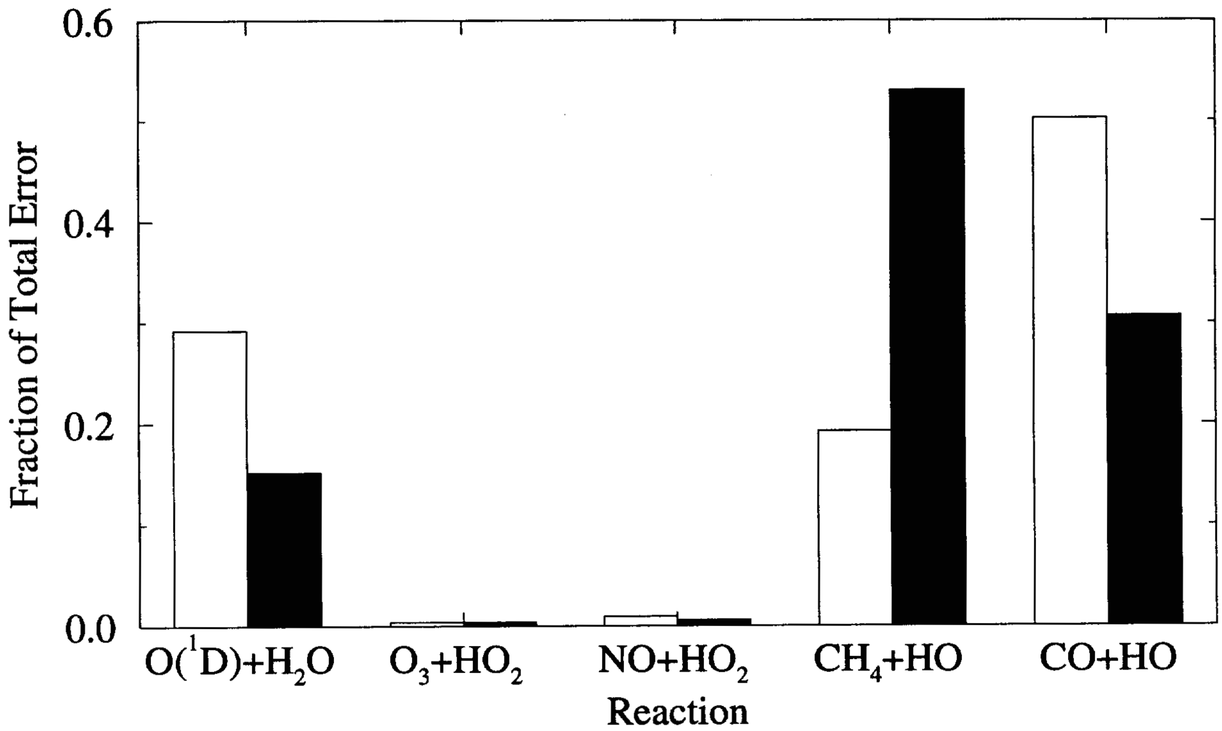

Figure 5.4: Model derived HO sensitivity to the reaction rate constants in the five most important reactions.

5.8 Total Error

In order to correctly ascertain the total error in model derived global HO concentration, a Monte Carlo simulation would again need to be run. The errors due to the specific processes discussed in the sections above are shown in Table 5.8. The overall error is done as discussed in the previous section with the added errors due to concentration uncertainties. The only difficulty is this situation is to determine the error in the $O(^1D)$ concentration. This was done in the usual way assuming that $O(^1D)$ is given by the following equation.

$$[O(^1D)] = \frac{J[O_3]}{K_6[O_2] + K_7[N_2]} \tag{5.15}$$

Further, I assume that the errors are due only to the O_3 mixing ratio and the photodissociation rate constant, J, for which I assign a value and error of $5{\cdot}10^{-6}$ and $4{\cdot}10^{-6}$. I have also assumed that the NO error is twice the NO_x error to take into account the effect of NO_2 on HO_2 concentrations. The error calculated in this manner is roughly 45%.

The most important sources of error are summarized in Table 5.8. A surprising feature is that the reaction rate constant uncertainty is quite important to the overall uncertainty in the derived HO concentration. It is important to note, however, that these results are *highly* simplified. A much more rigorous investigation of these issues is warranted.

Table 5.8: GCRC-ACM sensitivity to the most important input parameters.

Source	HO Error	
	lower	upper
CH_4 rate	4%	20%
CO rate	9%	11%
NO_x	9%	4%
$O(^1D)$	8%	6%
$O(^1D)$ rate	5%	6%
H_2O	2%	2%
CO	2%	1%
total	39%	51%

Chapter 6

Cloud Effects on Trace Gases

6.1 Introduction

Clouds can radically alter the distribution of HO in the atmosphere [Grant et al., 1992; Lu, 1993; Moraes and Khalil, 1993]. But clouds are quite variable in how they affect the distribution. Optically thick clouds, like cumulus, cause the actinic flux below then to be greatly reduced and so HO production is diminished. Optically thin clouds, like cirrus, generally increase the radiation below the cloud layer because they act as a diffuser. Above a cloud layer, the actinic flux is always greater than it would be otherwise due to the high reflectivity of clouds compared to the earth's surface.

The effect of clouds on the destruction of trace gases is not linearly related to their effect on HO concentrations. This is due to the dependence of the reaction rate constants on temperature and pressure, and to the fact that most trace gases are far more abundant in the lower atmosphere. The general equation governing the removal of such gases is given below.

$$D = \int_0^{z_t} K(T) C_{HO}(z) C_i(z) dz \tag{6.1}$$

Here, D is the total destruction of a given gas of concentration C_i due to HO removal, C_{HO} is the HO concentration, and z_t is the top of the atmosphere. As an example of the use of this formula, consider atmospheric CH_4. CH_4 is removed primarily in the troposphere, so in this case z_t is the tropopause height. The HO concentration is taken to be constant in the troposphere at 10^6 molec·cm^{-3} and the CH_4 *mixing ratio* is taken to be constant at 1700 ppbv.

$$D = \int_0^{12} (2.9 \cdot 10^{-12} e^{-1820/(288-6.5z)})\ (10^6)\ (1.7 \cdot 10^{-6})\ (2.55 \cdot 10^{19} e^{-z/8})\ dz \qquad (6.2)$$

In this equation, the temperature has been assumed linearly related to height (a good approximation for the troposphere). This can be expanded with a first order Taylor series.

$$\frac{1}{T} = \frac{1}{288 - 6.5z} \approx 288 + 6.5z \qquad (6.3)$$

The entire equation can thus be greatly simplified.

$$D = 1.3 \cdot 10^8 \int_0^{12} e^{-(6.3+0.27z)} dz \qquad (6.4)$$

When carried out, this equation yields $8.3 \cdot 10^5$ molec·cm^{-3} s^{-1} or 430 Tg·yr^{-}1.

Carrying this example further, suppose that a thin dense cloud is in the atmosphere at a height of 2 km. Following this, assume that there is no HO below the cloud and double HO for the two km above the cloud. Now the total destruction is slightly more complex.

$$D = 2.6 \cdot 10^8 \int_2^{4} e^{-(6.3+0.27z)} dz \ + \ 1.3 \cdot 10^8 \int_4^{12} e^{-(6.3+0.27z)} dz \qquad (6.5)$$

This yields a sink strength of $4.7 \cdot 10^5$ molec·cm^{-3} s^{-1} or 240 Tg·yr^{-1}, a reduction in sink strength of 44%. It should be noted what a large effect this simple redistribution of HO in the troposphere has on the total sink of methane. The total amount of HO in the troposphere has not changed. For higher clouds of this density the effect would be even greater. This simple calculation clearly shows that on a regional scale, clouds can have an enormous impact on the atmospheric oxidation capacity.

6.2 GCRC-ACM Determined Cloud Effects

Section 6.1 presented a simple illustrative example of the effect clouds have on the oxidation of trace gases. In this section, I present results using the GCRC-ACM. Because the real atmosphere is made up of clouds that increase and decrease HO, the results are much less obvious.

6.2.1 Cloud Model Accuracy

Before presenting results, it is important to establish the validity of the cloud model used in the ACM. Simple clouds models [Thompson, 1984; Madronich, 1987] accurately model radiative effects of clouds with albedos above 0.5. For clouds with smaller albedos, they greatly under-estimate the actinic flux below clouds because they assume that no direct radiation penetrates the cloud. The ACM cloud model takes the direct radiation transmission through clouds into effect and is thus much more accurate compared to these models.

The delta-Eddington method [Joseph et al., 1976] is traditionally used in atmospheric chemistry models that include micro-scale cloud effects. This model is quite accurate and is thus compared to the ACM cloud model. Figure 6.1 shows the excellent agreement between the two models even for low reflectivity clouds. Results are shown for ground albedos of 0.0 and 0.3. The results are even better for higher ground albedos. It is important to point out that where there are differences, the ACM cloud model predicts *more* actinic flux than the delta-Eddington model. This means the effect of clouds on trace gases, at least in this one way, will tend to be minimized.

6.2.2 HO Results

The ACM has been used to study the effects of clouds on the distribution of HO throughout the atmosphere. For the purposes of this study, the Oak Ridge cloud database was used, assuming random cloud overlapping for the high, middle, and low clouds [Warren et al., 1986a; Warren et al., 1986b]. The database provides information on the fraction of the sky that contains each type of cloud. The equations for determining the fraction of sky that contains various combinations of cloud cover are presented in Table 6.1

The optical depths of the high, middle, and low clouds were taken to be 0.5, 5, and 10, and their heights were taken to be approximately 9.5 km, 4.5 km, and 2.5 km depending upon latitude [London, 1952; Stephens et al., 1978]. For each global simulation the model was run for clear sky conditions and every combination of high, middle, and low

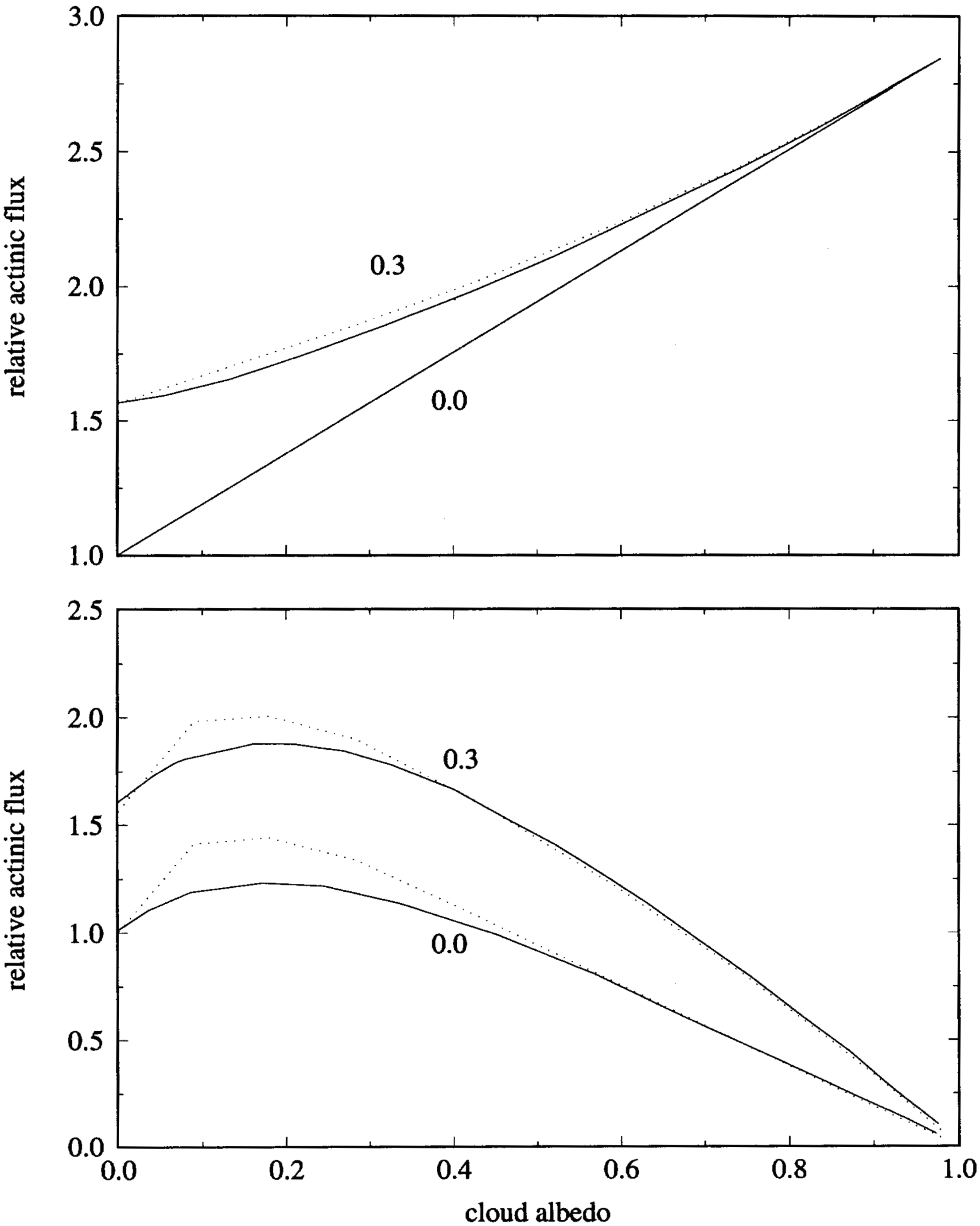

Figure 6.1: Comparison of above (top) and below (bottom) cloud actinic fluxes determined by delta-Eddington (solid line) and ACM (dotted line) models.

Table 6.1: Equations for determining the fraction of sky that contains various combinations of cloud cover given the total fractions of high (H), middle (M), and low (L) clouds.

Cloud Cover	Fraction
Clear	$(1-H)\cdot(1-M)\cdot(1-L)$
High Cloud Only	$H\cdot(1-M)\cdot(1-L)$
Middle Cloud Only	$(1-H)\cdot M\cdot(1-L)$
Low Cloud Only	$(1-H)\cdot(1-M)\cdot L$
High and Middle	$H\cdot M\cdot(1-L)$
High and Low	$H\cdot(1-M)\cdot L$
Middle and Low	$(1-H)\cdot M\cdot L$
High, Middle, and Low	$H\cdot M\cdot L$

cloudiness. A composite picture of the HO concentration for the globe was then made.

The distribution of HO in the atmosphere, including the effect of clouds, is shown in Figure 6.2 for the spring and Figure 6.3 for the winter. The distributions for the summer and fall are similar.

In general, the distribution of HO in the atmosphere is very similar to the three-dimensional model of Spivakovsky et al. [1990]. The distribution over land areas is qualitatively different than it is over oceanic areas, however. This is due to a number of factors. Ozone and NO_x concentrations are both higher over the land areas and the surface albedo of land is always higher than over oceans. When globally averaged, the predominance of the ocean is clear as see in the lower graph of Figure 6.4. This graph shows the raw concentrations in units of 10^5molec$\cdot$cm^{-3}. The top graph shows the difference in model simulations which assume a cloudless atmosphere as apposed to the current atmosphere's cloud distribution. The units are the same as in the bottom graph. Negative numbers indicate areas where the cloudless sky assumption over-estimates HO concentrations.

Because of the complexities of how clouds change the actinic flux in the atmosphere, clouds affect the HO concentrations in a much less stark manner than would be expected from the simple example given above. Clouds increase the HO concentration by at most 16% at any given location. They decrease HO but less, 16% at most. The effect on the global scale is, of course, much smaller because of the increase in HO in the upper atmosphere and decrease in the lower atmosphere. Globally, clouds increase tropospheric HO concentrations by roughly 4%. The effect on tropospheric trace gases is roughly the same size but in the opposite direction; the destruction of CH_4 and CO are reduced by roughly 3%. It is important to note, however, that the magnitude of the cloud effect is highly dependent upon the assumed albedo of oceanic areas. The numbers presented here are very conservative and could be substantially higher.

Another way to look at cloud effects is to consider a single cloud layer over varying optical depth and height. Figure 6.5 is the result of running the ACM at 15°N latitude for the spring with a ground albedo of 0 and 20%. This graph clearly shows that as cloud height increases, HO values decrease. As the optical depth increases, the effect is, in general, intensified. Figure 6.6 shows the same simulation as it relates to CH_4 removal. Note how the entire graph is shifted to lower cloud heights and optical depths.

6.2.3 Other Methods of HO Determination

Direct Measurements

The global or effective HO concentration will not be determined experimentally in the foreseeable future. This is due to two issues: measurement problems and the difficulty of averaging highly variable systems. In recent years, the measurement of HO in the troposphere has greatly improved [Mount, 1992; Platt and Hausmann, 1994], but the number of measurements has been very low. But even when measurements of HO are as ubiquitous as, say, CH_4 measurements are now, the global concentration of HO will still be known only very roughly. This is due to the fact that HO is an extremely reactive chemical in the atmosphere with a lifetime of roughly one second. Generally, however, comparisons between local experimental determinations of HO and model results have shown good agreement [Davis, Jr. et al., 1987].

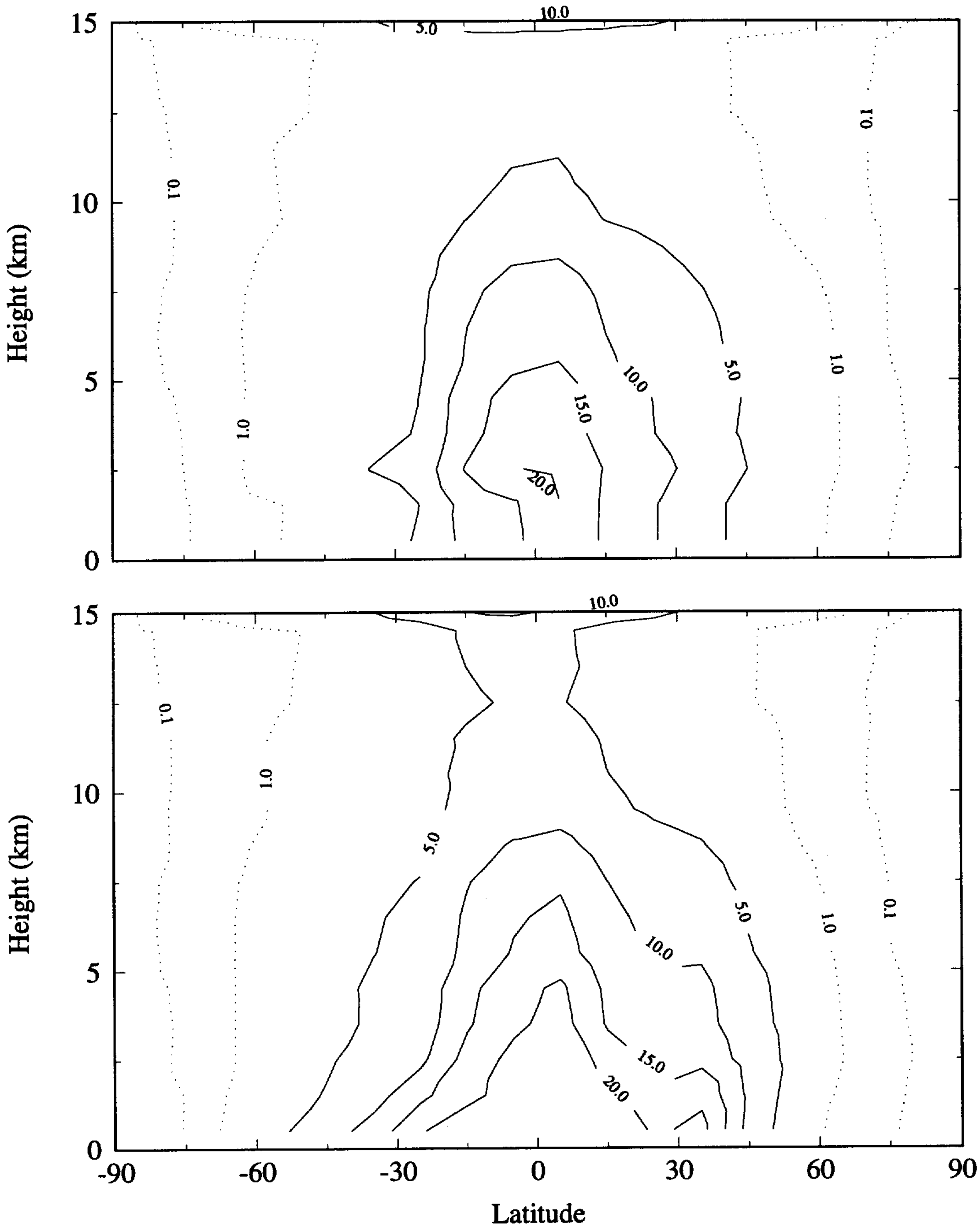

Figure 6.2: Tropospheric HO concentrations for land (bottom) and oceanic (top) areas for the spring. The lines are given in units of molec·cm^{-3}.

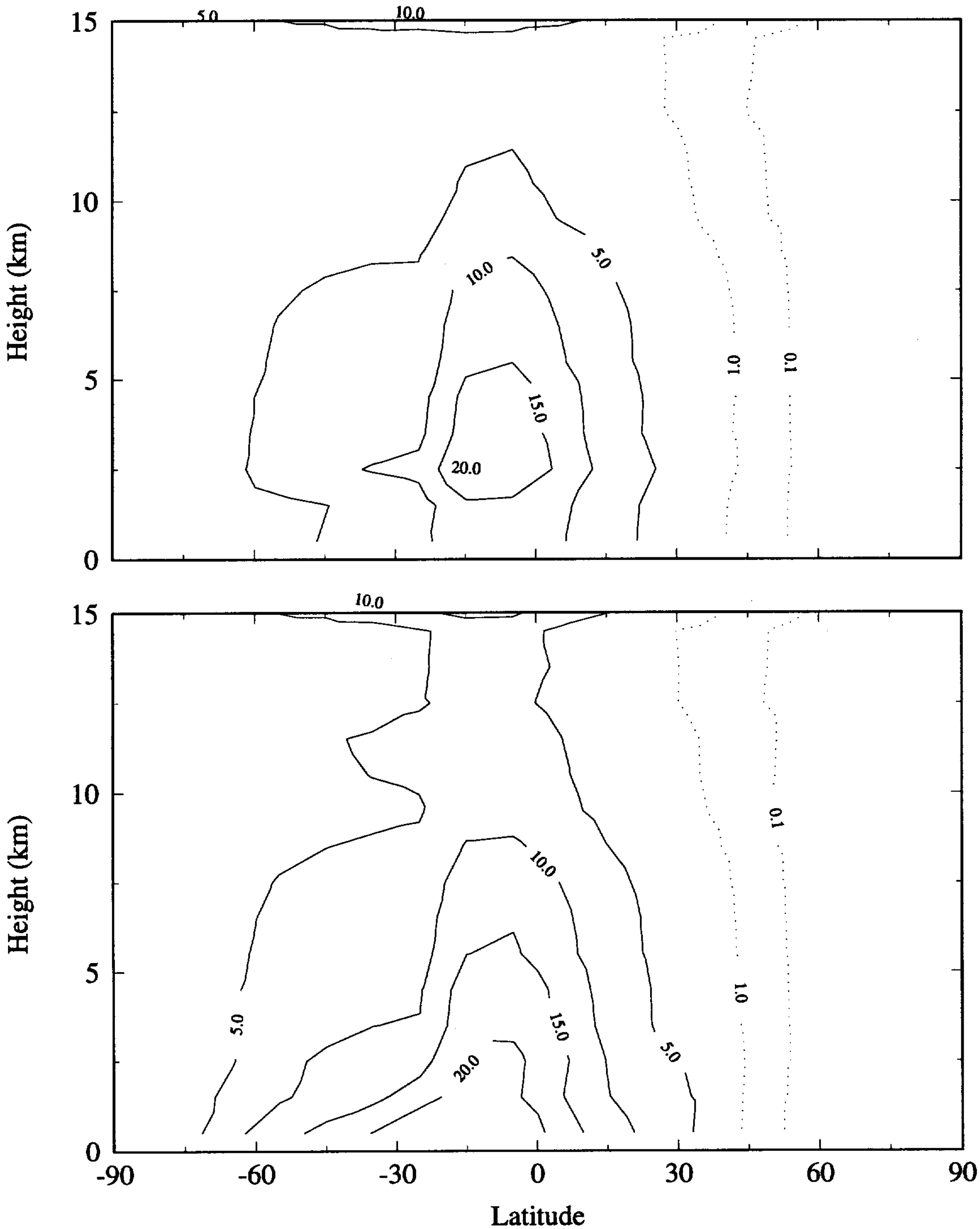

Figure 6.3: Tropospheric HO concentrations for land (bottom) and oceanic (top) areas for the winter. The lines are given in units of molec·cm^{-3}.

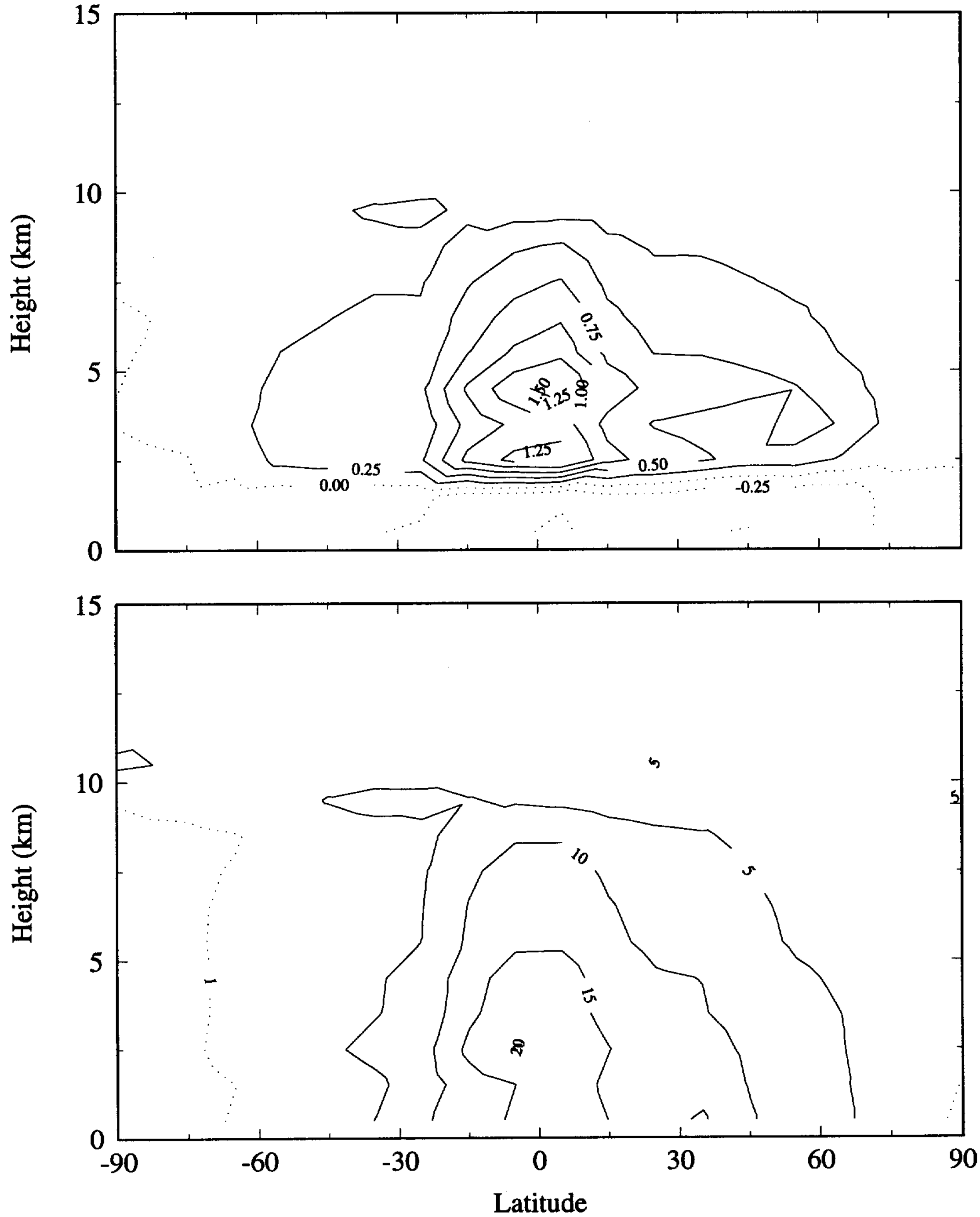

Figure 6.4: Globally and seasonally averaged tropospheric HO concentrations.

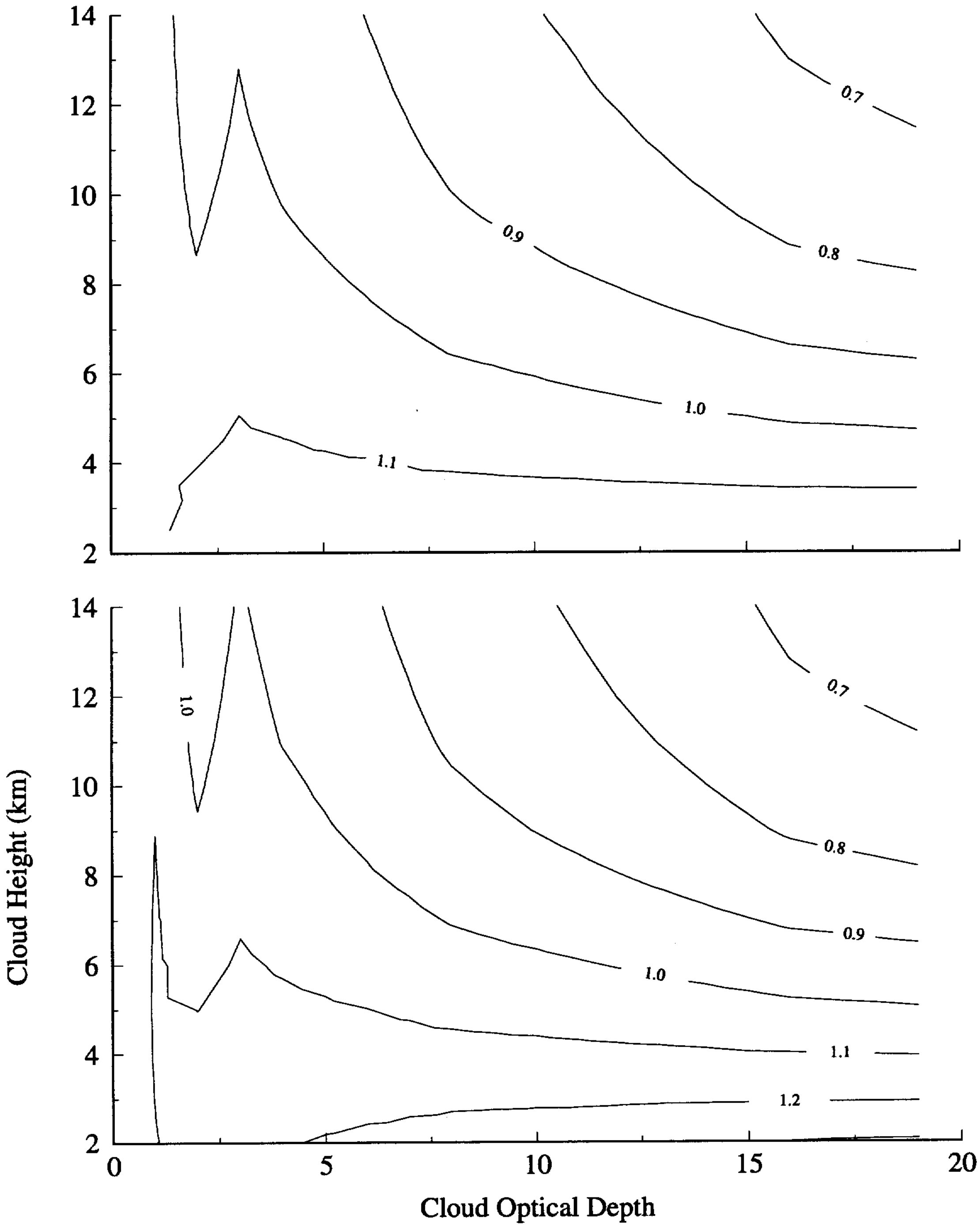

Figure 6.5: Total tropospheric HO at 15°N latitude for the spring with a ground albedo of 0 (top) and 20% (bottom). The units are in fraction of the clear sky value.

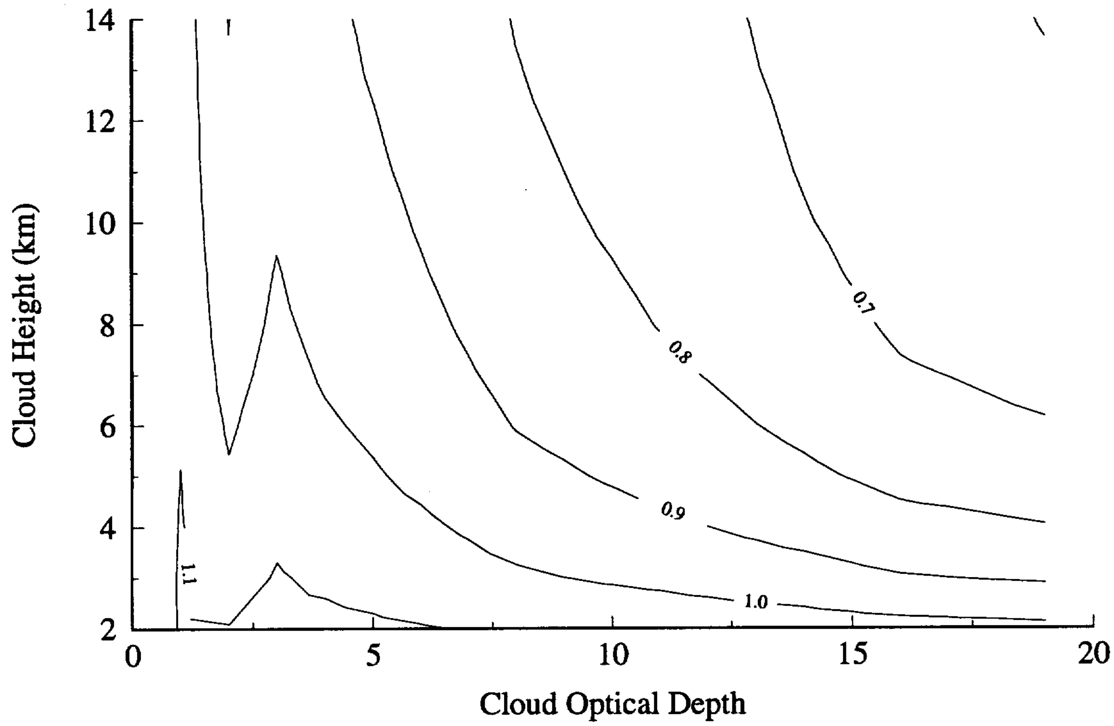

Figure 6.6: Total tropospheric CH_4 removal at 15°N latitude for the spring with a ground albedo of 0. The units are in fraction of the clear sky removal.

CH_3CCl_3 Derived Global HO Concentration

Without the use of experimental methods to derive a global estimate of HO, scientists have turned to other, less direct, means. The most prominent and accepted method is the use methyl chloroform (CH_3CCl_3) as a tracer [Lovelock, 1977; Singh, 1977].

A gas that is destroyed exclusively by HO may be used to determine the effective atmospheric concentration of HO.

$$\overline{C_{HO}} = \frac{1}{K_{eff} \cdot \tau} \tag{6.6}$$

$\overline{C_{HO}}$ is the globally averaged HO concentration, K_{eff} is the effective reaction rate constant of the gas with HO, and τ is the lifetime of the gas.

Overall, the calculated HO concentration is probably accurate but there are four sources of error in Equation 6.6. The first three are simply K_{eff}, τ, and the absolute calibration of CH_3CCl_3. The forth is not as obvious because it is implicit in the formulation of the problem. No real gas is destroyed entirely by reaction with HO. CH_3CCl_3 is believed to be removed primarily by reaction with HO but not exclusively, so this adds a further layer of complexity to the calculation.

Since 1984, the calculated atmospheric lifetime of methyl chloroform has stayed quite constant [Khalil and Rasmussen, 1984; Prinn et al., 1987; Prinn et al., 1992] despite large changes in the the value of K_{eff} and much more observational data on CH_3CCl_3 itself. Because it is dependent primarily on direct observations, the lifetime is perhaps the best known aspect of Equation 6.6. Two sources of error exist. The first is the absolute calibration of the CH_3CCl_3 concentration and the second is the source estimate. Quite recently, the absolute calibration of CH_3CCl_3 has been revised (I will try to get a reference for this before the printing of this thesis). This most recent revision will cause the predicted global HO value to increase.

It is possible that the stated emissions are higher than thought, which would tend to decrease the lifetime of CH_3CCl_3 while increasing the derived concentration of HO. CH_3CCl_3 is produced entirely by industrial processes, but exact figures of production from the former USSR, Japan, and China are unknown and have been difficult to estimate accurately [Prinn et al., 1983; Khalil and Rasmussen, 1984].

The sinks of CH_3CCl_3 are less certain than the sources. Early investigations assumed undetermined ("other") sources. Later, sinks were taken into account explicitly but only two were considered important: reaction with HO and stratospheric removal. These processes are thought to have lifetimes of roughly 6 and 60 years. Recent experimental data have shown that the ocean is a bigger sink than previously thought, with a lifetime of roughly 60-130 years [Butler et al., 1991]. Khalil and Rasmussen [1989] have suggested that soils could be as big a sink as oceans. Increased sink strength apart from HO will tend to decrease the derived HO concentration.

The reaction rate constant for Equation 6.6 has changed substantially over the last 15 years [DeMore et al., 1983; DeMore et al., 1990; DeMore et al., 1992] including a recent radical change [Talukdar et al., 1992]. The change in the NASA recommendations for the tropospheric reaction rate constant are shown in Figure 6.7.

Current estimates of global HO concentrations are shown in Table 6.2. The GCRC-ACM calculates the a global HO concentration which is within the uncertainties of all of the other derived concentrations.

Table 6.2: Comparison of the average global HO concentrations between the GCRC-ACM and other investigators. Units are given in 10^5 molec·cm^{-3}.

Investigator	HO Concentration
Khalil and Rasmussen [1984]	8±6
Spivakovsky et al. [1990]	8
Butler et al. [1991]	7.7
Pinto and Khalil [1991]	6
Prinn et al. [1992]	8.1±0.9
Thompson [1992]	6
This work with clouds	6.7±2.4/3.4
This work without clouds	6.5±2.5/3.3

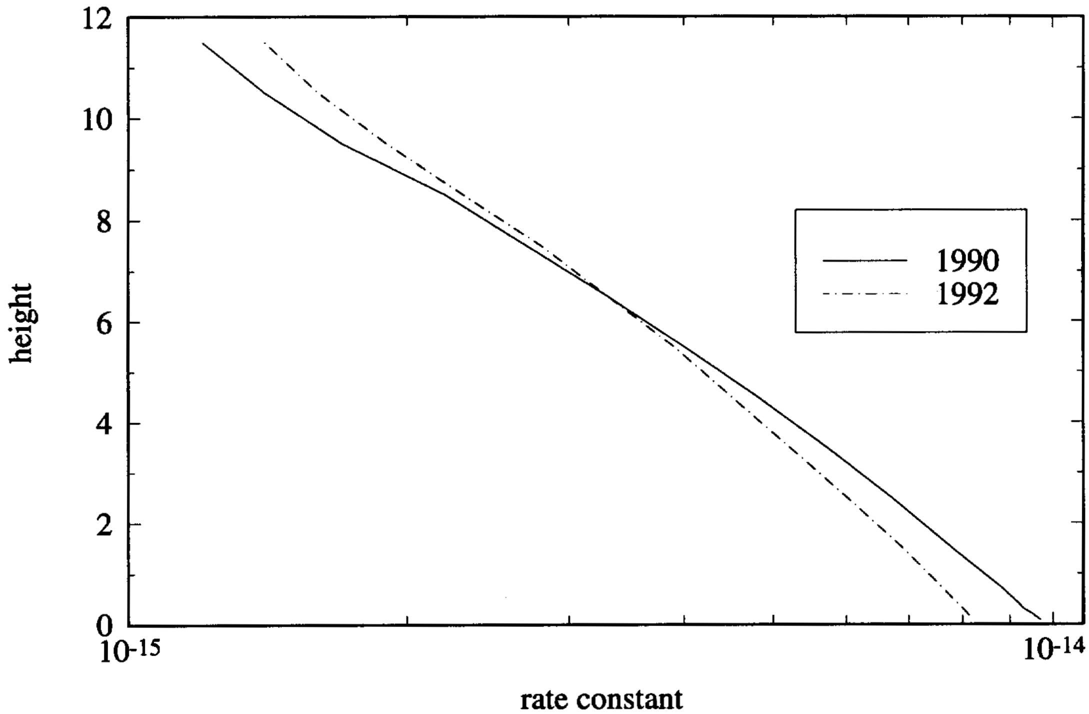

Figure 6.7: Changes to the reaction rate constant of CH_3CCl_3 with HO between 1990 and 1992.

Chapter 7

Atmospheric Chemistry of the Past

7.1 Introduction

In this chapter the GCRC-ACM will be used to calculate the HO concentration for the pre-industrial period and ice ages. In a sense, this is equivalent to a model sensitivity analysis because all of the important input parameters that are changed in each case. Such calculations have been done by a number of investigators and are summarized by Thompson [1992].

The data used for the pre-industrial and ice age periods is taken largely from Pinto and Khalil [1991] and are listed in Table 7.1. All of these values were used directly in the model with the exception of the O_3 and NO_y data. The standard O_3 data (developed in Chapter 4) was used in all cases and scaled to the Pinto values. The ACM, unlike many atmospheric chemistry models, holds NO_x constant and not NO_y. As a result, I chose NO_x values based upon the current understanding of the NO_x sources and sinks. Based upon this the global NO_x values should be roughly 33% and 25% of the present during the pre-industrial period and ice age. In addition, the water vapor was taken to be 70maximum in keeping with the Clausius-Clapeyron equation.

The results are listed in Table 7.2. Based upon the model sensitivity analysis certain aspects of changing HO concentrations are known. The lower CH_4 and CO concentrations should cause HO values to increase. But the lower O_3 and NO_x values should cause the HO values to decrease. In the case of the pre-industrial period, however, the O_3 change is the most dramatic feature and it dominates the effect causing the decrease

Table 7.1: Input parameters to the Pinto model. All values are given in ppbv.

Inputs	Modern	Pre-industrial	Ice age
CH_4	1650	750	350
NO_y	0.1	0.05	0.05
CO	110	57	28
H_2	500	230	150
O_3	22	14	12

in this period. It is interesting to note that the southern hemisphere change is much larger than the northern hemisphere change. In the southern hemisphere, CO values are not much great than they are believed to have been in the pre-industrial period. As a result, the HO concentration decreases because important sources are shut off but the most important sink is only decreased slightly. This result is consistent with the two- and three-dimensional models from the Max Planck Institute [Valentin, 1990; Crutzen and Zimmermann, 1991]. This same effect is found during the ice age too.

During the last glacial maximum, there is little change in the HO sources from the pre-industrial period. But the sinks have been cut in half during the same period. As a result, the HO concentration should be closer to the modern times. This is, in fact, the case. When the change in temperature (and water vapor) are not taken into account the HO concentration is the same as for the modern atmosphere. When this important factor *is* taken into account the change is roughly equivalent to the pre-industrial period. One final change was made, however. In order to take the higher albedo of the Northern land areas into account I have changed the albedo for all areas above 40°N to 0.8. This change makes the final HO concentration roughly equivalent to the pre-industrial period in the southern hemisphere but makes it exactly the same in the northern hemisphere.

One interesting uncertainty in this calculation is the effect of clouds in the ice age. The reduced temperature indicates there will be less water vapor but also a lowing of the relative humidity threshold for cloud formation. In addition the availability of cloud condensation nuclei is uncertain. As a result of these uncertainties I have used the modern cloud distribution but this is clearly an area in need of further study.

Table 7.2: Calculated HO values for the modern, pre-industrial, and ice age periods.

Period	North	South	Pinto
Modern	7.2	6.5	6.0
Pre-industrial	6.0	4.8	6.4
Ice Age	7.2	5.0	7.3

Chapter 8

Summary

This work has presented a new 2.5-dimensional model of the atmospheric chemistry of the world. This model, the Global Change Research Center Atmospheric Chemistry Model is generic in that it can be used to address most issues involved in homogeneous oxidation in the troposphere. The model, including source code and input data are available freely to the scientific community.

Generally, atmospheric chemistry models predict HO concentrations between 6 and $9 \cdot 10^5$molec·cm^{-3}. The reason for this variability is not fundamental differences in the chemistry used in the models. These models are critically dependent upon input parameters as discussed in Chapter 5. Given uncertainties in the input parameters, the errors are potentially high, on the order of 45%. The GCRC-ACM derived HO value of roughly $7 \cdot 10^5$molec·cm^{-3}is well within these errors.

Because of the large amount of data required for atmospheric chemistry models it is generally impractical to publish all of the input parameters. This is particularly true for the two most important input parameters, NO_x and O_3. This work corrects this problem to some extent because it provides all of the inputs to the GCRC-ACM making comparisons between it and other models a much simpler process.

The ACM includes a new cloud model which is quite accurate and does not require the solution of the radiative transfer equations. With the use of this model I have looked at the effects of clouds on HO and trace gases removed by HO. It has been known for some time that the radiative effects of clouds do not have a major impact on total tropospheric HO. But trace gas removal is not a linear function of a single tropospheric average HO concentration. As a result, any model which is used to look at the removal of biospheric trace gases destroyed by HO must include the effects of clouds. More work needs to be done to quantify this effect.

Another interesting aspect of the effect of clouds on atmospheric chemistry is that clouds tend to reduce the sensitivity of HO to changes in the model input parameters. For example, without clouds HO changes by 240% due to changes in NO_x from low to high values. With clouds the HO change is less than 200%. This adds further credence to the supposition of Pinto and Khalil [1991] that HO values have stayed relatively constant over very different climatic conditions.

This thesis lays the groundwork for the use of the ACM for addressing problems in the field of atmospheric chemistry. It also provides a solid framework to build upon. In the near future this model will be combined with the stratospheric ozone model currently under development in the GCRC.

Bibliography

Angle, R. P. and Sandhu, H. S. [1986]. Rural ozone concentrations in Alberta, Canada, *Atmospheric Environment* **20**(6): 1221–1228.

Bakwin, P. S., Jacob, D. J., Wofsy, S. C., Munger, J. W., Daube, B. C., Bradshaw, J. D., Sandholm, S. T., Talbot, R. W., Singh, H. B., Gregory, G. L. and Blake, D. R. [1994]. Reactive nitrogen oxides and ozone above a taiga woodland, *Journal of Geophysical Research* **99**(D1): 1927–1936.

Bakwin, P. S., Wofsy, S. C., Fan, S.-M. and Fitzjarrald, D. R. [1992]. Measurements of NO_x and NO_y concentrations and fluxes over Arctic tundra, *Journal of Geophysical Research* **97**(D15): 16,545–16,557.

Barrie, L. A. and Bottenheim, J. W. [1991]. Sulphur and nitrogen pollution in the arctic atmosphere, *in* W. Sturges (ed.), *Pollution of the arctic atmosphere*, Elsevier Press.

Bloxam, R. M., Brewer, A. W. and McElroy, C. T. [1975]. NO_2 measurements by absorption spectrophotometer: observations from the ground and high-altitude balloon, Churchill, Manitoba, July 1974, *Fourth conference on CIAP*, U. S. Department of Transportation, pp. 454–457.

Bollinger, M. J., Hahn, C. J., Parrish, D. D., Murphy, P. C., Albritton, D. L. and Fehsenfeld, F. C. [1984]. no_x measurements in clean continental air and analysis of the contributing meteorology, *Journal of Geophysical Research* **89**(D6): 9623–9631.

Bottenheim, J. W., Barrie, L. A. and Atlas, E. [1993]. The partitioning of nitrogen oxides in the lower arctic troposphere during spring 1988, *Journal of Atmospheric Chemistry* **17**: 15–27.

Bottenheim, J. W., Barrie, L. A., Atlas, E., Heidt, L. E., Niki, H., Rasmussen, R. A. and Shepson, P. B. [1990]. Depletion of lower tropospheric ozone during arctic spring: The polar sunrise experiment 1988, *Journal of Geophysical Research* **95**(D11): 18,555–18,568.

Bottenheim, J. W., Gallant, A. G. and Brice, K. A. [1986]. Measurements of NO_y species and O_3 at 82° N latitude, *Journal of Geophysical Research* **13**(1): 113–116.

Breeding, R. J., Lodge Jr., J. P., Pate, J. B., Sheesley, D. C., Klonis, H. B., Fogle, B., Anderson, J. A., Englert, T. R., Haagenson, P. L., McBeth, R. B., Morris, A. L., Pogue, R. and Wartburg, A. F. [1973]. Background trace gas concentrations in the Central United States, *Journal of Geophysical Research* **78**: 7057–7064.

Butler, J. H., Elkins, J. W., Thompson, T. M., Hall, B. D., Swanson, T. H. and Koropalov, V. [1991]. Oceanic consumption of CH_3CCl_3: implications for tropospheric OH, *Journal of Geophysical Research* **96**(D12): 22347–22355.

Carroll, M. A., Hastie, D. R., Ridley, B. A., Rodgers, M. O., Torres, A. L., Davis, D. D., Bradshaw, J. D., Sandholm, S. T., Schiff, H. I., Karecki, D. R., Harris, G. W., MacKay, G. I., Gregory, G. L., Condon, E. P., Trainer, M., Hubler, G., Montzka, D. D., Madronich, S., Albritton, D. L., Singh, H. B., Beck, S. M., Shipham, M. C. and Bachmeier, A. S. [1990]. Aircraft measurements of NO_x over the eastern Pacific and continental United States and implications for ozone production, *Journal of Geophysical Research* **95**(D7): 10,205–10,233.

Carroll, M. A., McFarland, M., Ridley, B. A. and Albritton, D. L. [1985]. Ground-based nitric oxide measurements at Wallops Island, Virginia, *Journal of Geophysical Research* **90**(D7): 12,853–12,860.

Carroll, M. A., Ridley, B. A., Montzka, D. D., Hubler, G., Walega, J. G., Norton, R. B., Huebert, B. J. and Grahek, F. E. [1992]. Measurements of nitric oxide and nitrogen dioxide during the Mauna Loa Observatory Photochemistry Experiment, *Journal of Geophysical Research* **97**(D10): 10,361–10,374.

Chatfield, R. and Harrison, H. [1977]. Tropospheric ozone 2. variations along a meridional band, *Journal of Geophysical Research* **82**(37): 5969–5976.

Cox, R. A. [1977]. Some measurements of ground level NO, NO_2 and O_3 concentrations at an unpolluted maritime site, *Tellus* **29**(4): 356–362.

Crutzen, P. J. [1988]. Tropospheric ozone: an overview, *in* I. S. A. Isaksen (ed.), *Tropospheric Ozone: Regional and Global Scale Interactions*, D. Reidel, Boston, pp. 3–11.

Crutzen, P. J. and Zimmermann, P. H. [1991]. *Tellus* **43B**: 136.

Davis, D. D., Chen, G., Chameides, W., Bradshaw, J., Sandholm, S., Rodgers, M., Schendal, J., Madronich, S., Sachse, G., Gregory, G., Anderson, B., Barrick, J., Shipham, M., Collins, J., Wade, L. and Blake, D. [1993]. A photostationary state analysis of the NO_2-NO system based on airborne observations from the subtropical/tropical north and south Atlantic, *Journal of Geophysical Research* **98**(D12): 23,501–23,523.

Davis, Jr., L. I., James, J. V., Wang, C. C., Guo, C., Morris, P. T. and Fishman, J. [1987]. OH measurement near the intertropical convergence zone in the Pacific, *Journal of Geophysical Research* **92**(D2): 2020–2024.

DeMore, W. B., Molina, M. J., Watson, R. T., Golden, D. M., Hampson, R. F., Kurylo, M. J., Howard, C. J. and Ravishankara, A. R. [1983]. Chemical kinetics and photochemical data for use in stratospheric modeling: evaluation no. 6, *Technical Report 83-62*, Jet Propulsion Laboratory.

DeMore, W. B., Sander, S. P., Golden, D. M., Hampson, R. F., Kurylo, M. J., Howard, C. J., Ravishankara, A. R., Kolb, C. E. and Molina, J. J. [1992]. Chemical kinetics and photochemical data for use in stratospheric modeling, *Technical Report 92-20*, Jet Propulsion Laboratory.

DeMore, W. B., Sander, S. P., Golden, D. M., Molina, M. J., Hampson, R. F., Kurylo, M. J., Howard, C. J. and Ravishankara, A. R. [1990]. Chemical kinetics and photochemical data for use in stratospheric modeling: evaluation no. 9, *Technical Report 90-1*, Jet Propulsion Laboratory.

Dickerson, R. R. [1984]. Measurements of reactive nitrogen compounds in the free troposphere, *Atmospheric Environment* **18**(12): 2585–2593.

Dickerson, R. R. [1985]. Reactive nitrogen compounds in the Arctic, *Journal of Geophysical Research* **90**(D6): 10,739–10,743.

Dickerson, R. R., Stedman, D. H. and Delany, A. C. [1982]. Direct measurements of ozone and nitrogen dioxide photolysis rates in the troposphere, *Journal of Geophysical Research* **87**: 4933.

Dignon, J. [1992]. NO_x and SO_x emissions from fossil fuels: A global distribution, *Atmospheric Environment* **26A**(6): 1157–1163.

Dignon, J. and Penner, J. E. [1991]. Biomass burning: A source of nitrogen oxides in the atmosphere, *in* J. S. Levine (ed.), *Global Biomass Burning*, The MIT Press, Cambridge, Massachusetts, pp. 370–375.

Drummond, J. W. [1977]. *Atmospheric measurements of nitric oxide using a chemiluminescent detector*, PhD thesis, University of Wyoming, Laramie.

Drummond, J. W., Ehhalt, D. H. and Volz, A. [1988]. Measurements of nitric oxide between 0-12 km altitude and 67°n to 60°s latitude obtained during STRATOZ III, *Journal of Geophysical Research* **93**(D12): 15,831–15,849.

Drummond, J. W. and Volz, A. [1982]. Simultaneous measurements of NO and NO_2 in the troposphere, *2nd Symposium composition of the nonurban troposphere*, American Meteorological Society, pp. 17–20.

Ehhalt, D. H. and Drummond, J. W. [1982]. The tropospheric cycle of NO_x, *in* H. W. Georgii and W. Jaeschke (eds), *Chemistry of the Unpolluted and Polluted Troposphere*, Reidel, Dordrecht, Holland, pp. 219–251.

Ehhalt, D. H. and Drummond, J. W. [1988]. NO_x sources and the tropospheric distribution of NO_x during STRATOZ III, *in* I. S. A. Isaksen (ed.), *Tropospheric Ozone*, D. Reidel Publishing Company, pp. 217–237.

Ehhalt, D. H., Rohrer, F. and Wahner, A. [1992]. Sources and distribution of NO_x in the upper troposphere at northern mid-latitudes, *Journal of Geophysical Research* **97**(D4): 3725–3738.

Fabian, P., Borchers, R., Flentje, G., Matthews, W. A., Sciler, W., Giehl, H., Bunse, K., Muller, F., Schmidt, U., Volz, A., Khedim, A. and Johnen, F. J. [1981]. The vertical distribution of stable trace gases at mid-latitudes, *Journal of Geophysical Research* **86**(C6): 5179–5184.

Fahey, D. W., Hubler, G., Parrish, D. D., Williams, E. J., Borton, R. B., Ridley, B. A., Singh, H. B., Liu, S. C. and Fehsenfeld, F. C. [1986]. Reactive nitrogen species in the troposphere: measurements of NO, NO_2, HNO_3, particulate nitrate, peroxyacetyl nitrate (PAN), O_3, and total reactive odd nitrogen (NO_y) at Niwot Ridge, Colorado, *Journal of Geophysical Research* **91**(D9): 9781–9793.

Fehsenfeld, F. C., Dickerson, R. R., Hubler, G., Luke, W. T., Nunnermacker, L. J., Williams, E. J., Roberts, J. M., Calvert, J. G., Curran, C. M., Delany, A. C., Eubank, C., Fahey, D. W., Fried, A., Gandrud, B. W., Langford, A. O., Murphy, P. C., Norton, R. B., Pickering, K. E. and Ridley, B. A. [1987]. A ground-based intercomparison of NO, NO_x, and NO_y measurement techniques, *Journal of Geophysical Research* **92**(D12): 14,710–14,722.

Fishman, J. and Crutzen, P. J. [1978]. The origin of ozone in the troposphere, *Nature* **274**: 855–858.

Fishman, J., Gregory, G. L., Sachse, G. W., Beck, S. M. and Hill, G. F. [1987]. Vertical profiles of ozone, carbon monoxide, and dew-point temperature obtained during GTE/CITE 1, October-November 1983, *Journal of Geophysical Research* **92**(D2): 2083–2094.

Fishman, J., Solomon, S. and Crutzen, P. J. [1979]. Observational and theoretical evidence in support of a significant in-situ photochemical source of tropospheric ozone, *Tellus* **31**: 432–446.

Fishman, J., Watson, C. E., Larsen, J. C. and Logan, J. A. [1990]. Distribution of tropospheric ozone determined from satellite data, *Journal of Geophysical Research* **95**(D4): 3599–3617.

Galbally, I. E. and Roy, C. R. [1981]. Ozone and nitrogen oxides in the southern hemisphere troposphere, *in* J. London (ed.), *Proceedings Quadrennial International Ozone Symposium*, pp. 431–438.

Gerhardt, P., Poppe, D. and Marenco, A. [1989]. Ozone, CO and NO_x distribution in the troposphere during STRATOZ III, *in* R. D. Bojkov and P. Fabian (eds), *Ozone in the atmosphere*, A. DEEPAK Publishing, Hampton, Virginia, pp. 467–470.

Grant, K. E., Grossman, A. S. and Connell, P. S. [1992]. Effects of cloud-radiation interactions on tropospheric chemistry, *Technical report*, Lawrence Livermore National Laboratory.

Gregory, G. L., Hoell, Jr., J. M., Beck, S. M., McDougal, D. S., Meyers, J. A. and Bruton, Jr., D. B. [1985]. Operational overview of wallops island instrument intercomparison: carbon monoxide, nitric oxide, and hydroxyl instrumentation, *Journal of Geophysical Research* **90**(D7): 12,808–12,818.

Hameed, S., Pinto, J. P. and Stewart, R. W. [1979]. Sensitivity of the predicted co-oh-ch$_4$ perturbation to tropospheric no$_x$ concentrations, *Journal of Geophysical Research* **84**(C2): 763–768.

Hansen, J., Russell, G., Rind, D., Stone, P., Lacis, A., Lebedeff, S., Ruedy, R. and Travis, L. [1983]. Efficient three-dimensional global models for climate studies: models I and II, *Monthly Weather Review* **111**(4): 609–662.

Helas, G. and Warneck, P. [1981]. Background NO_x mixing ratios in air masses over the North Atlantic Ocean, *Journal of Geophysical Research* **86**(C8): 7283–7290.

Hindmarsh, A. C. [1972]. Linear multistep methods for ordinary differential equations: method formulations, stability, and the methods of nordsieck and gear, *Technical report*, Lawrence Livermore National Laboratory.

Hindmarsh, A. C. [n.d.]. Availability of gear system in c, personal communication.

Isaksen, I. S. A. and Hov, O. [1987]. Calculation of trends in the tropospheric concentration of O_3, OH, CO, CH_4 and NO_x, *Tellus* **39B**: 271–285.

Jaffe, D. A., Honrath, R. E., Herring, J. A., Li, S.-M. and Kahl, J. D. [1991]. Measurements of nitrogen oxides at Barrow, Alaska during spring: evidence for regional and northern hemispheric sources of pollution, *Journal of Geophysical Research* **96**(D4): 7395–7405.

Johnston, P. V. and McKenzie, R. L. [1984]. Long-path absorption measurements of tropospheric NO_2 in rural New Zealand, *Geophysical Research Letters* **11**(1): 69–72.

Joseph, J. H., Wiscombe, W. J. and Weinman, J. A. [1976]. The delta-Eddington approximation for radiative flux transfer, *Journal of Atmospheric Science* **33**: 2452–2459.

Kaplan, W. A., Wofsy, S. C., Keller, M. and Da Costa, J. M. [1988]. Emission of NO and deposition of O_3 in a tropical forest system, *Journal of Geophysical Research* **93**(D2): 1389–1395.

Kelly, T. J., Stedman, D. H., Ritter, J. A. and Harvey, R. B. [1980]. Measurements of oxides of nitrogen and nitric acid in clean air, *Journal of Geophysical Research* **85**(C12): 7417–7425.

Kelly, T. J., Tanner, R. L., Newman, L., Galvin, P. J. and Kadlecek, J. A. [1984]. Trace gas and aerosol measurements at a remote site in the northeast U.S., *Atmospheric Environment* **18**(12): 2565–2576.

Kerr, J. B. and McElroy, C. T. [1976]. Measurement of stratospheric nitrogen dioxide from the AES stratospheric balloon program, *Atmosphere* **14**(3): 166–171.

Khalil, M. A. K. [1993]. Atmospheric trace gases: Sources, sinks, and role in global change, *A Global Warming Forum: Scientific, Economic, and Legal Overview*, CRC Press, chapter 17, pp. 357–389.

Khalil, M. A. K. and Rasmussen, R. A. [1984]. The atmospheric lifetime of methylchloroform, *Tellus* **36B**: 317–332.

Khalil, M. A. K. and Rasmussen, R. A. [1989]. The potential of soils as a sink of chlorofluorocarbons and other man-made chlorocarbons, *Geophysical Research Letters* **16**(7): 679–682.

Khalil, M. A. K. and Rasmussen, R. A. [1990a]. Atmospheric methane: recent global trends, *Environmental Science and Technology* **24**: 549–553.

Khalil, M. A. K. and Rasmussen, R. A. [1990b]. Atmospheric methane: recent global trends, *Environmental Science and Technology* **24**: 549–553.

Khalil, M. A. K. and Rasmussen, R. A. [1990c]. The global cycle of carbon monoxide: trends and mass balance, *Chemosphere* **20**(1-2): 227–242.

Khalil, M. A. K. and Rasmussen, R. A. [1994]. Global decrease in atmospheric carbon monoxide concentration, *Nature* **370**: 639–641.

Khalil, M. A. K., Shearer, M. J. and Rasmussen, R. A. [1993]. Methane sinks and distributions, *in* M. A. K. Khalil (ed.), *Atmospheric Methane: Sources, Sinks, and Role in Global Change*, Vol. I13, Springer-Verlag, Berlin, chapter 9, pp. 168–179.

Kley, D., Drummond, J. W., McFarland, M. and Liu, S. C. [1981]. Tropospheric profiles of no_x, *Journal of Geophysical Research* **86**(C4): 3153–3161.

Knapp, W. W., Bowersox, V. C., Chevone, B. I., Krupa, S. V., Lynch, J. A. and McFee, W. W. [1988]. Precipitation chemistry in the united states, 1: Summary of ion concentration variability 1979-1984, *Water Resources Institute Continuum*, Vol. 3, Center for Environmental Research, Cornell University.

Kondo, Y., Matthews, W. A., Iwata, A., Morita, Y. and Takagi, M. [1987]. Aircraft measurements of oxides of nitrogen along the eastern rim of the asian continent: Winter observations, *Journal of Atmospheric Chemistry* **5**(1): 37–58.

Law, K. S. and Pyle, J. A. [1993]. Modeling trace gas budgets in the troposphere, 1. ozone and odd nitrogen, *Journal of Geophysical Research* **98**(D10): 18377–18400.

Levy, H. [1971]. Normal atmosphere: large radical and formaldehyde concentrations predicted, *Science* **173**: 141–143.

Liu, S. C., McAfee, J. R. and Cicerone, R. J. [1984]. Radon 222 and tropospheric vertical transport, *Journal of Geophysical Research* **89**: 7291–7297.

Liu, S. C., McFarland, M., Kley, D., Zafiriou, O. and Huebert, B. [1983]. Tropospheric NO_x and O_3 budgets in the equatorial Pacific, *Journal of Geophysical Research* **88**(C2): 1360–1368.

Logan, J. A. [1983]. Nitrogen oxides in the troposphere: Global and regional budgets, *Journal of Geophysical Research* **88**(C15): 10,785–10807.

Logan, J. A. [1985]. Tropospheric ozone: seasonal behavior, trends, and anthropogenic influence, *Journal of Geophysical Research* **90**(D6): 10,463–10,482.

Logan, J. A. and Kirchhoff, V. W. J. H. [1986]. Seasonal variations of tropospheric ozone at Natal, Brazil, *Journal of Geophysical Research* **91**(D7): 7875–7881.

Logan, J. A., Prather, M. J., Wofsy, S. C. and McElroy, M. B. [1981]. Tropospheric chemistry: a global perspective, *Journal of Geophysical Research* **88**: 10785–10807.

London, J. [1952]. Study of radiational temperature changes, *Journal of Meteorology* **9**: 145–151.

Lovelock, J. E. [1977]. Methyl chloroform in the troposphere as an indicator of OH radical abundance, *Nature* **267**: 32–33.

Lu, Y. [1990]. *Modeling tropospheric OH chemistry*, Master's thesis, Oregon Graduate Institute.

Lu, Y. [1993]. *Model Calculations of Radiative Transfer and Tropospheric Chemistry*, PhD thesis, Oregon Graduate Institute.

Lu, Y. and Khalil, M. A. K. [1993]. Methane and carbon monoxide in OH chemistry: the effects of feedbacks and reservoirs generated by the reactive products, *Chemosphere* **26**: 641–656.

Luke, W. T. and Dickerson, R. R. [1987]. The flux of reactive nitrogen compounds from eastern North America to the western Atlantic Ocean, *Global Biogeochemical Cycles* **1**(4): 329–343.

Luther, F. M. and Gelinas, R. J. [1976]. Effect of molecular multiple scattering and surface albedo on atmospheric photodissociation rates, *Journal of Geophysical Research* **81**: 1125–1132.

Madronich, S. [1987]. Photodissociation in the atmosphere, 1. actinic flux and the effects of ground reflections and clouds, *Journal of Geophysical Research* **92**(D8): 9740–9752.

Manabe, S. and Wetherald, R. T. [1967]. Thermal equilibrium of the atmosphere with a given distribution of relative humidity, *Journal of Atmospheric Sciences* **24**(3): 241–259.

Marenco, A. and Said, F. [1989]. Meridional and vertical ozone distribution in the background troposphere (70°n-60°s; 0-12 km altitude) from scientific aircraft measurements during the STRATOZ III experiment (june 1984), *Atmospheric Environment* **23**(1): 201–214.

Marland, G., Rotty, R. M. and Treat, N. L. [1985]. CO_2 from fossil fuel burning: global distribution of emissions, *Tellus* **37B**: 243–258.

Matthews, E. [1983]. Global vegetation and land use: New high-resolution data bases for climate studies, *Journal of Climate and Applied Meteorology* **22**: 474–487.

McFarland, M., Kley, D., Drummond, J. W., Schmeltekopf, A. L. and Winkler, R. H. [1979]. Nitric oxide measurements in the equatorial pacific region, *Geophysical Research Letters* **6**(7): 605–608.

Mészáros, E. and Horváth, L. [1984]. Concentration and dry deposition of atmospheric sulfur and nitrogen compounds in Hungary, *Atmospheric Environment* **18**(9): 1725–1730.

Misanchuk, B. A., Hastie, D. R. and Schiff, H. I. [1987]. The distribution of nitrogen oxides off the east coast of North America, *Global Biogeochemical Cycles* **1**(4): 345–355.

Moraes, F. and Khalil, M. A. K. [1993]. The global effects of clouds on OH, *Eos* **74**(43): 179.

Mount, G. H. [1992]. The measurement of tropospheric OH by long path absorption, 1. instrumentation, *Journal of Geophysical Research* **97**(D2): 2427–2444.

Mulder, P. [1986]. Office note 84, *Technical report*, Data Support, National Center for Atmospheric Research.

National Center for Atmospheric Research [1983]. Ds750.1, *Technical report*, Data Support Section, Scientific Computing Division, NCAR.

National Oceanic and Atmospheric Administration [1976]. U. S. Standard Atmosphere, *Technical report*, NOAA, Washington, D.C.

Noxon, J. F. [1978]. Tropospheric NO_2, *Journal of Geophysical Research* **83**(C6): 3051–3057.

Noxon, J. F. [1980]. Correction, *Journal of Geophysical Research* **85**(C8): 4560–4561.

Noxon, J. F. [1981]. NO_x in the mid-Pacific troposphere, *Geophysical Research Letters* **8**(12): 1223–1226.

Noxon, J. F. [1983]. NO_3 and NO_2 in the mid-Pacific troposphere, *Journal of Geophysical Research* **88**(C15): 11,017–11,021.

Oltmans, S. J. [1981]. Surface ozone measurements in clean air, *Journal of Geophysical Research* **86**: 1174–1180.

Oltmans, S. J. and Komhyr, W. D. [1986]. Surface ozone distributions and variations from 1973-1984: measurements at the NOAA Geophysical Monitoring for Climatic Change baseline observatories, *Journal of Geophysical Research* **91**(D4): 5229–5236.

Oltmans, S. J., Komhyr, W. D., Franchois, P. R. and Matthews, W. A. [1989]. Tropospheric ozone: variations from surface and ECC ozonesonde observations, *in* R. D. Bojkov and P. Fabian (eds), *Ozone in the atmosphere*, A. DEEPAK Publishing, Hampton, Virginia, pp. 539–541.

Parrish, D. D., Buhr, M. P., Trainer, M., Norton, R. B., Shimshock, J. P., Fehsenfeld, F. C., Anlauf, K. G., Bottenheim, J. W., Tang, Y. Z., Wiebe, H. A., Roberts, J. M., Tanner, R. L., Newman, L., Bowersox, V. C., Olszyna, K. J., Bailey, E. M., Rodgers, M. O., Wang, T., Berresheim, H., Roychowdhury, U. K. and Demerjian, K. L. [1993]. The total reactive oxidized nitrogen levels and the partitioning between the individual species at six rural sites in eastern North America, *Journal of Geophysical Research* **98**(D2): 2927–2939.

Parrish, E. J. W. D. D. and Fehsenfeld, F. C. [1987]. Determination of nitrogen oxide emissions from soils: results from a grassland site in Colorado, United States, *Journal of Geophysical Research* **92**(D2): 2173–2179.

Penner, J. E., Atherton, C. S., Dignon, J., Ghan, S. J. and Walton, J. J. [1991]. Tropospheric nitrogen: A three-dimensional study of sources, distributions, and deposition, *Journal of Geophysical Research* **96**(D1): 959–990.

Pinto, J. and Khalil, M. A. K. [1991]. The stability of tropospheric OH during ice ages, inter-glacial epochs and modern times, *Tellus* **43B**: 347–352.

Platt, U. and Hausmann, M. [1994]. Spectroscopic measurement of the free radicals NO_3, BRO, IO, and OH in the troposphere, *Research on Chemical Intermediates* **20**(3-5): 557–578.

Platt, U. and Perner, D. [1980]. Direct measurements of atmospheric CH_2O, HNO_2, O_3, NO_2, and SO_2 by differential optical absorption in the near UV, *Journal of Geophysical Research* **85**(C12): 7453–7458.

Prather, M. J. [1994]. Lifetimes and eigenstates in atmospheric chemistry, *Geophysical Research Letters* **21**(9): 801–804.

Press, W. H., Flannery, B. P., Teukolsky, S. A. and Vetterling, W. T. [1988]. *Numerical Recipes in C*, Cambridge Press.

Prinn, R., Cunnold, D., Rasmussen, R., Simmonds, P., Alyea, F., Crawford, A., Fraser, P. and Rosen, R. [1987]. Atmospheric trends in methylchloroform and the global average for the hydroxyl radical, *Science* **238**: 945–950.

Prinn, R., Cunnold, D., Simmonds, P., Alyea, F., Boldi, R., Crawford, A., Fraser, P., Gutzler, D., Hartley, D., Rosen, R. and Rasmussen, R. [1992]. Global average concentration and trend for hydroxyl radicals deduced from ALE/GAGE trichloroethane (methyl chloroform) data for 1978-1990, *Journal of Geophysical Research* **97**(D2): 2445–2461.

Prinn, R. G., Rasmussen, R. A., Simmonds, P. G., Alyea, F. N., Cunnold, D. M., Lane, B. C., Cardelino, C. A. and Crawford, A. J. [1983]. The atmospheric lifetime experiment 5: results for CH_3CCl_3 based on three years of data, *Journal of Geophysical Research* **88**: 8415–8426.

Ridley, B. A. [1991]. Recent measurements of oxidized nitrogen compounds in the troposphere, *Atmospheric Environment* **25A**(9): 1905–1926.

Ridley, B. A., Carroll, M. A., Dunlap, D. D., Trainer, M., Sachse, G. W., Gregory, G. L. and Condon, E. P. [1989]. Measurements of NO_x over the eastern pacific ocean and southwestern united states during the spring 1984 NASA GTE aircraft program, *Journal of Geophysical Research*.

Ridley, B. A., Carroll, M. A. and Gregory, G. L. [1987]. Measurements of nitric oxide in the boundary layer and free troposphere over the Pacific Ocean, *Journal of Geophysical Research* **92**(D2): 2025–2047.

Ridley, B. A. and Howlett, L. C. [1974]. An instrument for nitric oxide measurements in the stratosphere, *Reviews of Scientific Instruments* **45**: 742–746.

Ritter, J. A., Stedman, D. H. and Kelly, T. J. [1979]. Ground-level measurements of nitric oxide, nitrogen dioxide and ozone in rural air, *in* D. Grosjean (ed.), *Nitrogenous air pollutants, chemical and biological implications*, Ann Arbor Science.

Robinson, E. and Robbins, R. C. [1970]. Gaseous nitrogen compound pollutants from urban and natural sources, *Journal of the air pollution control association* **20**(5): 303–306.

Rotty, R. M. [1987]. Estimates of seasonal variation in fossil fuel CO_2 emissions, *Tellus* **39B**: 184–202.

Roy, C. R., Galbally, I. E. and Ridley, B. A. [1980]. Stratospheric odd nitrogen, II, measurement of nitric oxide in the southern hemisphere, *Quarterly Journal of the Royal Meteorology Society* **106**: 887–894.

Sandholm, S. T., Bradshaw, J. D., Chen, G., Singh, H. B., Talbot, R. W., Gregory, G. L., Blake, D. R., Sachse, G. W., Browell, E. V., Barrick, J. D. W., Shipham, M. A., Bachmeier, A. S. and Owen, D. [1992]. Summertime tropospheric observations related to N_xO_y distribtuions and partitioning over Alaska: Arctic boundary layer expedition 3A, *Journal of Geophysical Research* **97**(D15): 16,481–16,509.

Sanhueza, E., Octavio, K. and Arrocha, A. [1985]. Surface ozone measurements in the Venezuelan tropical savannah, *Journal of Atmospheric Chemistry* **2**: 377–385.

Schiff, H. I., Pepper, D. and Ridley, B. A. [1979]. Tropospheric NO measurements up to 7 km, *Journal of Geophysical Research* **84**(C12): 7895–7897.

Schmidt, J., Khedim, A., Knapsa, D., Kulessa, G. and Johnen, F. J. [1984]. Stratospheric trace gas distributions observed in different seasons, *Advances in Space Research* **4**(4): 131–134.

Shaw Jr., R. W. and Paur, R. J. [1983]. Measurements of sulfur in gases and particles during sixteen months in the Ohio River Valley, *Atmospheric Environment* **17**(8): 1431–1438.

Simpson, D., Perrin, D. A., Varey, J. E. and Williams, M. L. [1990]. Dispersion modeling of nitrogen oxides in the United Kingdom, *Atmospheric Environment* **24A**(7): 1713–1733.

Singh, H. B. [1977]. Atmospheric halocarbons: evidence in favor of reduced hydroxyl radical concentrations in the troposphere, *Geophysical Research Letters* **4**: 101–104.

Smit, H. G. J., Kley, D., McKeen, S., Volz, A. and Gilge, S. [1989]. The latitudinal and vertical distribution of tropospheric ozone over the Atlantic Ocean in the southern and northern hemispheres, *in* R. D. Bojkov and P. Fabian (eds), *Ozone in the atmosphere*, A. DEEPAK Publishing, Hampton, Virginia, pp. 419–422.

Spencer, R. W. [1993]. Global oceanic precipitation from the MSU during 1979-91 and comparisons to other climatologies, *Journal of Climate* **6**(7): 1301–1326.

Spivakovsky, C. M., Yevich, R., Logan, J. A., Wofsy, S. C. and McElroy, M. B. [1990]. Tropospheric OH in a three-dimensional chemical tracer model: An assessment based on observations of CH_3CCl_3, *Journal of Geophysical Research* **95**(D11): 18,441–18,471.

Starr, W. L., Loewenstein, M. and Craig, R. A. [1979]. Measurement of NO and O_3 from u-2 aircraft: 1977 tropical convergence zone experiment, *Technical report*, NASA Tech. Memo, 78577.

Stedman, D. H. and McEwan, M. J. [1983]. Oxides of nitrogen at two sites in New Zealand, *Geophysical Research Letters* **10**(2): 168–171.

Stephens, G. L., Paltridge, G. W. and Platt, C. M. R. [1978]. Radiation profiles in extended water clouds. III: Observations, *Journal of Atmospheric Science* **35**: 2133–2141.

Talbot, R. W., Bradshaw, J. D., Sandholm, S. T., Singh, H. B., Sachse, G. W., Collins, J., Gregory, G. L., Anderson, B., Blake, D., Barrick, J., Browell, E. V., Klemm, K. I., Lefer, B. L., Klemm, O., Gorzelska, K., Olson, J., Herlth, D. and O'hara, D. [1994]. Summertime distribution and relations of reactive nitrogen species and no_y in the troposphere over canada, *Journal of Geophysical Research* **99**(D1): 1863–1885.

Talukdar, R. K., Mellouki, A., Schmoltner, A.-M., Watson, T., Montzka, S. and Ravishankara, A. R. [1992]. Kinetics of the OH reaction with methyl chloroform and its atmospheric implications, *Science* **257**: 227–230.

Taylor, F. W., Dudhia, A. and Rodgers, C. D. [1989]. Proposed reference models for nitrous oxide and methane in the middle atmosphere, *in* G. M. Keating (ed.), *Handbook for MAP, Vol. 31*, International Council of Scientific Unions, pp. 67–79.

Thompson, A. M. [1984]. The effect of clouds on photolysis rates and ozone formation in the unpolluted troposphere, *Journal of Geophysical Research* **89**(D1): 1341–1349.

Thompson, A. M. [1992]. The oxidizing capacity of the earth's atmosphere: Probably past and future changes, *Science* **256**: 1157–1165.

Torres, A. L. [1985]. Nitric oxide measurements at a nonurban eastern United States site: Wallops instrument results from July 1983 GTE/CITE mission, *Journal of Geophysical Research* **90**(D7): 12,875–12,880.

Turman, B. N. and Edgar, B. C. [1982]. Global lightning distributions at dawn and dusk, *Journal of Geophysical Research* **87**(C2): 1191–1206.

Valentin, K. M. [1990]. PhD thesis, Johannes-Gutenburg University.

Warneck, P. [1974]. On the role of OH and HO_2 radicals in the troposphere, *Tellus* **26**: 39–46.

Warneck, P. [1988]. *Chemistry of the Natural Atmosphere*, Vol. 41 of *International Geophysics Series*, Academic Press, Inc., San Diego.

Warren, S. G., Hahn, C. J., London, J., Chervin, R. M. and Jenne, R. L. [1986a]. Global distribution of total cloud cover and cloud type amounts over land, *Technical report*, NCAR.

Warren, S. G., Hahn, C. J., London, J., Chervin, R. M. and Jenne, R. L. [1986b]. Global distribution of total cloud cover and cloud type amounts over the ocean, *Technical report*, NCAR.

Winkler, P. [1989]. Meridional distribution of surface ozone over the atlantic (83°n-76°s), *in* R. D. Bojkov and P. Fabian (eds), *Ozone in the atmosphere*, A. DEEPAK Publishing, Hampton, Virginia, pp. 423–425.

Wuebbles, D. J. and Tamaresis, J. S. [1993]. The role of methane in the global environment, *in* M. A. K. Khalil (ed.), *Atmospheric Methane: Sources, Sinks, and Role in Global Change*, Vol. I13 of *NATO ASI Series*, Springer-Verlag, Berlin, chapter 20, pp. 469–513.

Appendix A

GCRC-ACM Source Code

A.1 Makefile

```
CC=cc
OPT=-O

OBJ = obj/acm.o \\
obj/acs.o \\
obj/j.o \\
obj/qy.o \\
obj/actinic.o \\
obj/terrxn.o \\
obj/getact.pent.o \\
obj/solvemat.o \\
obj/getline.o \\
obj/getdata.o \\
obj/getstdat.o \\
obj/getinit.o \\
obj/getcons.o \\
obj/output.o \\
obj/getk.o \\
obj/getj.o \\
obj/getacs.o

global: global.c
$(CC) $(OPT) -o global global.c

mkdist: mkdist.c
$(CC) $(OPT) -o mkdist mkdist.c

acm: $(OBJ)
$(CC) $(OPT) -o acm $(OBJ) -lm
obj/acm.o: acm.c acm.h
```

```
$(CC) $(OPT) -o obj/acm.o -c acm.c
obj/acs.o: acs.c acs.h
$(CC) $(OPT) -o obj/acs.o -c acs.c
obj/j.o: j.c acm.h actinic.h
$(CC) $(OPT) -o obj/j.o -c j.c
obj/qy.o: qy.c
$(CC) $(OPT) -o obj/qy.o -c qy.c
obj/actinic.o: actinic.c acm.h actinic.h
$(CC) $(OPT) -o obj/actinic.o -c actinic.c
obj/terrxn.o: terrxn.c
$(CC) $(OPT) -o obj/terrxn.o -c terrxn.c
obj/getact.o: getact.c acm.h actinic.h
$(CC) $(OPT) -o obj/getact.o -c getact.c
obj/solvemat.o: solvemat.c
$(CC) $(OPT) -o obj/solvemat.o -c solvemat.c
obj/getline.o: getline.c
$(CC) $(OPT) -o obj/getline.o -c getline.c
obj/getdata.o: getdata.c acm.h
$(CC) $(OPT) -o obj/getdata.o -c getdata.c
obj/getstdat.o: getstdat.c acm.h gases.h
$(CC) $(OPT) -o obj/getstdat.o -c getstdat.c
obj/getinit.o: getinit.c acm.h rxn.h gases.h solve.h
$(CC) $(OPT) -o obj/getinit.o -c getinit.c
obj/getcons.o: getcons.c acm.h rxn.h gases.h solve.h
$(CC) $(OPT) -o obj/getcons.o -c getcons.c
obj/output.o: output.c acm.h gases.h solve.h
$(CC) $(OPT) -o obj/output.o -c output.c
obj/getk.o: getk.c acm.h rxn.h kbinary.h kter.h
$(CC) $(OPT) -o obj/getk.o -c getk.c
obj/getj.o: getj.c acm.h rxn.h acs.h j.h
$(CC) $(OPT) -o obj/getj.o -c getj.c
obj/getacs.o: getacs.c acm.h acs.h j.h
$(CC) $(OPT) -o obj/getacs.o -c getacs.c
clean:
/bin/rm global mkdist acm obj/*
```

A.2 global.c

```
/*
 * global.c: Use the ACM to do a global run.
 */
#include <stdio.h>

/* This is [latitudes][heights][seasons][half][cloud type] */
```

```
double output[18][17][4][2][8];

main()
{
   int latitude, season, half;
   int i, z;
   char argument[256], clouds[80];
   int cloud_heights[3][18] = {{2,2,2,2,2,2,2,2,2,2,2,2,2,2,2,2,2,2},
                               {3,3,3,3,4,4,4,4,4,4,4,4,4,4,3,3,3,3},
                               {7,7,7,9,9,9,12,12,12,12,12,12,9,9,9,7,7,7}};

   for (latitude=-85;latitude<90;latitude+=10)
      for (season=0;season<4;season++)
         for (half=0;half<2;half++)
         {
            sprintf(argument,"./acm %d %d %d > .global \n",
                latitude, season, half);
            system(argument);
            get_output((latitude+85)/10,season,half,0);

            sprintf(argument,"./acm %d %d %d %d %g > .global \n",
                 latitude, season, half,
                 cloud_heights[0][(latitude+85)/10], 10.0);
            system(argument);
            get_output((latitude+85)/10,season,half,1);

            sprintf(argument,"./acm %d %d %d %d %g > .global \n",
                 latitude, season, half,
                 cloud_heights[1][(latitude+85)/10], 5.0);
            system(argument);
            get_output((latitude+85)/10,season,half,2);

            sprintf(argument,"./acm %d %d %d %d %g > .global \n",
                 latitude, season, half,
                 cloud_heights[2][(latitude+85)/10], 0.5);
            system(argument);
            get_output((latitude+85)/10,season,half,3);

            sprintf(argument,"./acm %d %d %d %d %g %d %g > .global \n",
                 latitude, season, half,
                 cloud_heights[0][(latitude+85)/10], 10.0,
                 cloud_heights[1][(latitude+85)/10], 5.0);
            system(argument);
            get_output((latitude+85)/10,season,half,4);
```

```
            sprintf(argument,"./acm %d %d %d %d %g %d %g > .global \n",
                 latitude, season, half,
                 cloud_heights[0][(latitude+85)/10], 10.0,
                 cloud_heights[2][(latitude+85)/10], 0.5);
            system(argument);
            get_output((latitude+85)/10,season,half,5);

            sprintf(argument,"./acm %d %d %d %d %g %d %g > .global \n",
                 latitude, season, half,
                 cloud_heights[1][(latitude+85)/10], 5.0,
                 cloud_heights[2][(latitude+85)/10], 0.5);
            system(argument);
            get_output((latitude+85)/10,season,half,6);

            sprintf(argument,"./acm %d %d %d %d %g %d %g > .global \n",
                 latitude, season, half,
                 cloud_heights[0][(latitude+85)/10], 10.0,
                 cloud_heights[1][(latitude+85)/10], 5.0,
                 cloud_heights[2][(latitude+85)/10], 0.5);
            system(argument);
            get_output((latitude+85)/10,season,half,7);

         }
   for (season=0;season<4;season++)
      for (latitude=-85;latitude<90;latitude+=10)
         for (half=0;half<2;half++)
            for (z=0;z<17;z++)
            {
               printf("%d %d %d %g",
                  season, latitude, half, (float)z+0.5);
               for (i=0;i<8;i++)
                  printf(" %g", output[(latitude+85)/10][z][season][half][i]);
               printf("\n");

            }
}

get_output(int latitude, int season, int half, int cloud)
{
   int i;
   double z;
   FILE *fp;
```

```
   if ( (fp=fopen(".global","r")) == NULL)
      exit(0);

   for (i=0;i<17;i++)
      fscanf(fp,"%lf %lf", &z, &(output[latitude][i][season][half][cloud]));
   fclose(fp);
}
```

A.3 mkdist.c

```
/*
 * mkdist.c: Make a global HO distribution based upon the output of
 * global.c
 */
#include <stdio.h>

/* This is [latitudes][heights][seasons][half][cloud type] */
double input[18][17][4][2][8];

main()
{
   int latitude, season, half;
   int i, j, z, tmp, lat;
   double HO, dtmp;
   double high[18][4], middle[18][4], low[18][4];
   double h[18][4], m[18][4], l[18][4], c[18][4],
          hm[18][4], hl[18][4], ml[18][4],
          hml[18][4];

   void getdata( char * , double [][]);

   for (season=0;season<4;season++)
      for (latitude=-85;latitude<90;latitude+=10)
 for (half=0;half<2;half++)
            for (z=0;z<17;z++)
    {
       scanf("%d %d %d %lf", &tmp, &tmp, &tmp, &dtmp);

       /* i is the cloud scenario */
       for (i=0;i<8;i++)
          scanf("%lf", &(input[(latitude+85)/10][z][season][half][i]));
    }

   /* First process the oceanic data */
```

```
  getdata("chighs.dat", high);
  getdata("cmids.dat", middle);
  getdata("clows.dat", low);
  for (i=0;i<18;i++)
  {
     for (j=0;j<4;j++)
     {
        h[i][j] = high[i][j]*(1.0-middle[i][j])*(1.0-low[i][j]);
m[i][j] = (1.0-high[i][j])*middle[i][j]*(1.0-low[i][j]);
l[i][j] = (1.0-high[i][j])*(1.0-middle[i][j])*low[i][j];
        hm[i][j] = high[i][j]*middle[i][j]*(1.0-low[i][j]);
        hl[i][j] = high[i][j]*(1.0-middle[i][j])*low[i][j];
        ml[i][j] = (1.0-high[i][j])*middle[i][j]*low[i][j];
        hml[i][j] = high[i][j]*middle[i][j]*low[i][j];
        c[i][j] = (1.0-high[i][j])*(1.0-middle[i][j])*(1.0-low[i][j]);
     }
  }
  fprintf(stderr,"Cloud Data Processed\n");

  for (season=0;season<4;season++)
     for (latitude=-85;latitude<90;latitude+=10)
        for (z=0;z<17;z++)
{
   printf("%d %d %d %g", season, latitude, 1, (float)z+0.5);
   lat = (latitude+85)/10;
   H0 = input[lat][z][season][1][0]*c[lat][season]
   + input[lat][z][season][1][1]*l[lat][season]
   + input[lat][z][season][1][2]*m[lat][season]
   + input[lat][z][season][1][3]*h[lat][season]
   + input[lat][z][season][1][4]*ml[lat][season]
   + input[lat][z][season][1][5]*hl[lat][season]
   + input[lat][z][season][1][6]*hm[lat][season]
   + input[lat][z][season][1][7]*hml[lat][season];
   printf(" %g", H0);
   H0 = input[lat][z][season][1][0];
   printf(" %g\n", H0);
}
  fprintf(stderr,"Sea Processing Done\n");

  /* Next process the land data */
  getdata("chighl.dat", high);
  getdata("cmidl.dat", middle);
  getdata("clowl.dat", low);
  for (i=0;i<18;i++)
```

```
   {
      for (j=0;j<4;j++)
      {
         h[i][j] = high[i][j]*(1.0-middle[i][j])*(1.0-low[i][j]);
 m[i][j] = (1.0-high[i][j])*middle[i][j]*(1.0-low[i][j]);
 l[i][j] = (1.0-high[i][j])*(1.0-middle[i][j])*low[i][j];
         hm[i][j] = high[i][j]*middle[i][j]*(1.0-low[i][j]);
         hl[i][j] = high[i][j]*(1.0-middle[i][j])*low[i][j];
         ml[i][j] = (1.0-high[i][j])*middle[i][j]*low[i][j];
         hml[i][j] = high[i][j]*middle[i][j]*low[i][j];
         c[i][j] = (1.0-high[i][j])*(1.0-middle[i][j])*(1.0-low[i][j]);
      }
   }

   for (season=0;season<4;season++)
      for (latitude=-85;latitude<90;latitude+=10)
         for (z=0;z<17;z++)
 {
    lat = (latitude+85)/10;
    printf("%d %d %d %g", season, latitude, 0, (float)z+0.5);
    HO = input[lat][z][season][0][0]*c[lat][season]
    + input[lat][z][season][0][1]*l[lat][season]
    + input[lat][z][season][0][2]*m[lat][season]
    + input[lat][z][season][0][3]*h[lat][season]
    + input[lat][z][season][0][4]*ml[lat][season]
    + input[lat][z][season][0][5]*hl[lat][season]
    + input[lat][z][season][0][6]*hm[lat][season]
    + input[lat][z][season][0][7]*hml[lat][season];
    printf(" %g", HO);
    HO = input[lat][z][season][0][0];
    printf(" %g\n", HO);
 }
}

void getdata(char *fn, double cloud[18][4])
{
   FILE *fp;
   int i, j, latitude;

   if ( (fp=fopen(fn,"r")) == NULL)
   {
      perror(fn);
      exit(1);
   }
```

```
  for (i=0;i<18;i++)
  {
     fscanf(fp,"%d", &latitude);
     for (j=0;j<4;j++)
     {
        fscanf(fp,"%lf", &(cloud[(latitude+85)/10][j]));
cloud[(latitude+85)/10][j] /= 100.0;
     }
  }

  fclose(fp);
}
```

A.4 acm.c

```
/* Program: acm
 *
 * Copyright 1993, 1994, 1995 F. Moraes and M.A.K. Khalil
 *
 * Permission to use, copy, modify, and distribute this software and its
 * documentation for any purpose and without fee is hereby granted, provided
 * that the above copyright notice appear in all copies and that both that
 * copyright notice and this permission notice appear in supporting
 * documentation. No representation is made about the suitability of this
 * software for any purpose.  It is provided "as is" without express or
 * implied warranty.
 *
 * Author: Francis Moraes (internet: francis@eeyore.atmos.ogi.edu)
 *         Global Change Research Center
 *         Oregon Graduate Institute
 *
 * Synopsis: This program simulates the chemistry of the troposphere as
 * detailed in "The Global Change Research Center Atmospheric
 * Chemistry Model" by F. Moraes. Copies are available from the
 * author at the e-mail address listed above.
 *
 * VARIABLES:
 *
 * T        Temperature in K
 * P        Pressure in N/m^2
 * M        Number Density in Molecules/m^3
 * I        Actinic Irradiance (Not currently used)
 * K*       K values for various reactions. These variable have the form
```

```
*           KA_B for reactions A + B -> C. These should eventually be made
*           into 2-D arrays for coupling with a climate model.
* J*        J values for various reactions. These are the same as the K
*           values except that the J* variables are 2-D arrays, the first
*           term holding the spatial data and the second the time data.
* albedo    The surface albedo.
* solve     Array of integers indicating whether a particular species
*           is to be solved for (1) or not (0).
* outputtype An integer value indicating what kind of output the user
*             desires: none (0), time (1), or altitude (2).
* output    Array of integers indicating which species concentrations
*           to be output.
* crit      The fractional change that any species can change from one
*           iteration to the next (one day to the next) for the model
*           to continue iterating.
* season    An integer value indicating the season (1=winter, 2=spring...)
*
* Global Variables
*
* For ease of programming, many variable have been made global. The
* concentrations have names as would be expected (eg. CH4, N2O). They
* are double arrays. The K values have names indicative of the two
* REACTING chemical species (eg. KOH_CH4 for OH + CH4 --> ...); they
* are also double arrays. The J values have names indicative of the
* starting compound (eg. JO3 for O3 --> O2 + O). Because the J values
* depend upon actinic flux they are two-dimensional double arrays.
*
* Functions
*
* get_par_data   This function opens the parameter file and reads the user
*                specified input parameters: solve, outputtype, output, and
*                albedo, listed above.
* get_std_atmos  This function calculates the temperature, pressure, and
*                number density of the atmosphere, inputs the concentration
*                of the 'static' (non-model determined) gases in mixing
*                ratio units, and converts the mixing ratios to units of
*                molecules/cm^3.
*
* get_K          This function determines the chemical constants for all of
*                the reactions in the model.
* get_actinic  This function determines the actinic flux for 10 nm wavelength
*              bands from 180 to 730 nm, for angles 0 to 86 degrees (in
*              approximately 10 degree bands), for all of the atmospheric
*              layers.
```

```
 * get_J        This function determines the photochemical constants for
 *              all of the reactions in the model.
 * get_initial_cons This function calculates the initial concentrations of
 *                  the 'reactive' (model determined) gases.
 * get_cons     This is the main loop of the model; it iteratively solves
 *              for the reactive species until convergence is achieved.
 * output_data  This function outputs the data, in the form given in the
 *              parameter file, to the standard output device (usually
 *              the screen).
 *
 * Program Flow
 *
 * The functions listed above give a pretty good idea of the flow of the
 * program. But generally:
 *
 *       o Get command line arguments.
 *       o Input parameters from start-up file.
 *       o Create the atmosphere (Temperature, Pressure, and Density).
 *       o Input the 'static' gas concentrations.
 *       o Calculate the K values.
 *       o Calculate the atmospheric actinic flux.
 *       o Calculate the J values.
 *       o Calculate the initial 'reactive' gas concentrations as a starting
 *         point for the iterative solution process.
 *       o Iteratively solve for the 'reactive' gas concentrations.
 *       o Output the results
 */

#include <stdio.h>
#include "acm.h"
#include "rxn.h"

#define PAR_FILE "dat/par.dat"
double no2qy1[19] = { 0.999, 0.998, 0.997, 0.996, 0.995, 0.994, 0.993,
                      0.992, 0.991, 0.990, 0.989, 0.988, 0.987, 0.986,
                      0.984, 0.983, 0.981, 0.979, 0.975 };
double no2qy2[44] = { 0.974, 0.973, 0.972, 0.971, 0.969, 0.967, 0.966,
                      0.964, 0.962, 0.960, 0.959, 0.957, 0.953, 0.950,
                      0.942, 0.922, 0.870, 0.820, 0.760, 0.695, 0.635,
                      0.560, 0.485, 0.425, 0.350, 0.290, 0.225, 0.185,
                      0.153, 0.130, 0.110, 0.094, 0.083, 0.070, 0.059,
                      0.048, 0.039, 0.030, 0.023, 0.018, 0.012, 0.008,
                      0.004, 0.000 };
```

```
main(int argc, char **argv)
{
   double crit = 0.001,
          T[SPACE_POINTS],
          P[SPACE_POINTS],
          M[SPACE_POINTS],
          Z[SPACE_POINTS][2],
          Kz[SPACE_POINTS+2],
          O3_column[SPACE_POINTS],
          albedo,
          cloud_optical_depth[3],
          surface_temperature,
          baseH2O;

   double nox;

   int season, i,
       solve[19], output[19], outputtype,
       cloud_layer_top[3] = { 0, 0, 0 };
   /* half of 2.5 dimensional model. Is this a land (0) or sea (1) run? */
   int half;

   extern double latitude, inclination;

   extern void get_par_data(char *, int *, int *, int *, double *),
               get_std_atmos(double *, double *, double *, double [][],
                             double *, int, double, double *, double *,int),
               get_acs(),
               get_actinic(double *, double *, double [][], double,
                           int *, double *, double *),
               get_initial_cons(int *, double [][], double *, double),
               get_cons(int *, double, double *, double [][], double *),
               output_data(int, int *, double [][], double *, double *),
               get_K(double *, double *, double *, double [][]),
               get_J(double *, double *, double *),
               exit_error(char *);

   extern double atof(char *);

   /* Input command line arguments */

   if (argc < 2)
   {
      fprintf(stderr,"Usage: acm lat sea half [ch co ...]\n");
```

```
   fprintf(stderr,"Where: lat is the latitude\n");
   fprintf(stderr,"       sea is the season (winter=0, spring=1, ...\n");
   fprintf(stderr,"       ch is cloud height\n");
   fprintf(stderr,"       co is cloud optical depth\n");
   fprintf(stderr,"There can be a maximum of 3 ch/co pairs\n");
   exit(1);
}

latitude = atof(argv[1])*PI/180.0;        /* change degrees to radians */
season = atoi(argv[2]);

/* Assign the solar inclination angle according to the season */
switch (season)
{
   case 0:
      inclination = -23.27;
      break;
   case 1:
      inclination = 0.0;
      break;
   case 2:
      inclination = 23.27;
      break;
   case 3:
      inclination = 0.0;
      break;
   default:
      exit_error("Season must be 0, 1, 2, or 3.");
}

inclination = inclination*PI/180.0;

half = atoi(argv[3]);
if (half != 0 && half != 1)
   exit_error("half must be either 0 (land) or 1 (sea).");

/* Input the cloud locations and optical depths */
if (argc > 4)
{
   cloud_layer_top[0] = atof(argv[4]);
   if (argc > 5)
      cloud_optical_depth[0] = atof(argv[5]);
   else
      exit_error("Cloud parameters must be given in pairs.");
```

```
}

if (argc > 6)
{
   cloud_layer_top[1] = atof(argv[6]);
   if (argc > 7)
      cloud_optical_depth[1] = atof(argv[7]);
   else
      exit_error("Cloud parameters must be given in pairs.");
}

if (argc > 8)
{
   cloud_layer_top[2] = atof(argv[8]);
   if (argc > 9)
      cloud_optical_depth[2] = atof(argv[9]);
   else
      exit_error("Cloud parameters must be given in pairs.");
}

/* Input the species to be solved for and output */
get_par_data(PAR_FILE,solve,&outputtype,output,&crit);

/* Input the temperature, pressure, and number density of the
 * atmosphere and the concentrations of the gases that the
 * model does not solve for (NOX, N2O, etc).
 */
get_std_atmos(T,M,P,Z,Kz,season,latitude,&albedo,O3_column,half);

/* Calculate the rate constants for the thermal reactions */
get_K(T,M,P,Z);

/* Calculate the absorption cross section of certain molecules */
get_acs();

/* Calculate the actinic flux */
get_actinic(T,M,Z,albedo,cloud_layer_top,cloud_optical_depth,O3_column);

/* Calculate the J values */
get_J(T,M,P);

/* Calculate initial concentrations */
get_initial_cons(solve,Z,M,nox);
```

```
    /* Iteratively solve concentrations */
    get_cons(solve, crit, Kz, Z, M-1);

    /* Output the results */
    output_data(outputtype,output,Z,M,P);

    return 0;
}
```

A.5 acs.c

```
/* Function: get...ACS (various functions)
 *
 * Copyright 1993 F. Moraes and M.A.K. Khalil
 *
 * Permission to use, copy, modify, and distribute this software and its
 * documentation for any purpose and without fee is hereby granted, provided
 * that the above copyright notice appear in all copies and that both that
 * copyright notice and this permission notice appear in supporting
 * documentation. No representation is made about the suitability of this
 * software for any purpose.  It is provided "as is" without express or
 * implied warranty.
 *
 * Author: Francis Moraes (internet: francis@eeyore.atmos.ogi.edu)
 *         Global Change Research Center
 *         Oregon Graduate Institute
 *
 * Synopsis: functions which determine the absorption cross section (ACS)
 * for the photodissociation in the OH model.
 *
 * FUNCTION FLOW
 *
 * Two independent procedures can be used for determining the ACS. The
 * first involves searching through a list of data for the proper value
 * and the second involves plugging the wavelength and temperature into
 * a formula. The second procedure is self explanatory but the first
 * requires more detail. The main() section of the program reads in a
 * starting wavelength, the ACS for the wavelengths starting at given
 * wavelength and ending at the next starting wavelength, and sometimes
 * a temperature parameter that modifies the ACS given. The functions
 * that use this approach then search the wavelengths until they find one
 * that is larger than the wavelength of interest and use the ACS of
 * the previous wavelength (the wavelengths run from lowest to highest).
 */
```

```
#include <math.h>
#include "acs.h"

double getO3ACS(double wavelength, double temperature)
{
   extern double O3ACS[][2];
   extern int O3ACS_NUM;
   int i;

   for (i=1;wavelength>=O3ACS[i][0] && i<O3ACS_NUM;i++)
      ;

   return O3ACS[i-1][1];
}

#define A0 6.4761E4
#define A1 -9.2170972E2
#define A2 4.535649
#define A3 -4.4589016E-3
#define A4 -4.035101E-5
#define A5 1.6878206E-7
#define A6 -2.652014E-10
#define A7 1.5534675E-13

#define B0 6.8123E3
#define B1 -5.1351E1
#define B2 1.1522E-1
#define B3 -3.0493E-5
#define B4 -1.0924E-7

double getH2O2ACS(double wavelength, double temperature)
{
   double chi, A, B;

   if (wavelength < 260 || wavelength > 350 ||
       temperature < 200 || temperature > 400)
   {
      return 0;
   }

   A = A0 + A1*wavelength + A2*pow(wavelength,2.0) + A3*pow(wavelength,3.0) +
       A4*pow(wavelength,4.0) + A5*pow(wavelength,5.0) +
       A6*pow(wavelength,6.0) + A7*pow(wavelength,7.0);
```

```
   B = B0 + B1*wavelength + B2*pow(wavelength,2.0) +
       B3*pow(wavelength,3.0) + B4*pow(wavelength,4.0);

   chi = 1.0 / ( 1.0 + exp(-1265.0/temperature));

   return (1.0E-21 * (chi*A + (1.0-chi)*B));
}

double getNO2ACS(double wavelength, double temperature)
{
   extern double NO2ACS[][3];
   extern int NO2ACS_NUM;
   int i;

   for (i=1;wavelength>=NO2ACS[i][0] && i<NO2ACS_NUM;i++)
      ;

   return (NO2ACS[i-1][1] + NO2ACS[i-1][2]*(temperature-273.15));
}

double getNO3ACS(double wavelength, double temperature)
{
   extern double NO3ACS[][2];
   extern int NO3ACS_NUM;
   int i;

   for (i=1;wavelength>=NO3ACS[i][0] && i<NO3ACS_NUM;i++)
      ;

   return (NO3ACS[i-1][1]);
}

double getHNO2ACS(double wavelength, double temperature)
{
   extern double HNO2ACS[][2];
   extern int HNO2ACS_NUM;
   int i;

   for (i=1;wavelength>=HNO2ACS[i][0] && i<HNO2ACS_NUM;i++)
      ;

   return (HNO2ACS[i-1][1]);
}
```

```
double getH2COACS(double wavelength, double temperature)
{
   extern double H2COACS[][2];
   extern int H2COACS_NUM;
   int i;

   for (i=1;wavelength>=H2COACS[i][0] && i<H2COACS_NUM;i++)
      ;

   return (H2COACS[i-1][1]);
}

#undef A0
#define A0 8.7756960795E-15
#undef A1
#define A1 -0.0490747133

double getCH3OOHACS(double wavelength, double temperature)
{
   if (wavelength < 210.0)
      return 0.0;
   else
      return (A0*exp(A1*wavelength));
}

double getHNO3ACS(double wavelength, double temperature)
{
   extern double HNO3ACS[][2];
   extern int HNO3ACS_NUM;
   int i;

   for (i=1;wavelength>=HNO3ACS[i][0] && i<HNO3ACS_NUM;i++)
      ;

   return (HNO3ACS[i-1][1]);
}

double getHO2NO2ACS(double wavelength, double temperature)
{
   extern double HO2NO2ACS[][2];
   extern int HO2NO2ACS_NUM;
   int i;
```

```
   for (i=1;wavelength>=HO2NO2ACS[i][0] && i<HO2NO2ACS_NUM;i++)
      ;

   return (HO2NO2ACS[i-1][1]);
}

double getN2O5ACS(double wavelength, double temperature)
{
   extern double N2O5ACS[][2];
   extern int N2O5ACS_NUM;
   int i;

   if (wavelength < 285.0)
   {
      for (i=1;wavelength>=N2O5ACS[i][0] && i<N2O5ACS_NUM;i++)
         ;
      return (N2O5ACS[i-1][1]);
   }
   else
      return (1.0E-20 * exp(2.735 + ((4728.5-17.127*wavelength)/temperature)));
}
```

A.6 actinic.c

```
/* Function: actinic
 *
 * Copyright 1993 F. Moraes and M.A.K. Khalil
 *
 * Permission to use, copy, modify, and distribute this software and its
 * documentation for any purpose and without fee is hereby granted, provided
 * that the above copyright notice appear in all copies and that both that
 * copyright notice and this permission notice appear in supporting
 * documentation. No representation is made about the suitability of this
 * software for any purpose.  It is provided "as is" without express or
 * implied warranty.
 *
 * Author: Francis Moraes (internet: francis@eeyore.atmos.ogi.edu)
 *         Global Change Research Center
 *         Oregon Graduate Institute
 *
 * Synopsis: Find the actinic flux given a wavelength, zenith angle,
 *             and height.
 *
 * FUNCTION FLOW
```

```
 *
 * The function simply looks up the actinic flux in a
 * three-dimensional array of values. The values were determined by the
 * function get_actinic(). The array, ActFlux[][][] has values ranging
 * from:
 *
 *       wavelength:        0 - 56 (180 nm - 730 nm)
 *       zenith angle:      0 -  9 (0 degrees - 86 degrees)
 *       height:            0 - 25 (0 km - 12 km)
 *
 * The function begins by checking to make sure that the wavelength is
 * within range. Next the wavelength is converted into the wavelength
 * bin (eg. 0 for wavelength = 180, 3 for wavelength = 210). Finally,
 * the program does a linear interpolation between the angle bins
 * above and below the given angle. Angles above 86 degrees return
 * a 0 flux.
 */

#include <math.h>
#include "acm.h"
#include "actinic.h"

double Actinic(int wavelength_bin, double angle, int height_bin)
{
   double per, slope, Flux, binsize;
   int angle_bin;
   extern int num_wavelength_bin;
   extern double ActFlux[WAVELENGTH_POINTS][ANGLE_POINTS][SPACE_POINTS],
                 ActAngle[ANGLE_POINTS],
                 ActBin[WAVELENGTH_POINTS];

   /* convert the angle from radians to degrees... */

   angle = 180.0 * angle / PI;

   if (ActBin[wavelength_bin] < LOW_WAVELENGTH)
      return 0.0;
   else if (ActBin[wavelength_bin] > HIGH_WAVELENGTH)
      return 0.0;

   angle_bin = (int) (angle/10.0);

   if (wavelength_bin == 0)
      binsize = ActBin[1] - ActBin[0];
```

```
   else if (wavelength_bin == num_wavelength_bins-1)
      binsize = ActBin[wavelength_bin] - ActBin[wavelength_bin-1];
   else
      binsize = (ActBin[wavelength_bin+1] - ActBin[wavelength_bin-1])/2.0;

   if (angle < 86.0)
   {
      slope = (ActFlux[wavelength_bin][angle_bin][height_bin] -
               ActFlux[wavelength_bin][angle_bin+1][height_bin]) /
              (ActAngle[angle_bin] - ActAngle[angle_bin+1]);
      Flux = binsize*(slope*(angle - ActAngle[angle_bin]) +
             ActFlux[wavelength_bin][angle_bin][height_bin]);

      return Flux;
   }

   return 0.0;
}
```

A.7 getacs.c

```
/* Function: get_acs
 *
 * Copyright 1993 F. Moraes and M.A.K. Khalil
 *
 * Permission to use, copy, modify, and distribute this software and its
 * documentation for any purpose and without fee is hereby granted, provided
 * that the above copyright notice appear in all copies and that both that
 * copyright notice and this permission notice appear in supporting
 * documentation. No representation is made about the suitability of this
 * software for any purpose.  It is provided "as is" without express or
 * implied warranty.
 *
 * Author: Francis Moraes (internet: francis@eeyore.atmos.ogi.edu)
 *         Global Change Research Center
 *         Oregon Graduate Institute
 *
 * Synopsis: Input all of the absorption cross section (ACS) data.
 *
 * VARIABLES:
 *
 * none
 *
 * GLOBAL VARIABLES:
```

```
 *
 * the ACS arrays
 *
 * FUNCTIONS:
 *
 * get_2_data: input data from a file that has two columns
 * get_3_data: input data from a file that has three columns
 *
 * PROGRAM FLOW:
 *
 * Input the absorption cross section data. The first number
 * is the beginning wavelength (in nm) and the second is the absorption
 * cross section for the wavelengths between the beginning wavelength
 * and the next beginning wavelength. This is the procedure for all of
 * the gases except for NO2
 *
 * Input the NO2 absorption cross section data. The first number
 * is the beginning wavelength (in nm), the second is the absorption
 * cross section for the wavelengths between the beginning wavelength
 * and the next beginning wavelength, and the third is the change in
 * ACS per unit (K) change of temperature.
 */

#include "acm.h"
#include "acs.h"
#include "j.h"

void get_acs()
{
   int i, j;

   extern int get_2_data(char *, double [][2]),
              get_3_data(char *, double [][3]);


   O3ACS_NUM = get_2_data(O3ACS_FILE,O3ACS);
   NO2ACS_NUM = get_3_data(NO2ACS_FILE,NO2ACS);
   NO3ACS_NUM = get_2_data(NO3ACS_FILE,NO3ACS);
   HNO2ACS_NUM = get_2_data(HNO2ACS_FILE,HNO2ACS);
   H2COACS_NUM = get_2_data(H2COACS_FILE,H2COACS);
   HNO3ACS_NUM = get_2_data(HNO3ACS_FILE,HNO3ACS);
   HO2NO2ACS_NUM = get_2_data(HO2NO2ACS_FILE,HO2NO2ACS);
   N2O5ACS_NUM = get_2_data(N2O5ACS_FILE,N2O5ACS);
}
```

A.8 getact.c

```
/* Function: get_actinic
 *
 * Copyright 1993 F. Moraes and M.A.K. Khalil
 *
 * Permission to use, copy, modify, and distribute this software and its
 * documentation for any purpose and without fee is hereby granted, provided
 * that the above copyright notice appear in all copies and that both that
 * copyright notice and this permission notice appear in supporting
 * documentation. No representation is made about the suitability of this
 * software for any purpose.  It is provided "as is" without express or
 * implied warranty.
 *
 * Purpose: Calculate the actinic flux at the all model layers for
 *           every wavelength for solar zenith angles 0, 10, 20, 30,
 *           40, 50, 60, 70, 78, 86 degrees. Other model components
 *           interpolate as necessary to get the exact zenith angle.
 *
 * Implementation: This function uses the two stream approximation to
 * calculate the actinic flux. It starts by initializing the ActAngle
 * array with the angles (in degrees) that relate to the ActFlux array.
 * It then inputs the solar radiation flux and the index of refraction
 * at the top of the atmosphere followed by the ozone column at all
 * of the model levels. An array is created for the use with the
 * numerical recipes linear system solution (this array is akin to the
 * A array in A*x = b). The total density of the atmosphere is calculated
 * (this is later used to determine the Rayleigh optical depth of each
 * layer of the atmosphere by dividing the Rayleigh optical depth of
 * the entire atmosphere by the percentage of the atmosphere in the given
 * atmospheric layer; this idea was given to me by Keith Grant).
 * Finally, for each wavelength, zenith angle, and atmospheric layer the
 * actinic flux is calculated. This is done by first determining the
 * Rayleigh and Ozone optical depths at each layer. From these values
 * the fraction of diffuse and direct light that is transmitted and
 * scattered at each depth can be determined. The optical depths are
 * also used to determine the direct radiation at each atmospheric
 * layer. Lastly, these values are used to fill the Fop (operator)
 * array and the Fconst (constant) array which are then solved to yield
 * the upward and downward fluxes of diffuse radiation which, with the
 * direct flux, are the actinic flux. This procedure is outlined in
 * Thompson (1984)
 *
 * PASSED VARIABLES:
```

```
*
* T             Array of temperature for each atmospheric layer
* M             Array of densities for each atmospheric layer
* Z             Array of atmospheric layer height (Z[][0]) and
*               atmospheric layer thickness (Z[][1]).
* albedo        The ground albedo
* cloud_layer_top The first atmospheric layer above the high,
*                middle, and low clouds. A zero value indicates
*                that there is no cloud.
* cloud_optical_depth The optical depth for the high, middle,
*                and low clouds.
*
* LOCAL VARIABLES:
*
* Fop            The operator array that is used for solving the set
*                of linear equation of diffuse radiation. This variable
*                is a two-dimensional array that corresponds to A in
*                the matrix equation:
*
*                                Fop.Fdiff = Fconst
*
*                Note however that there is no Fdiff variable. The
*                Numerical Recipes function that solves this equation
*                stores the Fdiff values in the Fconst vector. The
*                values that are stored in Fop correspond to both
*                upward AND downward diffuse radiation. The array
*                has elements of downward flux for the even numbered
*                elements (0, 2, 4, ...) and upward flux for the odd
*                numbered elements (1, 3, 5, ...). Since the matrix
*                equation is only penta-diagonal Fop is only five
*                elements wide.
* Fconst         The constant array in the matrix equation and the
*                resulting equation. See 'Fop' above.
* Fdir           An array of direct beam fluxes for each atmospheric
*                layer.
* Fscat_dir      An array of the fraction of direct light which is
*                scattered for each atmospheric layer.
* Fscat_diff     An array of the fraction of diffuse light which is
*                scattered for each atmospheric layer.
* Ftrans_diff    An array of the fraction of diffuse light which is
*                transmitted for each atmospheric layer.
* solar_flux     An array of the direct flux at the top of the
*                atmosphere for each wavelength bin. This flux is
*                given in 1 nm bands, even though the flux locations
```

```
*                 are not necessarily 1 nm apart.
* refraction      An array of the index of refraction of the atmosphere
*                 for each wavelength, kind of. The refraction array is
*                 input as one minus the index of refraction. This value
*                 is squared upon input and so refraction[] holds the
*                 values of (1 - refraction)^2.
* O3_column       An array of the O3 column at each atmospheric layer.
* deltaM          An array of the fraction of the total air in an
*                 atmospheric layer relative to the total air in the
*                 atmosphere.
* totalM          The total weighted atmospheric density.
* O3_optical_depth the ozone optical depth of a given atmospheric layer.
* Ray_optical_depth the Rayleigh optical depth of a given atmospheric
*                 layer.
* Base_Ray_optical_depth the Rayleigh optical depth of the entire
*                 atmosphere.
* angle           The angle of a given iteration, given in radians
* dir_cloud_albedo An array of cloud albedos relative to direct
*                 radiation for high, middle, and low clouds.
* diff_cloud_albedo An array of cloud albedos relative to diffuse
*                 radiation for high middle, and low clouds.
* wavelength_bin The integer counter for the wavelength iteration.
* angle_bin       The integer counter for the angle iteration.
*
* GLOBAL VARIABLES:
*
* num_wavelenght_bins is the number of wavelength bins.
* ActFlux         A three dimensional array which contains the actinic
*                 flux for each wavelength, zenith angle, and atmospheric
*                 layer (in that order).
* ActBin          An array containing the center wavelength (in nm) for
*                 each wavelength bin. Generally, the wavelength bin size
*                 is taken to be (ActBin[i+1] - ActBin[i-1])/2.
*
* FUNCTIONS
*
* initialize_angles This function fills the ActAngle array with the
*                 angles used in the model (0,10,20,30,40,50,60,70,78,86)
*                 each given in degrees.
*
* get_solar_data This function reads the solar_flux and refraction
*                 variables from file.
*
* get_data         A general function used here to input the ozone column
```

```
*               data.
*
* dmatrix       This is a Numerical Recipes function which allocates a
*               two-dimensional matrix. I am using this function because
*               of the weirdness of the NR C code, starting all arrays
*               at 1.
*
* get_layer_density This function fills the deltaM array with the
*               atmospheric fraction of the whole that a layer is.
*
* get_O3_optical_depth This function returns the optical depth of the
*               current layer and wavelength.
*
* getO3ACS      A general function to determine the absorption cross
*               section of ozone given a wavelength. It is used here
*               to determine the ozone optical depth of the atmosphere.
*
* fill_mat      This function loads the Fop and Fconst arrays with the
*               necessary values so that the diffuse radiation can be
*               solved for.
*
* solve_mat     This is a Numerical Recipes function which solves banded
*               matrices.
*
* AMdir       This function gives the normalized air mass that light
*             travels through at a given angle (it returns 1 for a
*             zenith angle of zero degrees).
*
* wavelength  This function returns the wavelength given a wavelength bin.
*
* avg         This function takes the average of two numbers.
*
* FUNCTION FLOW
*
*       o Initialize the angle array
*       o Input the solar and Ozone data
*       o Allocate memory for the linear equation solutions
*       o Determine the atmospheric fraction of each layer
*       o For each wavelength
*               o Calculate the Rayleigh optical depth of the atmosphere
*               o For each angle and space point
*                       o Calculate the Rayleigh and Ozone Optical depths
*                       o Calculate the transmitted and scattered light
*                         for diffuse and direct light
```

```
 *                      o Calculate the direct radiation
 *                      o Fill the diffuse operator array
 *                      o Solve for the diffuse radiation
 *
 */

#include <stdio.h>
#include <math.h>
#include "acm.h"
#include "actinic.h"

#define TOP_RAD_FILE "dat/solarflx.dat"
#define O3_COLUMN_FILE "dat/o3_column.dat"
#define RAY_CONST (1.044E-11)

get_actinic(double *T, double *M, double Z[][2], double albedo,
            int cloud_layer_top[], double cloud_optical_depth[],
            double *O3_column)
{
   double **Fop, Fconst[2*SPACE_POINTS],
          Fdir[SPACE_POINTS],
          Ftrans_diff[SPACE_POINTS],
          Fscat_diff[SPACE_POINTS],
          Fscat_dir[SPACE_POINTS],

          solar_flux[MAX],
          refraction[MAX],
          deltaM[SPACE_POINTS],

          O3_optical_depth,
          Ray_optical_depth,
          Base_Ray_optical_depth,

          angle,
          totalM = 0,
          dir_cloud_albedo[3] = { 0.0, 0.0, 0.0 },
          diff_cloud_albedo[3] = { 0.0, 0.0, 0.0 };

   int wavelength_bin,
       angle_bin,
       i, j, k;

   extern double ActFlux[WAVELENGTH_POINTS][ANGLE_POINTS][SPACE_POINTS],
                 ActBin[WAVELENGTH_POINTS];
```

```
extern int num_wavelength_bins;

extern double **dmatrix();

extern double AMdir(double),
              get_dir_albedo(double,double),
              get_diff_albedo(double),
              get_layer_density(double *, double [][], double *),
              get_O3_optical_depth(int, double *, double, double);

extern void solve_mat(),
            get_data(char *, double *, int),
            fill_mat(double **, double *, double *, double *,
                     double *, double *, int *, double *, double *,
                     double, double, double *),
            initialize_angles(double *);

extern int get_solar_data(double *, double *, double *);

/* Fill ActAngle with the 'standard' angles */
initialize_angles(ActAngle);

/* Input the solar data */
num_wavelength_bins = get_solar_data(ActBin,solar_flux,refraction);

/* Allocate space for use with matrix routines */
Fop = dmatrix(0,2*SPACE_POINTS-1,0,4);
for (i=0;i<2*SPACE_POINTS-1;i++)
   for (j=0;j<5;j++)
      Fop[i][j] = 0;

/* Calculate the total density of the atmosphere */
totalM = get_layer_density(M,Z,deltaM);

/* Calculate the diffuse radiation cloud albedo */
for (i=0;i<3;i++)
   diff_cloud_albedo[i] = get_diff_albedo(cloud_optical_depth[i]);

for (wavelength_bin=0;wavelength_bin<num_wavelength_bins;wavelength_bin++)
{
   /* Rayleigh Scattering Optical Depth of the entire atmosphere */
   Base_Ray_optical_depth = RAY_CONST*refraction[wavelength_bin]*
                            pow(1.0e-7*ActBin[wavelength_bin],-4.0);
```

```
for (angle_bin=0;angle_bin<ANGLE_POINTS;angle_bin++)
{
   /* zenith angle in radians */
   angle = PI*ActAngle[angle_bin]/180.0;

   for (k=SPACE_POINTS-1;k>=0;k--)
   {
      /* Ozone Optical Depth */
      O3_optical_depth = get_O3_optical_depth(k,O3_column,T[k],
                                              ActBin[wavelength_bin]);

      /* Rayleigh Scattering Optical Depth. */
      Ray_optical_depth = Base_Ray_optical_depth * deltaM[k];

      /* Fractional diffuse radiation transmission */
      Ftrans_diff[k] = exp(-(O3_optical_depth +
                             Ray_optical_depth)*AMdiff);

      /* Fractional diffuse radiation scattering */
      Fscat_diff[k] = exp(-O3_optical_depth*AMdiff)*
         (1.0 - exp(-Ray_optical_depth*AMdiff));

      /* Fractional direct radiation scattering */
      Fscat_dir[k] = exp(-O3_optical_depth*AMdir(angle))*
         (1.0 - exp(-Ray_optical_depth*AMdir(angle)));

      /* Calculate the direct radiation flux */
      if (k == SPACE_POINTS-1)
         Fdir[k] = solar_flux[wavelength_bin]*exp(-(O3_optical_depth +
                   Ray_optical_depth)*AMdir(angle));
      else if (k == cloud_layer_top[0]-1 /*&& k != 0*/)
            Fdir[k] = Fdir[k+1]*exp(-(O3_optical_depth +
                                      Ray_optical_depth +
                                  cloud_optical_depth[0])*
                                AMdir(angle));
      else if (k == cloud_layer_top[1]-1 /*&& k != 0*/)
            Fdir[k] = Fdir[k+1]*exp(-(O3_optical_depth +
                                      Ray_optical_depth +
                                  cloud_optical_depth[1])*
                                AMdir(angle));
      else if (k == cloud_layer_top[2]-1 /*&& k != 0*/)
            Fdir[k] = Fdir[k+1]*exp(-(O3_optical_depth +
                                      Ray_optical_depth +
                                  cloud_optical_depth[2])*
```

```
                                        AMdir(angle));
            else
               Fdir[k] = Fdir[k+1]*exp(-(O3_optical_depth +
                                              Ray_optical_depth)*AMdir(angle));

         }

         for (i=0;i<3;i++)
            dir_cloud_albedo[i] = get_dir_albedo(cloud_optical_depth[i],angle);

         fill_mat(Fop, Fconst, Fdir,
                       Ftrans_diff, Fscat_diff, Fscat_dir,
                       cloud_layer_top,
                       dir_cloud_albedo, diff_cloud_albedo,
                       albedo, angle,
                       cloud_optical_depth);

         solve_mat(Fop,2*SPACE_POINTS, 2, 2, Fconst);

         for (k=0;k<SPACE_POINTS;k++)
         {
            ActFlux[wavelength_bin][angle_bin][k] =
               Fdir[k] + Fconst[2*k] + Fconst[2*k+1];
         }
      }
   }
}

void initialize_angles(double *ActAngle)
{
   ActAngle[0] = 0.0;
   ActAngle[1] = 10.0;
   ActAngle[2] = 20.0;
   ActAngle[3] = 30.0;
   ActAngle[4] = 40.0;
   ActAngle[5] = 50.0;
   ActAngle[6] = 60.0;
   ActAngle[7] = 70.0;
   ActAngle[8] = 78.0;
   ActAngle[9] = 86.0;
}

int get_solar_data(double *ActBin, double *solar_flux, double *refraction)
{
```

```
   int k;
   FILE *fp;

   /* Input the solar flux at the top of the atmosphere and the
    * refraction of the atmosphere.
    *
    * The solar flux is given as a 1 nm wavelength band centered on
    * the given wavelength. Thus, when integrating, the solar flux
    * would be solar_flux[i]*(ActBin[i+1]-ActBin[i]).
    *
    * Note: the refraction array is input as (1 - refraction). This
    * value is then squared so that refraction[] holds the values
    * of (1 - refraction)^2.
    */
   if ( (fp=fopen(TOP_RAD_FILE,"r")) == NULL)
   {
      perror(TOP_RAD_FILE);
      exit(0);
   }

   for(k=0;fscanf(fp,"%lf %lf %lf",&(ActBin[k]), &(solar_flux[k]),
                                    &(refraction[k])) != EOF;k++)
      refraction[k] = pow(refraction[k],2.0);

   fclose(fp);

   /* Return the number of wavelength bins the data are divided into */
   return k;
}

double AMdir(double angle)
{
   return (35.0/sqrt( (1224.0 * pow(cos(angle),2.0) + 1.0)));
}

void fill_mat(double **Fop, double *Fconst, double *Fdir,
                    double *Ftrans_diff, double *Fscat_diff,
                    double *Fscat_dir,
                    int cloud_layer_top[],
                    double dir_cloud_albedo[],
                    double diff_cloud_albedo[],
                    double albedo, double angle, double od[])
{
   int i, k;
```

```
double avg(double *, int, int);

/* Fill the surface layer */
Fop[0][0] = 0.0;
Fop[0][1] = 0.0;
Fop[0][2] = 1.0;
Fop[0][3] = -0.5*avg(Fscat_diff,0,1);
Fop[0][4] = -(avg(Ftrans_diff,0,1) + 0.5*avg(Fscat_diff,0,1));
Fconst[0] = avg(Fscat_dir,0,1)*Fdir[1]*cos(angle);

Fop[1][0] = 0.0;
Fop[1][1] = -albedo - 0.5*avg(Fscat_diff,0,1);
Fop[1][2] = 1.0;
Fop[1][3] = 0.0;
Fop[1][4] = 0.0;
Fconst[1] = (Fscat_dir[0] + 2.0*albedo)*cos(angle)*Fdir[0];

/* Fill the matrix for all levels between the top atmospheric
   level and the surface layer */
for (k=1;k<SPACE_POINTS-1;k++)
{
   Fop[2*k][0] = 0.0;
   Fop[2*k][1] = 0.0;
   Fop[2*k][2] = 1.0;
   Fop[2*k][3] = -0.5*avg(Fscat_diff,k,k+1);
   Fop[2*k][4] = -(avg(Ftrans_diff,k,k+1) +
                 0.5*avg(Fscat_diff,k,k+1));
   Fconst[2*k] = avg(Fscat_dir,k,k+1)*Fdir[k+1]*cos(angle);

   Fop[2*k+1][0] = -(avg(Ftrans_diff,k,k-1) +
                   0.5*avg(Fscat_diff,k,k-1));
   Fop[2*k+1][1] = -0.5*avg(Fscat_diff,k,k-1);
   Fop[2*k+1][2] = 1.0;
   Fop[2*k+1][3] = 0.0;
   Fop[2*k+1][4] = 0.0;
   Fconst[2*k+1] = avg(Fscat_dir,k,k-1)*Fdir[k]*cos(angle);
}

/* Fill the matrix for the top atmospheric level */
k = SPACE_POINTS-1;

Fop[2*k][0] = 0.0;
Fop[2*k][1] = 0.0;
Fop[2*k][2] = 1.0;
```

```
   Fop[2*k][3] = -0.5*Fscat_diff[k];
   Fop[2*k][4] = 0.0;
   Fconst[2*k] = Fscat_dir[k]*Fdir[k]*cos(angle);

   Fop[2*k+1][0] = -avg(Ftrans_diff,k,k-1) - 0.5*avg(Fscat_diff,k,k-1);
   Fop[2*k+1][1] = -0.5*avg(Fscat_diff,k,k-1);
   Fop[2*k+1][2] = 1.0;
   Fop[2*k+1][3] = 0.0;
   Fop[2*k+1][4] = 0.0;
   Fconst[2*k+1] = avg(Fscat_dir,k,k-1)*Fdir[k]*cos(angle);

   for (i=0;i<3;i++)
   {
      if (cloud_layer_top[i] > 1)
      {
         /* This is the grid just below the cloud */
         Fop[2*(cloud_layer_top[i]-1)][0] =
                 Fop[2*(cloud_layer_top[i]-1)][1] = 0.0;
         Fop[2*(cloud_layer_top[i]-1)][2] = 1.0;
         Fop[2*(cloud_layer_top[i]-1)][3] = -diff_cloud_albedo[i];
         Fop[2*(cloud_layer_top[i]-1)][4] = -(1.0-diff_cloud_albedo[i]);

         /* Added 2.0 factor, found bug */
         Fconst[2*(cloud_layer_top[i]-1)] = (1.0-dir_cloud_albedo[i] -
                exp(-od[i]/cos(angle))) *
                 Fdir[cloud_layer_top[i]]*2.0*cos(angle);

         /* This is the grid just above the cloud */
         Fop[2*(cloud_layer_top[i])+1][0] = -(1.0-diff_cloud_albedo[i]);
         Fop[2*(cloud_layer_top[i])+1][1] = -diff_cloud_albedo[i];
         Fop[2*(cloud_layer_top[i])+1][2] = 1.0;
         Fop[2*(cloud_layer_top[i])+1][3] =
                Fop[2*(cloud_layer_top[i])+1][4] = 0;

         Fconst[2*(cloud_layer_top[i])+1] = Fdir[cloud_layer_top[i]+1]*
                 cos(angle)*(2.0*dir_cloud_albedo[i]);

      }
   }
}

double get_diff_albedo(double optical_depth)
{
   static double fixed_albedo[11] = {0.000,
```

```
                                        0.158,
                                        0.273,
                                        0.428,
                                        0.600,
                                        0.750,
                                        0.857,
                                        0.923,
                                        0.960,
                                        0.979,
                                        1.000};
   double albedol, albedou, albedo;
   int bin, int_optical_depth;

   if (optical_depth > 1000.0)
      return 1.0;

   int_optical_depth = (int) optical_depth;
   for (bin=0;(int_optical_depth/=2)>0;bin++)
      ;

   albedol = fixed_albedo[bin];
   albedou = fixed_albedo[bin+1];

   if (optical_depth > 2.0)
      albedo = (optical_depth-pow(2.0,(double)(bin)))*(albedou-albedol)/
                  (pow(2.0,(double)(bin+1)) - pow(2.0,(double)(bin))) +
                  albedol;
   else
      albedo = (optical_depth)*(albedou-albedol)/2.0 + albedol;

   return albedo;
}

double get_dir_albedo(double optical_depth, double angle)
{
   double albedo20l, albedo20u, albedo20;
   double albedo70l, albedo70u, albedo70;

   double albedo;
   int bin, int_optical_depth;

   static double fixed_albedo20[11] = {0.000,
                                        0.090,
                                        0.179,
```

```
                                          0.327,
                                          0.520,
                                          0.699,
                                          0.828,
                                          0.907,
                                          0.952,
                                          0.975,
                                          1.000};
static double fixed_albedo70[11] = {0.000,
                                          0.311,
                                          0.438,
                                          0.567,
                                          0.697,
                                          0.811,
                                          0.892,
                                          0.942,
                                          0.970,
                                          0.984,
                                          1.000};

if (optical_depth > 1000.0)
   return 1.0;

int_optical_depth = (int) optical_depth;
for (bin=0;(int_optical_depth/=2)>0;bin++)
   ;

albedo20l = fixed_albedo20[bin];
albedo20u = fixed_albedo20[bin+1];
albedo70l = fixed_albedo70[bin];
albedo70u = fixed_albedo70[bin+1];

if (optical_depth > 2.0)
{
   albedo20 = (optical_depth-pow(2.0,(double)(bin)))*(albedo20u-albedo20l)/
              (pow(2.0,(double)(bin+1)) - pow(2.0,(double)(bin))) +
              albedo20l;
   albedo70 = (optical_depth-pow(2.0,(double)(bin)))*(albedo70u-albedo70l)/
              (pow(2.0,(double)(bin+1)) - pow(2.0,(double)(bin))) +
              albedo70l;
}
else
{
   albedo20 = (optical_depth)*(albedo20u-albedo20l)/2.0 + albedo20l;
```

```
    albedo70 = (optical_depth)*(albedo70u-albedo70l)/2.0 + albedo70l;
  }

  /* 0.87266 = 50 degrees, the difference between 70 and 20 */
  albedo = angle*(albedo70-albedo20)/0.87266 + albedo20;

  return albedo;
}

double avg(double arr[], int i, int j)
{
  return ((arr[i]+arr[j])/2.0);
}

double get_layer_density(double *M, double Z[][2], double *deltaM)
{
  double totalM = 0;
  int k;

  for (k=0;k<SPACE_POINTS;k++)
    totalM += (M[k]*Z[k][1]);
  for (k=0;k<SPACE_POINTS;k++)
    deltaM[k] = M[k]*Z[k][1]/totalM;

  return totalM;
}

double get_O3_optical_depth(int k, double *O3_column, double temp,
                            double actinic_flux_bin)
{
  double O3_optical_depth;
  extern double getO3ACS(double, double);

  if (k == SPACE_POINTS-1)
    O3_optical_depth = O3_column[k] * getO3ACS(actinic_flux_bin,temp);
  else
    O3_optical_depth = (O3_column[k]-O3_column[k+1]) *
                       getO3ACS(actinic_flux_bin,temp);

  return O3_optical_depth;
}
```

A.9 getcons.c

```
/* Function: get_cons
 *
 * Copyright 1993 F. Moraes and M.A.K. Khalil
 *
 * Permission to use, copy, modify, and distribute this software and its
 * documentation for any purpose and without fee is hereby granted, provided
 * that the above copyright notice appear in all copies and that both that
 * copyright notice and this permission notice appear in supporting
 * documentation. No representation is made about the suitability of this
 * software for any purpose.  It is provided "as is" without express or
 * implied warranty.
 *
 * Author: Francis Moraes (internet: francis@eeyore.atmos.ogi.edu)
 *         Global Change Research Center
 *         Oregon Graduate Institute
 *
 * Synopsis: Given initial values for the 'reactive' species in the model,
 *           this function iteratively solves for the species using the
 *           complete chemistry (unlike the initial values which were
 *           based upon a subset of the chemistry affecting the species).
 *
 * VARIABLES:
 *
 * Kz is an array that hold Kz values for various atmospheric layers. I have
 * set up this array so that Kz[1] is the Kz value BETWEEN the 0 and 1
 * layers, thus it is really Kz[1/2]. This makes the calculations simpler.
 *
 * GLOBAL VARIABLES:
 *
 * This function uses the usual concentrations, and reaction constants.
 *
 * FUNCTIONS:
 *
 * change        This function calculates the relative change in
 *               concentrations.
 * avgM          Average two M (density) values.
 * getM          Get a particular M (density) value, takes care of array
 *               ends.
 * trans        Transport code put into a function to simplify coding.
 *               There are two terms, one for the numerator and one for
 *               the denominator.
 *
 * PROGRAM FLOW:
 *
```

```
 * The convergence variable is set to 0 and as long as,
 * after every complete iteration, it is still 0 the function will
 * continue to iterate. At the begin of each iteration sequence, the
 * convergence variable is set to 1.  For each time step and each spatial
 * step, the new concentration is solved for. If the relative fractional
 * change of a species is more than the criterion value (crit) then the
 * convergence variable is set back to 0. This procedure is completed
 * until convergence is attained. The only tricky part about all of this
 * is that, since time is cyclical, the last time step is the same as
 * the first time step. To simplify the code (actually to reduce the amount
 * of code), it is necessary to copy the last time-step data into the
 * first time step.
 */

#include <math.h>
#include <stdio.h>

#include "acm.h"
#include "rxn.h"
#include "gases.h"
#include "solve.h"

#define DELTAT (86400.0/TIME_POINTS)

void get_cons(int *solve, double crit, double *Kz, double Z[][2], double *M)
{
   int i, j, convergence = 0, iteration = 0;
   double a, b, c, oldcon, rho, rhop, rhom, newCH4[SPACE_POINTS+2];

   double change(double, double),
             avgM(int, double *),
             getM(int, double *),
          trans(int, double [][], int, int, double, double, double *);

   double p1, p2, p3, p4, d1, d2, d3;

   extern void get_data(char *, double *, int);

   while (convergence == 0)
   {
      convergence = 1;

      for (j=0;j<TIME_POINTS;j++)
      {
```

```
for (i=1;i<SPACE_POINTS+1;i++)
{
   rho = DELTAT / (Z[i-1][1]*Z[i-1][1]);

   if (i == 1)
   {
      rhop = DELTAT/(Z[i-1][1]*((Z[i][1]+Z[i-1][1])/2.0))*
                Kz[i+1]*avgM(i+1,M);
      rhom = 0;
   }
   else if (i == SPACE_POINTS)
   {
      rhom = DELTAT/(Z[i-1][1]*((Z[i-2][1]+Z[i-1][1])/2.0))*
                Kz[i]*avgM(i,M);
      rhop = 0;
   }
   else
   {
      rhop = DELTAT/(Z[i-1][1]*((Z[i][1]+Z[i-1][1])/2.0))*
                Kz[i+1]*avgM(i+1,M);
      rhom = DELTAT/(Z[i-1][1]*((Z[i-2][1]+Z[i-1][1])/2.0))*
                Kz[i]*avgM(i,M);
   }
   rhop = rhom = 0.0;

   if (solve[IO1D] == 1)
   {
      oldcon = O1D[i][j+1];

      O1D[i][j+1] = (JO3[i][j]*O3[i][j])/
                    (KO1D_N2[i]*N2[i] + KO1D_O2[i]*O2[i] +
                     KO1D_H2O[i]*H2O[i] + KO1D_H2[i]*H2[i] +
                     KH2_O1D[i]*H2[i] +
                     (KO1D_CH4a[i]+KO1D_CH4b[i])*CH4[i][j]);

      if (change(oldcon,O1D[i][j+1]) > crit)
         convergence = 0;
   }

   if (solve[IO] == 1)
   {
      oldcon = O[i][j+1];
      O[i][j+1] = ((JNO2[i][j+1]*NO2[i][j+1] +
                    JO3b[i][j]*O3[i][j] +
```

```
                    JNO3b[i][j+1]*NO3[i][j+1] +
                    KOH_OHa[i]*OH[i][j+1]*OH[i][j+1] +
                    /* Only a small percent of this reaction */
                    /* produces H2O+O */
                    0.02 * KH_HO2[i]*H[i][j+1]*HO2[i][j+1] +
                    (KO1D_N2[i]*N2[i] + KO1D_O2[i]*O2[i])*
                    O1D[i][j+1]))/
                    (KO_O2[i]*O2[i] + KO_NO2[i]*NO2[i][j+1] +
                     KNO_O[i]*NO[i][j+1] + KOH_O[i]*OH[i][j+1] +
                     KH2_O[i]*H2[i] +
                     KHO2_O[i]*HO2[i][j+1] +
                     KH2O2_O[i]*H2O2[i][j+1] +
                     KH2CO_O[i]*H2CO[i][j+1] +
                     KO_O3[i]*O3[i][j]);

   if (change(oldcon,O[i][j+1]) > crit)
      convergence = 0;
}

if (solve[IH])
{
   oldcon = H[i][j+1];

   H[i][j+1] = (JH2COa[i][j]*H2CO[i][j+1] +
               KH2_O[i]*H2[i]*O[i][j+1] +
               KH2_O1D[i]*H2[i]*O1D[i][j+1] +
               (KOH_O[i]*O[i][j+1] +
                KOH_H2[i]*H2[i] + KOH_CO[i]*CO[i])*OH[i][j+1]) /
               (KH_O2[i]*O2[i] + KH_HO2[i]*HO2[i][j+1] +
                KH_O3[i]*O3[i][j]);

   if (change(oldcon,H[i][j+1]) > crit)
      convergence = 0;
}

if (solve[IH2O2] == 1)
{
   oldcon = H2O2[i][j+1];

   H2O2[i][j+1] = (((KHO2_HO2a[i]+KHO2_HO2b[i]) *
                  HO2[i][j+1]*HO2[i][j+1] +
                  KOH_OHb[i]*OH[i][j+1]*OH[i][j+1])*DELTAT +
                  H2O2[i][j] +
                  trans(0,H2O2,i,j,rhop,rhom,M))/
```

```
                    ((KOH_H2O2[i]*OH[i][j+1] + Khet[i] +
                     KH2O2_O[i]*O[i][j+1] +
                     JH2O2[i][j+1])*DELTAT + 1.0 +
                    trans(1,H2O2,i,j,rhop,rhom,M));

   if (change(oldcon,H2O2[i][j+1]) > crit)
      convergence = 0;
}

if (solve[INO] == 1)
{
   oldcon = NO[i][j+1];
   NO[i][j+1] = ((JNO2[i][j+1]*NOX[i] +
                  KO_NO2[i]*NO2[i][j]*O[i][j+1] +
                  JNO3a[i][j+1]*NO3[i][j+1])*
                 DELTAT + NO[i][j] + trans(0,NO,i,j,rhop,rhom,M))/
                ((KCH3O2_NO[i]*CH3O2[i][j+1] +
                  KNO_HO2[i]*HO2[i][j+1] + KNO_O3[i]*O3[i][j] +
                  KNO_NO3[i]*NO3[i][j+1] +
                  KNO_O[i]*O[i][j+1] +
                  JNO2[i][j+1])*DELTAT + 1.0 +
                  trans(1,NO,i,j,rhop,rhom,M));

   if (change(oldcon,NO[i][j+1]) > crit)
      convergence = 0;
}

if (solve[INO2] == 1)
{
   oldcon = NO2[i][j+1];
   NO2[i][j+1] = ((KN2O5[i]*N2O5[i][j+1] +
                   KNO_O[i]*NO[i][j+1] +
                   /* See page 7 of notebook */
                   2.0*JHO2NO2[i][j+1]*HO2NO2[i][j+1] +
                   KHO2NO2[i]*HO2NO2[i][j+1] +
                   JNO3b[i][j+1]*NO3[i][j+1] +
                   JN2O5[i][j+1]*N2O5[i][j+1] +
                   JHNO3[i][j+1]*HNO3[i] +
                   KOH_HO2NO2[i]*OH[i][j+1]*HO2NO2[i][j+1] +
                   (KNO_HO2[i]*HO2[i][j+1] + KNO_O3[i]*O3[i][j] +
                    2.0*KNO_NO3[i]*NO3[i][j+1] +
                    KCH3O2_NO[i]*CH3O2[i][j+1])*NOX[i])*DELTAT +
                    NO2[i][j] + trans(0,NO2,i,j,rhop,rhom,M))/
                 ((KOH_NO2[i]*OH[i][j+1] +
```

```
                    KO_NO2[i]*O[i][j+1] +
                    (KNO_HO2[i] /*+ KNO_HO2[i]*/)*
                    HO2[i][j+1] + (KNO2_NO3[i] + 2.0*KNO_NO3[i]) *
                    NO3[i][j+1] + (/*KNO2_CH3O2[i]+*/KCH3O2_NO[i])*
                    CH3O2[i][j+1] + JNO2[i][j+1] +
                    (KNO2_O3[i]+KNO_O3[i])*O3[i][j])*DELTAT + 1.0 +
                    trans(1,NO2,i,j,rhop,rhom,M));

   if (change(oldcon,NO2[i][j+1]) > crit)
      convergence = 0;
}

if (solve[IHO2NO2] == 1)
{
   oldcon = HO2NO2[i][j+1];
   HO2NO2[i][j+1] = (KHO2_NO2[i]*HO2[i][j+1]*NO2[i][j+1]*DELTAT +
                     HO2NO2[i][j] +
                     0.0*trans(0,HO2NO2,i,j,rhop,rhom,M))/
                    /* Assuming AMT, only HO2NO2->HO2+NO2 */
                    /* See notebook, page 7 */
                    ((Khet[i] + KHO2NO2[i] + 2.0*JHO2NO2[i][j+1] +
                      KOH_HO2NO2[i]*OH[i][j+1]) * DELTAT + 1.0 +
                     0.0*trans(1,HO2NO2,i,j,rhop,rhom,M));

   if (change(oldcon,HO2NO2[i][j+1]) > crit)
      convergence = 0;
}

if (solve[INO3] == 1)
{
   oldcon = NO3[i][j+1];
   NO3[i][j+1] = (((KN2O5[i]+JN2O5[i][j+1])*N2O5[i][j+1] +
                    KOH_HNO3[i]*OH[i][j+1]*HNO3[i] +
                    KNO2_O3[i]*NO2[i][j+1]*O3[i][j])*DELTAT +
                    NO3[i][j] + trans(0,NO3,i,j,rhop,rhom,M))/
                  ((KNO2_NO3[i]*NO2[i][j+1] + JNO3a[i][j+1] +
                    JNO3b[i][j+1]+KNO_NO3[i]*NO[i][j+1])*DELTAT +
                   1.0 + trans(1,NO3,i,j,rhop,rhom,M));

   if (change(oldcon,NO3[i][j+1]) > crit)
      convergence = 0;
}

if (solve[IN2O5] == 1)
```

```
{
   oldcon = N2O5[i][j+1];
   N2O5[i][j+1] = (KNO2_NO3[i]*NO2[i][j+1]*NO3[i][j+1]*DELTAT +
                   N2O5[i][j] + trans(0,N2O5,i,j,rhop,rhom,M))/
                   ((KN2O5[i]+JN2O5[i][j+1])*DELTAT + 1.0 +
                   trans(1,N2O5,i,j,rhop,rhom,M));

   if (change(oldcon,N2O5[i][j+1]) > crit)
      convergence = 0;
}

if (solve[ICH3] == 1)
{
   oldcon = CH3[i][j+1];
   CH3[i][j+1] = ((KO1D_CH4a[i]*O1D[i][j+1]+KOH_CH4[i]*OH[i][j+1])*
                  CH4[i][j]*DELTAT + CH3[i][j] +
                  trans(0,CH3,i,j,rhop,rhom,M))/
                 (KCH3_O2[i]*O2[i]*DELTAT + 1.0 +
                 trans(1,CH3,i,j,rhop,rhom,M));

   if (change(oldcon,CH3[i][j+1]) > crit)
      convergence = 0;
}

if (solve[ICH3O2] == 1)
{
   oldcon = CH3O2[i][j+1];
   a = KCH3O2_CH3O2[i]*DELTAT;
   b = (/*KNO2_CH3O2[i]*NO2[i][j+1] +*/ KCH3O2_HO2[i]*HO2[i][j+1] +
        KCH3O2_NO[i]*NO[i][j+1])*DELTAT + 1.0;
   c = (KCH3_O2[i]*O2[i]*CH3[i][j+1] +
        KOH_CH3OOH[i]*OH[i][j+1]*CH3OOH[i][j+1])*DELTAT +
        CH3O2[i][j];
   CH3O2[i][j+1] = 2.0 * c / ( b + sqrt(b*b + 4*a*c) );

   if (change(oldcon,CH3O2[i][j+1]) > crit)
      convergence = 0;
}

if (solve[ICH3OOH] == 1)
{
   oldcon = CH3OOH[i][j+1];
   CH3OOH[i][j+1] = (KCH3O2_HO2[i]*CH3O2[i][j+1] *
                     HO2[i][j+1]*DELTAT + CH3OOH[i][j] +
```

```
                     trans(0,CH3OOH,i,j,rhop,rhom,M))/
                    ((Khet[i] + JCH3OOH[i][j+1] +
                      KOH_CH3OOH[i]*OH[i][j+1])*DELTAT + 1.0 +
                      trans(1,CH3OOH,i,j,rhop,rhom,M));

   if (change(oldcon,CH3OOH[i][j+1]) > crit)
      convergence = 0;
}

if (solve[ICH3O] == 1)
{
   oldcon = CH3O[i][j+1];
   CH3O[i][j+1] = ((JCH3OOH[i][j+1]*CH3OOH[i][j+1] +
                    KCH3O2_NO[i]*CH3O2[i][j+1]*NO[i][j+1])*DELTAT +
                   CH3O[i][j] + trans(0,CH3O,i,j,rhop,rhom,M))/
                   (KCH3O_O2[i]*O2[i]*DELTAT + 1.0 +
                   trans(1,CH3O,i,j,rhop,rhom,M));

   if (change(oldcon,CH3O[i][j+1]) > crit)
      convergence = 0;
}

if (solve[IH2CO] == 1)
{
   oldcon = H2CO[i][j+1];
   H2CO[i][j+1] = ((KO1D_CH4b[i]*O1D[i][j+1]*CH4[i][j] +
                    KCH3O_O2[i]*CH3O[i][j+1]*O2[i] /*+
                    KCH3O2_CH3O2[i]*CH3O2[i][j+1]*CH3O2[i][j+1]*/) *
                   DELTAT + H2CO[i][j] +
                   trans(0,H2CO,i,j,rhop,rhom,M))/
                  ((Khet[i] + JH2COa[i][j+1] + JH2COb[i][j+1] +
                    KH2CO_O[i]*O[i][j+1] +
                    KOH_H2CO[i]*OH[i][j+1])*DELTAT + 1.0 +
                    trans(1,H2CO,i,j,rhop,rhom,M));

   if (change(oldcon,H2CO[i][j+1]) > crit)
      convergence = 0;
}

if (solve[IHCO] == 1)
{
   oldcon = HCO[i][j+1];
   HCO[i][j+1] = ((JH2COa[i][j+1]*H2CO[i][j+1] +
                   KH2CO_O[i]*H2CO[i][j+1]*O[i][j+1] +
```

```
                 KOH_H2CO[i]*OH[i][j+1]*H2CO[i][j+1])*DELTAT +
                HCO[i][j] + trans(0,HCO,i,j,rhop,rhom,M)) /
                (KHCO_O2[i]*O2[i]*DELTAT + 1.0 +
                trans(1,HCO,i,j,rhop,rhom,M));

   if (change(oldcon,HCO[i][j+1]) > crit)
      convergence = 0;
}

if (solve[IHO2] == 1)
{
   oldcon = HO2[i][j+1];

   a = (KHO2_HO2a[i] + KHO2_HO2b[i]);
   b = (KHO2_O3[i]*O3[i][j+1] + KOH_HO2[i]*OH[i][j+1] +
        KNO_HO2[i]*NO[i][j+1] + KHO2_NO2[i]*NO2[i][j+1] +
        KCH3O2_HO2[i]*CH3O2[i][j+1]);
   c = -((KOH_O3[i]*O3[i][j+1] + KOH_H2O2[i]*H2O2[i][j+1])*
        OH[i][j+1] + KCH3O_O2[i]*CH3O[i][j+1]*O2[i] +
        KH_O2[i]*H[i][j+1]*O2[i] +
        KH2O2_O[i]*H2O2[i][j+1]*O[i][j+1] +
        KHCO_O2[i]*HCO[i][j+1]*O2[i] +

        2.0*JHO2NO2[i][j+1]*HO2NO2[i][j+1] +
        KHO2NO2[i]*HO2NO2[i][j+1]);

   HO2[i][j+1] = -2.0 * c / ( b + sqrt(b*b - 4*a*c) );

   if (change(oldcon,HO2[i][j+1]) > crit)
      convergence = 0;
}

if (solve[IOH] == 1)
{
   oldcon = OH[i][j+1];
   OH[i][j+1] = ((
                2.0*JH2O2[i][j+1]*H2O2[i][j+1] +
                JHNO3[i][j+1]*HNO3[i] +
                KH_O3[i]*H[i][j+1]*O3[i][j] +
                /* The 0.9 term comes from the fact that */
                /* only about 90% of this reaction produces */
                /* HO+HO. The rest produces H2+O2 and H2O+O */
                2.0*0.9*KH_HO2[i]*H[i][j+1]*HO2[i][j+1] +
                KH2CO_O[i]*H2CO[i][j+1]*O[i][j+1] +
```

```
                    KH2O2_O[i]*H2O2[i][j+1]*O[i][j+1] +
                    KHO2_O[i]*HO2[i][j+1]*O[i][j+1] +
                    KH2_O[i]*O[i][j+1]*H2[i] +
                    KH2_O1D[i]*O1D[i][j+1]*H2[i] +
                    JCH3OOH[i][j+1]*CH3OOH[i][j+1] +
                    (2.0*KO1D_H2O[i]*H2O[i] + KO1D_H2[i]*H2[i] +
                     KO1D_CH4a[i]*CH4[i][j+1] )*O1D[i][j+1] +
                    (KHO2_O3[i]*O3[i][j+1] + KNO_HO2[i]*NO[i][j+1])*
                    HO2[i][j+1]) * DELTAT + OH[i][j] +
                    trans(0,OH,i,j,rhop,rhom,M))/
                   (((KOH_NO2[i]*NO2[i][j+1]) +
                    KOH_H2[i]*H2[i] + KOH_O3[i]*O3[i][j+1] +
                    KOH_HO2[i]*HO2[i][j+1] +
                    KOH_H2O2[i]*H2O2[i][j+1] +
                    KOH_CO[i]*CO[i] +
                    KOH_CH4[i]*CH4[i][j+1] +
                    KOH_H2CO[i]*H2CO[i][j+1] +
                    KOH_CH3OOH[i]*CH3OOH[i][j+1])*DELTAT + 1.0 +
                    trans(1,OH,i,j,rhop,rhom,M));

         if (change(oldcon,OH[i][j+1]) > crit)
            convergence = 0;

      }
   }

   /* now put the last element in the first element;
      this is because the time is cyclical. */

   if (j == TIME_POINTS-1)
   {
      for (i=1;i<SPACE_POINTS+1;i++)
      {
         O1D[i][0] = O1D[i][TIME_POINTS];
         O[i][0] = O[i][TIME_POINTS];
         OH[i][0] = OH[i][TIME_POINTS];
         H[i][0] = H[i][TIME_POINTS];
         HO2[i][0] = HO2[i][TIME_POINTS];
         H2O2[i][0] = H2O2[i][TIME_POINTS];
         NO[i][0] = NO[i][TIME_POINTS];
         HNO2[i][0] = HNO2[i][TIME_POINTS];
         NO2[i][0] = NO2[i][TIME_POINTS];
         HO2NO2[i][0] = HO2NO2[i][TIME_POINTS];
         NO3[i][0] = NO3[i][TIME_POINTS];
```

```
                N205[i][0] = N205[i][TIME_POINTS];
                CH3[i][0] = CH3[i][TIME_POINTS];
                CH302[i][0] = CH302[i][TIME_POINTS];
                CH300H[i][0] = CH300H[i][TIME_POINTS];
                CH30[i][0] = CH30[i][TIME_POINTS];
                H2CO[i][0] = H2CO[i][TIME_POINTS];
                HCO[i][0] = HCO[i][TIME_POINTS];
            }
         }
      }
   }
}

double change(double old,double new)
{
   if (new > 0)
      return fabs((old-new)/new);
   else
      return 0.0;
}

double avgM(int pos, double *M)
{
   if (pos == 0)
      return (M[0]);
   else if (pos == SPACE_POINTS)
      return (M[SPACE_POINTS-1]);
   else
      return ((M[pos-1]+M[pos])/2);
}
double getM(int pos, double *M)
{
   if (pos == 0)
      return M[1];
   else if (pos == SPACE_POINTS)
      return M[SPACE_POINTS-1];
   else
      return M[pos];
}

double trans(int which, double con[SPACE_POINTS+2][TIME_POINTS+1],
             int i, int j, double rhop, double rhom, double *M)
{
   double retval;
```

```
   if (which == 0)
   {
      retval = rhom*con[i-1][j]/getM(i-1,M) +
               rhop*con[i+1][j]/getM(i+1,M);
   }
   else
      retval = rhom/getM(i,M) + rhop/getM(i,M);

   return retval;
}
```

A.10 getdata.c

```
/* Function: get...data (various functions)
 *
 * Copyright 1993 F. Moraes and M.A.K. Khalil
 *
 * Permission to use, copy, modify, and distribute this software and its
 * documentation for any purpose and without fee is hereby granted, provided
 * that the above copyright notice appear in all copies and that both that
 * copyright notice and this permission notice appear in supporting
 * documentation. No representation is made about the suitability of this
 * software for any purpose.  It is provided "as is" without express or
 * implied warranty.
 *
 * Purpose: This file contains five functions for inputing data from file:
 *
 *       get_data: This function reads a data file which consists of a
 *               single number per row. The number is assumed to be
 *               double precision.
 *
 *       get_2_data: This function reads a data file which consists of
 *               two numbers per row. The numbers are assumed to be double
 *               precision.
 *
 *       get_3_data: This function reads a data file which consists of
 *               three numbers per row. The numbers are assumed to be double
 *               precision.
 *
 *       get_par_data: This function reads the parameter file data. Because
 *               this file will be changed often, this function is smarter
 *               than the other functions in terms of reading the data. In
 *               particular, this function skips commented lines (lines that
```

```
 *              begin with the '#' character).
 *
 *      get_seasonal_data: This function reads a data file which consists
 *              of 6 columns of numbers representing the latitude, height,
 *              and then winter, spring, summer, fall concentrations of a
 *              given gas. It extracts the correct season for use in the
 *              model
 *
 * In addition, this file contains a general purpose utility function,
 * exit_error, which prints an error message to the standard error and
 * exits the program.
 */

#include <stdio.h>
#include "acm.h"

/* FUNCTION: get_data
 *
 * PASSED VARIABLES
 *
 * fname        The name of the data file to be opened.
 * data                 An array to hold the data read
 * max                  The maximum number of data points to read
 */

void get_data(char *fname, double *data, int max)
{
   FILE *fp;
   int i;
   extern void exit_error(char *);

   if ( (fp=fopen(fname,"r")) == NULL)
      exit_error(fname);

   for (i=0;fscanf(fp,"%lf", data+i) != EOF && i<max;i++)
      ;

   fclose(fp);
}

/* FUNCTION: get_data
 *
 * PASSED VARIABLES
 *
```

```
 * fname        The name of the data file to be opened.
 * data                 A 2-D array into which the data is read.
 */

int get_2_data(char *fname, double data[][2])
{
   int i;
   FILE *fp;
   extern void exit_error(char *);

   if ( (fp=fopen(fname,"r")) == NULL)
      exit_error(fname);

   for (i=0;fscanf(fp,"%lf %lf", &(data[i][0]), &(data[i][1])) != EOF;i++)
      ;

   fclose(fp);

   return i;
}

/* FUNCTION: get_data
 *
 * PASSED VARIABLES
 *
 * fname        The name of the data file to be opened.
 * data                 A 3-D array into which the data is read.
 */

int get_3_data(char *fname, double data[][3])
{
   int i;
   FILE *fp;
   extern void exit_error(char *);

   if ( (fp=fopen(fname,"r")) == NULL)
      exit_error(fname);

   for (i=0;fscanf(fp,"%lf %lf %lf", &(data[i][0]),
                                     &(data[i][1]),
                                     &(data[i][2])) != EOF;i++)
      ;

   fclose(fp);
```

```
   return i;
}

/* FUNCTION: get_data
 *
 * PASSED VARIABLES
 *
 * fname        The name of the data file to be opened.
 * a                An array whose elements correspond to each of the
 *                chemicals in the model and which tell the model
 *                whether to solve for the chemical (1) or not (0).
 * b                The type of output requested by the user:
 *                      0       none
 *                      1       time
 *                      2       height
 *                      3       total column
 *                      4       diurnally averaged height
 * c                The same as for 'a' except that it determines
 *                whether the chemical will be output and if so how.
 * albedo        The ground albedo
 * cloud_layer_top A three element array indicating where high,
 *                middle, and low clouds occur (a zero value indicates
 *                that there is no cloud)
 * cloud_optical_depth A three element array indicating the optical
 *                depth of the high, middle, and low clouds.
 * baseH2O        The surface relative humidity.
 */

void get_par_data(char *fname,int *a, int *b, int *c, double *crit)
/* double *albedo,
                  int cloud_layer_top[],
                  double cloud_optical_depth[], double *baseH2O) */
{
   FILE *fp;
   char s[256];
   extern int getline(FILE *, char *);
   extern void exit_error(char *);
   int i;

   if ( (fp=fopen("par.dat","r")) == NULL)
   {
      if ( (fp=fopen(fname,"r")) == NULL)
      {
```

```
            fprintf(stderr, "Error reading file %s.\n", fname);
            exit(1);
         }
      }

      if (getline(fp,s) == EOF)
         exit_error(fname);

      sscanf(s,"%d %d %d %d %d %d %d %d %d %d %d %d %d %d %d %d %d %d %d",
            &a[0], &a[1], &a[2], &a[3], &a[4], &a[5], &a[6], &a[7],
            &a[8], &a[9], &a[10], &a[11], &a[12], &a[13], &a[14],
            &a[15], &a[16], &a[17], &a[18]);

      if (getline(fp,s) == EOF)
         exit_error(fname);

      sscanf(s,"%d", b);

      if (getline(fp,s) == EOF)
         exit_error(fname);

      sscanf(s,"%d %d %d %d %d %d %d %d %d %d %d %d %d %d %d %d %d %d %d",
            &c[0], &c[1], &c[2], &c[3], &c[4], &c[5], &c[6], &c[7],
            &c[8], &c[9], &c[10], &c[11], &c[12], &c[13], &c[14],
            &c[15], &c[16], &c[17], &c[18]);

      if (getline(fp,s) == EOF)
         exit_error(fname);

      sscanf(s,"%lf", crit);

      fclose(fp);

      return;
}

get_seasonal_data(char *fname, double *con, int num, double lat, int season)
{
      int i, j, skip;
      double c[4], z;
      char s[256];
      FILE *fp;
      extern void exit_error(char *);
```

```
   if ( (fp=fopen(fname,"r")) == NULL)
   {
      fprintf(stderr, "Error reading file %s.\n", fname);
      exit(1);
   }

   skip = (170 - ((int) (180*lat/3.1415) + 85))/10;

   for (i=0;i<skip;i++)
     {
      for (j=0;j<num;j++)
        {
         if (getline(fp,s) == EOF)
            exit_error(fname);
        }
     }

   for (j=0;j<num;j++)
   {
      if (getline(fp,s) == EOF)
         exit_error(fname);

      sscanf(s,"%d %lf %lf %lf %lf %lf", &lat, &z, c+0, c+1, c+2, c+3);
      con[j] = c[season];
   }

   fclose(fp);

   return;
}

void exit_error(char *str)
{
   perror(str);
   exit(1);
}
```

A.11 getinit.c

```
/* Function: get_init
 *
 * Copyright 1993 F. Moraes and M.A.K. Khalil
 *
 * Permission to use, copy, modify, and distribute this software and its
```

```
 * documentation for any purpose and without fee is hereby granted, provided
 * that the above copyright notice appear in all copies and that both that
 * copyright notice and this permission notice appear in supporting
 * documentation. No representation is made about the suitability of this
 * software for any purpose.  It is provided "as is" without express or
 * implied warranty.
 *
 * Author: Francis Moraes (internet: francis@eeyore.atmos.ogi.edu)
 *         Global Change Research Center
 *         Oregon Graduate Institute
 *
 * Synopsis: Calculate initial values for iterative solution.
 *
 * VARIABLES:
 *
 * none to speak of
 *
 * GLOBAL VARIABLES:
 *
 * The usual concentration and rate constant variables.
 *
 * FUNCTIONS:
 *
 * none
 *
 * PROGRAM FLOW:
 *
 * Initial values are determined base upon known quantities.
 *
 */

#include <math.h>
#include <stdio.h>
#include "acm.h"
#include "rxn.h"
#include "gases.h"
#include "solve.h"

void get_initial_cons(int *solve, double Z[][2],double *M, double nox)
{
   int i, j;
   double a, b, c;
   FILE *fp;
```

```
for (j=0;j<=TIME_POINTS;j++)
{
   for (i=1;i<SPACE_POINTS+1;i++)
   {
      if (solve[IO1D] == 1)
         O1D[i][j] = O3[i][j] * JO3[i][j] /
                     ( KO1D_N2[i]*N2[i] + KO1D_O2[i]*O2[i] +
                       KO1D_H2O[i]*H2O[i] );
      else
         O1D[i][j] = 0.0;

      if (solve[IO] == 1)
         O[i][j] = ( KO1D_N2[i]*N2[i] + KO1D_O2[i]*O2[i] ) * O1D[i][j] /
                   ( KO_O2[i] * O2[i] );
      else
         O[i][j] = 0.0;

      if (solve[IOH] == 1)
         OH[i][j] = 2.0 * KO1D_H2O[i] * O1D[i][j] * H2O[i] /
                    ( KOH_CO[i] * CO[i] + KOH_CH4[i] * CH4[i-1][j] );
      else
         OH[i][j] = 0.0;

      if (solve[IH] == 1)
         H[i][j] = ( (KO1D_H2[i]*O1D[i][j] + KOH_H2[i]*OH[i][j])*H2[i] +
                     KOH_CO[i]*OH[i][j]*CO[i] ) / (KH_O2[i]*O2[i]);
      else
         H[i][j] = 0.0;

      if (solve[IHO2] == 1)
      {
         a = KHO2_HO2a[i] + KHO2_HO2b[i];
         b = KHO2_O3[i]*O3[i][j] + KOH_HO2[i]*OH[i][j];
         c = KOH_O3[i]*OH[i][j]*O3[i][j] + KH_O2[i]*H[i][j]*O2[i];
         HO2[i][j] = 2.0 * c / ( b + sqrt(b*b + 4*a*c) );
      }
      else
         HO2[i][j] = 0.0;

      if (solve[IH2O2] == 1)
      {
         if ( (a=(KOH_H2O2[i]*OH[i][j] + Khet[i] + JH2O2[i][j])) > 0.0)
            H2O2[i][j] = (KHO2_HO2a[i]+KHO2_HO2b[i])*HO2[i][j]*HO2[i][j]/a;
         else
```

```
        H2O2[i][j] = 0.0;
    }
    else
        H2O2[i][j] = 0.0;

    if (solve[INO] == 1)
        NO[i][j] = (2.0*KO1D_N2O[i]*O1D[i][j]*N2O[i] + JNO2[i][j]*NOX[i] )/
                   (KNO_HO2[i]*HO2[i][j] + KNO_O3[i]*O3[i][j] + JNO2[i][j]+
                    KOH_NO[i]*OH[i][j] );
    else
        NO[i][j] = 0.0;

    if (solve[IHNO2] == 1)
    {
        if ( (a=(Khet[i] + JHNO2[i][j])) > 0.0)
            HNO2[i][j] = KOH_NO[i]*OH[i][j]*NO[i][j] / a;
        else
            HNO2[i][j] = 0.0;
    }
    else
        HNO2[i][j] = 0.0;

    if (solve[INO2] == 1)
        NO2[i][j] = ( JHNO3[i][j]*HNO3[i] + KNO_HO2[i]*NOX[i]*HO2[i][j]+
                      KNO_O3[i]*NOX[i]*O3[i][j] ) / ( KOH_NO2[i]*OH[i][j] +
                      (KHO2_NO2[i]+KNO_HO2[i])*HO2[i][j] + JNO2[i][j] +
                      (KNO_O3[i]+KNO2_O3[i])*O3[i][j] );
    else
    {
        NO2[i][j] = nox*M[i-1]*1e-12;
        NO[i][j] = .25*NO2[i][j];
    }

    if (solve[IHO2NO2] == 1)
        HO2NO2[i][j] = KHO2_NO2[i]*HO2[i][j]*NO2[i][j] /
                       ( Khet[i] + KHO2NO2[i] + JHO2NO2[i][j] );
    else
        HO2NO2[i][j] = 0.0;

    if (solve[INO3] == 1)
        NO3[i][j] = ( JHO2NO2[i][j]*HO2NO2[i][j] +
                      KNO2_O3[i]*NO2[i][j]*O3[i][j] ) /
                    ( KNO2_NO3[i]*NO2[i][j] + JNO3a[i][j] + JNO3b[i][j] +
                      KNO_NO3[i]*NO[i][j] );
```

```
else
   NO3[i][j] = 0.0;

if (solve[IN2O5] == 1)
   N2O5[i][j] = KNO2_NO3[i]*NO2[i][j]*NO3[i][j]/(KN2O5[i]+JN2O5[i][j]);
else
   N2O5[i][j] = 0.0;

if (solve[ICH3] == 1)
   CH3[i][j] = (KO1D_CH4a[i]*O1D[i][j] + KOH_CH4[i]*OH[i][j])*
               CH4[i-1][j] / ( KCH3_O2[i]*O2[i] );
else
   CH3[i][j] = 0.0;

if (solve[ICH3O2] == 1)
{
   a = 3.0 * KCH3O2_CH3O2[i];
   b = KNO2_CH3O2[i]*NO2[i][j] + KCH3O2_HO2[i]*HO2[i][j] +
       KCH3O2_NO[i]*NO[i][j];
   c = KCH3_O2[i] * O2[i] * CH3[i][j];
   CH3O2[i][j] = 2.0 * c / ( b + sqrt(b*b + 4*a*c) );
}
else
   CH3O2[i][j] = 0.0;

if (solve[ICH3OOH] == 1)
{
   if ( (a=Khet[i] + JCH3OOH[i][j] + KOH_CH3OOH[i]*OH[i][j]) > 0.0)
      CH3OOH[i][j] = KCH3O2_HO2[i]*CH3O2[i][j]*HO2[i][j] / a;
   else
      CH3OOH[i][j] = 0.0;
}
else
   CH3OOH[i][j] = 0.0;

if (solve[ICH3O] == 1)
   CH3O[i][j] = ( 2.0*KCH3O2_CH3O2[i]*CH3O2[i][j]*CH3O2[i][j] +
                  JCH3OOH[i][j] + KCH3O2_NO[i]*CH3O2[i][j]*NO[i][j] ) /
                ( KCH3O_O2[i]*O2[i] );
else
   CH3O[i][j] = 0.0;

if (solve[IH2CO] == 1)
{
```

```
      if ((a=(Khet[i]+JH2COa[i][j]+JH2COb[i][j]+KOH_H2CO[i]*OH[i][j]))>0)
         H2CO[i][j] = ( KO1D_CH4b[i]*O1D[i][j]*CH4[i-1][j] +
                        KCH3O_O2[i]*CH3O[i][j]*O2[i] +
                        KCH3O2_CH3O2[i]*CH3O2[i][j]*CH3O2[i][j] ) / a;
      else
         H2CO[i][j] = 0.0;
   }
   else
      H2CO[i][j] = 0.0;

   if (solve[IHCO] == 1)
      HCO[i][j] = ( JH2COa[i][j]*H2CO[i][j] +
                    KOH_H2CO[i]*OH[i][j]*H2CO[i][j] )/(KHCO_O2[i]*O2[i]);
   else
      HCO[i][j] = 0.0;
}

O1D[0][j] = O1D[1][j];
O1D[SPACE_POINTS+1][j] = O1D[SPACE_POINTS][j];
O[0][j] = O[1][j];
O[SPACE_POINTS+1][j] = O[SPACE_POINTS][j];
OH[0][j] = OH[1][j];
OH[SPACE_POINTS+1][j] = OH[SPACE_POINTS][j];
H[0][j] = H[1][j];
H[SPACE_POINTS+1][j] = H[SPACE_POINTS][j];
HO2[0][j] = HO2[1][j];
HO2[SPACE_POINTS+1][j] = HO2[SPACE_POINTS][j];
H2O2[0][j] = H2O2[1][j];
H2O2[SPACE_POINTS+1][j] = H2O2[SPACE_POINTS][j];
NO[0][j] = NO[1][j];
NO[SPACE_POINTS+1][j] = NO[SPACE_POINTS][j];
HNO2[0][j] = HNO2[1][j];
HNO2[SPACE_POINTS+1][j] = HNO2[SPACE_POINTS][j];
NO2[0][j] = NO2[1][j];
NO2[SPACE_POINTS+1][j] = NO2[SPACE_POINTS][j];
HO2NO2[0][j] = HO2NO2[1][j];
HO2NO2[SPACE_POINTS+1][j] = HO2NO2[SPACE_POINTS][j];
NO3[0][j] = NO3[1][j];
NO3[SPACE_POINTS+1][j] = NO3[SPACE_POINTS][j];
N2O5[0][j] = N2O5[1][j];
N2O5[SPACE_POINTS+1][j] = N2O5[SPACE_POINTS][j];
CH3[0][j] = CH3[1][j];
CH3[SPACE_POINTS+1][j] = CH3[SPACE_POINTS][j];
CH3O2[0][j] = CH3O2[1][j];
```

```
    CH3O2[SPACE_POINTS+1][j] = CH3O2[SPACE_POINTS][j];
    CH3OOH[0][j] = CH3OOH[1][j];
    CH3OOH[SPACE_POINTS+1][j] = CH3OOH[SPACE_POINTS][j];
    CH3O[0][j] = CH3O[1][j];
    CH3O[SPACE_POINTS+1][j] = CH3O[SPACE_POINTS][j];
    H2CO[0][j] = H2CO[1][j];
    H2CO[SPACE_POINTS+1][j] = H2CO[SPACE_POINTS][j];
    HCO[0][j] = HCO[1][j];
    HCO[SPACE_POINTS+1][j] = HCO[SPACE_POINTS][j];
  }
}
```

A.12 getj.c

```
/* Function: get_J
 *
 * Copyright 1993 F. Moraes and M.A.K. Khalil
 *
 * Permission to use, copy, modify, and distribute this software and its
 * documentation for any purpose and without fee is hereby granted, provided
 * that the above copyright notice appear in all copies and that both that
 * copyright notice and this permission notice appear in supporting
 * documentation. No representation is made about the suitability of this
 * software for any purpose.  It is provided "as is" without express or
 * implied warranty.
 *
 * Author: Francis Moraes (internet: francis@eeyore.atmos.ogi.edu)
 *         Global Change Research Center
 *         Oregon Graduate Institute
 *
 * Synopsis: Calculate J (photochemical recation) values.
 *
 * VARIABLES:
 *
 * T        temperature
 * M        density
 * P        pressure
 *
 * GLOBAL VARIABLES:
 *
 * All of the photochemical reaction variables (J-whatever)
 *
 * FUNCTIONS:
 *
```

```
 * Several getJ-whatever functions which determine the J value for
 * a given chemical species.
 *
 * PROGRAM FLOW:
 *
 * For each time of day and vertical layer calculate the J value for
 * for each chemical species.
 */

#include <stdio.h>
#include "acm.h"
#include "rxn.h"
#include "acs.h"
#include "j.h"

void get_J(double *T, double *M, double *P)
{
   int i, j;

   double tmp = 0.0;
   extern double getJO3(double, int, int),
                 getJO3b(double, int, int),
                 getJH2O2(double, int, int),
                 getJNO2(double, int, int),
                 getJNO3a(double, int, int),
                 getJNO3b(double, int, int),
                 getJHNO2(double, int, int),
                 getJH2COa(double, int, int),
                 getJH2COb(double, int, double, int),
                 getJCH3OOH(double, int, int),
                 getJHNO3(double, int, int),
                 getJHO2NO2(double, int, int),
                 getJN2O5(double, int, int);

   for (i=1;i<SPACE_POINTS+1;i++)
   {
      for (j=0;j<=TIME_POINTS;j++)
      {
         JO3[i][j] = getJO3(T[i-1],j,i-1);
         JO3b[i][j] = getJO3b(T[i-1],j,i-1);
         JH2O2[i][j] = getJH2O2(T[i-1],j,i-1);
         JNO2[i][j] = getJNO2(T[i-1],j,i-1);
         JNO3a[i][j] = getJNO3a(T[i-1],j,i-1);
         JNO3b[i][j] = getJNO3b(T[i-1],j,i-1);
```

```
        JHNO2[i][j] = getJHNO2(T[i-1],j,i-1);
        JH2COa[i][j] = getJH2COa(T[i-1],j,i-1);
        JH2COb[i][j] = getJH2COb(T[i-1],j,P[i-1],i-1);
        JCH3OOH[i][j] = getJCH3OOH(T[i-1],j,i-1);
        JHNO3[i][j] = getJHNO3(T[i-1],j,i-1);
        JHO2NO2[i][j] = getJHO2NO2(T[i-1],j,i-1);
        JN2O5[i][j] = getJN2O5(T[i-1],j,i-1);
      }
    }
}
```

A.13 getk.c

```
/* Function: get_K
 *
 * Copyright 1993 F. Moraes and M.A.K. Khalil
 *
 * Permission to use, copy, modify, and distribute this software and its
 * documentation for any purpose and without fee is hereby granted, provided
 * that the above copyright notice appear in all copies and that both that
 * copyright notice and this permission notice appear in supporting
 * documentation. No representation is made about the suitability of this
 * software for any purpose.  It is provided "as is" without express or
 * implied warranty.
 *
 * Purpose: Determine the K values for all of the reactions in the model
 *            for each of the atmospheric layers.
 *
 * PASSED VARIABLES:
 *
 * T         Array of temperature for each atmospheric layer
 * M         Array of densities for each atmospheric layer
 * P         Array of pressures for each atmospheric layer
 *
 * GLOBAL VARIABLES:
 *
 * This function uses all of the K* global variables. These are
 * given in the files kbinary.h and kter.h.
 *
 * FUNCTIONS:
 *
 * This function calls no other functions. It uses defines exclusively.
 * These are given in the file rxn.h.
 *
```

```
 * FUNCTION FLOW:
 *
 *       o For each atmospheric layer
 *               o Calculate the K values for all of the gases
 */

#include "acm.h"
#include "rxn.h"
#include "kbinary.h"
#include "kter.h"

void get_K(double *T, double *M, double *P, double Z[][2])
{
   int i;
   double K0, K2, K3;

   for (i=1;i<SPACE_POINTS+1;i++)
   {
      /* binary reactions */

      KO1D_N2[i] = getKO1D_N2(T[i-1]);
      KO1D_O2[i] = getKO1D_O2(T[i-1]);
      KO1D_H2O[i] = getKO1D_H2O;
      KO1D_H2[i] = getKO1D_H2;
      KO1D_CH4a[i] = getKO1D_CH4a;
      KO1D_CH4b[i] = getKO1D_CH4b;
      KO1D_N2O[i] = getKO1D_N2O;
      KOH_H2[i] = getKOH_H2(T[i-1]);
      KOH_O3[i] = getKOH_O3(T[i-1]);
      KHO2_O3[i] = getKHO2_O3(T[i-1]);
      KOH_HO2[i] = getKOH_HO2(T[i-1]);
      KHO2_HO2a[i] = getKHO2_HO2a(T[i-1]);
      KHO2_HO2b[i] = getKHO2_HO2b(M[i-1],T[i-1]);
      KOH_H2O2[i] = getKOH_H2O2(T[i-1]);
      KNO_HO2[i] = getKNO_HO2(T[i-1]);
      KNO_O3[i] = getKNO_O3(T[i-1]);
      KNO_NO3[i] = getKNO_NO3(T[i-1]);
      KNO2_O3[i] = getKNO2_O3(T[i-1]);
      KOH_CO[i] = getKOH_CO(P[i-1]/P[0]);
      KOH_CH4[i] = getKOH_CH4(T[i-1]);
      KOH_H2CO[i] = getKOH_H2CO;
      KOH_CH3OOH[i] = getKOH_CH3OOH;
      KCH3O_O2[i] = getKCH3O_O2(T[i-1]);
      KHCO_O2[i] = getKHCO_O2(T[i-1]);
```

```
    KCH3O2_CH3O2[i] = getKCH3O2_CH3O2(T[i-1]);
    KCH3O2_HO2[i] = getKCH3O2_HO2(T[i-1]);
    KCH3O2_NO[i] = getKCH3O2_NO(T[i-1]);
    /* New O3 reactions */
    KO_O3[i] = getKO_O3(T[i-1]);
    KO_NO2[i] = getKO_NO2(T[i-1]);
    KH_O3[i] = getKH_O3(T[i-1]);
    KOH_O[i] = getKOH_O(T[i-1]);
    KHO2_O[i] = getKHO2_O(T[i-1]);
    KH2O2_O[i] = getKH2O2_O(T[i-1]);

    K0 = 7.2e-15*exp(785/T[i-1]);
    K2 = 4.1e-16*exp(1440/T[i-1]);
    K3 = 1.9e-33*exp(725/T[i-1]);
    KOH_HNO3[i] = K0 + K3*M[i-1]/(1.0 + K3*M[i-1]/K2);

    KOH_OHa[i] = getKOH_OHa(T[i-1]);
    KOH_OHb[i] = getKOH_OHb(T[i-1],M[i-1]);
    KH_HO2[i] = getKH_HO2(T[i-1]);
    KH2CO_O[i] = getKH2CO_O(T[i-1]);
    KH2_O[i] = getKH2_O(T[i-1]);
    KH2_O1D[i] = getKH2_O1D(T[i-1]);
    KOH_HO2NO2[i] = getKOH_HO2NO2(T[i-1]);

    /* termolecular reactions */

    KH_O2[i] = getKH_O2(T[i-1],M[i-1]);
    KO_O2[i] = getKO_O2(T[i-1],M[i-1]);
    KCH3_O2[i] = getKCH3_O2(T[i-1],M[i-1]);
    KOH_NO[i] = getKOH_NO(T[i-1],M[i-1]);
    KOH_NO2[i] = getKOH_NO2(T[i-1],M[i-1]);
    KHO2_NO2[i] = getKHO2_NO2(T[i-1],M[i-1]);
    KNO_O[i] = getKNO_O(T[i-1],M[i-1]);
    KNO2_NO3[i] = getKNO2_NO3(T[i-1],M[i-1]);
    KNO2_CH3O2[i] = getKNO2_CH3O2(T[i-1],M[i-1]);
    KN2O5[i] = getKN2O5(T[i-1],M[i-1]);
    KHO2NO2[i] = getKHO2NO2(T[i-1],M[i-1]);
}

/* Heterogeneous reactions */

for (i=1;i<SPACE_POINTS+1;i++)
{
    if (Z[i-1][0] < 400000.0)
```

```
         Khet[i] = 2.31e-6;
      else
         Khet[i] = 2.31e-6 * exp(1.6*(4.0 - Z[i-1][0]/100000.0));
   }
}
```

A.14 getline.c

```
/* Function: getline
 *
 * Copyright 1993 F. Moraes and M.A.K. Khalil
 *
 * Permission to use, copy, modify, and distribute this software and its
 * documentation for any purpose and without fee is hereby granted, provided
 * that the above copyright notice appear in all copies and that both that
 * copyright notice and this permission notice appear in supporting
 * documentation. No representation is made about the suitability of this
 * software for any purpose.  It is provided "as is" without express or
 * implied warranty.
 *
 * Author: Francis Moraes (internet: francis@eeyore.atmos.ogi.edu)
 *         Global Change Research Center
 *         Oregon Graduate Institute
 *
 * Synopsis: Reads a line from file. If the line begins with a pound
 *            sign (#) another line is read because that line is assumed
 *            a comment.
 */

#include <stdio.h>

getline(FILE *fp, char s[])
{
   int i;

   do
   {
      for (i=0;(s[i]=fgetc(fp))!='\n';i++)
         if (s[i] == (char)EOF)
            return EOF;
   }
   while (s[0] == '#');
   s[i] = 0;
   return 0;
```

```
}
```

A.15 getstdat.c

```
/* Function: get_std_atmos
 *
 * Copyright 1993 F. Moraes and M.A.K. Khalil
 *
 * Permission to use, copy, modify, and distribute this software and its
 * documentation for any purpose and without fee is hereby granted, provided
 * that the above copyright notice appear in all copies and that both that
 * copyright notice and this permission notice appear in supporting
 * documentation. No representation is made about the suitability of this
 * software for any purpose.  It is provided "as is" without express or
 * implied warranty.
 *
 * Purpose: Setup the standard parts of the atmosphere, mostly by reading
 *     from files.
 *
 * PASSED VARIABLES:
 *
 * T Array of temperatures for each atmospheric layer
 * M Array of densities for each atmospheric layer
 * P Array of pressures for each atmospheric layer
 * Z Array of atmospheric layer heights (Z[][0]) and
 * atmospheric layer thickness (Z[][1])
 * Kz Array of vertical transport coefficients
 * surface_rel_humidity The surface relative humidity
 *
 * LOCAL VARIABLES:
 *
 * sat_vapor The saturation vapor pressure for a given atmospheric layer
 * rel_humidity The relative humidity for a given atmospheric layer
 *
 * FUNCTIONS
 *
 * get_data A general function used here to input the gas concentrations
 * of the non-reactive gases as well as other data
 *
 * exit_error A utility function which prints an error message and exits
 *
 * FUNCTION FLOW:
 *
 * o Read the non-reactive gas concentrations from file, assuming
```

```
 *   them to be given in mixing ratios
 * o Read the vertical transport coefficients
 * o For each atmospheric layer
 * o Read Z[][0], Z[][1], T[], P[], M[]
 * o Calculate the water vapor using the method of
 *   Manabe and Wetherald (1967)
 * o Convert the gas mixing ratios to concentrations
 */

#include <math.h>
#include <stdio.h>
#include "acm.h"
#include "gases.h"

#define O3_FILE "dat/o3.dat"
#define LAND_O3_FILE "dat/o3land.dat"
#define SEA_O3_FILE "dat/o3sea.dat"
#define LAND_NOX_FILE "dat/noxland.dat"
#define SEA_NOX_FILE "dat/noxsea.dat"
#define LAND_CO_FILE "dat/coland.dat"
#define SEA_CO_FILE "dat/cosea.dat"
#define H2O_FILE "dat/h2o.dat"
#define LAND_H2O_FILE "dat/h2oland.dat"
#define SEA_H2O_FILE "dat/h2osea.dat"
#define CH4_FILE "dat/ch4.dat"
#define N2_FILE "dat/n2.dat"
#define O2_FILE "dat/o2.dat"
#define H2_FILE "dat/h2.dat"
#define N2O_FILE "dat/n2o.dat"
#define Kz_FILE "dat/kz.dat"
#define TEMP_FILE "dat/temp.dat"
#define LAND_TEMP_FILE "dat/templand.dat"
#define SEA_TEMP_FILE "dat/tempsea.dat"
#define ALBEDO_FILE "dat/albedo.dat"
#define STDATM_FILE "dat/stdatm.dat"
#define O3_COL_FILE "dat/o3_col.dat"

#define H 800000.0
#define CMKM 100000.0
#define DU 2.69e16
#define MO 2.6e19
#define MAXIT 100
#define A 5.08e18
#define NTRY 50
```

```
#define FACTOR 1.6

#define LAND 0
#define SEA 1

void get_std_atmos(double *T, double *M, double *P, double Z[][2], double *Kz,
                   int season, double latitude, double *albedo, double *O3_col,
   int half)
/* half: of 2.5 dimensional model. Is it land (0) or sea (1)? */
{
   int i, j;
   int tropopause;
   double Zt;
   double boundary;
   double tmp, sat_vapor, rel_humidity;
   double O3temp[SPACE_POINTS+2], CH4temp[SPACE_POINTS+2];
   double hno3;
   double o3a, o3b, o3b1=-1.0, o3b2=1.0, o3c, o3d, alpha, beta;
   double O3total = 0;
   double scaleO3, tropO3, tropO3M=0;
   FILE *fp;

   double get_land_sea_data(int, int, char *);
   int get_tropopause_height(double, double [][2]);
   extern void get_data(char *, double *, int),
               exit_error(char *);

   get_data(N2_FILE,N2+1,SPACE_POINTS);
   get_data(O2_FILE,O2+1,SPACE_POINTS);
   get_data(H2_FILE,H2+1,SPACE_POINTS);
   get_data(N2O_FILE,N2O+1,SPACE_POINTS);
   get_data(Kz_FILE,Kz,SPACE_POINTS+2);

   get_seasonal_data(CH4_FILE,CH4temp+1,SPACE_POINTS,latitude,season);

   /* NOX and H2O files list data in mixing ratios */

   if (half == LAND)
   {
      get_seasonal_data(LAND_H2O_FILE,H2O+1,SPACE_POINTS,latitude,season);
      get_seasonal_data(LAND_TEMP_FILE,T,SPACE_POINTS,latitude,season);
      get_seasonal_data(LAND_NOX_FILE,NOX+1,SPACE_POINTS,latitude,season);
      get_seasonal_data(LAND_O3_FILE,O3temp+1,SPACE_POINTS,latitude,season);
      get_seasonal_data(LAND_CO_FILE,CO+1,SPACE_POINTS,latitude,season);
```

```
}
else if (half == SEA)
{
   get_seasonal_data(SEA_H2O_FILE,H2O+1,SPACE_POINTS,latitude,season);
   get_seasonal_data(SEA_TEMP_FILE,T,SPACE_POINTS,latitude,season);
   get_seasonal_data(SEA_NOX_FILE,NOX+1,SPACE_POINTS,latitude,season);
   get_seasonal_data(SEA_O3_FILE,O3temp+1,SPACE_POINTS,latitude,season);
   get_seasonal_data(SEA_CO_FILE,CO+1,SPACE_POINTS,latitude,season);
}
else
{
   fprintf(stderr,"Major error\n");
   exit(1);
}

/* This gets the ground albedo for the given latitude */
*albedo = get_land_sea_data(half, season, "dat/albedo");

/* get the tropospheric constant HNO3 */
hno3 = get_land_sea_data(half, season, "dat/hno3")*1.0e-12;

if ( (fp=fopen(STDATM_FILE,"r")) == NULL)
   exit_error(STDATM_FILE);
for (i=0;i<SPACE_POINTS;i++)
   fscanf(fp,"%lf %lf %lf %lf %lf", &Z[i][0], &Z[i][1], &tmp, P+i, M+i);
fclose(fp);

tropopause = get_tropopause_height(latitude*180.0/PI,Z);

/* Here we convert mixing ratios to concentrations... */
for (i=0;i<SPACE_POINTS;i++)
{
   for (j=0;j<TIME_POINTS+1;j++)
   {
CH4[i+1][j] = CH4temp[i+1];
O3[i+1][j] = O3temp[i+1];
   }

   NOX[i+1] = NOX[i+1]*M[i];
   HNO3[i+1] = hno3*M[i];

   H2[i+1] = H2[i+1]*M[i];
   H2O[i+1] = H2O[i+1]*M[i];
   N2[i+1] = N2[i+1]*M[i];
```

```
    O2[i+1] = O2[i+1]*M[i];
    N2O[i+1] = N2O[i+1]*M[i];
  }

  /* Calculate the Ozone column density */
  O3_col[SPACE_POINTS-1] = O3temp[SPACE_POINTS]*Z[SPACE_POINTS-1][1];

  for (i=SPACE_POINTS-2;i>=0;i--)
    O3_col[i] = O3_col[i+1] + O3temp[i+1]*Z[i][1];

}

double get_land_sea_data(int half, int season, char *base)
{
  FILE *fp;
  double tmp, con[4];
  char filename[20];
  int i, j;

  strcpy(filename,base);
  if (half == 0)
  {
    strcat(filename,"land.dat");
    if ( (fp=fopen(filename,"r")) == NULL)
       exit_error(filename);
  }
  else if (half == 1)
  {
    strcat(filename,"sea.dat");
    if ( (fp=fopen(filename,"r")) == NULL)
       exit_error(filename);
  }

  j = ((int)(180*latitude/PI+5.0)+85)/10;
  for (i=0;i<=j;i++)
  {
    fscanf(fp,"%lf %lf %lf %lf %lf", &tmp, con,con+1,con+2,con+3);
  }
  fclose(fp);

  return (con[season]);
}

int get_tropopause_height(double lat, double Z[][2])
```

```
{
   int i;

   if (lat < 0.0)
      lat = (-lat);

   if (lat < 30)
   {
      for (i=0;Z[i][0]<1500000.0;i++)
 ;
      return i-1;
   }
   else if (lat < 60.0)
   {
      for (i=0;Z[i][0]<1200000.0;i++)
 ;
      return i-1;
   }
   else
   {
      for (i=0;Z[i][0]<800000.0;i++)
 ;
      return i-1;
   }
}
```

A.16 j.c

```
/* Function: getJ... (various functions)
 *
 * Copyright 1993 F. Moraes and M.A.K. Khalil
 *
 * Permission to use, copy, modify, and distribute this software and its
 * documentation for any purpose and without fee is hereby granted, provided
 * that the above copyright notice appear in all copies and that both that
 * copyright notice and this permission notice appear in supporting
 * documentation. No representation is made about the suitability of this
 * software for any purpose.  It is provided "as is" without express or
 * implied warranty.
 *
 * Author: Francis Moraes (internet: francis@eeyore.atmos.ogi.edu)
 *         Global Change Research Center
 *         Oregon Graduate Institute
 *
```

```
 * Synopsis: functions which determine the photodissociation constant
 * for various gases. These functions are dependent upon the functions
 * in the files QY.c and ACS.c and the function Actinic.
 *
 * FUNCTION FLOW
 *
 * All of the functions are the same. They calculate the
 * zenith angle for use in the Actinic() function then they integrate
 * over all wavelengths (in 10 nm increments) the quantum yield times (QY)
 * the absorption cross section (ACS) times the actinic flux.
 */

#include <math.h>
#include <stdio.h>
#include "acm.h"
#include "actinic.h"

#define MAX_ZENITH (PI*86.0/180.0)

double getJO3(double temperature, int timestep, int k)
{
   double J = 0.0, lambda, zenith;
   int i;
   extern int num_wavelength_bins;
   extern double latitude, inclination;

   extern double get_zenith(int),
                 O3QY(double,double),
                 getO3ACS(double,double),
                 Actinic(int,double,int);

   zenith = get_zenith(timestep);

   if (zenith > MAX_ZENITH)
      return 0.0;

   /* ACS: 170 - 720 nm
    * QY:    0 - 320 nm
    * Actinic: 180 - 730 nm
    * Thus we integrate over lambda 180 - 330 nm
    */
   for (i=0;ActBin[i]<180.0;i++)
      ;
   if (i>0)
```

```
    i--;
  for (;ActBin[i]<330.0;i++)
    J += (O3QY(ActBin[i],temperature)*
          getO3ACS(ActBin[i],temperature)*
          Actinic(i,zenith,k));

  return J;
}

double getJO3b(double temperature, int timestep, int k)
{
  double J = 0.0, lambda, zenith;
  int i;
  extern int num_wavelength_bins;
  extern double latitude, inclination;

  extern double get_zenith(int),
                O3QYb(double,double),
                getO3ACS(double,double),
                Actinic(int,double,int);

  zenith = get_zenith(timestep);

  if (zenith > MAX_ZENITH)
    return 0.0;

  /* ACS: 170 - 720 nm
   * QY:    0 - 320 nm
   * Actinic: 180 - 730 nm
   * Thus we integrate over lambda 180 - 330 nm
   */
  for (i=0;ActBin[i]<180.0;i++)
    ;
  if (i>0)
    i--;
  for (;ActBin[i]<320.0;i++)
    J += (O3QYb(ActBin[i],temperature)*
          getO3ACS(ActBin[i],temperature)*
          Actinic(i,zenith,k));

  return J;
}

double getJH2O2(double temperature, int timestep, int k)
```

```
{
   double J = 0.0, lambda, zenith;
   int i;
   extern int num_wavelength_bins;
   extern double latitude, inclination;

   extern double get_zenith(int),
                 H2O2QY(double,double),
                 getH2O2ACS(double,double),
                 Actinic(int,double,int);

   zenith = get_zenith(timestep);

   if (zenith > MAX_ZENITH)
      return 0.0;

   /* ACS: 260 - 350 nm
    * QY:   0 - INF nm
    * Actinic: 180 - 730 nm
    * Thus we integrate over lambda 260 - 350 nm
    */
   for (i=0;ActBin[i]<260.0;i++)
      ;
   if (i>0)
      i--;
   for (;ActBin[i]<350.0;i++)
      J += (H2O2QY(ActBin[i],temperature)*
            getH2O2ACS(ActBin[i],temperature)*
            Actinic(i,zenith,k));

   return J;
}

double getJNO2(double temperature, int timestep, int k)
{
   double J = 0.0, lambda, zenith;
   int i;
   extern int num_wavelength_bins;
   extern double latitude, inclination;

   extern double get_zenith(int),
                 NO2QY(double,double),
                 getNO2ACS(double,double),
                 Actinic(int,double,int);
```

```
   zenith = get_zenith(timestep);

   if (zenith > MAX_ZENITH)
      return 0.0;

   /* ACS: 200 - 430 nm
    * QY:    0 - 430 nm
    * Actinic: 180 - 730 nm
    * Thus we integrate over lambda 200 - 430 nm
    */

   for (i=0;ActBin[i]<200.0;i++)
      ;
   if (i>0)
      i--;
   for (;ActBin[i]<430.0;i++)
   {
      J += (NO2QY(ActBin[i],temperature)*
            getNO2ACS(ActBin[i],temperature)*
            Actinic(i,zenith,k));
   }

   return J;
}

double getJNO3a(double temperature, int timestep, int k)
{
   double J = 0.0, lambda, zenith;
   int i;
   extern int num_wavelength_bins;
   extern double latitude, inclination;

   extern double get_zenith(int),
                 NO3aQY(double,double),
                 getNO3ACS(double,double),
                 Actinic(int,double,int);

   zenith = get_zenith(timestep);

   if (zenith > MAX_ZENITH)
      return 0.0;

   /* ACS: 400 - 720 nm
```

```
 * QY:    0 - 590 nm
 * Actinic: 180 - 730 nm
 * Thus we integrate over lambda 400 - 590 nm
 */
if (zenith < 1.51)
   J = 0.022*cos(zenith);
else
   J = 0;

return J;
}

double getJNO3b(double temperature, int timestep, int k)
{
   double J = 0.0, lambda, zenith;
   int i;
   extern int num_wavelength_bins;
   extern double latitude, inclination;

   extern double get_zenith(int),
                 NO3bQY(double,double),
                 getNO3ACS(double,double),
                 Actinic(int,double,int);

   zenith = get_zenith(timestep);

   if (zenith > MAX_ZENITH)
      return 0.0;

   /* ACS: 400 - 720 nm
    * QY:    0 - 650 nm
    * Actinic: 180 - 730 nm
    * Thus we integrate over lambda 400 - 650 nm
    */
   for (i=0;ActBin[i]<400.0;i++)
      ;
   if (i>0)
      i--;
   for (;ActBin[i]<650.0;i++)
      J += (NO3bQY(ActBin[i],temperature)*
            getNO3ACS(ActBin[i],temperature)*
            Actinic(i,zenith,k));

   return J;
```

```
}

double getJHNO2(double temperature, int timestep, int k)
{
   double J = 0.0, lambda, zenith;
   int i;
   extern int num_wavelength_bins;
   extern double latitude, inclination;

   extern double get_zenith(int),
                 HNO2QY(double,double),
                 getHNO2ACS(double,double),
                 Actinic(int,double,int);

   zenith = get_zenith(timestep);

   if (zenith > MAX_ZENITH)
      return 0.0;

   /* ACS: 310 - 400 nm
    * QY:    0 - INF nm
    * Actinic: 180 - 730 nm
    * Thus we integrate over lambda 300 - 410 nm
    */
   for (i=0;ActBin[i]<310.0;i++)
      ;
   if (i>0)
      i--;
   for (;ActBin[i]<400.0;i++)
      J += (HNO2QY(ActBin[i],temperature)*
            getHNO2ACS(ActBin[i],temperature)*
            Actinic(i,zenith,k));

   return J;
}

double getJH2COa(double temperature, int timestep, int k)
{
   double J = 0.0, lambda, zenith;
   int i;
   extern int num_wavelength_bins;
   extern double latitude, inclination;

   extern double get_zenith(int),
```

```
                 H2COaQY(double,double),
                 getH2COACS(double,double),
                 Actinic(int,double,int);

   zenith = get_zenith(timestep);

   if (zenith > MAX_ZENITH)
      return 0.0;

   /* ACS: 240 - 310 nm
    * QY:   0 - 340 nm
    * Actinic: 180 - 730 nm
    * Thus we integrate over lambda 240 - 340 nm
    */
   for (i=0;ActBin[i]<240.0;i++)
      ;
   if (i>0)
      i--;
   for (;ActBin[i]<310.0;i++)
      J += (H2COaQY(ActBin[i],temperature)*
            getH2COACS(ActBin[i],temperature)*
            Actinic(i,zenith,k));

   return J;
}

double getJH2COb(double temperature, int timestep, double pressure, int k)
{
   double J = 0.0, lambda, zenith;
   int i;
   extern int num_wavelength_bins;
   extern double latitude, inclination;

   extern double get_zenith(int),
                 H2CObQY(double,double,double),
                 getH2COACS(double,double),
                 Actinic(int,double,int);

   zenith = get_zenith(timestep);

   if (zenith > MAX_ZENITH)
      return 0.0;

   /* ACS: 240 - 310 nm <== Unsure of this
```

```
 * QY:    0 - INF nm
 * Actinic: 180 - 730 nm
 * Thus we integrate over lambda 240 - 730 nm
 */
for (i=0;ActBin[i]<240.0;i++)
   ;
if (i>0)
   i--;
for (;ActBin[i]<310.0;i++)
   J += (H2CObQY(ActBin[i],temperature,pressure)*
         getH2COACS(ActBin[i],temperature)*
         Actinic(i,zenith,k));

return J;
}

double getJCH3OOH(double temperature, int timestep, int k)
{
   double J = 0.0, lambda, zenith;
   int i;
   extern int num_wavelength_bins;
   extern double latitude, inclination;

   extern double get_zenith(int),
                 CH3OOHQY(double,double),
                 getCH3OOHACS(double,double),
                 Actinic(int,double,int);

   zenith = get_zenith(timestep);

   if (zenith > MAX_ZENITH)
      return 0.0;

   /* ACS: 210 - INF nm
    * QY:    0 - INF nm
    * Actinic: 180 - 730 nm
    * Thus we integrate over lambda 210 - 730 nm
    */
   for (i=0;ActBin[i]<210.0;i++)
      ;
   if (i>0)
      i--;
   for (;ActBin[i]<730.0;i++)
      J += (CH3OOHQY(ActBin[i],temperature)*
```

```
            getCH3OOHACS(ActBin[i],temperature)*
            Actinic(i,zenith,k));

   return J;
}

double getJHNO3(double temperature, int timestep, int k)
{
   double J = 0.0, lambda, zenith;
   int i;
   extern int num_wavelength_bins;
   extern double latitude, inclination;

   extern double get_zenith(int),
                 HNO3QY(double,double),
                 getHNO3ACS(double,double),
                 Actinic(int,double,int);

   zenith = get_zenith(timestep);

   if (zenith > MAX_ZENITH)
      return 0.0;

   /* ACS: 190 - 340 nm
    * QY:    0 - INF nm
    * Actinic: 180 - 730 nm
    * Thus we integrate over lambda 190 - 340 nm
    */
   for (i=0;ActBin[i]<190.0;i++)
      ;
   if (i>0)
      i--;
   for (;ActBin[i]<340.0;i++)
      J += (HNO3QY(ActBin[i],temperature)*
            getHNO3ACS(ActBin[i],temperature)*
            Actinic(i,zenith,k));

   return J;
}

double getJHO2NO2(double temperature, int timestep, int k)
{
   double J = 0.0, lambda, zenith;
   int i;
```

```
    extern int num_wavelength_bins;
    extern double latitude, inclination;

    extern double get_zenith(int),
                  HO2NO2QY(double,double),
                  getHO2NO2ACS(double,double),
                  Actinic(int,double,int);

    zenith = get_zenith(timestep);

    if (zenith > MAX_ZENITH)
       return 0.0;

    /* ACS: 190 - 330 nm
     * QY:    0 - INF nm
     * Actinic: 180 - 730 nm
     * Thus we integrate over lambda 190 - 330 nm
     */
    for (i=0;ActBin[i]<190.0;i++)
       ;
    if (i>0)
       i--;
    for (;ActBin[i]<330.0;i++)
       J += (HO2NO2QY(ActBin[i],temperature)*
             getHO2NO2ACS(ActBin[i],temperature)*
             Actinic(i,zenith,k));

    return J;
}

double getJN2O5(double temperature, int timestep, int k)
{
    double J = 0.0, lambda, zenith;
    int i;
    extern int num_wavelength_bins;
    extern double latitude, inclination;

    extern double get_zenith(int),
                  N2O5QY(double,double),
                  getN2O5ACS(double,double),
                  Actinic(int,double,int);

    zenith = get_zenith(timestep);
```

```
   if (zenith > MAX_ZENITH)
      return 0.0;

   /* ACS: 200 - 280 nm
    * QY:    0 - INF nm
    * Actinic: 180 - 730 nm
    * Thus we integrate over lambda 200 - 280 nm
    */
   for (i=0;ActBin[i]<200.0;i++)
      ;
   if (i>0)
      i--;
   for (;ActBin[i]<380.0;i++)
      J += (N205QY(ActBin[i],temperature)*
            getN205ACS(ActBin[i],temperature)*
            Actinic(i,zenith,k));

   return J;
}

double get_zenith(int timestep)
{
   double zenith;
   extern double inclination, latitude;

   zenith = acos(sin(inclination)*sin(latitude) +
                 cos(inclination)*cos(latitude) *
                 cos(PI*(double)(timestep-TIME_POINTS/2) /
     ((double)TIME_POINTS/2.0)));

   return zenith;
}
```

A.17 output.c

```
/* Function: output_data
 *
 * Copyright 1993 F. Moraes and M.A.K. Khalil
 *
 * Permission to use, copy, modify, and distribute this software and its
 * documentation for any purpose and without fee is hereby granted, provided
 * that the above copyright notice appear in all copies and that both that
 * copyright notice and this permission notice appear in supporting
 * documentation. No representation is made about the suitability of this
```

```
 * software for any purpose.  It is provided "as is" without express or
 * implied warranty.
 *
 * Author: Francis Moraes (internet: francis@eeyore.atmos.ogi.edu)
 *         Global Change Research Center
 *         Oregon Graduate Institute
 *
 * Synopsis: This function outputs concentration data from the ACM.
 *
 * VARIABLES:
 *
 * outputtype An integer which indicates the type of output: none (0)
 * time (1), height (2), diurnally averaged height (3),
 * or total column (4). See in the code below for details.
 * output An array which indicates which species to output data
 * for and what time of day or vertical layer to output
 * (this is ignored for outputtype of 3 or 4)
 * Z A 2-D array which indicates the vertical grid layer
 * heights (Z[][0]) and thicknesses (Z[][1]) both in cm.
 * M An array which holds the density for each grid layer
 *
 * GLOBAL VARIABLES:
 *
 * All of the gas concentration arrays are global.
 *
 * FUNCTIONS:
 *
 * none.
 *
 * PROGRAM FLOW:
 *
 * The program simply checks the outputtype variable and then iterates
 * through time or space (depending upon the value of outputtype) outputting
 * values where appropriate.
 */

#include <stdio.h>
#include "acm.h"
#include "gases.h"
#include "rxn.h"
#include "solve.h"
#undef SPACE_POINTS
#define SPACE_POINTS 17
```

```
void output_data(int outputtype, int *output, double Z[][2], double *M,
double *P)
{
   int i, j;
   double totalcon, totz;
   double totalno, totalno2;

   /* An outputtype of 1 causes the program to output concentrations
    * at every time of the data for a given atmospheric layer. The
    * atmospheric layer is given in the output array. If an element
    * of this array is less than zero the corresponding concentration
    * is not output. The code does not check to see if the atmospheric
    * layer is valid (less than SPACE_POINTS).
    */
   if (outputtype == 1)
   {
      for (j=0;j<TIME_POINTS;j++)
      {
         printf("%g", (float)(j)/(float)TIME_POINTS);

         if (output[IO1D] >= 0)
            printf(" %.2e", O1D[output[IO1D]][j]);
         if (output[IO] >= 0)
            printf(" %.2e", O[output[IO]][j]);
         if (output[IOH] >= 0)
            printf(" %.2e", OH[output[IOH]][j]);
         if (output[IH] >= 0)
            printf(" %.2e", H[output[IH]][j]);
         if (output[IHO2] >= 0)
            printf(" %.2e", HO2[output[IHO2]][j]);
         if (output[IH2O2] >= 0)
            printf(" %.2e", H2O2[output[IH2O2]][j]);
         if (output[INO] >= 0)
            printf(" %.2e", NO[output[INO]][j]);
         if (output[IHNO2] >= 0)
            printf(" %.2e", HNO2[output[IHNO2]][j]);
         if (output[INO2] >= 0)
            printf(" %.2e", NO2[output[INO2]][j]);
         if (output[IHO2NO2] >= 0)
            printf(" %.2e", HO2NO2[output[IHO2NO2]][j]);
         if (output[INO3] >= 0)
            printf(" %.2e", NO3[output[INO3]][j]);
         if (output[IN2O5] >= 0)
            printf(" %.2e", N2O5[output[IN2O5]][j]);
```

```
        if (output[ICH3] >= 0)
           printf(" %.2e", CH3[output[ICH3]][j]);
        if (output[ICH3O2] >= 0)
           printf(" %.2e", CH3O2[output[ICH3O2]][j]);
        if (output[ICH3OOH] >= 0)
           printf(" %.2e", CH3OOH[output[ICH3OOH]][j]);
        if (output[ICH3O] >= 0)
           printf(" %.2e", CH3O[output[ICH3O]][j]);
        if (output[IH2CO] >= 0)
           printf(" %.2e", H2CO[output[IH2CO]][j]);
        if (output[IHCO] >= 0)
           printf(" %.2e", HCO[output[IHCO]][j]);
        if (output[ICH4] >= 0)
           printf(" %.2e", CH4[output[ICH4]][j]);
        printf("\n");
     }
  }
  /* An outputtype of 2 causes the program to output concentrations
   * at every atmospheric layer for a given time of day. The time
   * (time step, actually) is given in the output array. If an element
   * of this array is less than zero the corresponding concentration
   * is not output. The code does not check to make sure the time
   * step given is valid (less than TIME_STEPS).
   */
  else if (outputtype == 2)
  {
     for (i=1;i<SPACE_POINTS+1;i++)
     {
        printf("%g", Z[i-1][0]/100000.0);

        if (output[IO1D] >= 0)
           printf(" %.2e", O1D[i][output[IO1D]]);
        if (output[IO] >= 0)
           printf(" %.2e", O[i][output[IO]]);
        if (output[IOH] >= 0)
           printf(" %.2e", OH[i][output[IOH]]/M[i-1]);
        if (output[IH] >= 0)
           printf(" %.2e", H[i][output[IH]]);
        if (output[IHO2] >= 0)
           printf(" %.2e", HO2[i][output[IHO2]]/M[i-1]);
        if (output[IH2O2] >= 0)
           printf(" %.2e", H2O2[i][output[IH2O2]]);
        if (output[INO] >= 0)
           printf(" %.2e", NO[i][output[INO]]);
```

```
        if (output[IHNO2] >= 0)
           printf(" %.2e", HNO2[i][output[IHNO2]]);
        if (output[INO2] >= 0)
           printf(" %.2e", NO2[i][output[INO2]]);
        if (output[IHO2NO2] >= 0)
           printf(" %.2e", HO2NO2[i][output[IHO2NO2]]);
        if (output[INO3] >= 0)
           printf(" %.2e", NO3[i][output[INO3]]);
        if (output[IN2O5] >= 0)
           printf(" %.2e", N2O5[i][output[IN2O5]]);
        if (output[ICH3] >= 0)
           printf(" %.2e", CH3[i][output[ICH3]]);
        if (output[ICH3O2] >= 0)
           printf(" %.2e", CH3O2[i][output[ICH3O2]]);
        if (output[ICH3OOH] >= 0)
           printf(" %.2e", CH3OOH[i][output[ICH3OOH]]);
        if (output[ICH3O] >= 0)
           printf(" %.2e", CH3O[i][output[ICH3O]]);
        if (output[IH2CO] >= 0)
           printf(" %.2e", H2CO[i][output[IH2CO]]);
        if (output[IHCO] >= 0)
           printf(" %.2e", HCO[i][output[IHCO]]);
        if (output[ICH4] >= 0)
           printf(" %.2e", CH4[i][output[ICH4]]);
        printf("\n");
     }
  }
  /* An outputtype of 3 causes the program to output diurnally
   * averaged concentrations at every atmospheric layer. The
   * output array tells the program only whether to output or
   * not (less than zero).
   */
  else if (outputtype == 3)
  {
     for (i=1;i<SPACE_POINTS+1;i++)
     {
/*
        printf("%10g %10g", Z[i-1][0]/100000.0, P[i-1]/P[0]);
*/
        printf("%10g", Z[i-1][0]/100000.0);

        if (output[IO1D] >= 0)
        {
           totalcon = 0.0;
```

```
        for (j=0;j<TIME_POINTS;j++)
           totalcon += (O1D[i][j]);
        printf(" %10.2e", totalcon/TIME_POINTS);
     }
     if (output[IO] >= 0)
     {
        totalcon = 0.0;
        for (j=0;j<TIME_POINTS;j++)
           totalcon += (O[i][j]);
        printf(" %10.2e", totalcon/TIME_POINTS);
     }
     if (output[IOH] >= 0)
     {
        totalcon = 0.0;
        for (j=0;j<TIME_POINTS;j++)
           totalcon += (OH[i][j]);
        printf(" %10.2e", totalcon/TIME_POINTS);
/*
totalno = totalno2 = 0.0;
        for (j=0;j<TIME_POINTS;j++)
{
           totalno += (NO[i][j]);
           totalno2 += (NO2[i][j]);
}
        printf(" %.2e", totalno2/totalno);
*/
     }
     if (output[IH] >= 0)
     {
        totalcon = 0.0;
        for (j=0;j<TIME_POINTS;j++)
           totalcon += (H[i][j]);
        printf(" %10.2e", totalcon/TIME_POINTS);
     }
     if (output[IHO2] >= 0)
     {
        totalcon = 0.0;
        for (j=0;j<TIME_POINTS;j++)
           totalcon += (HO2[i][j]);
        printf(" %10.2e", totalcon/TIME_POINTS);
     }
     if (output[IH2O2] >= 0)
     {
        totalcon = 0.0;
```

```
    for (j=0;j<TIME_POINTS;j++)
       totalcon += (H2O2[i][j]);
    printf(" %10.2e", totalcon/TIME_POINTS);
 }
 if (output[INO] >= 0)
 {
    totalcon = 0.0;
    for (j=0;j<TIME_POINTS;j++)
       totalcon += (NO[i][j]);
    printf(" %10.2e", totalcon/TIME_POINTS);
 }
 if (output[IHNO2] >= 0)
 {
    totalcon = 0.0;
    for (j=0;j<TIME_POINTS;j++)
       totalcon += (HNO2[i][j]);
    printf(" %10.2e", totalcon/TIME_POINTS);
 }
 if (output[INO2] >= 0)
 {
    totalcon = 0.0;
    for (j=0;j<TIME_POINTS;j++)
       totalcon += (NO2[i][j]);
    printf(" %10.2e", totalcon/TIME_POINTS);
 }
 if (output[IHO2NO2] >= 0)
 {
    totalcon = 0.0;
    for (j=0;j<TIME_POINTS;j++)
       totalcon += (HO2NO2[i][j]);
    printf(" %10.2e", totalcon/TIME_POINTS);
 }
 if (output[INO3] >= 0)
 {
    totalcon = 0.0;
    for (j=0;j<TIME_POINTS;j++)
       totalcon += (NO3[i][j]);
    printf(" %10.2e", totalcon/TIME_POINTS);
 }
 if (output[IN2O5] >= 0)
 {
    totalcon = 0.0;
    for (j=0;j<TIME_POINTS;j++)
       totalcon += (N2O5[i][j]);
```

```
   printf(" %10.2e", totalcon/TIME_POINTS);
}
if (output[ICH3] >= 0)
{
   totalcon = 0.0;
   for (j=0;j<TIME_POINTS;j++)
      totalcon += (CH3[i][j]);
   printf(" %10.2e", totalcon/TIME_POINTS);
}
if (output[ICH3O2] >= 0)
{
   totalcon = 0.0;
   for (j=0;j<TIME_POINTS;j++)
      totalcon += (CH3O2[i][j]);
   printf(" %10.2e", totalcon/TIME_POINTS);
}
if (output[ICH3OOH] >= 0)
{
   totalcon = 0.0;
   for (j=0;j<TIME_POINTS;j++)
      totalcon += (CH3OOH[i][j]);
   printf(" %10.2e", totalcon/TIME_POINTS);
}
if (output[ICH3O] >= 0)
{
   totalcon = 0.0;
   for (j=0;j<TIME_POINTS;j++)
      totalcon += (CH3O[i][j]);
   printf(" %10.2e", totalcon/TIME_POINTS);
}
if (output[IH2CO] >= 0)
{
   totalcon = 0.0;
   for (j=0;j<TIME_POINTS;j++)
      totalcon += (H2CO[i][j]);
   printf(" %10.2e", totalcon/TIME_POINTS);
}
if (output[IHCO] >= 0)
{
   totalcon = 0.0;
   for (j=0;j<TIME_POINTS;j++)
      totalcon += (HCO[i][j]);
   printf(" %10.2e", totalcon/TIME_POINTS);
}
```

```
        if (output[ICH4] >= 0)
        {
           totalcon = 0.0;
           for (j=0;j<TIME_POINTS;j++)
              totalcon += (CH4[i][j]);
           printf(" %.2e", totalcon/TIME_POINTS);
        }
        printf("\n");
     }
  }
  /* An outputtype of 4 causes the program the total column
   * concentration. The output array tells the program only
   * whether to output or not (less than zero).
   */
  else if (outputtype == 4)
  {
     if (output[IO1D] >= 0)
     {
        totalcon = totz = 0.0;
        for (i=1;i<16+1;i++)
        {
           for (j=0;j<TIME_POINTS;j++)
              totalcon += (O1D[i][j]*Z[i][1]);
           totz += Z[i][1];
        }
        printf(" %.2e", totalcon/(totz*TIME_POINTS));
     }
     if (output[IO] >= 0)
     {
        totalcon = totz = 0.0;
        for (i=1;i<16+1;i++)
        {
           for (j=0;j<TIME_POINTS;j++)
              totalcon += (O[i][j]*Z[i][1]);
   totz += Z[i][1];
}
        printf(" %.2e", totalcon/(totz*TIME_POINTS));
     }
     if (output[IOH] >= 0)
     {
        totalcon = totz = 0.0;

        for (i=1;i<16+1;i++)
{
```

```
          for (j=0;j<TIME_POINTS;j++)
             totalcon += (OH[i][j]*Z[i-1][1]);
   totz += Z[i][1];
}
        printf(" %.2e", totalcon/(totz*TIME_POINTS));
        for (i=1;i<16+1;i++)
{
          for (j=0;j<TIME_POINTS;j++)
             totalcon += (OH[i][j]*Z[i-1][1]);
   totz += Z[i-1][1]*M[i-1];
}
        printf(" %.2e", totalcon/(totz*TIME_POINTS));
     }
     if (output[IH] >= 0)
     {
        totalcon = totz = 0.0;
        for (i=1;i<16+1;i++)
{
          for (j=0;j<TIME_POINTS;j++)
             totalcon += (H[i][j]*Z[i-1][1]);
   totz += Z[i-1][1];
}
        printf(" %.2e", totalcon/(totz*TIME_POINTS));
     }
     if (output[IHO2] >= 0)
     {
        totalcon = totz = 0.0;
        for (i=1;i<16+1;i++)
{
          for (j=0;j<TIME_POINTS;j++)
             totalcon += (HO2[i][j]*Z[i][1]);
   totz += Z[i][1];
}
        printf(" %.2e", totalcon/(totz*TIME_POINTS));
        for (i=1;i<16+1;i++)
{
          for (j=0;j<TIME_POINTS;j++)
             totalcon += (HO2[i][j]*Z[i-1][1]);
   totz += Z[i-1][1]*M[i-1];
}
        printf(" %.2e", totalcon/(totz*TIME_POINTS));
     }
     if (output[IH2O2] >= 0)
     {
```

```
        totalcon = totz = 0.0;
        for (i=1;i<16+1;i++)
{
           for (j=0;j<TIME_POINTS;j++)
              totalcon += (H2O2[i][j]*Z[i][1]);
   totz += Z[i][1];
}
        printf(" %.2e", totalcon/(totz*TIME_POINTS));
     }
     if (output[INO] >= 0)
     {
        totalcon = totz = 0.0;
        for (i=1;i<16+1;i++)
{
           for (j=0;j<TIME_POINTS;j++)
              totalcon += (NO[i][j]*Z[i][1]);
   totz += Z[i][1];
}
        printf(" %.2e", totalcon/(totz*TIME_POINTS));
     }
     if (output[IHNO2] >= 0)
     {
        totalcon = totz = 0.0;
        for (i=1;i<16+1;i++)
{
           for (j=0;j<TIME_POINTS;j++)
              totalcon += (HNO2[i][j]*Z[i][1]);
   totz += Z[i][1];
}
        printf(" %.2e", totalcon/(totz*TIME_POINTS));
     }
     if (output[INO2] >= 0)
     {
        totalcon = totz = 0.0;
        for (i=1;i<16+1;i++)
{
           for (j=0;j<TIME_POINTS;j++)
              totalcon += (NO2[i][j]*Z[i][1]);
   totz += Z[i][1];
}
        printf(" %.2e", totalcon/(totz*TIME_POINTS));
     }
     if (output[IHO2NO2] >= 0)
     {
```

```
        totalcon = totz = 0.0;
        for (i=1;i<16+1;i++)
{
          for (j=0;j<TIME_POINTS;j++)
            totalcon += (HO2NO2[i][j]*Z[i][1]);
   totz += Z[i][1];
}
        printf(" %.2e", totalcon/(totz*TIME_POINTS));
      }
      if (output[INO3] >= 0)
      {
        totalcon = totz = 0.0;
        for (i=1;i<16+1;i++)
{
          for (j=0;j<TIME_POINTS;j++)
            totalcon += (NO3[i][j]*Z[i][1]);
   totz += Z[i][1];
}
        printf(" %.2e", totalcon/(totz*TIME_POINTS));
      }
      if (output[IN2O5] >= 0)
      {
        totalcon = totz = 0.0;
        for (i=1;i<16+1;i++)
{
          for (j=0;j<TIME_POINTS;j++)
            totalcon += (N2O5[i][j]*Z[i][1]);
   totz += Z[i][1];
}
        printf(" %.2e", totalcon/(totz*TIME_POINTS));
      }
      if (output[ICH3] >= 0)
      {
        totalcon = totz = 0.0;
        for (i=1;i<16+1;i++)
{
          for (j=0;j<TIME_POINTS;j++)
            totalcon += (CH3[i][j]*Z[i][1]);
   totz += Z[i][1];
}
        printf(" %.2e", totalcon/(totz*TIME_POINTS));
      }
      if (output[ICH3O2] >= 0)
      {
```

```
        totalcon = totz = 0.0;
        for (i=1;i<16+1;i++)
{
           for (j=0;j<TIME_POINTS;j++)
              totalcon += (CH3O2[i][j]*Z[i][1]);
   totz += Z[i][1];
}
        printf(" %.2e", totalcon/(totz*TIME_POINTS));
     }
     if (output[ICH3OOH] >= 0)
     {
        totalcon = totz = 0.0;
        for (i=1;i<16+1;i++)
{
           for (j=0;j<TIME_POINTS;j++)
              totalcon += (CH3OOH[i][j]*Z[i][1]);
   totz += Z[i][1];
}
        printf(" %.2e", totalcon/(totz*TIME_POINTS));
     }
     if (output[ICH3O] >= 0)
     {
        totalcon = totz = 0.0;
        for (i=1;i<16+1;i++)
{
           for (j=0;j<TIME_POINTS;j++)
              totalcon += (CH3O[i][j]*Z[i][1]);
   totz += Z[i][1];
}
        printf(" %.2e", totalcon/(totz*TIME_POINTS));
     }
     if (output[IH2CO] >= 0)
     {
        totalcon = totz = 0.0;
        for (i=1;i<16+1;i++)
{
           for (j=0;j<TIME_POINTS;j++)
              totalcon += (H2CO[i][j]*Z[i][1]);
   totz += Z[i][1];
}
        printf(" %.2e", totalcon/(totz*TIME_POINTS));
     }
     if (output[IHCO] >= 0)
     {
```

```
        totalcon = totz = 0.0;
        for (i=1;i<16+1;i++)
{
           for (j=0;j<TIME_POINTS;j++)
              totalcon += (HCO[i][j]*Z[i][1]);
   totz += Z[i][1];
}
        printf(" %.2e", totalcon/(totz*TIME_POINTS));
     }
     if (output[ICH4] >= 0)
     {
        totalcon = totz = 0.0;
        for (i=1;i<SPACE_POINTS+1;i++)
{
           for (j=0;j<TIME_POINTS;j++)
              totalcon += (CH4[i][j]*Z[i][1]);
   totz += Z[i][1];
}
        printf(" %.2e", totalcon/(totz*TIME_POINTS));
     }
     printf("\n");
  }
}
```

A.18 qy.c

```
/* Function: ...QY (various functions)
 *
 * Copyright 1993 F. Moraes and M.A.K. Khalil
 *
 * Permission to use, copy, modify, and distribute this software and its
 * documentation for any purpose and without fee is hereby granted, provided
 * that the above copyright notice appear in all copies and that both that
 * copyright notice and this permission notice appear in supporting
 * documentation. No representation is made about the suitability of this
 * software for any purpose.  It is provided "as is" without express or
 * implied warranty.
 *
 * Author: Francis Moraes (internet: francis@eeyore.atmos.ogi.edu)
 *         Global Change Research Center
 *         Oregon Graduate Institute
 *
 * Synopsis: This file contains all of the functions for determining
 * the quantum yields for all of the photodissociation processes used
```

```
 * in the model.
 */

#include <stdio.h>
#include <math.h>

/* function: O3QY(double lambda, double temperature)
 *
 * purpose: Calculate the quantum yield for the photolysis of Ozone
 * to O(1D) in the wavelength region 305 to 320 nm. Wavelengths below
 * this will be given quantum yields of 0.95 and wavelengths above it
 * will be given quantum yields of zero. This subroutine is only valid
 * for temperatures in [220,300] Kelvin. Temperatures not in this
 * region are given either 220 K or 300 K (depending whether low or
 * high) and processed but the glob variable error_flag is set. The
 * data used for this subroutine comes from ``Chemical Kinetics and
 * Photochemical Data for Use in Stratospheric Modeling'' by DeMore
 * et al.
 */

#define A00  0.94932
#define A01 -0.00017039
#define A02  0.0000014072
#define A0(T) (A00 + A01*(T) + A02*(T)*(T))

#define A10 -0.024052
#define A11  0.0010479
#define A12 -0.000010655
#define A1(T) (A10 + A11*(T) + A12*(T)*(T))

#define A20  0.018771
#define A21 -0.00036401
#define A22 -0.000018587
#define A2(T) (A20 + A21*(T) + A22*(T)*(T))

#define A30 -0.01454
#define A31 -0.000047787
#define A32  0.0000081277
#define A3(T) (A30 + A31*(T) + A32*(T)*(T))

#define A40  0.0023287
#define A41  0.000019891
#define A42 -0.0000011801
#define A4(T) (A40 + A41*(T) + A42*(T)*(T))
```

```
#define A50 -0.00014471
#define A51 -0.0000017188
#define A52  0.000000072661
#define A5(T) (A50 + A51*(T) + A52*(T)*(T))

#define A60  0.000003183
#define A61  0.000000046209
#define A62 -0.0000000016266
#define A6(T) (A60 + A61*(T) + A62*(T)*(T))

double O3QY(lambda,temperature)
double lambda, temperature;
{
   double qy;
   /*
   if (lambda < 305.0)
      return 0.95;
   else if (lambda > 320.0)
      return 0.0;

   if (temperature > 300.0)
      temperature = 300.0;
   else if (temperature < 220.0)
      temperature = 220.0;

   temperature = 298.0 - temperature;
   lambda = lambda - 305.0;

   qy = A0(temperature) + A1(temperature)*lambda +
A2(temperature)*pow(lambda,2.0) +
A3(temperature)*pow(lambda,3.0) +
A4(temperature)*pow(lambda,4.0) +
A5(temperature)*pow(lambda,5.0) +
A6(temperature)*pow(lambda,6.0);

   if (qy < 0.02)
      qy = 0.0;
   return qy;
   */

  if(lambda <310)
     return 0.9;
  if(lambda <320)
```

```
    return 0.15;
  else
    return 0.0;
}

double O3QYb(lambda,temperature)
double lambda, temperature;
{
   if (lambda < 320.0)
      return 0.1;
   else
      return 0.9;
}

/* function: H2O2QY(double lambda, double temperature)
 *
 * Purpose: Calculate the quantum yield of H2O2. Apparently this number
 * is always 1.0 because I can find no information on it.
 */

double H2O2QY(lambda,temperature)
double lambda, temperature;
{
   return 1.0;
}

/* function: NO2QY(double lambda, double temperature)
 *
 * Purpose: Calculate the quantum yield of NO2.
 *
 * Implementation: The data in NASA 90-1 were fit using parabolic approximation
 * for the wavelengths from 285 to 394 and a forth order polynomial for the
 * wavelengths from 395 to 423.
 */

#undef A0
#define A0  0.9955302581
#undef A1
#define A1  0.0001790401
#undef A2
#define A2 -0.0000046925

#define B0 -1510.7327103
#define B1    49.226740374
```

```
#define B2    -0.5976602682
#define B3     0.0032073379
#define B4    -0.000006424


double NO2QY(lambda, temperature)
double lambda, temperature;
{
   int i, j;
   extern double no2qy1[19], no2qy2[44];

   if (lambda < 285.0)
      return 1.0;
   else if (lambda < 395.0)
      return (A0 + A1*(lambda-285.0) + A2*pow(lambda-285.0,2.0));
   else if (lambda < 423.0)
      return ( B0 + B1*(lambda-285.0) + B2*pow(lambda-285.0,2.0) +
               B3*pow(lambda-285.0,3.0) + B4*pow(lambda-285.0,4.0) );
   else
      return 0.0;
}

/*
 * The functions for the NO3 quantum yields were derived from Atkinson
 * and Lloyd (1984). Note that the total quantum yield is above zero.
 */

#undef A0
#define A0 0.5
#undef A1
#define A1 30.0
#undef A2
#define A2 589.0

double NO3aQY(lambda, temperature)
double lambda, temperature;
{
   if (lambda < A2)
      return 0.0;
   else
      return (A0 * exp(A1*(1.0-lambda/A2)));
}

#undef A0
```

```
#define A0 93.877800729
#undef A1
#define A1 -0.283519671
#undef A2
#define A2 0.0002139621

double NO3bQY(lambda, temperature)
double lambda, temperature;
{
   if (lambda < 592.67110079)
      return 1.0;
   else if (lambda < 648.09488675)
      return (A0 + A1*lambda + A2*pow(lambda,2.0));
   else
      return 0.0;
}

double HNO2QY(lambda,temperature)
double lambda, temperature;
{
   return 1.0;
}

#undef A0
#define A0 120.075505828
#undef A1
#define A1 -1.336996892
#undef A2
#define A2 0.0049254662
#undef A3
#define A3 -0.000005981

double H2COaQY(lambda, temperature)
double lambda, temperature;
{
   if (lambda < 240.0)
      return 0.21;
   else if (lambda < 340.0)
      return (A0 + A1*lambda + A2*pow(lambda,2.0) + A3*pow(lambda,3.0));
   else
      return 0.0;
}

#undef A0
```

```
#define A0 5529.8069309
#undef A1
#define A1 -98.797426552
#undef A2
#define A2 0.7025906395
#undef A3
#define A3 -0.0024853642
#undef A4
#define A4 0.0000043728
#undef A5
#define A5 -0.0000000031
#undef A6
#define A6 4.4827141E-11

double H2CObQY(double lambda, double temperature, double pressure)
{
   if (lambda < 301.25)
      return 0.251;
   else if (lambda < 303.75)
      return 0.247;
   else if (lambda < 306.25)
      return 0.247;
   else if (lambda < 308.75)
      return 0.252;
   else if (lambda < 311.25)
      return 0.261;
   else if (lambda < 313.75)
      return 0.276;
   else if (lambda < 316.25)
      return 0.316;
   else if (lambda < 318.75)
      return 0.368;
   else if (lambda < 321.75)
      return 0.423;
   else if (lambda < 323.75)
      return 0.480;
   else if (lambda < 326.25)
      return 0.550;
   else if (lambda < 328.75)
      return 0.634;
   else if (lambda < 331.25)
      return 0.697;
   else if (lambda < 333.75)
      return 0.739;
```

```
   else if (lambda < 336.25)
      return 0.728;
   else if (lambda < 338.75)
      return 0.667;
   else if (lambda < 341.25)
      return 0.602;
   else if (lambda < 343.75)
      return 0.535;
   else if (lambda < 346.25)
      return 0.469;
   else if (lambda < 348.75)
      return 0.405;
   else if (lambda < 351.25)
      return 0.337;
   else if (lambda < 353.75)
      return 0.265;
   else
      return 0.197;
}

double CH3OOHQY(double lambda, double temperature)
{
   return 1.0;
}

double HNO3QY(double lambda, double temperature)
{
   return 1.0;
}

double HO2NO2QY(double lambda, double temperature)
{
   return 0.333;
}

double N2O5QY(double lambda, double temperature)
{
   return 1.0;
}
```

A.19 solvemat.c

```
/* Copyright 1988 and 1992 by Press, Teukolsky, Vetterling, and Flannery */
```

```
#include <stdio.h>
#include <stddef.h>
#include <stdlib.h>
#include <math.h>

#define SWAP(a,b) {dum=(a);(a)=(b);(b)=dum;}
#define TINY 1.0e-20

#define NR_END 1
#define FREE_ARG char*

void solve_mat(), bandec(), banbks(), tridag(), free_submatrix(), nrerror();
double **dmatrix();
double **submatrix();

void solve_mat(double **a,int n,int ml,int mu, double *b)
{
   double **al, **aa, d;
   unsigned long indx[200];

   al = dmatrix(1,n,1,ml);
   aa = submatrix(a,0,(n-1),0,(ml+mu),1,1);
   bandec(aa,n,ml,mu,al,indx-1,&d);
   banbks(aa,n,ml,mu,al,indx-1,b-1);
   free_submatrix(aa,1,n,1,ml);
   free(al);
}

void bandec(double **a,
    unsigned long n,
    int m1,
    int m2,
    double **al,
    unsigned long indx[],
    double *d)
{
   unsigned long i, j, k, l;
   int mm;
   double dum;

   mm = m1 + m2 + 1;
   l = m1;
```

```
  for (i=1;i<=m1;i++)
  {
     for (j=m1+2-i;j<=mm;j++)
a[i][j-1] = a[i][j];
     l--;
     for (j=mm-l;j<=mm;j++)
a[i][j] = 0.0;
  }
  *d = 1.0;
  l = m1;
  for (k=1;k<=n;k++)
  {
     dum = a[k][1];
     i=k;
     if (l < n)
l++;
     for (j=k+1;j<=l;j++)
     {
if (fabs(a[j][1]) > fabs(dum))
{
   dum = a[j][1];
   i = j;
}
     }
     indx[k] = i;
     if (dum == 0.0)
a[k][1] = TINY;
     if (i != k)
     {
*d = -(*d);
for (j=1;j<=mm;j++)
   SWAP(a[k][j],a[i][j]);
     }
     for (i=k+1;i<=l;i++)
     {
dum = a[i][1] / a[k][1];
al[k][i-k] = dum;
for (j=2;j<=mm;j++)
   a[i][j-1] = a[i][j] - dum*a[k][j];
a[i][mm] = 0.0;
     }
  }
}
```

```
void banbks(double **a,
    unsigned long n,
    int m1,
    int m2,
    double **al,
    unsigned long indx[],
    double b[])
{
   unsigned long i, k, l;
   int mm;
   double dum;

   mm = m1 + m2 + 1;
   l = m1;
   for (k=1;k<=n;k++)
   {
      i = indx[k];
      if (i != k)
 SWAP(b[k],b[i])
      if (l < n)
 l++;
      for (i=k+1;i<=l;i++)
 b[i] -= al[k][i-k]*b[k];
   }
   l = 1;
   for (i=n;i>=1;i--)
   {
      dum = b[i];
      for (k=2;k<=l;k++)
 dum -= a[i][k]*b[k+i-1];
      b[i] = dum / a[i][1];
      if (l < mm)
 l++;
   }
}

void tridag(a,b,c,r,u,n)
double a[], b[], c[], r[], u[];
int n;
{
   int j;
   double bet, *gam, *vector();
   void nrerror();
```

```
   gam = (double *) malloc(n*sizeof(double));

   if (b[1] == 0.0)
      nrerror("Error 1 in Tridag");
   u[1]=r[1]/(bet=b[1]);
   for (j=2;j<=n;j++)
   {
      gam[j] = c[j-1]/bet;
      bet = b[j] - a[j]*gam[j];
      if (bet == 0.0)
 nrerror("Error 2 in Tridag");
      u[j] = (r[j]-a[j]*u[j-1])/bet;
   }
   for (j=(n-1);j>=1;j--)
      u[j] -= gam[j+1]*u[j+1];
   free(gam);
}

double **dmatrix(long nrl, long nrh, long ncl, long nch)
{
   long i, nrow=nrh-nrl+1, ncol=nch-ncl+1;
   double **m;

   m = (double **) malloc((size_t)((nrow+NR_END)*sizeof(double*)));
   if (!m) nrerror("allocation failure 1 in matrix()");
   m += NR_END;
   m -= nrl;

   m[nrl] = (double *) malloc((size_t)((nrow*ncol+NR_END)*sizeof(double)));
   if (!m[nrl]) nrerror("allocation failure 2 in matrix()");
   m[nrl] += NR_END;
   m[nrl] -= ncl;

   for (i=nrl+1;i<=nrh;i++) m[i] = m[i-1]+ncol;

   return m;
}

double **submatrix(double **a, long oldrl, long oldrh, long oldcl, long oldch,
long newrl, long newcl)
{
   long i, j, nrow=oldrh-oldrl+1, ncol=oldcl-newcl;
   double **m;
```

```
    m = (double **) malloc((size_t) ((nrow+NR_END)*sizeof(double*)));
    if (!m) nrerror("allocation failure in submatrix()");
    m += NR_END;
    m -= newrl;

    for (i=oldrl,j=newrl;i<=oldrh;i++,j++)
        m[j] = a[i]+ncol;

    return m;
}

void free_submatrix(double **b, long nrl, long nrh, long ncl, long nch)
{
    free((FREE_ARG) (b+nrl-NR_END));
}

void nrerror(char error_text[])
{
    fprintf(stderr,"%s\n", error_text);
    fprintf(stderr,"...now exiting to system...\n");
    exit(1);
}

void thomas(double **a, int n, double *b)
{
    int i, k;
    double *u, **aa, *x;

   for (i=1;i<n;i++)
   {
      a[i][1] = a[i][1]/a[i-1][2];
      a[i][2] = a[i][2] - a[i][1]*a[i-1][3];
   }

   for (i=1;i<n;i++)
      b[i]=b[i]-a[i][1]*b[i-1];

   x[n-1] = b[n-1]/a[n-1][1];
   for (k=1;k<n;k++)
   {
           i=n-k+1;
           x[i] = (b[i]-a[i][2]*x[i-1])/a[i][1];
   }
```

```
  for(i=0;i<n;i++)
     b[i]=x[i];
}
```

A.20 terrxn.c

```
/* Function: TerRxn
 *
 * Copyright 1993 F. Moraes and M.A.K. Khalil
 *
 * Permission to use, copy, modify, and distribute this software and its
 * documentation for any purpose and without fee is hereby granted, provided
 * that the above copyright notice appear in all copies and that both that
 * copyright notice and this permission notice appear in supporting
 * documentation. No representation is made about the suitability of this
 * software for any purpose.  It is provided "as is" without express or
 * implied warranty.
 *
 * Author: Francis Moraes (internet: francis@eeyore.atmos.ogi.edu)
 *         Global Change Research Center
 *         Oregon Graduate Institute
 *
 * PURPOSE: This function calculates the termolecular reaction rate
 * given the temperature (T), number density (M), and the four reaction
 * parameters (see DeMore et al.).
 *
 * VARIABLES:
 *
 * T: Temperature
 * numden: Number Density
 * K300: Low pressure K limit at 300 kelvin
 * N: Low pressure temperature factor
 * KINF300: High pressure K limit at 300 kelvin
 * M: High pressure temperature factor
 */

#include <math.h>

double TerRxn(T, numden, K300, N, KINF300, M)
double T, numden, K300, N, KINF300, M;
{
   double K0, KINF;

   K0   = K300    * pow(T/300.0,-N);
```

```
   KINF = KINF300 * pow(T/300.0,-M);

   return (( KO * numden / ( 1.0 + KO * numden / KINF ) ) *
          pow(0.6,1.0/(1.0+pow(log10(KO*numden/KINF),2.0))));
}
```

A.21 acm.h

```
#ifndef PI
#define PI      3.1415926536
#endif

#define SPACE_POINTS 22
#define TIME_POINTS 24

double inclination,
       latitude;
```

A.22 acs.h

```
#ifndef MAX
#define MAX 150
#endif
/*
   List of absorption cross sections for ozone at various wavelengths.
   The 0 column contains the wavelengths and the 1 column contains the
   absorption cross sections.
 */
double O3ACS[MAX][2],
/*
   List of absorption cross sections for other gases at various wavelengths.
   The 0 column contains the wavelengths, the 1 column contains the
   absorption cross sections, and the 2 column contains the linear
   change in ACS per Kelvin temperature change.
 */
       NO2ACS[MAX][3],
       NO3ACS[MAX][2],
       HNO2ACS[MAX][2],
       H2COACS[MAX][2],
       HNO3ACS[MAX][2],
       HO2NO2ACS[MAX][2],
       N2O5ACS[MAX][2];
```

```
/* The number of elements in the ACS arrays. */

int O3ACS_NUM,
    NO2ACS_NUM,
    NO3ACS_NUM,
    HNO2ACS_NUM,
    H2COACS_NUM,
    HNO3ACS_NUM,
    HO2NO2ACS_NUM,
    N2O5ACS_NUM;
```

A.23 actinic.h

```
#ifndef MAX
#define MAX 150
#endif

#define WAVELENGTH_POINTS 144
#define ANGLE_POINTS 10

#define LOW_WAVELENGTH 200.0
#define HIGH_WAVELENGTH 852.5

int num_wavelength_bins;

double ActFlux[WAVELENGTH_POINTS][ANGLE_POINTS][SPACE_POINTS];
double ActAngle[ANGLE_POINTS], ActBin[WAVELENGTH_POINTS];

#define AMdiff 1.66
```

A.24 gases.h

```
    double O1D[SPACE_POINTS+2][TIME_POINTS+1],
           O[SPACE_POINTS+2][TIME_POINTS+1],
           OH[SPACE_POINTS+2][TIME_POINTS+1],
           HO2[SPACE_POINTS+2][TIME_POINTS+1],
           H2O2[SPACE_POINTS+2][TIME_POINTS+1],
           H[SPACE_POINTS+2][TIME_POINTS+1],
           NO[SPACE_POINTS+2][TIME_POINTS+1],
           NO2[SPACE_POINTS+2][TIME_POINTS+1],
           NO3[SPACE_POINTS+2][TIME_POINTS+1],
           N2O5[SPACE_POINTS+2][TIME_POINTS+1],
           HNO2[SPACE_POINTS+2][TIME_POINTS+1],
```

```
        HO2NO2[SPACE_POINTS+2][TIME_POINTS+1],
        CH3[SPACE_POINTS+2][TIME_POINTS+1],
        H2CO[SPACE_POINTS+2][TIME_POINTS+1],
        CH3O[SPACE_POINTS+2][TIME_POINTS+1],
        CH3O2[SPACE_POINTS+2][TIME_POINTS+1],
        CH3OOH[SPACE_POINTS+2][TIME_POINTS+1],
        HCO[SPACE_POINTS+2][TIME_POINTS+1],
        CH4[SPACE_POINTS+2][TIME_POINTS+1];

  double CO[SPACE_POINTS+1],
        NOX[SPACE_POINTS+1],
        H2O[SPACE_POINTS+1],
        HNO3[SPACE_POINTS+1],
        O3[SPACE_POINTS+2][TIME_POINTS+1],
        N2[SPACE_POINTS+1],
        O2[SPACE_POINTS+1],
        H2[SPACE_POINTS+1],
        N2O[SPACE_POINTS+1],
        CH4_FLUX[SPACE_POINTS];
```

A.25 j.h

```
/* absorption cross section data files */
#define O3ACS_FILE "dat/o3acs.dat"
#define NO2ACS_FILE "dat/no2acs.dat"
#define NO3ACS_FILE "dat/no3acs.dat"
#define HNO2ACS_FILE "dat/hno2acs.dat"
#define H2COACS_FILE "dat/h2coacs.dat"
#define HNO3ACS_FILE "dat/hno3acs.dat"
#define HO2NO2ACS_FILE "dat/hno4acs.dat"
#define N2O5ACS_FILE "dat/n2o5acs.dat"
```

A.26 kbinary.h

```
/* header file: binary.h
 *
 * purpose: This file contains all of the binary reactions that are
 * used in the model. The first letter of the definition indicated that
 * it is a K value (thermal reaction). The next set of letters and
 * numbers are the first reactant and the second (separated by an
 * underscore) is the second.
 *
 * The functions are dependent upon temperature (T), pressure (P), and
```

```
 * number density (M).
 */

#include <math.h>

#define getKO1D_N2(T) (1.8E-11 * exp(110.0/(T)))
#define getKO1D_O2(T) (3.2E-11 * exp(70.0/(T)))
#define getKO1D_H2O (2.2E-10)
#define getKO1D_H2 (1.0E-10)
#define getKO1D_CH4a (1.4E-10)
#define getKO1D_CH4b (1.4E-11)
#define getKO1D_N2O (6.7E-11)
#define getKOH_H2(T) (5.5E-12 * exp(-2000.0/(T)))
#define getKOH_O3(T) (1.6E-12 * exp(-940.0/(T)))
#define getKHO2_O3(T) (1.1E-14 * exp(-500.0/(T)))
#define getKOH_HO2(T) (4.8E-11 * exp(250.0/(T)))
#define getKHO2_HO2a(T) (2.3E-13 * exp(600.0/(T)))
#define getKHO2_HO2b(M,T) (1.7E-33 * (M) * exp(1000.0/(T)))
#define getKOH_H2O2(T) (2.9E-12 * exp(-160.0/(T)))
#define getKNO_HO2(T) (3.7E-12 * exp(250.0/(T)))
#define getKNO_O3(T) (2.0E-12 * exp(-1400.0/(T)))
#define getKNO_NO3(T) (1.5E-11 * exp(250.0/(T)))
#define getKNO2_O3(T) (1.2E-13 * exp(-2450/(T)))
#define getKOH_CO(P) (1.5E-13 * (1.0 + 0.6*(P)))
#define getKOH_CH4(T) (2.9E-12 * exp(-1820.0/(T)))
#define getKOH_H2CO (1.0E-11)
#define getKOH_CH3OOH (1.0E-11)
#define getKCH3O_O2(T) (3.9E-14 * exp(-900.0/(T)))
#define getKHCO_O2(T) (3.5E-12 * exp(140.0/(T)))
#define getKCH3O2_CH3O2(T) (1.6E-13 * exp(220.0/(T)))
#define getKCH3O2_HO2(T) (7.7E-14 * exp(1300.0/(T)))
#define getKCH3O2_NO(T) (4.2E-12 * exp(180.0/(T)))

#define getKO_O3(T) (8.0E-12 * exp(-2060.0/(T)))
#define getKO_NO2(T) (6.5E-12 * exp(120.0/(T)))
#define getKH_O3(T) (1.4E-10 * exp(-470.0/(T)))
#define getKOH_O(T) (2.2e-11 * exp(120.0/(T)))
#define getKHO2_O(T) (3.0e-11 * exp(200.0/(T)))
#define getKH2O2_O(T) (1.4e-12 * exp(-2000.0/(T)))
#define getKOH_OHa(T) (4.2e-12 * exp(-240.0/(T)))
#define getKH_HO2(T) (8.1e-11)
#define getKH2CO_O(T) (3.4e-11 * exp(-1600.0/(T)))
#define getKH2_O(T) (1.6e-11 * exp(-2230.0/(T)))
#define getKH2_O1D(T) (1.0e-10)
```

```
#define getKOH_HO2NO2(T) (1.3e-12 * exp(380.0/(T)))
```

A.27 kter.h

```
/* header file: Kter.h
 *
 * purpose: This file contains all of the termolecular reactions that are
 * used in the model. The first letter of the definition indicated that
 * it is a K value (thermal reaction). The next set of letters and
 * numbers are the first reactant and the second (separated by an
 * underscore) is the second.
 *
 * The functions are dependent upon temperature (T), pressure (P), and
 * number density (M).
 */

#include <math.h>

#define getKH_O2(T,M) (TerRxn((T),(M),5.7E-32,1.6,7.5E-11,0.0))
/* Note: The high pressure limit is assumed to be equal to the low
 * pressure limit for O + O2 -> O3
 */
#define getKO_O2(T,M) (6.0E-34*pow((T)/300.0,2.3)*(M))
#define getKCH3_O2(T,M) (TerRxn((T),(M),4.5E-31,3.0,1.8E-12,1.7))
#define getKOH_NO(T,M) (TerRxn((T),(M),7.0E-31,2.6,1.5E-11,0.5))
#define getKOH_NO2(T,M) (TerRxn((T),(M),2.6E-30,3.2,2.4E-11,1.3))
#define getKHO2_NO2(T,M) (TerRxn((T),(M),1.8E-31,3.2,4.7E-12,1.4))
#define getKNO_O(T,M) (TerRxn((T),(M),9.9E-32,1.5,3.0E-11,0.0))
#define getKNO2_NO3(T,M) (TerRxn((T),(M),2.2E-30,3.9,1.5E-12,0.7))
#define getKNO2_CH3O2(T,M) (TerRxn((T),(M),1.5E-30,4.0,6.5E-12,2.0))
#define getKN2O5(T,M) (getKNO2_NO3((T),(M)) * 5.65E26 * exp(-11001.0/(T)))
#define getKHO2NO2(T,M) (1.3E14 * exp(-10418.0/(T)))

#define getKOH_OHb(T,M) (TerRxn((T),(M),6.9E-31,0.8,1.5E-11,0.0))

double TerRxn(double,double,double,double,double,double);
```

A.28 rxn.h

```
double KO1D_N2[SPACE_POINTS+1],
       KO1D_O2[SPACE_POINTS+1],
       KO1D_H2O[SPACE_POINTS+1],
       KO1D_H2[SPACE_POINTS+1],
```

```
        KO1D_CH4a[SPACE_POINTS+1],
        KO1D_CH4b[SPACE_POINTS+1],
        KO1D_N2O[SPACE_POINTS+1],
        KOH_H2[SPACE_POINTS+1],
        KOH_O3[SPACE_POINTS+1],
        KHO2_O3[SPACE_POINTS+1],
        KOH_HO2[SPACE_POINTS+1],
        KHO2_HO2a[SPACE_POINTS+1],
        KHO2_HO2b[SPACE_POINTS+1],
        KOH_H2O2[SPACE_POINTS+1],
        KNO_HO2[SPACE_POINTS+1],
        KNO_O3[SPACE_POINTS+1],
        KNO_NO3[SPACE_POINTS+1],
        KNO2_O3[SPACE_POINTS+1],
        KOH_CO[SPACE_POINTS+1],
        KOH_CH4[SPACE_POINTS+1],
        KOH_H2CO[SPACE_POINTS+1],
        KOH_CH3OOH[SPACE_POINTS+1],
        KCH3O_O2[SPACE_POINTS+1],
        KHCO_O2[SPACE_POINTS+1],
        KCH3O2_CH3O2[SPACE_POINTS+1],
        KCH3O2_HO2[SPACE_POINTS+1],
        KCH3O2_NO[SPACE_POINTS+1],

        KO_O3[SPACE_POINTS+1],
        KO_NO2[SPACE_POINTS+1],
        KH_O3[SPACE_POINTS+1],
        KOH_O[SPACE_POINTS+1],
KHO2_O[SPACE_POINTS+1],
KH2O2_O[SPACE_POINTS+1],
KOH_HNO3[SPACE_POINTS+1],
KOH_OHa[SPACE_POINTS+1],
KOH_OHb[SPACE_POINTS+1],
KH_HO2[SPACE_POINTS+1],
KH2CO_O[SPACE_POINTS+1],
KH2_O[SPACE_POINTS+1],
KH2_O1D[SPACE_POINTS+1],
KOH_HO2NO2[SPACE_POINTS+1];

 /* K values for Termolecular Reactions */

 double KH_O2[SPACE_POINTS+1],
        KO_O2[SPACE_POINTS+1],
        KCH3_O2[SPACE_POINTS+1],
```

```
        KOH_NO[SPACE_POINTS+1],
        KOH_NO2[SPACE_POINTS+1],
        KHO2_NO2[SPACE_POINTS+1],
        KNO_O[SPACE_POINTS+1],
        KNO2_NO3[SPACE_POINTS+1],
        KNO2_CH3O2[SPACE_POINTS+1],
        KN2O5[SPACE_POINTS+1],
        KHO2NO2[SPACE_POINTS+1];

double KOH_HNO3[SPACE_POINTS+1];

/* K values for heterogeneous chemistry */

double Khet[SPACE_POINTS+1];
double JO3[SPACE_POINTS+1][TIME_POINTS+1],
       JO3b[SPACE_POINTS+1][TIME_POINTS+1],
       JH2O2[SPACE_POINTS+1][TIME_POINTS+1],
       JNO2[SPACE_POINTS+1][TIME_POINTS+1],
       JNO3a[SPACE_POINTS+1][TIME_POINTS+1],
       JNO3b[SPACE_POINTS+1][TIME_POINTS+1],
       JHNO2[SPACE_POINTS+1][TIME_POINTS+1],
       JH2COa[SPACE_POINTS+1][TIME_POINTS+1],
       JH2COb[SPACE_POINTS+1][TIME_POINTS+1],
       JCH3OOH[SPACE_POINTS+1][TIME_POINTS+1],
       JHNO3[SPACE_POINTS+1][TIME_POINTS+1],
       JHO2NO2[SPACE_POINTS+1][TIME_POINTS+1],
       JN2O5[SPACE_POINTS+1][TIME_POINTS+1];
```

A.29 solve.h

```
/* index values for the solve and output arrays */

#define IO1D 0
#define IO 1
#define IOH 2
#define IH 3
#define IHO2 4
#define IH2O2 5
#define INO 6
#define IHNO2 7
#define INO2 8
#define IHO2NO2 9
#define INO3 10
#define IN2O5 11
```

```
#define ICH3 12
#define ICH302 13
#define ICH300H 14
#define ICH30 15
#define IH2CO 16
#define IHCO 17
#define ICH4 18
```

Appendix B

GCRC-ACM Input Data

B.1 albedoland.dat

-85	0.50	0.50	0.50	0.50
-75	0.50	0.50	0.50	0.50
-65	0.20	0.20	0.20	0.20
-55	0.23	0.23	0.23	0.23
-45	0.22	0.22	0.22	0.22
-35	0.24	0.24	0.24	0.24
-25	0.22	0.22	0.22	0.22
-15	0.17	0.17	0.17	0.17
-5	0.14	0.14	0.14	0.14
5	0.14	0.14	0.14	0.14
15	0.18	0.18	0.18	0.18
25	0.26	0.26	0.26	0.26
35	0.22	0.22	0.22	0.22
45	0.21	0.21	0.21	0.21
55	0.17	0.17	0.17	0.17
65	0.17	0.17	0.17	0.17
75	0.25	0.25	0.25	0.25
85	0.45	0.45	0.45	0.45

B.2 albedosea.dat

-85	0.04	0.04	0.04	0.04
-75	0.04	0.04	0.04	0.04
-65	0.04	0.04	0.04	0.04
-55	0.04	0.04	0.04	0.04
-45	0.04	0.04	0.04	0.04
-35	0.04	0.04	0.04	0.04
-25	0.04	0.04	0.04	0.04
-15	0.04	0.04	0.04	0.04
-5	0.04	0.04	0.04	0.04
5	0.04	0.04	0.04	0.04
15	0.04	0.04	0.04	0.04
25	0.04	0.04	0.04	0.04
35	0.04	0.04	0.04	0.04
45	0.04	0.04	0.04	0.04
55	0.04	0.04	0.04	0.04
65	0.04	0.04	0.04	0.04
75	0.04	0.04	0.04	0.04
85	0.04	0.04	0.04	0.04

B.3 ch4.dat

85	0.5	4.4E+13	4.3E+13	4.2E+13	4.3E+13
85	1.5	4.0E+13	3.9E+13	3.8E+13	3.9E+13
85	2.5	3.6E+13	3.5E+13	3.5E+13	3.5E+13
85	3.5	3.2E+13	3.2E+13	3.1E+13	3.2E+13
85	4.5	2.9E+13	2.9E+13	2.8E+13	2.9E+13
85	5.5	2.6E+13	2.6E+13	2.5E+13	2.6E+13
85	6.5	2.3E+13	2.3E+13	2.3E+13	2.3E+13
85	7.5	2.1E+13	2.1E+13	2.0E+13	2.1E+13
85	8.5	1.9E+13	1.8E+13	1.8E+13	1.8E+13
85	9.5	1.7E+13	1.6E+13	1.6E+13	1.6E+13
85	10.5	1.5E+13	1.4E+13	1.4E+13	1.4E+13
85	11.5	1.3E+13	1.2E+13	1.2E+13	1.2E+13
85	12.5	1.1E+13	1.1E+13	1.0E+13	1.1E+13
85	13.5	9.1E+12	8.9E+12	8.8E+12	8.9E+12
85	14.5	7.3E+12	7.2E+12	7.1E+12	7.2E+12
85	18.5	3.3E+12	3.3E+12	3.2E+12	3.3E+12
85	24.5	1.5E+12	1.5E+12	1.5E+12	1.5E+12
85	29.5	6.9E+11	6.8E+11	6.7E+11	6.8E+11
85	34.5	3.2E+11	3.1E+11	3.1E+11	3.1E+11
85	39.5	1.5E+11	1.5E+11	1.5E+11	1.5E+11
85	44.5	7.4E+10	7.3E+10	7.2E+10	7.3E+10
85	49.5	3.9E+10	3.8E+10	3.7E+10	3.8E+10
75	0.5	4.3E+13	4.3E+13	4.2E+13	4.3E+13
75	1.5	3.9E+13	3.9E+13	3.8E+13	3.9E+13
75	2.5	3.6E+13	3.5E+13	3.4E+13	3.5E+13
75	3.5	3.2E+13	3.2E+13	3.1E+13	3.2E+13
75	4.5	2.9E+13	2.8E+13	2.8E+13	2.8E+13
75	5.5	2.6E+13	2.6E+13	2.5E+13	2.6E+13
75	6.5	2.3E+13	2.3E+13	2.2E+13	2.3E+13
75	7.5	2.1E+13	2.0E+13	2.0E+13	2.0E+13
75	8.5	1.8E+13	1.8E+13	1.8E+13	1.8E+13
75	9.5	1.6E+13	1.6E+13	1.6E+13	1.6E+13
75	10.5	1.4E+13	1.4E+13	1.4E+13	1.4E+13

75	11.5	1.3E+13	1.2E+13	1.2E+13	1.2E+13
75	12.5	1.1E+13	1.1E+13	1.0E+13	1.1E+13
75	13.5	9.0E+12	8.8E+12	8.7E+12	8.8E+12
75	14.5	7.2E+12	7.1E+12	7.0E+12	7.1E+12
75	18.5	3.3E+12	3.3E+12	3.2E+12	3.3E+12
75	24.5	1.5E+12	1.5E+12	1.5E+12	1.5E+12
75	29.5	6.9E+11	6.8E+11	6.6E+11	6.8E+11
75	34.5	3.2E+11	3.1E+11	3.1E+11	3.1E+11
75	39.5	1.5E+11	1.5E+11	1.5E+11	1.5E+11
75	44.5	7.4E+10	7.2E+10	7.1E+10	7.2E+10
75	49.5	3.8E+10	3.8E+10	3.7E+10	3.8E+10
65	0.5	4.3E+13	4.2E+13	4.2E+13	4.2E+13
65	1.5	3.9E+13	3.8E+13	3.8E+13	3.8E+13
65	2.5	3.5E+13	3.5E+13	3.4E+13	3.5E+13
65	3.5	3.2E+13	3.1E+13	3.1E+13	3.1E+13
65	4.5	2.9E+13	2.8E+13	2.8E+13	2.8E+13
65	5.5	2.6E+13	2.5E+13	2.5E+13	2.5E+13
65	6.5	2.3E+13	2.3E+13	2.2E+13	2.3E+13
65	7.5	2.1E+13	2.0E+13	2.0E+13	2.0E+13
65	8.5	1.8E+13	1.8E+13	1.8E+13	1.8E+13
65	9.5	1.6E+13	1.6E+13	1.6E+13	1.6E+13
65	10.5	1.4E+13	1.4E+13	1.4E+13	1.4E+13
65	11.5	1.2E+13	1.2E+13	1.2E+13	1.2E+13
65	12.5	1.1E+13	1.0E+13	1.0E+13	1.0E+13
65	13.5	8.9E+12	8.8E+12	8.6E+12	8.8E+12
65	14.5	7.2E+12	7.1E+12	6.9E+12	7.1E+12
65	18.5	3.3E+12	3.2E+12	3.2E+12	3.2E+12
65	24.5	1.5E+12	1.5E+12	1.4E+12	1.5E+12
65	29.5	6.8E+11	6.7E+11	6.6E+11	6.7E+11
65	34.5	3.1E+11	3.1E+11	3.0E+11	3.1E+11
65	39.5	1.5E+11	1.5E+11	1.4E+11	1.5E+11
65	44.5	7.3E+10	7.2E+10	7.1E+10	7.2E+10
65	49.5	3.8E+10	3.7E+10	3.7E+10	3.7E+10
55	0.5	4.3E+13	4.2E+13	4.1E+13	4.2E+13
55	1.5	3.9E+13	3.8E+13	3.7E+13	3.8E+13
55	2.5	3.5E+13	3.4E+13	3.4E+13	3.4E+13
55	3.5	3.2E+13	3.1E+13	3.1E+13	3.1E+13
55	4.5	2.8E+13	2.8E+13	2.7E+13	2.8E+13
55	5.5	2.6E+13	2.5E+13	2.5E+13	2.5E+13
55	6.5	2.3E+13	2.2E+13	2.2E+13	2.2E+13
55	7.5	2.0E+13	2.0E+13	2.0E+13	2.0E+13
55	8.5	1.8E+13	1.8E+13	1.8E+13	1.8E+13
55	9.5	1.6E+13	1.6E+13	1.6E+13	1.6E+13
55	10.5	1.4E+13	1.4E+13	1.4E+13	1.4E+13
55	11.5	1.2E+13	1.2E+13	1.2E+13	1.2E+13
55	12.5	1.1E+13	1.0E+13	1.0E+13	1.0E+13
55	13.5	8.8E+12	8.7E+12	8.6E+12	8.7E+12
55	14.5	7.1E+12	7.0E+12	6.9E+12	7.0E+12
55	18.5	3.3E+12	3.2E+12	3.1E+12	3.2E+12
55	24.5	1.5E+12	1.5E+12	1.4E+12	1.5E+12
55	29.5	6.8E+11	6.7E+11	6.5E+11	6.7E+11
55	34.5	3.1E+11	3.1E+11	3.0E+11	3.1E+11
55	39.5	1.5E+11	1.5E+11	1.4E+11	1.5E+11
55	44.5	7.2E+10	7.1E+10	7.0E+10	7.1E+10
55	49.5	3.8E+10	3.7E+10	3.7E+10	3.7E+10
45	0.5	4.2E+13	4.2E+13	4.1E+13	4.2E+13
45	1.5	3.8E+13	3.8E+13	3.7E+13	3.8E+13
45	2.5	3.5E+13	3.4E+13	3.4E+13	3.4E+13
45	3.5	3.1E+13	3.1E+13	3.0E+13	3.1E+13
45	4.5	2.8E+13	2.8E+13	2.7E+13	2.8E+13
45	5.5	2.5E+13	2.5E+13	2.4E+13	2.5E+13
45	6.5	2.3E+13	2.2E+13	2.2E+13	2.2E+13
45	7.5	2.0E+13	2.0E+13	2.0E+13	2.0E+13
45	8.5	1.8E+13	1.8E+13	1.7E+13	1.8E+13
45	9.5	1.6E+13	1.6E+13	1.5E+13	1.6E+13
45	10.5	1.4E+13	1.4E+13	1.4E+13	1.4E+13
45	11.5	1.2E+13	1.2E+13	1.2E+13	1.2E+13
45	12.5	1.0E+13	1.0E+13	1.0E+13	1.0E+13
45	13.5	8.8E+12	8.6E+12	8.5E+12	8.6E+12
45	14.5	7.1E+12	6.9E+12	6.8E+12	6.9E+12
45	18.5	3.2E+12	3.2E+12	3.1E+12	3.2E+12
45	24.5	1.5E+12	1.4E+12	1.4E+12	1.4E+12
45	29.5	6.7E+11	6.6E+11	6.5E+11	6.6E+11
45	34.5	3.1E+11	3.0E+11	3.0E+11	3.0E+11
45	39.5	1.5E+11	1.4E+11	1.4E+11	1.4E+11
45	44.5	7.2E+10	7.1E+10	6.9E+10	7.1E+10
45	49.5	3.8E+10	3.7E+10	3.6E+10	3.7E+10
35	0.5	4.2E+13	4.1E+13	4.1E+13	4.1E+13
35	1.5	3.8E+13	3.7E+13	3.7E+13	3.7E+13
35	2.5	3.4E+13	3.4E+13	3.3E+13	3.4E+13
35	3.5	3.1E+13	3.1E+13	3.0E+13	3.1E+13
35	4.5	2.8E+13	2.8E+13	2.7E+13	2.8E+13
35	5.5	2.5E+13	2.5E+13	2.4E+13	2.5E+13
35	6.5	2.2E+13	2.2E+13	2.2E+13	2.2E+13
35	7.5	2.0E+13	2.0E+13	1.9E+13	2.0E+13
35	8.5	1.8E+13	1.8E+13	1.7E+13	1.8E+13
35	9.5	1.6E+13	1.6E+13	1.5E+13	1.6E+13
35	10.5	1.4E+13	1.4E+13	1.4E+13	1.4E+13
35	11.5	1.2E+13	1.2E+13	1.2E+13	1.2E+13
35	12.5	1.0E+13	1.0E+13	1.0E+13	1.0E+13
35	13.5	8.7E+12	8.6E+12	8.4E+12	8.6E+12
35	14.5	7.0E+12	6.9E+12	6.8E+12	6.9E+12
35	18.5	3.2E+12	3.1E+12	3.1E+12	3.1E+12
35	24.5	1.5E+12	1.4E+12	1.4E+12	1.4E+12
35	29.5	6.7E+11	6.5E+11	6.4E+11	6.5E+11
35	34.5	3.1E+11	3.0E+11	3.0E+11	3.0E+11
35	39.5	1.5E+11	1.4E+11	1.4E+11	1.4E+11
35	44.5	7.1E+10	7.0E+10	6.9E+10	7.0E+10
35	49.5	3.7E+10	3.7E+10	3.6E+10	3.7E+10
25	0.5	4.2E+13	4.1E+13	4.0E+13	4.1E+13
25	1.5	3.8E+13	3.7E+13	3.6E+13	3.7E+13
25	2.5	3.4E+13	3.4E+13	3.3E+13	3.4E+13

25	3.5	3.1E+13	3.0E+13	3.0E+13	3.0E+13
25	4.5	2.8E+13	2.7E+13	2.7E+13	2.7E+13
25	5.5	2.5E+13	2.4E+13	2.4E+13	2.4E+13
25	6.5	2.2E+13	2.2E+13	2.2E+13	2.2E+13
25	7.5	2.0E+13	2.0E+13	1.9E+13	2.0E+13
25	8.5	1.8E+13	1.7E+13	1.7E+13	1.7E+13
25	9.5	1.6E+13	1.5E+13	1.5E+13	1.5E+13
25	10.5	1.4E+13	1.4E+13	1.3E+13	1.4E+13
25	11.5	1.2E+13	1.2E+13	1.2E+13	1.2E+13
25	12.5	1.0E+13	1.0E+13	1.0E+13	1.0E+13
25	13.5	8.6E+12	8.5E+12	8.3E+12	8.5E+12
25	14.5	7.0E+12	6.8E+12	6.7E+12	6.8E+12
25	18.5	3.2E+12	3.1E+12	3.1E+12	3.1E+12
25	24.5	1.4E+12	1.4E+12	1.4E+12	1.4E+12
25	29.5	6.6E+11	6.5E+11	6.4E+11	6.5E+11
25	34.5	3.0E+11	3.0E+11	2.9E+11	3.0E+11
25	39.5	1.4E+11	1.4E+11	1.4E+11	1.4E+11
25	44.5	7.1E+10	6.9E+10	6.8E+10	6.9E+10
25	49.5	3.7E+10	3.6E+10	3.6E+10	3.6E+10
15	0.5	4.1E+13	4.1E+13	4.0E+13	4.1E+13
15	1.5	3.7E+13	3.7E+13	3.6E+13	3.7E+13
15	2.5	3.4E+13	3.3E+13	3.3E+13	3.3E+13
15	3.5	3.1E+13	3.0E+13	3.0E+13	3.0E+13
15	4.5	2.8E+13	2.7E+13	2.7E+13	2.7E+13
15	5.5	2.5E+13	2.4E+13	2.4E+13	2.4E+13
15	6.5	2.2E+13	2.2E+13	2.1E+13	2.2E+13
15	7.5	2.0E+13	1.9E+13	1.9E+13	1.9E+13
15	8.5	1.8E+13	1.7E+13	1.7E+13	1.7E+13
15	9.5	1.6E+13	1.5E+13	1.5E+13	1.5E+13
15	10.5	1.4E+13	1.4E+13	1.3E+13	1.4E+13
15	11.5	1.2E+13	1.2E+13	1.2E+13	1.2E+13
15	12.5	1.0E+13	1.0E+13	9.9E+12	1.0E+13
15	13.5	8.6E+12	8.4E+12	8.3E+12	8.4E+12
15	14.5	6.9E+12	6.8E+12	6.6E+12	6.8E+12
15	18.5	3.1E+12	3.1E+12	3.0E+12	3.1E+12
15	24.5	1.4E+12	1.4E+12	1.4E+12	1.4E+12
15	29.5	6.5E+11	6.4E+11	6.3E+11	6.4E+11
15	34.5	3.0E+11	3.0E+11	2.9E+11	3.0E+11
15	39.5	1.4E+11	1.4E+11	1.4E+11	1.4E+11
15	44.5	7.0E+10	6.9E+10	6.8E+10	6.9E+10
15	49.5	3.7E+10	3.6E+10	3.5E+10	3.6E+10
5	0.5	4.1E+13	4.0E+13	4.0E+13	4.0E+13
5	1.5	3.7E+13	3.6E+13	3.6E+13	3.6E+13
5	2.5	3.4E+13	3.3E+13	3.2E+13	3.3E+13
5	3.5	3.0E+13	3.0E+13	2.9E+13	3.0E+13
5	4.5	2.7E+13	2.7E+13	2.6E+13	2.7E+13
5	5.5	2.4E+13	2.4E+13	2.4E+13	2.4E+13
5	6.5	2.2E+13	2.2E+13	2.1E+13	2.2E+13
5	7.5	2.0E+13	1.9E+13	1.9E+13	1.9E+13
5	8.5	1.7E+13	1.7E+13	1.7E+13	1.7E+13
5	9.5	1.5E+13	1.5E+13	1.5E+13	1.5E+13
5	10.5	1.4E+13	1.3E+13	1.3E+13	1.3E+13
5	11.5	1.2E+13	1.2E+13	1.1E+13	1.2E+13
5	12.5	1.0E+13	1.0E+13	9.8E+12	1.0E+13
5	13.5	8.5E+12	8.3E+12	8.2E+12	8.3E+12
5	14.5	6.8E+12	6.7E+12	6.6E+12	6.7E+12
5	18.5	3.1E+12	3.1E+12	3.0E+12	3.1E+12
5	24.5	1.4E+12	1.4E+12	1.4E+12	1.4E+12
5	29.5	6.5E+11	6.4E+11	6.3E+11	6.4E+11
5	34.5	3.0E+11	2.9E+11	2.9E+11	2.9E+11
5	39.5	1.4E+11	1.4E+11	1.4E+11	1.4E+11
5	44.5	6.9E+10	6.8E+10	6.7E+10	6.8E+10
5	49.5	3.6E+10	3.6E+10	3.5E+10	3.6E+10
-5	0.5	3.9E+13	4.0E+13	4.1E+13	4.0E+13
-5	1.5	3.6E+13	3.6E+13	3.7E+13	3.6E+13
-5	2.5	3.2E+13	3.3E+13	3.3E+13	3.3E+13
-5	3.5	2.9E+13	3.0E+13	3.0E+13	3.0E+13
-5	4.5	2.6E+13	2.7E+13	2.7E+13	2.7E+13
-5	5.5	2.3E+13	2.4E+13	2.4E+13	2.4E+13
-5	6.5	2.1E+13	2.1E+13	2.2E+13	2.1E+13
-5	7.5	1.9E+13	1.9E+13	1.9E+13	1.9E+13
-5	8.5	1.7E+13	1.7E+13	1.7E+13	1.7E+13
-5	9.5	1.5E+13	1.5E+13	1.5E+13	1.5E+13
-5	10.5	1.3E+13	1.3E+13	1.4E+13	1.3E+13
-5	11.5	1.1E+13	1.2E+13	1.2E+13	1.2E+13
-5	12.5	9.7E+12	9.9E+12	1.0E+13	9.9E+12
-5	13.5	8.1E+12	8.3E+12	8.4E+12	8.3E+12
-5	14.5	6.5E+12	6.7E+12	6.8E+12	6.7E+12
-5	18.5	3.0E+12	3.0E+12	3.1E+12	3.0E+12
-5	24.5	1.4E+12	1.4E+12	1.4E+12	1.4E+12
-5	29.5	6.2E+11	6.3E+11	6.4E+11	6.3E+11
-5	34.5	2.9E+11	2.9E+11	3.0E+11	2.9E+11
-5	39.5	1.4E+11	1.4E+11	1.4E+11	1.4E+11
-5	44.5	6.6E+10	6.8E+10	6.9E+10	6.8E+10
-5	49.5	3.5E+10	3.5E+10	3.6E+10	3.5E+10
-15	0.5	3.9E+13	4.0E+13	4.0E+13	4.0E+13
-15	1.5	3.5E+13	3.6E+13	3.7E+13	3.6E+13
-15	2.5	3.2E+13	3.3E+13	3.3E+13	3.3E+13
-15	3.5	2.9E+13	2.9E+13	3.0E+13	2.9E+13
-15	4.5	2.6E+13	2.6E+13	2.7E+13	2.6E+13
-15	5.5	2.3E+13	2.4E+13	2.4E+13	2.4E+13
-15	6.5	2.1E+13	2.1E+13	2.2E+13	2.1E+13
-15	7.5	1.9E+13	1.9E+13	1.9E+13	1.9E+13
-15	8.5	1.7E+13	1.7E+13	1.7E+13	1.7E+13
-15	9.5	1.5E+13	1.5E+13	1.5E+13	1.5E+13
-15	10.5	1.3E+13	1.3E+13	1.3E+13	1.3E+13
-15	11.5	1.1E+13	1.2E+13	1.2E+13	1.2E+13
-15	12.5	9.6E+12	9.9E+12	1.0E+13	9.9E+12
-15	13.5	8.1E+12	8.2E+12	8.4E+12	8.2E+12
-15	14.5	6.5E+12	6.6E+12	6.7E+12	6.6E+12
-15	18.5	3.0E+12	3.0E+12	3.1E+12	3.0E+12
-15	24.5	1.3E+12	1.4E+12	1.4E+12	1.4E+12

-15	29.5	6.2E+11	6.3E+11	6.4E+11	6.3E+11
-15	34.5	2.8E+11	2.9E+11	2.9E+11	2.9E+11
-15	39.5	1.3E+11	1.4E+11	1.4E+11	1.4E+11
-15	44.5	6.6E+10	6.7E+10	6.9E+10	6.7E+10
-15	49.5	3.5E+10	3.5E+10	3.6E+10	3.5E+10
-25	0.5	3.9E+13	4.0E+13	4.0E+13	4.0E+13
-25	1.5	3.5E+13	3.6E+13	3.7E+13	3.6E+13
-25	2.5	3.2E+13	3.3E+13	3.3E+13	3.3E+13
-25	3.5	2.9E+13	2.9E+13	3.0E+13	2.9E+13
-25	4.5	2.6E+13	2.6E+13	2.7E+13	2.6E+13
-25	5.5	2.3E+13	2.4E+13	2.4E+13	2.4E+13
-25	6.5	2.1E+13	2.1E+13	2.2E+13	2.1E+13
-25	7.5	1.9E+13	1.9E+13	1.9E+13	1.9E+13
-25	8.5	1.7E+13	1.7E+13	1.7E+13	1.7E+13
-25	9.5	1.5E+13	1.5E+13	1.5E+13	1.5E+13
-25	10.5	1.3E+13	1.3E+13	1.3E+13	1.3E+13
-25	11.5	1.1E+13	1.2E+13	1.2E+13	1.2E+13
-25	12.5	9.6E+12	9.9E+12	1.0E+13	9.9E+12
-25	13.5	8.1E+12	8.2E+12	8.4E+12	8.2E+12
-25	14.5	6.5E+12	6.6E+12	6.7E+12	6.6E+12
-25	18.5	3.0E+12	3.0E+12	3.1E+12	3.0E+12
-25	24.5	1.3E+12	1.4E+12	1.4E+12	1.4E+12
-25	29.5	6.2E+11	6.3E+11	6.4E+11	6.3E+11
-25	34.5	2.8E+11	2.9E+11	2.9E+11	2.9E+11
-25	39.5	1.3E+11	1.4E+11	1.4E+11	1.4E+11
-25	44.5	6.6E+10	6.7E+10	6.9E+10	6.7E+10
-25	49.5	3.5E+10	3.5E+10	3.6E+10	3.5E+10
-35	0.5	3.9E+13	4.0E+13	4.0E+13	4.0E+13
-35	1.5	3.5E+13	3.6E+13	3.7E+13	3.6E+13
-35	2.5	3.2E+13	3.3E+13	3.3E+13	3.3E+13
-35	3.5	2.9E+13	2.9E+13	3.0E+13	2.9E+13
-35	4.5	2.6E+13	2.6E+13	2.7E+13	2.6E+13
-35	5.5	2.3E+13	2.4E+13	2.4E+13	2.4E+13
-35	6.5	2.1E+13	2.1E+13	2.2E+13	2.1E+13
-35	7.5	1.9E+13	1.9E+13	1.9E+13	1.9E+13
-35	8.5	1.7E+13	1.7E+13	1.7E+13	1.7E+13
-35	9.5	1.5E+13	1.5E+13	1.5E+13	1.5E+13
-35	10.5	1.3E+13	1.3E+13	1.3E+13	1.3E+13
-35	11.5	1.1E+13	1.2E+13	1.2E+13	1.2E+13
-35	12.5	9.6E+12	9.9E+12	1.0E+13	9.9E+12
-35	13.5	8.1E+12	8.2E+12	8.4E+12	8.2E+12
-35	14.5	6.5E+12	6.6E+12	6.7E+12	6.6E+12
-35	18.5	3.0E+12	3.0E+12	3.1E+12	3.0E+12
-35	24.5	1.3E+12	1.4E+12	1.4E+12	1.4E+12
-35	29.5	6.2E+11	6.3E+11	6.4E+11	6.3E+11
-35	34.5	2.8E+11	2.9E+11	2.9E+11	2.9E+11
-35	39.5	1.3E+11	1.4E+11	1.4E+11	1.4E+11
-35	44.5	6.6E+10	6.7E+10	6.9E+10	6.7E+10
-35	49.5	3.5E+10	3.5E+10	3.6E+10	3.5E+10
-45	0.5	3.9E+13	4.0E+13	4.0E+13	4.0E+13
-45	1.5	3.5E+13	3.6E+13	3.7E+13	3.6E+13
-45	2.5	3.2E+13	3.3E+13	3.3E+13	3.3E+13
-45	3.5	2.9E+13	2.9E+13	3.0E+13	2.9E+13
-45	4.5	2.6E+13	2.6E+13	2.7E+13	2.6E+13
-45	5.5	2.3E+13	2.4E+13	2.4E+13	2.4E+13
-45	6.5	2.1E+13	2.1E+13	2.2E+13	2.1E+13
-45	7.5	1.9E+13	1.9E+13	1.9E+13	1.9E+13
-45	8.5	1.7E+13	1.7E+13	1.7E+13	1.7E+13
-45	9.5	1.5E+13	1.5E+13	1.5E+13	1.5E+13
-45	10.5	1.3E+13	1.3E+13	1.3E+13	1.3E+13
-45	11.5	1.1E+13	1.2E+13	1.2E+13	1.2E+13
-45	12.5	9.6E+12	9.9E+12	1.0E+13	9.9E+12
-45	13.5	8.1E+12	8.2E+12	8.4E+12	8.2E+12
-45	14.5	6.5E+12	6.6E+12	6.7E+12	6.6E+12
-45	18.5	3.0E+12	3.0E+12	3.1E+12	3.0E+12
-45	24.5	1.3E+12	1.4E+12	1.4E+12	1.4E+12
-45	29.5	6.2E+11	6.3E+11	6.4E+11	6.3E+11
-45	34.5	2.8E+11	2.9E+11	2.9E+11	2.9E+11
-45	39.5	1.3E+11	1.4E+11	1.4E+11	1.4E+11
-45	44.5	6.6E+10	6.7E+10	6.9E+10	6.7E+10
-45	49.5	3.5E+10	3.5E+10	3.6E+10	3.5E+10
-55	0.5	3.9E+13	4.0E+13	4.0E+13	4.0E+13
-55	1.5	3.5E+13	3.6E+13	3.7E+13	3.6E+13
-55	2.5	3.2E+13	3.3E+13	3.3E+13	3.3E+13
-55	3.5	2.9E+13	2.9E+13	3.0E+13	2.9E+13
-55	4.5	2.6E+13	2.6E+13	2.7E+13	2.6E+13
-55	5.5	2.3E+13	2.4E+13	2.4E+13	2.4E+13
-55	6.5	2.1E+13	2.1E+13	2.2E+13	2.1E+13
-55	7.5	1.9E+13	1.9E+13	1.9E+13	1.9E+13
-55	8.5	1.7E+13	1.7E+13	1.7E+13	1.7E+13
-55	9.5	1.5E+13	1.5E+13	1.5E+13	1.5E+13
-55	10.5	1.3E+13	1.3E+13	1.3E+13	1.3E+13
-55	11.5	1.1E+13	1.2E+13	1.2E+13	1.2E+13
-55	12.5	9.6E+12	9.9E+12	1.0E+13	9.9E+12
-55	13.5	8.1E+12	8.2E+12	8.4E+12	8.2E+12
-55	14.5	6.5E+12	6.6E+12	6.7E+12	6.6E+12
-55	18.5	3.0E+12	3.0E+12	3.1E+12	3.0E+12
-55	24.5	1.3E+12	1.4E+12	1.4E+12	1.4E+12
-55	29.5	6.2E+11	6.3E+11	6.4E+11	6.3E+11
-55	34.5	2.8E+11	2.9E+11	2.9E+11	2.9E+11
-55	39.5	1.3E+11	1.4E+11	1.4E+11	1.4E+11
-55	44.5	6.6E+10	6.7E+10	6.9E+10	6.7E+10
-55	49.5	3.5E+10	3.5E+10	3.6E+10	3.5E+10
-65	0.5	3.9E+13	4.0E+13	4.0E+13	4.0E+13
-65	1.5	3.5E+13	3.6E+13	3.7E+13	3.6E+13
-65	2.5	3.2E+13	3.3E+13	3.3E+13	3.3E+13
-65	3.5	2.9E+13	2.9E+13	3.0E+13	2.9E+13
-65	4.5	2.6E+13	2.6E+13	2.7E+13	2.6E+13
-65	5.5	2.3E+13	2.4E+13	2.4E+13	2.4E+13
-65	6.5	2.1E+13	2.1E+13	2.2E+13	2.1E+13
-65	7.5	1.9E+13	1.9E+13	1.9E+13	1.9E+13
-65	8.5	1.7E+13	1.7E+13	1.7E+13	1.7E+13

-65	9.5	1.5E+13	1.5E+13	1.5E+13	1.5E+13
-65	10.5	1.3E+13	1.3E+13	1.3E+13	1.3E+13
-65	11.5	1.1E+13	1.2E+13	1.2E+13	1.2E+13
-65	12.5	9.6E+12	9.9E+12	1.0E+13	9.9E+12
-65	13.5	8.1E+12	8.2E+12	8.4E+12	8.2E+12
-65	14.5	6.5E+12	6.6E+12	6.7E+12	6.6E+12
-65	18.5	3.0E+12	3.0E+12	3.1E+12	3.0E+12
-65	24.5	1.3E+12	1.4E+12	1.4E+12	1.4E+12
-65	29.5	6.2E+11	6.3E+11	6.4E+11	6.3E+11
-65	34.5	2.8E+11	2.9E+11	2.9E+11	2.9E+11
-65	39.5	1.3E+11	1.4E+11	1.4E+11	1.4E+11
-65	44.5	6.6E+10	6.7E+10	6.9E+10	6.7E+10
-65	49.5	3.5E+10	3.5E+10	3.6E+10	3.5E+10
-75	0.5	3.9E+13	4.0E+13	4.0E+13	4.0E+13
-75	1.5	3.5E+13	3.6E+13	3.7E+13	3.6E+13
-75	2.5	3.2E+13	3.3E+13	3.3E+13	3.3E+13
-75	3.5	2.9E+13	2.9E+13	3.0E+13	2.9E+13
-75	4.5	2.6E+13	2.6E+13	2.7E+13	2.6E+13
-75	5.5	2.3E+13	2.4E+13	2.4E+13	2.4E+13
-75	6.5	2.1E+13	2.1E+13	2.2E+13	2.1E+13
-75	7.5	1.9E+13	1.9E+13	1.9E+13	1.9E+13
-75	8.5	1.7E+13	1.7E+13	1.7E+13	1.7E+13
-75	9.5	1.5E+13	1.5E+13	1.5E+13	1.5E+13
-75	10.5	1.3E+13	1.3E+13	1.3E+13	1.3E+13
-75	11.5	1.1E+13	1.2E+13	1.2E+13	1.2E+13
-75	12.5	9.6E+12	9.9E+12	1.0E+13	9.9E+12
-75	13.5	8.1E+12	8.2E+12	8.4E+12	8.2E+12
-75	14.5	6.5E+12	6.6E+12	6.7E+12	6.6E+12
-75	18.5	3.0E+12	3.0E+12	3.1E+12	3.0E+12
-75	24.5	1.3E+12	1.4E+12	1.4E+12	1.4E+12
-75	29.5	6.2E+11	6.3E+11	6.4E+11	6.3E+11
-75	34.5	2.8E+11	2.9E+11	2.9E+11	2.9E+11
-75	39.5	1.3E+11	1.4E+11	1.4E+11	1.4E+11
-75	44.5	6.6E+10	6.7E+10	6.9E+10	6.7E+10
-75	49.5	3.5E+10	3.5E+10	3.6E+10	3.5E+10
-85	0.5	3.9E+13	4.0E+13	4.0E+13	4.0E+13
-85	1.5	3.5E+13	3.6E+13	3.7E+13	3.6E+13
-85	2.5	3.2E+13	3.3E+13	3.3E+13	3.3E+13
-85	3.5	2.9E+13	2.9E+13	3.0E+13	2.9E+13
-85	4.5	2.6E+13	2.6E+13	2.7E+13	2.6E+13
-85	5.5	2.3E+13	2.4E+13	2.4E+13	2.4E+13
-85	6.5	2.1E+13	2.1E+13	2.2E+13	2.1E+13
-85	7.5	1.9E+13	1.9E+13	1.9E+13	1.9E+13
-85	8.5	1.7E+13	1.7E+13	1.7E+13	1.7E+13
-85	9.5	1.5E+13	1.5E+13	1.5E+13	1.5E+13
-85	10.5	1.3E+13	1.3E+13	1.3E+13	1.3E+13
-85	11.5	1.1E+13	1.2E+13	1.2E+13	1.2E+13
-85	12.5	9.6E+12	9.9E+12	1.0E+13	9.9E+12
-85	13.5	8.1E+12	8.2E+12	8.4E+12	8.2E+12
-85	14.5	6.5E+12	6.6E+12	6.7E+12	6.6E+12
-85	18.5	3.0E+12	3.0E+12	3.1E+12	3.0E+12
-85	24.5	1.3E+12	1.4E+12	1.4E+12	1.4E+12
-85	29.5	6.2E+11	6.3E+11	6.4E+11	6.3E+11
-85	34.5	2.8E+11	2.9E+11	2.9E+11	2.9E+11
-85	39.5	1.3E+11	1.4E+11	1.4E+11	1.4E+11
-85	44.5	6.6E+10	6.7E+10	6.9E+10	6.7E+10
-85	49.5	3.5E+10	3.5E+10	3.6E+10	3.5E+10

B.4 coland.dat

85	0.5	3.5E+12	2.9E+12	2.5E+12	2.9E+12
85	1.5	3.2E+12	2.6E+12	2.2E+12	2.6E+12
85	2.5	2.8E+12	2.4E+12	2.0E+12	2.4E+12
85	3.5	2.4E+12	2.2E+12	1.8E+12	2.2E+12
85	4.5	2.3E+12	1.9E+12	1.7E+12	1.9E+12
85	5.5	2.1E+12	1.7E+12	1.5E+12	1.7E+12
85	6.5	1.8E+12	1.6E+12	1.2E+12	1.6E+12
85	7.5	1.6E+12	1.4E+12	1.2E+12	1.4E+12
85	8.5	1.4E+12	1.2E+12	1.0E+12	1.2E+12
85	9.5	1.3E+12	1.1E+12	9.0E+11	1.1E+12
85	10.5	1.0E+12	9.7E+11	8.1E+11	9.7E+11
85	11.5	9.8E+11	8.4E+11	7.0E+11	8.4E+11
85	12.5	8.4E+11	7.2E+11	6.0E+11	7.2E+11
85	13.5	7.1E+11	6.1E+11	5.1E+11	6.1E+11
85	14.5	5.7E+11	4.9E+11	4.1E+11	4.9E+11
85	18.5	2.6E+11	2.2E+11	1.8E+11	2.2E+11
85	24.5	1.2E+11	1.0E+11	8.4E+10	1.0E+11
85	29.5	5.4E+10	4.6E+10	3.8E+10	4.6E+10
85	34.5	2.5E+10	2.1E+10	1.7E+10	2.1E+10
85	39.5	1.2E+10	1.0E+10	8.4E+09	1.0E+10
85	44.5	5.9E+09	4.9E+09	4.1E+09	4.9E+09
85	49.5	3.0E+09	2.6E+09	2.2E+09	2.6E+09
75	0.5	3.5E+12	2.9E+12	2.5E+12	2.9E+12
75	1.5	3.2E+12	2.6E+12	2.2E+12	2.6E+12
75	2.5	2.8E+12	2.4E+12	2.0E+12	2.4E+12
75	3.5	2.4E+12	2.2E+12	1.8E+12	2.2E+12
75	4.5	2.3E+12	1.9E+12	1.7E+12	1.9E+12
75	5.5	2.1E+12	1.7E+12	1.5E+12	1.7E+12
75	6.5	1.8E+12	1.6E+12	1.2E+12	1.6E+12
75	7.5	1.6E+12	1.4E+12	1.2E+12	1.4E+12
75	8.5	1.4E+12	1.2E+12	1.0E+12	1.2E+12
75	9.5	1.3E+12	1.1E+12	9.0E+11	1.1E+12
75	10.5	1.0E+12	9.7E+11	8.1E+11	9.7E+11
75	11.5	9.8E+11	8.4E+11	7.0E+11	8.4E+11
75	12.5	8.4E+11	7.2E+11	6.0E+11	7.2E+11
75	13.5	7.1E+11	6.1E+11	5.1E+11	6.1E+11
75	14.5	5.7E+11	4.9E+11	4.1E+11	4.9E+11
75	18.5	2.6E+11	2.2E+11	1.8E+11	2.2E+11
75	24.5	1.2E+11	1.0E+11	8.4E+10	1.0E+11
75	29.5	5.4E+10	4.6E+10	3.8E+10	4.6E+10
75	34.5	2.5E+10	2.1E+10	1.7E+10	2.1E+10

75	39.5	1.2E+10	1.0E+10	8.4E+09	1.0E+10
75	44.5	5.9E+09	4.9E+09	4.1E+09	4.9E+09
75	49.5	3.0E+09	2.6E+09	2.2E+09	2.6E+09
65	0.5	3.5E+12	2.9E+12	2.5E+12	2.9E+12
65	1.5	3.2E+12	2.6E+12	2.2E+12	2.6E+12
65	2.5	2.8E+12	2.4E+12	2.0E+12	2.4E+12
65	3.5	2.4E+12	2.2E+12	1.8E+12	2.2E+12
65	4.5	2.3E+12	1.9E+12	1.7E+12	1.9E+12
65	5.5	2.1E+12	1.7E+12	1.5E+12	1.7E+12
65	6.5	1.8E+12	1.6E+12	1.2E+12	1.6E+12
65	7.5	1.6E+12	1.4E+12	1.2E+12	1.4E+12
65	8.5	1.4E+12	1.2E+12	1.0E+12	1.2E+12
65	9.5	1.3E+12	1.1E+12	9.0E+11	1.1E+12
65	10.5	1.0E+12	9.7E+11	8.1E+11	9.7E+11
65	11.5	9.8E+11	8.4E+11	7.0E+11	8.4E+11
65	12.5	8.4E+11	7.2E+11	6.0E+11	7.2E+11
65	13.5	7.1E+11	6.1E+11	5.1E+11	6.1E+11
65	14.5	5.7E+11	4.9E+11	4.1E+11	4.9E+11
65	18.5	2.6E+11	2.2E+11	1.8E+11	2.2E+11
65	24.5	1.2E+11	1.0E+11	8.4E+10	1.0E+11
65	29.5	5.4E+10	4.6E+10	3.8E+10	4.6E+10
65	34.5	2.5E+10	2.1E+10	1.7E+10	2.1E+10
65	39.5	1.2E+10	1.0E+10	8.4E+09	1.0E+10
65	44.5	5.9E+09	4.9E+09	4.1E+09	4.9E+09
65	49.5	3.0E+09	2.6E+09	2.2E+09	2.6E+09
55	0.5	4.2E+12	3.5E+12	3.0E+12	3.5E+12
55	1.5	3.8E+12	3.1E+12	2.6E+12	3.1E+12
55	2.5	2.8E+12	2.4E+12	2.0E+12	2.4E+12
55	3.5	2.4E+12	2.2E+12	1.8E+12	2.2E+12
55	4.5	2.3E+12	1.9E+12	1.7E+12	1.9E+12
55	5.5	2.1E+12	1.7E+12	1.5E+12	1.7E+12
55	6.5	1.8E+12	1.6E+12	1.2E+12	1.6E+12
55	7.5	1.6E+12	1.4E+12	1.2E+12	1.4E+12
55	8.5	1.4E+12	1.2E+12	1.0E+12	1.2E+12
55	9.5	1.3E+12	1.1E+12	9.0E+11	1.1E+12
55	10.5	1.0E+12	9.7E+11	8.1E+11	9.7E+11
55	11.5	9.8E+11	8.4E+11	7.0E+11	8.4E+11
55	12.5	8.4E+11	7.2E+11	6.0E+11	7.2E+11
55	13.5	7.1E+11	6.1E+11	5.1E+11	6.1E+11
55	14.5	5.7E+11	4.9E+11	4.1E+11	4.9E+11
55	18.5	2.6E+11	2.2E+11	1.8E+11	2.2E+11
55	24.5	1.2E+11	1.0E+11	8.4E+10	1.0E+11
55	29.5	5.4E+10	4.6E+10	3.8E+10	4.6E+10
55	34.5	2.5E+10	2.1E+10	1.7E+10	2.1E+10
55	39.5	1.2E+10	1.0E+10	8.4E+09	1.0E+10
55	44.5	5.9E+09	4.9E+09	4.1E+09	4.9E+09
55	49.5	3.0E+09	2.6E+09	2.2E+09	2.6E+09
45	0.5	4.6E+12	3.8E+12	3.3E+12	3.8E+12
45	1.5	4.2E+12	3.4E+12	2.9E+12	3.4E+12
45	2.5	2.8E+12	2.4E+12	2.0E+12	2.4E+12
45	3.5	2.4E+12	2.2E+12	1.8E+12	2.2E+12
45	4.5	2.3E+12	1.9E+12	1.7E+12	1.9E+12
45	5.5	2.1E+12	1.7E+12	1.5E+12	1.7E+12
45	6.5	1.8E+12	1.6E+12	1.2E+12	1.6E+12
45	7.5	1.6E+12	1.4E+12	1.2E+12	1.4E+12
45	8.5	1.4E+12	1.2E+12	1.0E+12	1.2E+12
45	9.5	1.3E+12	1.1E+12	9.0E+11	1.1E+12
45	10.5	1.0E+12	9.7E+11	8.1E+11	9.7E+11
45	11.5	9.8E+11	8.4E+11	7.0E+11	8.4E+11
45	12.5	8.4E+11	7.2E+11	6.0E+11	7.2E+11
45	13.5	7.1E+11	6.1E+11	5.1E+11	6.1E+11
45	14.5	5.7E+11	4.9E+11	4.1E+11	4.9E+11
45	18.5	2.6E+11	2.2E+11	1.8E+11	2.2E+11
45	24.5	1.2E+11	1.0E+11	8.4E+10	1.0E+11
45	29.5	5.4E+10	4.6E+10	3.8E+10	4.6E+10
45	34.5	2.5E+10	2.1E+10	1.7E+10	2.1E+10
45	39.5	1.2E+10	1.0E+10	8.4E+09	1.0E+10
45	44.5	5.9E+09	4.9E+09	4.1E+09	4.9E+09
45	49.5	3.0E+09	2.6E+09	2.2E+09	2.6E+09
35	0.5	4.0E+12	3.2E+12	2.8E+12	3.2E+12
35	1.5	3.6E+12	2.9E+12	2.4E+12	2.9E+12
35	2.5	2.6E+12	2.2E+12	1.8E+12	2.2E+12
35	3.5	2.4E+12	2.0E+12	1.6E+12	2.0E+12
35	4.5	2.2E+12	1.8E+12	1.4E+12	1.8E+12
35	5.5	2.0E+12	1.6E+12	1.4E+12	1.6E+12
35	6.5	1.8E+12	1.4E+12	1.2E+12	1.4E+12
35	7.5	1.5E+12	1.3E+12	1.1E+12	1.3E+12
35	8.5	1.3E+12	1.1E+12	9.0E+11	1.1E+12
35	9.5	1.2E+12	1.0E+12	8.4E+11	1.0E+12
35	10.5	1.1E+12	9.0E+11	7.4E+11	9.0E+11
35	11.5	9.2E+11	7.8E+11	6.4E+11	7.8E+11
35	12.5	7.9E+11	6.7E+11	5.5E+11	6.7E+11
35	13.5	6.6E+11	5.6E+11	4.6E+11	5.6E+11
35	14.5	5.3E+11	4.5E+11	3.7E+11	4.5E+11
35	18.5	2.3E+11	2.1E+11	1.7E+11	2.1E+11
35	24.5	1.1E+11	9.3E+10	7.7E+10	9.3E+10
35	29.5	5.1E+10	4.3E+10	3.5E+10	4.3E+10
35	34.5	2.2E+10	2.0E+10	1.6E+10	2.0E+10
35	39.5	1.1E+10	9.3E+09	7.7E+09	9.3E+09
35	44.5	5.4E+09	4.6E+09	3.8E+09	4.6E+09
35	49.5	2.8E+09	2.4E+09	2.0E+09	2.4E+09
25	0.5	3.2E+12	2.8E+12	2.3E+12	2.8E+12
25	1.5	3.0E+12	2.5E+12	1.8E+12	2.5E+12
25	2.5	2.3E+12	1.9E+12	1.5E+12	1.9E+12
25	3.5	2.1E+12	1.7E+12	1.3E+12	1.7E+12
25	4.5	1.9E+12	1.5E+12	1.3E+12	1.5E+12
25	5.5	1.6E+12	1.4E+12	1.0E+12	1.4E+12
25	6.5	1.4E+12	1.2E+12	1.0E+12	1.2E+12
25	7.5	1.3E+12	1.1E+12	8.4E+11	1.1E+12
25	8.5	1.2E+12	9.7E+11	7.5E+11	9.7E+11
25	9.5	1.0E+12	8.6E+11	6.6E+11	8.6E+11
25	10.5	9.2E+11	7.6E+11	6.0E+11	7.6E+11

25	11.5	8.0E+11	6.6E+11	5.2E+11	6.6E+11
25	12.5	6.9E+11	5.7E+11	4.5E+11	5.7E+11
25	13.5	5.7E+11	4.7E+11	3.7E+11	4.7E+11
25	14.5	4.6E+11	3.8E+11	3.0E+11	3.8E+11
25	18.5	2.1E+11	1.7E+11	1.3E+11	1.7E+11
25	24.5	9.6E+10	7.8E+10	6.2E+10	7.8E+10
25	29.5	4.4E+10	3.6E+10	2.8E+10	3.6E+10
25	34.5	1.9E+10	1.7E+10	1.3E+10	1.7E+10
25	39.5	9.6E+09	7.8E+09	6.2E+09	7.8E+09
25	44.5	4.7E+09	3.9E+09	2.9E+09	3.9E+09
25	49.5	2.4E+09	2.0E+09	1.6E+09	2.0E+09
15	0.5	2.8E+12	2.3E+12	1.6E+12	2.3E+12
15	1.5	2.5E+12	2.0E+12	1.6E+12	2.0E+12
15	2.5	1.9E+12	1.5E+12	1.1E+12	1.5E+12
15	3.5	1.6E+12	1.4E+12	1.0E+12	1.4E+12
15	4.5	1.6E+12	1.2E+12	1.0E+12	1.2E+12
15	5.5	1.5E+12	1.1E+12	8.2E+11	1.1E+12
15	6.5	1.2E+12	9.9E+11	7.3E+11	9.9E+11
15	7.5	1.1E+12	8.8E+11	6.6E+11	8.8E+11
15	8.5	1.0E+12	7.8E+11	5.8E+11	7.8E+11
15	9.5	8.8E+11	7.0E+11	5.0E+11	7.0E+11
15	10.5	7.9E+11	6.1E+11	4.5E+11	6.1E+11
15	11.5	6.7E+11	5.3E+11	3.9E+11	5.3E+11
15	12.5	5.8E+11	4.6E+11	3.4E+11	4.6E+11
15	13.5	4.8E+11	3.8E+11	2.8E+11	3.8E+11
15	14.5	3.9E+11	3.1E+11	2.3E+11	3.1E+11
15	18.5	1.8E+11	1.4E+11	1.0E+11	1.4E+11
15	24.5	8.0E+10	6.4E+10	4.6E+10	6.4E+10
15	29.5	3.7E+10	2.9E+10	2.1E+10	2.9E+10
15	34.5	1.7E+10	1.3E+10	1.1E+10	1.3E+10
15	39.5	8.0E+09	6.4E+09	4.6E+09	6.4E+09
15	44.5	4.1E+09	3.1E+09	2.3E+09	3.1E+09
15	49.5	2.2E+09	1.6E+09	1.2E+09	1.6E+09
5	0.5	2.4E+12	1.7E+12	1.2E+12	1.7E+12
5	1.5	2.0E+12	1.6E+12	1.1E+12	1.6E+12
5	2.5	1.6E+12	1.2E+12	7.4E+11	1.2E+12
5	3.5	1.3E+12	1.1E+12	6.4E+11	1.1E+12
5	4.5	1.3E+12	9.5E+11	6.3E+11	9.5E+11
5	5.5	1.2E+12	8.5E+11	5.7E+11	8.5E+11
5	6.5	1.0E+12	7.6E+11	5.0E+11	7.6E+11
5	7.5	9.2E+11	6.8E+11	4.4E+11	6.8E+11
5	8.5	8.2E+11	6.0E+11	4.0E+11	6.0E+11
5	9.5	7.2E+11	5.4E+11	3.4E+11	5.4E+11
5	10.5	6.3E+11	4.7E+11	3.1E+11	4.7E+11
5	11.5	5.5E+11	4.1E+11	2.7E+11	4.1E+11
5	12.5	4.7E+11	3.5E+11	2.3E+11	3.5E+11
5	13.5	4.0E+11	3.0E+11	2.0E+11	3.0E+11
5	14.5	3.2E+11	2.4E+11	1.6E+11	2.4E+11
5	18.5	1.5E+11	1.1E+11	7.0E+10	1.1E+11
5	24.5	6.7E+10	4.9E+10	3.3E+10	4.9E+10
5	29.5	2.9E+10	2.3E+10	1.5E+10	2.3E+10
5	34.5	1.4E+10	1.0E+10	7.2E+09	1.0E+10
5	39.5	6.7E+09	4.9E+09	3.3E+09	4.9E+09
5	44.5	3.2E+09	2.4E+09	1.6E+09	2.4E+09
5	49.5	1.7E+09	1.3E+09	7.0E+08	1.3E+09
-5	0.5	1.4E+12	1.4E+12	1.4E+12	1.4E+12
-5	1.5	1.3E+12	1.3E+12	1.3E+12	1.3E+12
-5	2.5	9.9E+11	9.9E+11	9.9E+11	9.9E+11
-5	3.5	9.0E+11	9.0E+11	9.0E+11	9.0E+11
-5	4.5	8.1E+11	8.1E+11	8.1E+11	8.1E+11
-5	5.5	7.2E+11	7.2E+11	7.2E+11	7.2E+11
-5	6.5	6.5E+11	6.5E+11	6.5E+11	6.5E+11
-5	7.5	5.8E+11	5.8E+11	5.8E+11	5.8E+11
-5	8.5	5.1E+11	5.1E+11	5.1E+11	5.1E+11
-5	9.5	4.6E+11	4.6E+11	4.6E+11	4.6E+11
-5	10.5	4.0E+11	4.0E+11	4.0E+11	4.0E+11
-5	11.5	3.5E+11	3.5E+11	3.5E+11	3.5E+11
-5	12.5	3.0E+11	3.0E+11	3.0E+11	3.0E+11
-5	13.5	2.5E+11	2.5E+11	2.5E+11	2.5E+11
-5	14.5	2.0E+11	2.0E+11	2.0E+11	2.0E+11
-5	18.5	9.2E+10	9.2E+10	9.2E+10	9.2E+10
-5	24.5	4.2E+10	4.2E+10	4.2E+10	4.2E+10
-5	29.5	1.9E+10	1.9E+10	1.9E+10	1.9E+10
-5	34.5	8.8E+09	8.8E+09	8.8E+09	8.8E+09
-5	39.5	4.2E+09	4.2E+09	4.2E+09	4.2E+09
-5	44.5	2.1E+09	2.1E+09	2.1E+09	2.1E+09
-5	49.5	1.1E+09	1.1E+09	1.1E+09	1.1E+09
-15	0.5	1.4E+12	1.4E+12	1.4E+12	1.4E+12
-15	1.5	1.3E+12	1.3E+12	1.3E+12	1.3E+12
-15	2.5	9.9E+11	9.9E+11	9.9E+11	9.9E+11
-15	3.5	9.0E+11	9.0E+11	9.0E+11	9.0E+11
-15	4.5	8.1E+11	8.1E+11	8.1E+11	8.1E+11
-15	5.5	7.2E+11	7.2E+11	7.2E+11	7.2E+11
-15	6.5	6.5E+11	6.5E+11	6.5E+11	6.5E+11
-15	7.5	5.8E+11	5.8E+11	5.8E+11	5.8E+11
-15	8.5	5.1E+11	5.1E+11	5.1E+11	5.1E+11
-15	9.5	4.6E+11	4.6E+11	4.6E+11	4.6E+11
-15	10.5	4.0E+11	4.0E+11	4.0E+11	4.0E+11
-15	11.5	3.5E+11	3.5E+11	3.5E+11	3.5E+11
-15	12.5	3.0E+11	3.0E+11	3.0E+11	3.0E+11
-15	13.5	2.5E+11	2.5E+11	2.5E+11	2.5E+11
-15	14.5	2.0E+11	2.0E+11	2.0E+11	2.0E+11
-15	18.5	9.2E+10	9.2E+10	9.2E+10	9.2E+10
-15	24.5	4.2E+10	4.2E+10	4.2E+10	4.2E+10
-15	29.5	1.9E+10	1.9E+10	1.9E+10	1.9E+10
-15	34.5	8.8E+09	8.8E+09	8.8E+09	8.8E+09
-15	39.5	4.2E+09	4.2E+09	4.2E+09	4.2E+09
-15	44.5	2.1E+09	2.1E+09	2.1E+09	2.1E+09
-15	49.5	1.1E+09	1.1E+09	1.1E+09	1.1E+09
-25	0.5	1.2E+12	1.2E+12	1.2E+12	1.2E+12
-25	1.5	1.1E+12	1.1E+12	1.1E+12	1.1E+12
-25	2.5	9.9E+11	9.9E+11	9.9E+11	9.9E+11

-25	3.5	9.0E+11	9.0E+11	9.0E+11	9.0E+11
-25	4.5	8.1E+11	8.1E+11	8.1E+11	8.1E+11
-25	5.5	7.2E+11	7.2E+11	7.2E+11	7.2E+11
-25	6.5	6.5E+11	6.5E+11	6.5E+11	6.5E+11
-25	7.5	5.8E+11	5.8E+11	5.8E+11	5.8E+11
-25	8.5	5.1E+11	5.1E+11	5.1E+11	5.1E+11
-25	9.5	4.6E+11	4.6E+11	4.6E+11	4.6E+11
-25	10.5	4.0E+11	4.0E+11	4.0E+11	4.0E+11
-25	11.5	3.5E+11	3.5E+11	3.5E+11	3.5E+11
-25	12.5	3.0E+11	3.0E+11	3.0E+11	3.0E+11
-25	13.5	2.5E+11	2.5E+11	2.5E+11	2.5E+11
-25	14.5	2.0E+11	2.0E+11	2.0E+11	2.0E+11
-25	18.5	9.2E+10	9.2E+10	9.2E+10	9.2E+10
-25	24.5	4.2E+10	4.2E+10	4.2E+10	4.2E+10
-25	29.5	1.9E+10	1.9E+10	1.9E+10	1.9E+10
-25	34.5	8.8E+09	8.8E+09	8.8E+09	8.8E+09
-25	39.5	4.2E+09	4.2E+09	4.2E+09	4.2E+09
-25	44.5	2.1E+09	2.1E+09	2.1E+09	2.1E+09
-25	49.5	1.1E+09	1.1E+09	1.1E+09	1.1E+09
-35	0.5	1.2E+12	1.2E+12	1.2E+12	1.2E+12
-35	1.5	1.1E+12	1.1E+12	1.1E+12	1.1E+12
-35	2.5	9.9E+11	9.9E+11	9.9E+11	9.9E+11
-35	3.5	9.0E+11	9.0E+11	9.0E+11	9.0E+11
-35	4.5	8.1E+11	8.1E+11	8.1E+11	8.1E+11
-35	5.5	7.2E+11	7.2E+11	7.2E+11	7.2E+11
-35	6.5	6.5E+11	6.5E+11	6.5E+11	6.5E+11
-35	7.5	5.8E+11	5.8E+11	5.8E+11	5.8E+11
-35	8.5	5.1E+11	5.1E+11	5.1E+11	5.1E+11
-35	9.5	4.6E+11	4.6E+11	4.6E+11	4.6E+11
-35	10.5	4.0E+11	4.0E+11	4.0E+11	4.0E+11
-35	11.5	3.5E+11	3.5E+11	3.5E+11	3.5E+11
-35	12.5	3.0E+11	3.0E+11	3.0E+11	3.0E+11
-35	13.5	2.5E+11	2.5E+11	2.5E+11	2.5E+11
-35	14.5	2.0E+11	2.0E+11	2.0E+11	2.0E+11
-35	18.5	9.2E+10	9.2E+10	9.2E+10	9.2E+10
-35	24.5	4.2E+10	4.2E+10	4.2E+10	4.2E+10
-35	29.5	1.9E+10	1.9E+10	1.9E+10	1.9E+10
-35	34.5	8.8E+09	8.8E+09	8.8E+09	8.8E+09
-35	39.5	4.2E+09	4.2E+09	4.2E+09	4.2E+09
-35	44.5	2.1E+09	2.1E+09	2.1E+09	2.1E+09
-35	49.5	1.1E+09	1.1E+09	1.1E+09	1.1E+09
-45	0.5	1.2E+12	1.2E+12	1.2E+12	1.2E+12
-45	1.5	1.1E+12	1.1E+12	1.1E+12	1.1E+12
-45	2.5	9.9E+11	9.9E+11	9.9E+11	9.9E+11
-45	3.5	9.0E+11	9.0E+11	9.0E+11	9.0E+11
-45	4.5	8.1E+11	8.1E+11	8.1E+11	8.1E+11
-45	5.5	7.2E+11	7.2E+11	7.2E+11	7.2E+11
-45	6.5	6.5E+11	6.5E+11	6.5E+11	6.5E+11
-45	7.5	5.8E+11	5.8E+11	5.8E+11	5.8E+11
-45	8.5	5.1E+11	5.1E+11	5.1E+11	5.1E+11
-45	9.5	4.6E+11	4.6E+11	4.6E+11	4.6E+11
-45	10.5	4.0E+11	4.0E+11	4.0E+11	4.0E+11
-45	11.5	3.5E+11	3.5E+11	3.5E+11	3.5E+11
-45	12.5	3.0E+11	3.0E+11	3.0E+11	3.0E+11
-45	13.5	2.5E+11	2.5E+11	2.5E+11	2.5E+11
-45	14.5	2.0E+11	2.0E+11	2.0E+11	2.0E+11
-45	18.5	9.2E+10	9.2E+10	9.2E+10	9.2E+10
-45	24.5	4.2E+10	4.2E+10	4.2E+10	4.2E+10
-45	29.5	1.9E+10	1.9E+10	1.9E+10	1.9E+10
-45	34.5	8.8E+09	8.8E+09	8.8E+09	8.8E+09
-45	39.5	4.2E+09	4.2E+09	4.2E+09	4.2E+09
-45	44.5	2.1E+09	2.1E+09	2.1E+09	2.1E+09
-45	49.5	1.1E+09	1.1E+09	1.1E+09	1.1E+09
-55	0.5	1.2E+12	1.2E+12	1.2E+12	1.2E+12
-55	1.5	1.1E+12	1.1E+12	1.1E+12	1.1E+12
-55	2.5	9.9E+11	9.9E+11	9.9E+11	9.9E+11
-55	3.5	9.0E+11	9.0E+11	9.0E+11	9.0E+11
-55	4.5	8.1E+11	8.1E+11	8.1E+11	8.1E+11
-55	5.5	7.2E+11	7.2E+11	7.2E+11	7.2E+11
-55	6.5	6.5E+11	6.5E+11	6.5E+11	6.5E+11
-55	7.5	5.8E+11	5.8E+11	5.8E+11	5.8E+11
-55	8.5	5.1E+11	5.1E+11	5.1E+11	5.1E+11
-55	9.5	4.6E+11	4.6E+11	4.6E+11	4.6E+11
-55	10.5	4.0E+11	4.0E+11	4.0E+11	4.0E+11
-55	11.5	3.5E+11	3.5E+11	3.5E+11	3.5E+11
-55	12.5	3.0E+11	3.0E+11	3.0E+11	3.0E+11
-55	13.5	2.5E+11	2.5E+11	2.5E+11	2.5E+11
-55	14.5	2.0E+11	2.0E+11	2.0E+11	2.0E+11
-55	18.5	9.2E+10	9.2E+10	9.2E+10	9.2E+10
-55	24.5	4.2E+10	4.2E+10	4.2E+10	4.2E+10
-55	29.5	1.9E+10	1.9E+10	1.9E+10	1.9E+10
-55	34.5	8.8E+09	8.8E+09	8.8E+09	8.8E+09
-55	39.5	4.2E+09	4.2E+09	4.2E+09	4.2E+09
-55	44.5	2.1E+09	2.1E+09	2.1E+09	2.1E+09
-55	49.5	1.1E+09	1.1E+09	1.1E+09	1.1E+09
-65	0.5	1.2E+12	1.2E+12	1.2E+12	1.2E+12
-65	1.5	1.1E+12	1.1E+12	1.1E+12	1.1E+12
-65	2.5	9.9E+11	9.9E+11	9.9E+11	9.9E+11
-65	3.5	9.0E+11	9.0E+11	9.0E+11	9.0E+11
-65	4.5	8.1E+11	8.1E+11	8.1E+11	8.1E+11
-65	5.5	7.2E+11	7.2E+11	7.2E+11	7.2E+11
-65	6.5	6.5E+11	6.5E+11	6.5E+11	6.5E+11
-65	7.5	5.8E+11	5.8E+11	5.8E+11	5.8E+11
-65	8.5	5.1E+11	5.1E+11	5.1E+11	5.1E+11
-65	9.5	4.6E+11	4.6E+11	4.6E+11	4.6E+11
-65	10.5	4.0E+11	4.0E+11	4.0E+11	4.0E+11
-65	11.5	3.5E+11	3.5E+11	3.5E+11	3.5E+11
-65	12.5	3.0E+11	3.0E+11	3.0E+11	3.0E+11
-65	13.5	2.5E+11	2.5E+11	2.5E+11	2.5E+11
-65	14.5	2.0E+11	2.0E+11	2.0E+11	2.0E+11
-65	18.5	9.2E+10	9.2E+10	9.2E+10	9.2E+10
-65	24.5	4.2E+10	4.2E+10	4.2E+10	4.2E+10

-65	29.5	1.9E+10	1.9E+10	1.9E+10	1.9E+10
-65	34.5	8.8E+09	8.8E+09	8.8E+09	8.8E+09
-65	39.5	4.2E+09	4.2E+09	4.2E+09	4.2E+09
-65	44.5	2.1E+09	2.1E+09	2.1E+09	2.1E+09
-65	49.5	1.1E+09	1.1E+09	1.1E+09	1.1E+09
-75	0.5	1.2E+12	1.2E+12	1.2E+12	1.2E+12
-75	1.5	1.1E+12	1.1E+12	1.1E+12	1.1E+12
-75	2.5	9.9E+11	9.9E+11	9.9E+11	9.9E+11
-75	3.5	9.0E+11	9.0E+11	9.0E+11	9.0E+11
-75	4.5	8.1E+11	8.1E+11	8.1E+11	8.1E+11
-75	5.5	7.2E+11	7.2E+11	7.2E+11	7.2E+11
-75	6.5	6.5E+11	6.5E+11	6.5E+11	6.5E+11
-75	7.5	5.8E+11	5.8E+11	5.8E+11	5.8E+11
-75	8.5	5.1E+11	5.1E+11	5.1E+11	5.1E+11
-75	9.5	4.6E+11	4.6E+11	4.6E+11	4.6E+11
-75	10.5	4.0E+11	4.0E+11	4.0E+11	4.0E+11
-75	11.5	3.5E+11	3.5E+11	3.5E+11	3.5E+11
-75	12.5	3.0E+11	3.0E+11	3.0E+11	3.0E+11
-75	13.5	2.5E+11	2.5E+11	2.5E+11	2.5E+11
-75	14.5	2.0E+11	2.0E+11	2.0E+11	2.0E+11
-75	18.5	9.2E+10	9.2E+10	9.2E+10	9.2E+10
-75	24.5	4.2E+10	4.2E+10	4.2E+10	4.2E+10
-75	29.5	1.9E+10	1.9E+10	1.9E+10	1.9E+10
-75	34.5	8.8E+09	8.8E+09	8.8E+09	8.8E+09
-75	39.5	4.2E+09	4.2E+09	4.2E+09	4.2E+09
-75	44.5	2.1E+09	2.1E+09	2.1E+09	2.1E+09
-75	49.5	1.1E+09	1.1E+09	1.1E+09	1.1E+09
-85	0.5	1.2E+12	1.2E+12	1.2E+12	1.2E+12
-85	1.5	1.1E+12	1.1E+12	1.1E+12	1.1E+12
-85	2.5	9.9E+11	9.9E+11	9.9E+11	9.9E+11
-85	3.5	9.0E+11	9.0E+11	9.0E+11	9.0E+11
-85	4.5	8.1E+11	8.1E+11	8.1E+11	8.1E+11
-85	5.5	7.2E+11	7.2E+11	7.2E+11	7.2E+11
-85	6.5	6.5E+11	6.5E+11	6.5E+11	6.5E+11
-85	7.5	5.8E+11	5.8E+11	5.8E+11	5.8E+11
-85	8.5	5.1E+11	5.1E+11	5.1E+11	5.1E+11
-85	9.5	4.6E+11	4.6E+11	4.6E+11	4.6E+11
-85	10.5	4.0E+11	4.0E+11	4.0E+11	4.0E+11
-85	11.5	3.5E+11	3.5E+11	3.5E+11	3.5E+11
-85	12.5	3.0E+11	3.0E+11	3.0E+11	3.0E+11
-85	13.5	2.5E+11	2.5E+11	2.5E+11	2.5E+11
-85	14.5	2.0E+11	2.0E+11	2.0E+11	2.0E+11
-85	18.5	9.2E+10	9.2E+10	9.2E+10	9.2E+10
-85	24.5	4.2E+10	4.2E+10	4.2E+10	4.2E+10
-85	29.5	1.9E+10	1.9E+10	1.9E+10	1.9E+10
-85	34.5	8.8E+09	8.8E+09	8.8E+09	8.8E+09
-85	39.5	4.2E+09	4.2E+09	4.2E+09	4.2E+09
-85	44.5	2.1E+09	2.1E+09	2.1E+09	2.1E+09
-85	49.5	1.1E+09	1.1E+09	1.1E+09	1.1E+09

B.5 cosea.dat

85	0.5	3.5E+12	2.9E+12	2.5E+12	2.9E+12
85	1.5	3.2E+12	2.6E+12	2.2E+12	2.6E+12
85	2.5	2.8E+12	2.4E+12	2.0E+12	2.4E+12
85	3.5	2.4E+12	2.2E+12	1.8E+12	2.2E+12
85	4.5	2.3E+12	1.9E+12	1.7E+12	1.9E+12
85	5.5	2.1E+12	1.7E+12	1.5E+12	1.7E+12
85	6.5	1.8E+12	1.6E+12	1.2E+12	1.6E+12
85	7.5	1.6E+12	1.4E+12	1.2E+12	1.4E+12
85	8.5	1.4E+12	1.2E+12	1.0E+12	1.2E+12
85	9.5	1.3E+12	1.1E+12	9.0E+11	1.1E+12
85	10.5	1.0E+12	9.7E+11	8.1E+11	9.7E+11
85	11.5	9.8E+11	8.4E+11	7.0E+11	8.4E+11
85	12.5	8.4E+11	7.2E+11	6.0E+11	7.2E+11
85	13.5	7.1E+11	6.1E+11	5.1E+11	6.1E+11
85	14.5	5.7E+11	4.9E+11	4.1E+11	4.9E+11
85	18.5	2.6E+11	2.2E+11	1.8E+11	2.2E+11
85	24.5	1.2E+11	1.0E+11	8.4E+10	1.0E+11
85	29.5	5.4E+10	4.6E+10	3.8E+10	4.6E+10
85	34.5	2.5E+10	2.1E+10	1.7E+10	2.1E+10
85	39.5	1.2E+10	1.0E+10	8.4E+09	1.0E+10
85	44.5	5.9E+09	4.9E+09	4.1E+09	4.9E+09
85	49.5	3.0E+09	2.6E+09	2.2E+09	2.6E+09
75	0.5	3.5E+12	2.9E+12	2.5E+12	2.9E+12
75	1.5	3.2E+12	2.6E+12	2.2E+12	2.6E+12
75	2.5	2.8E+12	2.4E+12	2.0E+12	2.4E+12
75	3.5	2.4E+12	2.2E+12	1.8E+12	2.2E+12
75	4.5	2.3E+12	1.9E+12	1.7E+12	1.9E+12
75	5.5	2.1E+12	1.7E+12	1.5E+12	1.7E+12
75	6.5	1.8E+12	1.6E+12	1.2E+12	1.6E+12
75	7.5	1.6E+12	1.4E+12	1.2E+12	1.4E+12
75	8.5	1.4E+12	1.2E+12	1.0E+12	1.2E+12
75	9.5	1.3E+12	1.1E+12	9.0E+11	1.1E+12
75	10.5	1.0E+12	9.7E+11	8.1E+11	9.7E+11
75	11.5	9.8E+11	8.4E+11	7.0E+11	8.4E+11
75	12.5	8.4E+11	7.2E+11	6.0E+11	7.2E+11
75	13.5	7.1E+11	6.1E+11	5.1E+11	6.1E+11
75	14.5	5.7E+11	4.9E+11	4.1E+11	4.9E+11
75	18.5	2.6E+11	2.2E+11	1.8E+11	2.2E+11
75	24.5	1.2E+11	1.0E+11	8.4E+10	1.0E+11
75	29.5	5.4E+10	4.6E+10	3.8E+10	4.6E+10
75	34.5	2.5E+10	2.1E+10	1.7E+10	2.1E+10
75	39.5	1.2E+10	1.0E+10	8.4E+09	1.0E+10
75	44.5	5.9E+09	4.9E+09	4.1E+09	4.9E+09
75	49.5	3.0E+09	2.6E+09	2.2E+09	2.6E+09
65	0.5	3.5E+12	2.9E+12	2.5E+12	2.9E+12
65	1.5	3.2E+12	2.6E+12	2.2E+12	2.6E+12
65	2.5	2.8E+12	2.4E+12	2.0E+12	2.4E+12
65	3.5	2.4E+12	2.2E+12	1.8E+12	2.2E+12
65	4.5	2.3E+12	1.9E+12	1.7E+12	1.9E+12

65	5.5	2.1E+12	1.7E+12	1.5E+12	1.7E+12
65	6.5	1.8E+12	1.6E+12	1.2E+12	1.6E+12
65	7.5	1.6E+12	1.4E+12	1.2E+12	1.4E+12
65	8.5	1.4E+12	1.2E+12	1.0E+12	1.2E+12
65	9.5	1.3E+12	1.1E+12	9.0E+11	1.1E+12
65	10.5	1.0E+12	9.7E+11	8.1E+11	9.7E+11
65	11.5	9.8E+11	8.4E+11	7.0E+11	8.4E+11
65	12.5	8.4E+11	7.2E+11	6.0E+11	7.2E+11
65	13.5	7.1E+11	6.1E+11	5.1E+11	6.1E+11
65	14.5	5.7E+11	4.9E+11	4.1E+11	4.9E+11
65	18.5	2.6E+11	2.2E+11	1.8E+11	2.2E+11
65	24.5	1.2E+11	1.0E+11	8.4E+10	1.0E+11
65	29.5	5.4E+10	4.6E+10	3.8E+10	4.6E+10
65	34.5	2.5E+10	2.1E+10	1.7E+10	2.1E+10
65	39.5	1.2E+10	1.0E+10	8.4E+09	1.0E+10
65	44.5	5.9E+09	4.9E+09	4.1E+09	4.9E+09
65	49.5	3.0E+09	2.6E+09	2.2E+09	2.6E+09
55	0.5	3.5E+12	2.9E+12	2.5E+12	2.9E+12
55	1.5	3.2E+12	2.6E+12	2.2E+12	2.6E+12
55	2.5	2.8E+12	2.4E+12	2.0E+12	2.4E+12
55	3.5	2.4E+12	2.2E+12	1.8E+12	2.2E+12
55	4.5	2.3E+12	1.9E+12	1.7E+12	1.9E+12
55	5.5	2.1E+12	1.7E+12	1.5E+12	1.7E+12
55	6.5	1.8E+12	1.6E+12	1.2E+12	1.6E+12
55	7.5	1.6E+12	1.4E+12	1.2E+12	1.4E+12
55	8.5	1.4E+12	1.2E+12	1.0E+12	1.2E+12
55	9.5	1.3E+12	1.1E+12	9.0E+11	1.1E+12
55	10.5	1.0E+12	9.7E+11	8.1E+11	9.7E+11
55	11.5	9.8E+11	8.4E+11	7.0E+11	8.4E+11
55	12.5	8.4E+11	7.2E+11	6.0E+11	7.2E+11
55	13.5	7.1E+11	6.1E+11	5.1E+11	6.1E+11
55	14.5	5.7E+11	4.9E+11	4.1E+11	4.9E+11
55	18.5	2.6E+11	2.2E+11	1.8E+11	2.2E+11
55	24.5	1.2E+11	1.0E+11	8.4E+10	1.0E+11
55	29.5	5.4E+10	4.6E+10	3.8E+10	4.6E+10
55	34.5	2.5E+10	2.1E+10	1.7E+10	2.1E+10
55	39.5	1.2E+10	1.0E+10	8.4E+09	1.0E+10
55	44.5	5.9E+09	4.9E+09	4.1E+09	4.9E+09
55	49.5	3.0E+09	2.6E+09	2.2E+09	2.6E+09
45	0.5	3.5E+12	2.9E+12	2.5E+12	2.9E+12
45	1.5	3.2E+12	2.6E+12	2.2E+12	2.6E+12
45	2.5	2.8E+12	2.4E+12	2.0E+12	2.4E+12
45	3.5	2.4E+12	2.2E+12	1.8E+12	2.2E+12
45	4.5	2.3E+12	1.9E+12	1.7E+12	1.9E+12
45	5.5	2.1E+12	1.7E+12	1.5E+12	1.7E+12
45	6.5	1.8E+12	1.6E+12	1.2E+12	1.6E+12
45	7.5	1.6E+12	1.4E+12	1.2E+12	1.4E+12
45	8.5	1.4E+12	1.2E+12	1.0E+12	1.2E+12
45	9.5	1.3E+12	1.1E+12	9.0E+11	1.1E+12
45	10.5	1.0E+12	9.7E+11	8.1E+11	9.7E+11
45	11.5	9.8E+11	8.4E+11	7.0E+11	8.4E+11
45	12.5	8.4E+11	7.2E+11	6.0E+11	7.2E+11
45	13.5	7.1E+11	6.1E+11	5.1E+11	6.1E+11
45	14.5	5.7E+11	4.9E+11	4.1E+11	4.9E+11
45	18.5	2.6E+11	2.2E+11	1.8E+11	2.2E+11
45	24.5	1.2E+11	1.0E+11	8.4E+10	1.0E+11
45	29.5	5.4E+10	4.6E+10	3.8E+10	4.6E+10
45	34.5	2.5E+10	2.1E+10	1.7E+10	2.1E+10
45	39.5	1.2E+10	1.0E+10	8.4E+09	1.0E+10
45	44.5	5.9E+09	4.9E+09	4.1E+09	4.9E+09
45	49.5	3.0E+09	2.6E+09	2.2E+09	2.6E+09
35	0.5	3.3E+12	2.7E+12	2.3E+12	2.7E+12
35	1.5	3.0E+12	2.4E+12	2.0E+12	2.4E+12
35	2.5	2.6E+12	2.2E+12	1.8E+12	2.2E+12
35	3.5	2.4E+12	2.0E+12	1.6E+12	2.0E+12
35	4.5	2.2E+12	1.8E+12	1.4E+12	1.8E+12
35	5.5	2.0E+12	1.6E+12	1.4E+12	1.6E+12
35	6.5	1.8E+12	1.4E+12	1.2E+12	1.4E+12
35	7.5	1.5E+12	1.3E+12	1.1E+12	1.3E+12
35	8.5	1.3E+12	1.1E+12	9.0E+11	1.1E+12
35	9.5	1.2E+12	1.0E+12	8.4E+11	1.0E+12
35	10.5	1.1E+12	9.0E+11	7.4E+11	9.0E+11
35	11.5	9.2E+11	7.8E+11	6.4E+11	7.8E+11
35	12.5	7.9E+11	6.7E+11	5.5E+11	6.7E+11
35	13.5	6.6E+11	5.6E+11	4.6E+11	5.6E+11
35	14.5	5.3E+11	4.5E+11	3.7E+11	4.5E+11
35	18.5	2.3E+11	2.1E+11	1.7E+11	2.1E+11
35	24.5	1.1E+11	9.3E+10	7.7E+10	9.3E+10
35	29.5	5.1E+10	4.3E+10	3.5E+10	4.3E+10
35	34.5	2.2E+10	2.0E+10	1.6E+10	2.0E+10
35	39.5	1.1E+10	9.3E+09	7.7E+09	9.3E+09
35	44.5	5.4E+09	4.6E+09	3.8E+09	4.6E+09
35	49.5	2.8E+09	2.4E+09	2.0E+09	2.4E+09
25	0.5	2.7E+12	2.3E+12	1.9E+12	2.3E+12
25	1.5	2.5E+12	2.1E+12	1.5E+12	2.1E+12
25	2.5	2.3E+12	1.9E+12	1.5E+12	1.9E+12
25	3.5	2.1E+12	1.7E+12	1.3E+12	1.7E+12
25	4.5	1.9E+12	1.5E+12	1.3E+12	1.5E+12
25	5.5	1.6E+12	1.4E+12	1.0E+12	1.4E+12
25	6.5	1.4E+12	1.2E+12	1.0E+12	1.2E+12
25	7.5	1.3E+12	1.1E+12	8.4E+11	1.1E+12
25	8.5	1.2E+12	9.7E+11	7.5E+11	9.7E+11
25	9.5	1.0E+12	8.6E+11	6.6E+11	8.6E+11
25	10.5	9.2E+11	7.6E+11	6.0E+11	7.6E+11
25	11.5	8.0E+11	6.6E+11	5.2E+11	6.6E+11
25	12.5	6.9E+11	5.7E+11	4.5E+11	5.7E+11
25	13.5	5.7E+11	4.7E+11	3.7E+11	4.7E+11
25	14.5	4.6E+11	3.8E+11	3.0E+11	3.8E+11
25	18.5	2.1E+11	1.7E+11	1.3E+11	1.7E+11
25	24.5	9.6E+10	7.8E+10	6.2E+10	7.8E+10
25	29.5	4.4E+10	3.6E+10	2.8E+10	3.6E+10
25	34.5	1.9E+10	1.7E+10	1.3E+10	1.7E+10

25	39.5	9.6E+09	7.8E+09	6.2E+09	7.8E+09
25	44.5	4.7E+09	3.9E+09	2.9E+09	3.9E+09
25	49.5	2.4E+09	2.0E+09	1.6E+09	2.0E+09
15	0.5	2.3E+12	1.9E+12	1.3E+12	1.9E+12
15	1.5	2.1E+12	1.7E+12	1.3E+12	1.7E+12
15	2.5	1.9E+12	1.5E+12	1.1E+12	1.5E+12
15	3.5	1.6E+12	1.4E+12	1.0E+12	1.4E+12
15	4.5	1.6E+12	1.2E+12	1.0E+12	1.2E+12
15	5.5	1.5E+12	1.1E+12	8.2E+11	1.1E+12
15	6.5	1.2E+12	9.9E+11	7.3E+11	9.9E+11
15	7.5	1.1E+12	8.8E+11	6.6E+11	8.8E+11
15	8.5	1.0E+12	7.8E+11	5.8E+11	7.8E+11
15	9.5	8.8E+11	7.0E+11	5.0E+11	7.0E+11
15	10.5	7.9E+11	6.1E+11	4.5E+11	6.1E+11
15	11.5	6.7E+11	5.3E+11	3.9E+11	5.3E+11
15	12.5	5.8E+11	4.6E+11	3.4E+11	4.6E+11
15	13.5	4.8E+11	3.8E+11	2.8E+11	3.8E+11
15	14.5	3.9E+11	3.1E+11	2.3E+11	3.1E+11
15	18.5	1.8E+11	1.4E+11	1.0E+11	1.4E+11
15	24.5	8.0E+10	6.4E+10	4.6E+10	6.4E+10
15	29.5	3.7E+10	2.9E+10	2.1E+10	2.9E+10
15	34.5	1.7E+10	1.3E+10	1.1E+10	1.3E+10
15	39.5	8.0E+09	6.4E+09	4.6E+09	6.4E+09
15	44.5	4.1E+09	3.1E+09	2.3E+09	3.1E+09
15	49.5	2.2E+09	1.6E+09	1.2E+09	1.6E+09
5	0.5	2.0E+12	1.4E+12	1.0E+12	1.4E+12
5	1.5	1.7E+12	1.3E+12	9.0E+11	1.3E+12
5	2.5	1.6E+12	1.2E+12	7.4E+11	1.2E+12
5	3.5	1.3E+12	1.1E+12	6.4E+11	1.1E+12
5	4.5	1.3E+12	9.5E+11	6.3E+11	9.5E+11
5	5.5	1.2E+12	8.5E+11	5.7E+11	8.5E+11
5	6.5	1.0E+12	7.6E+11	5.0E+11	7.6E+11
5	7.5	9.2E+11	6.8E+11	4.4E+11	6.8E+11
5	8.5	8.2E+11	6.0E+11	4.0E+11	6.0E+11
5	9.5	7.2E+11	5.4E+11	3.4E+11	5.4E+11
5	10.5	6.3E+11	4.7E+11	3.1E+11	4.7E+11
5	11.5	5.5E+11	4.1E+11	2.7E+11	4.1E+11
5	12.5	4.7E+11	3.5E+11	2.3E+11	3.5E+11
5	13.5	4.0E+11	3.0E+11	2.0E+11	3.0E+11
5	14.5	3.2E+11	2.4E+11	1.6E+11	2.4E+11
5	18.5	1.5E+11	1.1E+11	7.0E+10	1.1E+11
5	24.5	6.7E+10	4.9E+10	3.3E+10	4.9E+10
5	29.5	2.9E+10	2.3E+10	1.5E+10	2.3E+10
5	34.5	1.4E+10	1.0E+10	7.2E+09	1.0E+10
5	39.5	6.7E+09	4.9E+09	3.3E+09	4.9E+09
5	44.5	3.2E+09	2.4E+09	1.6E+09	2.4E+09
5	49.5	1.7E+09	1.3E+09	7.0E+08	1.3E+09
-5	0.5	1.2E+12	1.2E+12	1.2E+12	1.2E+12
-5	1.5	1.1E+12	1.1E+12	1.1E+12	1.1E+12
-5	2.5	9.9E+11	9.9E+11	9.9E+11	9.9E+11
-5	3.5	9.0E+11	9.0E+11	9.0E+11	9.0E+11

-5	4.5	8.1E+11	8.1E+11	8.1E+11	8.1E+11
-5	5.5	7.2E+11	7.2E+11	7.2E+11	7.2E+11
-5	6.5	6.5E+11	6.5E+11	6.5E+11	6.5E+11
-5	7.5	5.8E+11	5.8E+11	5.8E+11	5.8E+11
-5	8.5	5.1E+11	5.1E+11	5.1E+11	5.1E+11
-5	9.5	4.6E+11	4.6E+11	4.6E+11	4.6E+11
-5	10.5	4.0E+11	4.0E+11	4.0E+11	4.0E+11
-5	11.5	3.5E+11	3.5E+11	3.5E+11	3.5E+11
-5	12.5	3.0E+11	3.0E+11	3.0E+11	3.0E+11
-5	13.5	2.5E+11	2.5E+11	2.5E+11	2.5E+11
-5	14.5	2.0E+11	2.0E+11	2.0E+11	2.0E+11
-5	18.5	9.2E+10	9.2E+10	9.2E+10	9.2E+10
-5	24.5	4.2E+10	4.2E+10	4.2E+10	4.2E+10
-5	29.5	1.9E+10	1.9E+10	1.9E+10	1.9E+10
-5	34.5	8.8E+09	8.8E+09	8.8E+09	8.8E+09
-5	39.5	4.2E+09	4.2E+09	4.2E+09	4.2E+09
-5	44.5	2.1E+09	2.1E+09	2.1E+09	2.1E+09
-5	49.5	1.1E+09	1.1E+09	1.1E+09	1.1E+09
-15	0.5	1.2E+12	1.2E+12	1.2E+12	1.2E+12
-15	1.5	1.1E+12	1.1E+12	1.1E+12	1.1E+12
-15	2.5	9.9E+11	9.9E+11	9.9E+11	9.9E+11
-15	3.5	9.0E+11	9.0E+11	9.0E+11	9.0E+11
-15	4.5	8.1E+11	8.1E+11	8.1E+11	8.1E+11
-15	5.5	7.2E+11	7.2E+11	7.2E+11	7.2E+11
-15	6.5	6.5E+11	6.5E+11	6.5E+11	6.5E+11
-15	7.5	5.8E+11	5.8E+11	5.8E+11	5.8E+11
-15	8.5	5.1E+11	5.1E+11	5.1E+11	5.1E+11
-15	9.5	4.6E+11	4.6E+11	4.6E+11	4.6E+11
-15	10.5	4.0E+11	4.0E+11	4.0E+11	4.0E+11
-15	11.5	3.5E+11	3.5E+11	3.5E+11	3.5E+11
-15	12.5	3.0E+11	3.0E+11	3.0E+11	3.0E+11
-15	13.5	2.5E+11	2.5E+11	2.5E+11	2.5E+11
-15	14.5	2.0E+11	2.0E+11	2.0E+11	2.0E+11
-15	18.5	9.2E+10	9.2E+10	9.2E+10	9.2E+10
-15	24.5	4.2E+10	4.2E+10	4.2E+10	4.2E+10
-15	29.5	1.9E+10	1.9E+10	1.9E+10	1.9E+10
-15	34.5	8.8E+09	8.8E+09	8.8E+09	8.8E+09
-15	39.5	4.2E+09	4.2E+09	4.2E+09	4.2E+09
-15	44.5	2.1E+09	2.1E+09	2.1E+09	2.1E+09
-15	49.5	1.1E+09	1.1E+09	1.1E+09	1.1E+09
-25	0.5	1.2E+12	1.2E+12	1.2E+12	1.2E+12
-25	1.5	1.1E+12	1.1E+12	1.1E+12	1.1E+12
-25	2.5	9.9E+11	9.9E+11	9.9E+11	9.9E+11
-25	3.5	9.0E+11	9.0E+11	9.0E+11	9.0E+11
-25	4.5	8.1E+11	8.1E+11	8.1E+11	8.1E+11
-25	5.5	7.2E+11	7.2E+11	7.2E+11	7.2E+11
-25	6.5	6.5E+11	6.5E+11	6.5E+11	6.5E+11
-25	7.5	5.8E+11	5.8E+11	5.8E+11	5.8E+11
-25	8.5	5.1E+11	5.1E+11	5.1E+11	5.1E+11
-25	9.5	4.6E+11	4.6E+11	4.6E+11	4.6E+11
-25	10.5	4.0E+11	4.0E+11	4.0E+11	4.0E+11

-25	11.5	3.5E+11	3.5E+11	3.5E+11	3.5E+11
-25	12.5	3.0E+11	3.0E+11	3.0E+11	3.0E+11
-25	13.5	2.5E+11	2.5E+11	2.5E+11	2.5E+11
-25	14.5	2.0E+11	2.0E+11	2.0E+11	2.0E+11
-25	18.5	9.2E+10	9.2E+10	9.2E+10	9.2E+10
-25	24.5	4.2E+10	4.2E+10	4.2E+10	4.2E+10
-25	29.5	1.9E+10	1.9E+10	1.9E+10	1.9E+10
-25	34.5	8.8E+09	8.8E+09	8.8E+09	8.8E+09
-25	39.5	4.2E+09	4.2E+09	4.2E+09	4.2E+09
-25	44.5	2.1E+09	2.1E+09	2.1E+09	2.1E+09
-25	49.5	1.1E+09	1.1E+09	1.1E+09	1.1E+09
-35	0.5	1.2E+12	1.2E+12	1.2E+12	1.2E+12
-35	1.5	1.1E+12	1.1E+12	1.1E+12	1.1E+12
-35	2.5	9.9E+11	9.9E+11	9.9E+11	9.9E+11
-35	3.5	9.0E+11	9.0E+11	9.0E+11	9.0E+11
-35	4.5	8.1E+11	8.1E+11	8.1E+11	8.1E+11
-35	5.5	7.2E+11	7.2E+11	7.2E+11	7.2E+11
-35	6.5	6.5E+11	6.5E+11	6.5E+11	6.5E+11
-35	7.5	5.8E+11	5.8E+11	5.8E+11	5.8E+11
-35	8.5	5.1E+11	5.1E+11	5.1E+11	5.1E+11
-35	9.5	4.6E+11	4.6E+11	4.6E+11	4.6E+11
-35	10.5	4.0E+11	4.0E+11	4.0E+11	4.0E+11
-35	11.5	3.5E+11	3.5E+11	3.5E+11	3.5E+11
-35	12.5	3.0E+11	3.0E+11	3.0E+11	3.0E+11
-35	13.5	2.5E+11	2.5E+11	2.5E+11	2.5E+11
-35	14.5	2.0E+11	2.0E+11	2.0E+11	2.0E+11
-35	18.5	9.2E+10	9.2E+10	9.2E+10	9.2E+10
-35	24.5	4.2E+10	4.2E+10	4.2E+10	4.2E+10
-35	29.5	1.9E+10	1.9E+10	1.9E+10	1.9E+10
-35	34.5	8.8E+09	8.8E+09	8.8E+09	8.8E+09
-35	39.5	4.2E+09	4.2E+09	4.2E+09	4.2E+09
-35	44.5	2.1E+09	2.1E+09	2.1E+09	2.1E+09
-35	49.5	1.1E+09	1.1E+09	1.1E+09	1.1E+09
-45	0.5	1.2E+12	1.2E+12	1.2E+12	1.2E+12
-45	1.5	1.1E+12	1.1E+12	1.1E+12	1.1E+12
-45	2.5	9.9E+11	9.9E+11	9.9E+11	9.9E+11
-45	3.5	9.0E+11	9.0E+11	9.0E+11	9.0E+11
-45	4.5	8.1E+11	8.1E+11	8.1E+11	8.1E+11
-45	5.5	7.2E+11	7.2E+11	7.2E+11	7.2E+11
-45	6.5	6.5E+11	6.5E+11	6.5E+11	6.5E+11
-45	7.5	5.8E+11	5.8E+11	5.8E+11	5.8E+11
-45	8.5	5.1E+11	5.1E+11	5.1E+11	5.1E+11
-45	9.5	4.6E+11	4.6E+11	4.6E+11	4.6E+11
-45	10.5	4.0E+11	4.0E+11	4.0E+11	4.0E+11
-45	11.5	3.5E+11	3.5E+11	3.5E+11	3.5E+11
-45	12.5	3.0E+11	3.0E+11	3.0E+11	3.0E+11
-45	13.5	2.5E+11	2.5E+11	2.5E+11	2.5E+11
-45	14.5	2.0E+11	2.0E+11	2.0E+11	2.0E+11
-45	18.5	9.2E+10	9.2E+10	9.2E+10	9.2E+10
-45	24.5	4.2E+10	4.2E+10	4.2E+10	4.2E+10
-45	29.5	1.9E+10	1.9E+10	1.9E+10	1.9E+10
-45	34.5	8.8E+09	8.8E+09	8.8E+09	8.8E+09
-45	39.5	4.2E+09	4.2E+09	4.2E+09	4.2E+09
-45	44.5	2.1E+09	2.1E+09	2.1E+09	2.1E+09
-45	49.5	1.1E+09	1.1E+09	1.1E+09	1.1E+09
-55	0.5	1.2E+12	1.2E+12	1.2E+12	1.2E+12
-55	1.5	1.1E+12	1.1E+12	1.1E+12	1.1E+12
-55	2.5	9.9E+11	9.9E+11	9.9E+11	9.9E+11
-55	3.5	9.0E+11	9.0E+11	9.0E+11	9.0E+11
-55	4.5	8.1E+11	8.1E+11	8.1E+11	8.1E+11
-55	5.5	7.2E+11	7.2E+11	7.2E+11	7.2E+11
-55	6.5	6.5E+11	6.5E+11	6.5E+11	6.5E+11
-55	7.5	5.8E+11	5.8E+11	5.8E+11	5.8E+11
-55	8.5	5.1E+11	5.1E+11	5.1E+11	5.1E+11
-55	9.5	4.6E+11	4.6E+11	4.6E+11	4.6E+11
-55	10.5	4.0E+11	4.0E+11	4.0E+11	4.0E+11
-55	11.5	3.5E+11	3.5E+11	3.5E+11	3.5E+11
-55	12.5	3.0E+11	3.0E+11	3.0E+11	3.0E+11
-55	13.5	2.5E+11	2.5E+11	2.5E+11	2.5E+11
-55	14.5	2.0E+11	2.0E+11	2.0E+11	2.0E+11
-55	18.5	9.2E+10	9.2E+10	9.2E+10	9.2E+10
-55	24.5	4.2E+10	4.2E+10	4.2E+10	4.2E+10
-55	29.5	1.9E+10	1.9E+10	1.9E+10	1.9E+10
-55	34.5	8.8E+09	8.8E+09	8.8E+09	8.8E+09
-55	39.5	4.2E+09	4.2E+09	4.2E+09	4.2E+09
-55	44.5	2.1E+09	2.1E+09	2.1E+09	2.1E+09
-55	49.5	1.1E+09	1.1E+09	1.1E+09	1.1E+09
-65	0.5	1.2E+12	1.2E+12	1.2E+12	1.2E+12
-65	1.5	1.1E+12	1.1E+12	1.1E+12	1.1E+12
-65	2.5	9.9E+11	9.9E+11	9.9E+11	9.9E+11
-65	3.5	9.0E+11	9.0E+11	9.0E+11	9.0E+11
-65	4.5	8.1E+11	8.1E+11	8.1E+11	8.1E+11
-65	5.5	7.2E+11	7.2E+11	7.2E+11	7.2E+11
-65	6.5	6.5E+11	6.5E+11	6.5E+11	6.5E+11
-65	7.5	5.8E+11	5.8E+11	5.8E+11	5.8E+11
-65	8.5	5.1E+11	5.1E+11	5.1E+11	5.1E+11
-65	9.5	4.6E+11	4.6E+11	4.6E+11	4.6E+11
-65	10.5	4.0E+11	4.0E+11	4.0E+11	4.0E+11
-65	11.5	3.5E+11	3.5E+11	3.5E+11	3.5E+11
-65	12.5	3.0E+11	3.0E+11	3.0E+11	3.0E+11
-65	13.5	2.5E+11	2.5E+11	2.5E+11	2.5E+11
-65	14.5	2.0E+11	2.0E+11	2.0E+11	2.0E+11
-65	18.5	9.2E+10	9.2E+10	9.2E+10	9.2E+10
-65	24.5	4.2E+10	4.2E+10	4.2E+10	4.2E+10
-65	29.5	1.9E+10	1.9E+10	1.9E+10	1.9E+10
-65	34.5	8.8E+09	8.8E+09	8.8E+09	8.8E+09
-65	39.5	4.2E+09	4.2E+09	4.2E+09	4.2E+09
-65	44.5	2.1E+09	2.1E+09	2.1E+09	2.1E+09
-65	49.5	1.1E+09	1.1E+09	1.1E+09	1.1E+09
-75	0.5	1.2E+12	1.2E+12	1.2E+12	1.2E+12
-75	1.5	1.1E+12	1.1E+12	1.1E+12	1.1E+12
-75	2.5	9.9E+11	9.9E+11	9.9E+11	9.9E+11

-75	3.5	9.0E+11	9.0E+11	9.0E+11	9.0E+11
-75	4.5	8.1E+11	8.1E+11	8.1E+11	8.1E+11
-75	5.5	7.2E+11	7.2E+11	7.2E+11	7.2E+11
-75	6.5	6.5E+11	6.5E+11	6.5E+11	6.5E+11
-75	7.5	5.8E+11	5.8E+11	5.8E+11	5.8E+11
-75	8.5	5.1E+11	5.1E+11	5.1E+11	5.1E+11
-75	9.5	4.6E+11	4.6E+11	4.6E+11	4.6E+11
-75	10.5	4.0E+11	4.0E+11	4.0E+11	4.0E+11
-75	11.5	3.5E+11	3.5E+11	3.5E+11	3.5E+11
-75	12.5	3.0E+11	3.0E+11	3.0E+11	3.0E+11
-75	13.5	2.5E+11	2.5E+11	2.5E+11	2.5E+11
-75	14.5	2.0E+11	2.0E+11	2.0E+11	2.0E+11
-75	18.5	9.2E+10	9.2E+10	9.2E+10	9.2E+10
-75	24.5	4.2E+10	4.2E+10	4.2E+10	4.2E+10
-75	29.5	1.9E+10	1.9E+10	1.9E+10	1.9E+10
-75	34.5	8.8E+09	8.8E+09	8.8E+09	8.8E+09
-75	39.5	4.2E+09	4.2E+09	4.2E+09	4.2E+09
-75	44.5	2.1E+09	2.1E+09	2.1E+09	2.1E+09
-75	49.5	1.1E+09	1.1E+09	1.1E+09	1.1E+09
-85	0.5	1.2E+12	1.2E+12	1.2E+12	1.2E+12
-85	1.5	1.1E+12	1.1E+12	1.1E+12	1.1E+12
-85	2.5	9.9E+11	9.9E+11	9.9E+11	9.9E+11
-85	3.5	9.0E+11	9.0E+11	9.0E+11	9.0E+11
-85	4.5	8.1E+11	8.1E+11	8.1E+11	8.1E+11
-85	5.5	7.2E+11	7.2E+11	7.2E+11	7.2E+11
-85	6.5	6.5E+11	6.5E+11	6.5E+11	6.5E+11
-85	7.5	5.8E+11	5.8E+11	5.8E+11	5.8E+11
-85	8.5	5.1E+11	5.1E+11	5.1E+11	5.1E+11
-85	9.5	4.6E+11	4.6E+11	4.6E+11	4.6E+11
-85	10.5	4.0E+11	4.0E+11	4.0E+11	4.0E+11
-85	11.5	3.5E+11	3.5E+11	3.5E+11	3.5E+11
-85	12.5	3.0E+11	3.0E+11	3.0E+11	3.0E+11
-85	13.5	2.5E+11	2.5E+11	2.5E+11	2.5E+11
-85	14.5	2.0E+11	2.0E+11	2.0E+11	2.0E+11
-85	18.5	9.2E+10	9.2E+10	9.2E+10	9.2E+10
-85	24.5	4.2E+10	4.2E+10	4.2E+10	4.2E+10
-85	29.5	1.9E+10	1.9E+10	1.9E+10	1.9E+10
-85	34.5	8.8E+09	8.8E+09	8.8E+09	8.8E+09
-85	39.5	4.2E+09	4.2E+09	4.2E+09	4.2E+09
-85	44.5	2.1E+09	2.1E+09	2.1E+09	2.1E+09
-85	49.5	1.1E+09	1.1E+09	1.1E+09	1.1E+09

B.6 h2.dat

```
5.0E-07
5.0E-07
5.0E-07
5.0E-07
5.0E-07
5.0E-07
5.0E-07
5.0E-07
5.0E-07
5.0E-07
5.0E-07
5.0E-07
5.0E-07
5.0E-07
5.0E-07
5.0E-07
5.0E-07
5.0E-07
4.0E-07
3.0E-07
2.5E-07
2.0E-07
```

B.7 h2coacs.dat

240.00	3.0E-22
250.00	1.3E-21
260.00	4.7E-21
270.00	8.6E-21
280.00	1.9E-20
290.00	2.5E-20
301.25	1.4E-20
303.75	4.3E-20
306.25	3.3E-20
308.75	2.2E-20
311.25	9.3E-21
313.75	3.4E-20
316.25	3.9E-20
318.75	1.7E-20
321.25	1.1E-20
323.75	4.7E-21
326.25	4.4E-20
328.75	2.3E-20
331.25	1.3E-20
333.75	1.2E-21
336.25	1.3E-21
338.75	3.4E-20
341.25	9.4E-21
343.75	1.4E-20
346.25	4.0E-23
348.75	9.0E-23
351.25	1.7E-21
353.75	1.8E-20
356.25	3.5E-22

B.8 h2oland.dat

```
85  0.5 5.6E-04 1.1E-03 5.0E-03 1.5E-03
85  1.5 7.7E-04 1.3E-03 4.1E-03 1.4E-03
85  2.5 5.7E-04 9.3E-04 2.8E-03 1.0E-03
85  3.5 4.0E-04 6.3E-04 1.9E-03 7.0E-04
85  4.5 2.6E-04 4.0E-04 1.2E-03 4.5E-04
85  5.5 1.3E-04 2.0E-04 6.2E-04 2.3E-04
85  6.5 8.6E-05 1.3E-04 4.2E-04 1.5E-04
85  7.5 5.4E-05 8.3E-05 2.6E-04 9.3E-05
85  8.5 2.5E-05 3.9E-05 1.2E-04 4.3E-05
85  9.5 7.1E-06 1.2E-05 3.4E-05 1.1E-05
85 10.5 4.7E-06 7.5E-06 2.2E-05 7.6E-06
85 11.5 3.6E-06 5.6E-06 1.6E-05 6.1E-06
85 12.5 1.7E-06 2.0E-06 5.3E-06 2.7E-06
85 13.5 1.4E-06 1.3E-06 3.5E-06 1.8E-06
85 14.5 1.2E-06 6.3E-07 1.7E-06 8.4E-07
85 18.5 9.7E-06 1.4E-05 4.8E-05 1.4E-05
85 24.5 9.7E-06 1.4E-05 4.8E-05 1.4E-05
85 29.5 9.7E-06 1.4E-05 4.8E-05 1.4E-05
85 34.5 9.7E-06 1.4E-05 4.8E-05 1.4E-05
85 39.5 9.7E-06 1.4E-05 4.8E-05 1.4E-05
85 44.5 9.7E-06 1.4E-05 4.8E-05 1.4E-05
85 49.5 9.7E-06 1.4E-05 4.8E-05 1.4E-05
75  0.5 9.0E-04 1.6E-03 5.9E-03 2.6E-03
75  1.5 9.5E-04 1.5E-03 4.7E-03 2.0E-03
75  2.5 6.6E-04 1.0E-03 3.1E-03 1.4E-03
75  3.5 4.3E-04 6.7E-04 2.0E-03 8.8E-04
75  4.5 2.7E-04 4.2E-04 1.3E-03 5.6E-04
75  5.5 1.3E-04 2.0E-04 6.2E-04 2.7E-04
75  6.5 8.9E-05 1.4E-04 4.1E-04 1.8E-04
75  7.5 5.6E-05 8.6E-05 2.6E-04 1.1E-04
75  8.5 2.7E-05 4.1E-05 1.2E-04 5.1E-05
75  9.5 8.0E-06 1.2E-05 3.5E-05 1.3E-05
75 10.5 5.1E-06 7.9E-06 2.3E-05 8.5E-06
75 11.5 3.8E-06 5.9E-06 1.7E-05 6.6E-06
75 12.5 1.7E-06 2.0E-06 6.0E-06 2.7E-06
75 13.5 1.4E-06 1.3E-06 4.0E-06 1.8E-06
75 14.5 1.2E-06 6.3E-07 1.9E-06 8.4E-07
75 18.5 9.7E-06 1.7E-05 4.0E-05 1.6E-05
75 24.5 9.7E-06 1.7E-05 4.0E-05 1.6E-05
75 29.5 9.7E-06 1.7E-05 4.0E-05 1.6E-05
75 34.5 9.7E-06 1.7E-05 4.0E-05 1.6E-05
75 39.5 9.7E-06 1.7E-05 4.0E-05 1.6E-05
75 44.5 9.7E-06 1.7E-05 4.0E-05 1.6E-05
75 49.5 9.7E-06 1.7E-05 4.0E-05 1.6E-05
65  0.5 8.2E-04 2.5E-03 1.0E-02 3.3E-03
65  1.5 9.6E-04 1.9E-03 6.9E-03 2.5E-03
65  2.5 6.9E-04 1.3E-03 4.5E-03 1.7E-03
65  3.5 4.8E-04 8.4E-04 2.8E-03 1.1E-03
65  4.5 3.1E-04 5.3E-04 1.8E-03 6.9E-04
65  5.5 1.5E-04 2.6E-04 8.4E-04 3.4E-04
65  6.5 1.0E-04 1.8E-04 5.6E-04 2.3E-04
65  7.5 6.4E-05 1.1E-04 3.5E-04 1.4E-04
65  8.5 3.0E-05 5.2E-05 1.7E-04 6.5E-05
65  9.5 8.8E-06 1.5E-05 5.3E-05 1.8E-05
65 10.5 5.6E-06 9.3E-06 3.3E-05 1.2E-05
65 11.5 4.1E-06 6.7E-06 2.5E-05 8.9E-06
65 12.5 1.7E-06 2.0E-06 8.0E-06 3.3E-06
65 13.5 1.4E-06 1.3E-06 5.3E-06 2.2E-06
65 14.5 1.2E-06 6.3E-07 2.5E-06 1.1E-06
65 18.5 1.1E-05 2.1E-05 3.4E-05 1.7E-05
65 24.5 1.1E-05 2.1E-05 3.4E-05 1.7E-05
65 29.5 1.1E-05 2.1E-05 3.4E-05 1.7E-05
65 34.5 1.1E-05 2.1E-05 3.4E-05 1.7E-05
65 39.5 1.1E-05 2.1E-05 3.4E-05 1.7E-05
65 44.5 1.1E-05 2.1E-05 3.4E-05 1.7E-05
65 49.5 1.1E-05 2.1E-05 3.4E-05 1.7E-05
55  0.5 1.2E-03 3.2E-03 9.6E-03 5.3E-03
55  1.5 1.1E-03 2.5E-03 6.9E-03 3.8E-03
55  2.5 8.3E-04 1.8E-03 4.5E-03 2.4E-03
55  3.5 5.8E-04 1.2E-03 2.8E-03 1.5E-03
55  4.5 3.7E-04 7.8E-04 1.8E-03 9.9E-04
55  5.5 1.8E-04 3.9E-04 8.4E-04 4.9E-04
55  6.5 1.2E-04 2.6E-04 5.6E-04 3.3E-04
55  7.5 7.7E-05 1.6E-04 3.6E-04 2.1E-04
55  8.5 3.6E-05 7.7E-05 1.7E-04 9.9E-05
55  9.5 9.7E-06 2.2E-05 5.4E-05 2.9E-05
55 10.5 6.0E-06 1.3E-05 3.3E-05 1.9E-05
55 11.5 4.4E-06 8.8E-06 2.4E-05 1.5E-05
55 12.5 1.3E-06 2.0E-06 7.3E-06 5.3E-06
55 13.5 8.8E-07 1.3E-06 4.9E-06 3.5E-06
55 14.5 4.2E-07 6.3E-07 2.3E-06 1.7E-06
55 18.5 1.3E-05 2.0E-05 3.1E-05 2.0E-05
55 24.5 1.3E-05 2.0E-05 3.1E-05 2.0E-05
55 29.5 1.3E-05 2.0E-05 3.1E-05 2.0E-05
55 34.5 1.3E-05 2.0E-05 3.1E-05 2.0E-05
55 39.5 1.3E-05 2.0E-05 3.1E-05 2.0E-05
55 44.5 1.3E-05 2.0E-05 3.1E-05 2.0E-05
55 49.5 1.3E-05 2.0E-05 3.1E-05 2.0E-05
45  0.5 3.5E-03 6.0E-03 1.3E-02 8.7E-03
45  1.5 2.4E-03 4.5E-03 1.0E-02 5.8E-03
45  2.5 1.6E-03 2.9E-03 6.3E-03 3.7E-03
45  3.5 9.9E-04 1.8E-03 3.7E-03 2.2E-03
45  4.5 6.4E-04 1.1E-03 2.4E-03 1.4E-03
45  5.5 3.2E-04 5.6E-04 1.2E-03 7.3E-04
45  6.5 2.2E-04 3.7E-04 8.1E-04 4.9E-04
45  7.5 1.4E-04 2.4E-04 5.2E-04 3.2E-04
45  8.5 6.6E-05 1.1E-04 2.6E-04 1.6E-04
45  9.5 2.0E-05 3.2E-05 9.4E-05 5.4E-05
45 10.5 1.3E-05 1.9E-05 5.6E-05 3.3E-05
45 11.5 9.0E-06 1.3E-05 3.9E-05 2.4E-05
```

45	12.5	2.7E-06	2.7E-06	9.3E-06	6.6E-06
45	13.5	1.8E-06	1.8E-06	6.2E-06	4.4E-06
45	14.5	8.4E-07	8.4E-07	3.0E-06	2.1E-06
45	18.5	1.6E-05	1.8E-05	3.5E-05	2.7E-05
45	24.5	1.6E-05	1.8E-05	3.5E-05	2.7E-05
45	29.5	1.6E-05	1.8E-05	3.5E-05	2.7E-05
45	34.5	1.6E-05	1.8E-05	3.5E-05	2.7E-05
45	39.5	1.6E-05	1.8E-05	3.5E-05	2.7E-05
45	44.5	1.6E-05	1.8E-05	3.5E-05	2.7E-05
45	49.5	1.6E-05	1.8E-05	3.5E-05	2.7E-05
35	0.5	8.6E-03	1.1E-02	2.0E-02	1.5E-02
35	1.5	5.4E-03	7.0E-03	1.3E-02	9.6E-03
35	2.5	3.1E-03	4.2E-03	7.9E-03	5.5E-03
35	3.5	1.7E-03	2.4E-03	4.6E-03	3.0E-03
35	4.5	1.1E-03	1.6E-03	3.0E-03	2.0E-03
35	5.5	6.2E-04	8.7E-04	1.6E-03	1.1E-03
35	6.5	4.3E-04	5.9E-04	1.1E-03	7.4E-04
35	7.5	2.7E-04	3.8E-04	7.4E-04	4.8E-04
35	8.5	1.4E-04	1.9E-04	3.8E-04	2.5E-04
35	9.5	5.1E-05	6.1E-05	1.5E-04	9.7E-05
35	10.5	3.1E-05	3.5E-05	8.5E-05	5.7E-05
35	11.5	2.1E-05	2.4E-05	5.8E-05	4.0E-05
35	12.5	5.3E-06	4.7E-06	1.3E-05	9.3E-06
35	13.5	3.5E-06	3.1E-06	8.4E-06	6.2E-06
35	14.5	1.7E-06	1.5E-06	4.0E-06	3.0E-06
35	18.5	2.9E-05	3.0E-05	4.3E-05	3.8E-05
35	24.5	2.9E-05	3.0E-05	4.3E-05	3.8E-05
35	29.5	2.9E-05	3.0E-05	4.3E-05	3.8E-05
35	34.5	2.9E-05	3.0E-05	4.3E-05	3.8E-05
35	39.5	2.9E-05	3.0E-05	4.3E-05	3.8E-05
35	44.5	2.9E-05	3.0E-05	4.3E-05	3.8E-05
35	49.5	2.9E-05	3.0E-05	4.3E-05	3.8E-05
25	0.5	1.4E-02	1.7E-02	2.3E-02	2.0E-02
25	1.5	8.9E-03	1.1E-02	1.5E-02	1.3E-02
25	2.5	5.1E-03	6.4E-03	8.6E-03	7.3E-03
25	3.5	2.8E-03	3.6E-03	4.9E-03	4.0E-03
25	4.5	1.9E-03	2.4E-03	3.3E-03	2.6E-03
25	5.5	9.8E-04	1.3E-03	1.8E-03	1.4E-03
25	6.5	6.7E-04	9.1E-04	1.2E-03	9.6E-04
25	7.5	4.4E-04	5.8E-04	8.0E-04	6.2E-04
25	8.5	2.3E-04	2.9E-04	4.1E-04	3.2E-04
25	9.5	8.6E-05	1.0E-04	1.5E-04	1.2E-04
25	10.5	5.0E-05	6.0E-05	8.5E-05	6.8E-05
25	11.5	3.3E-05	4.1E-05	5.8E-05	4.6E-05
25	12.5	6.6E-06	8.6E-06	1.3E-05	1.0E-05
25	13.5	4.4E-06	5.7E-06	8.4E-06	6.6E-06
25	14.5	2.1E-06	2.7E-06	4.0E-06	3.2E-06
25	18.5	4.8E-05	5.1E-05	5.7E-05	5.4E-05
25	24.5	4.8E-05	5.1E-05	5.7E-05	5.4E-05
25	29.5	4.8E-05	5.1E-05	5.7E-05	5.4E-05
25	34.5	4.8E-05	5.1E-05	5.7E-05	5.4E-05
25	39.5	4.8E-05	5.1E-05	5.7E-05	5.4E-05
25	44.5	4.8E-05	5.1E-05	5.7E-05	5.4E-05
25	49.5	4.8E-05	5.1E-05	5.7E-05	5.4E-05
15	0.5	1.8E-02	2.1E-02	2.5E-02	2.3E-02
15	1.5	1.2E-02	1.3E-02	1.6E-02	1.5E-02
15	2.5	6.5E-03	7.7E-03	9.9E-03	9.2E-03
15	3.5	3.5E-03	4.3E-03	5.9E-03	5.4E-03
15	4.5	2.4E-03	2.9E-03	3.9E-03	3.5E-03
15	5.5	1.3E-03	1.6E-03	2.1E-03	1.9E-03
15	6.5	8.9E-04	1.1E-03	1.5E-03	1.3E-03
15	7.5	5.7E-04	6.8E-04	9.3E-04	8.1E-04
15	8.5	2.8E-04	3.3E-04	4.6E-04	4.0E-04
15	9.5	9.3E-05	1.1E-04	1.5E-04	1.3E-04
15	10.5	5.5E-05	6.2E-05	8.8E-05	7.6E-05
15	11.5	3.7E-05	4.2E-05	5.9E-05	5.1E-05
15	12.5	8.0E-06	8.6E-06	1.2E-05	1.1E-05
15	13.5	5.3E-06	5.7E-06	8.0E-06	7.1E-06
15	14.5	2.5E-06	2.7E-06	3.8E-06	3.4E-06
15	18.5	5.0E-05	5.4E-05	6.7E-05	5.7E-05
15	24.5	5.0E-05	5.4E-05	6.7E-05	5.7E-05
15	29.5	5.0E-05	5.4E-05	6.7E-05	5.7E-05
15	34.5	5.0E-05	5.4E-05	6.7E-05	5.7E-05
15	39.5	5.0E-05	5.4E-05	6.7E-05	5.7E-05
15	44.5	5.0E-05	5.4E-05	6.7E-05	5.7E-05
15	49.5	5.0E-05	5.4E-05	6.7E-05	5.7E-05
5	0.5	2.4E-02	2.6E-02	2.5E-02	2.6E-02
5	1.5	1.6E-02	1.8E-02	1.7E-02	1.7E-02
5	2.5	9.6E-03	1.1E-02	1.1E-02	1.1E-02
5	3.5	5.7E-03	6.7E-03	6.7E-03	6.7E-03
5	4.5	3.8E-03	4.4E-03	4.4E-03	4.5E-03
5	5.5	2.1E-03	2.4E-03	2.4E-03	2.5E-03
5	6.5	1.4E-03	1.6E-03	1.7E-03	1.7E-03
5	7.5	9.0E-04	1.0E-03	1.1E-03	1.1E-03
5	8.5	4.4E-04	5.0E-04	5.2E-04	5.3E-04
5	9.5	1.4E-04	1.5E-04	1.7E-04	1.8E-04
5	10.5	8.2E-05	8.8E-05	9.7E-05	1.0E-04
5	11.5	5.5E-05	5.9E-05	6.5E-05	6.8E-05
5	12.5	1.1E-05	1.1E-05	1.3E-05	1.3E-05
5	13.5	7.5E-06	7.5E-06	8.4E-06	8.8E-06
5	14.5	3.6E-06	3.6E-06	4.0E-06	4.2E-06
5	18.5	6.2E-05	6.3E-05	7.5E-05	6.7E-05
5	24.5	6.2E-05	6.3E-05	7.5E-05	6.7E-05
5	29.5	6.2E-05	6.3E-05	7.5E-05	6.7E-05
5	34.5	6.2E-05	6.3E-05	7.5E-05	6.7E-05
5	39.5	6.2E-05	6.3E-05	7.5E-05	6.7E-05
5	44.5	6.2E-05	6.3E-05	7.5E-05	6.7E-05
5	49.5	6.2E-05	6.3E-05	7.5E-05	6.7E-05
-5	0.5	2.5E-02	2.6E-02	2.2E-02	2.4E-02
-5	1.5	1.6E-02	1.7E-02	1.4E-02	1.6E-02
-5	2.5	1.0E-02	1.0E-02	8.6E-03	1.0E-02
-5	3.5	6.4E-03	6.4E-03	5.1E-03	6.3E-03

-5	4.5	4.3E-03	4.2E-03	3.3E-03	4.1E-03
-5	5.5	2.3E-03	2.3E-03	1.6E-03	2.1E-03
-5	6.5	1.6E-03	1.6E-03	1.1E-03	1.4E-03
-5	7.5	1.0E-03	1.0E-03	7.0E-04	9.0E-04
-5	8.5	5.2E-04	4.8E-04	3.5E-04	4.4E-04
-5	9.5	1.8E-04	1.5E-04	1.1E-04	1.4E-04
-5	10.5	1.0E-04	8.6E-05	6.7E-05	8.4E-05
-5	11.5	6.8E-05	5.7E-05	4.5E-05	5.6E-05
-5	12.5	1.3E-05	1.1E-05	9.3E-06	1.1E-05
-5	13.5	8.4E-06	7.1E-06	6.2E-06	7.1E-06
-5	14.5	4.0E-06	3.4E-06	3.0E-06	3.4E-06
-5	18.5	7.2E-05	7.2E-05	8.4E-05	7.8E-05
-5	24.5	7.2E-05	7.2E-05	8.4E-05	7.8E-05
-5	29.5	7.2E-05	7.2E-05	8.4E-05	7.8E-05
-5	34.5	7.2E-05	7.2E-05	8.4E-05	7.8E-05
-5	39.5	7.2E-05	7.2E-05	8.4E-05	7.8E-05
-5	44.5	7.2E-05	7.2E-05	8.4E-05	7.8E-05
-5	49.5	7.2E-05	7.2E-05	8.4E-05	7.8E-05
-15	0.5	2.2E-02	2.2E-02	1.7E-02	1.9E-02
-15	1.5	1.5E-02	1.4E-02	1.1E-02	1.2E-02
-15	2.5	8.8E-03	8.1E-03	6.1E-03	7.5E-03
-15	3.5	5.1E-03	4.4E-03	3.2E-03	4.3E-03
-15	4.5	3.4E-03	2.9E-03	2.0E-03	2.7E-03
-15	5.5	1.8E-03	1.5E-03	9.4E-04	1.3E-03
-15	6.5	1.2E-03	1.0E-03	6.3E-04	8.7E-04
-15	7.5	7.8E-04	6.3E-04	4.1E-04	5.5E-04
-15	8.5	3.8E-04	3.1E-04	2.1E-04	2.7E-04
-15	9.5	1.2E-04	1.0E-04	7.3E-05	9.2E-05
-15	10.5	7.2E-05	5.8E-05	4.3E-05	5.3E-05
-15	11.5	4.8E-05	3.8E-05	2.9E-05	3.5E-05
-15	12.5	9.3E-06	7.3E-06	6.0E-06	6.6E-06
-15	13.5	6.2E-06	4.9E-06	4.0E-06	4.4E-06
-15	14.5	3.0E-06	2.3E-06	1.9E-06	2.1E-06
-15	18.5	6.0E-05	6.2E-05	8.8E-05	7.8E-05
-15	24.5	6.0E-05	6.2E-05	8.8E-05	7.8E-05
-15	29.5	6.0E-05	6.2E-05	8.8E-05	7.8E-05
-15	34.5	6.0E-05	6.2E-05	8.8E-05	7.8E-05
-15	39.5	6.0E-05	6.2E-05	8.8E-05	7.8E-05
-15	44.5	6.0E-05	6.2E-05	8.8E-05	7.8E-05
-15	49.5	6.0E-05	6.2E-05	8.8E-05	7.8E-05
-25	0.5	1.9E-02	1.7E-02	1.3E-02	1.4E-02
-25	1.5	1.1E-02	1.1E-02	7.5E-03	8.5E-03
-25	2.5	6.4E-03	5.8E-03	3.9E-03	4.8E-03
-25	3.5	3.5E-03	3.0E-03	1.9E-03	2.6E-03
-25	4.5	2.3E-03	2.0E-03	1.3E-03	1.7E-03
-25	5.5	1.3E-03	1.0E-03	6.7E-04	9.2E-04
-25	6.5	8.9E-04	7.2E-04	4.7E-04	6.3E-04
-25	7.5	5.7E-04	4.6E-04	3.0E-04	4.1E-04
-25	8.5	2.8E-04	2.4E-04	1.6E-04	2.1E-04
-25	9.5	9.8E-05	8.8E-05	6.4E-05	7.9E-05
-25	10.5	5.6E-05	5.1E-05	3.8E-05	4.6E-05
-25	11.5	3.7E-05	3.4E-05	2.6E-05	3.1E-05
-25	12.5	6.6E-06	6.6E-06	6.0E-06	6.0E-06
-25	13.5	4.4E-06	4.4E-06	4.0E-06	4.0E-06
-25	14.5	2.1E-06	2.1E-06	1.9E-06	1.9E-06
-25	18.5	4.8E-05	5.2E-05	7.9E-05	6.6E-05
-25	24.5	4.8E-05	5.2E-05	7.9E-05	6.6E-05
-25	29.5	4.8E-05	5.2E-05	7.9E-05	6.6E-05
-25	34.5	4.8E-05	5.2E-05	7.9E-05	6.6E-05
-25	39.5	4.8E-05	5.2E-05	7.9E-05	6.6E-05
-25	44.5	4.8E-05	5.2E-05	7.9E-05	6.6E-05
-25	49.5	4.8E-05	5.2E-05	7.9E-05	6.6E-05
-35	0.5	1.3E-02	1.2E-02	1.0E-02	1.0E-02
-35	1.5	7.9E-03	7.3E-03	5.6E-03	5.9E-03
-35	2.5	4.5E-03	4.0E-03	3.0E-03	3.4E-03
-35	3.5	2.5E-03	2.1E-03	1.5E-03	1.9E-03
-35	4.5	1.7E-03	1.5E-03	1.0E-03	1.3E-03
-35	5.5	1.0E-03	8.8E-04	6.0E-04	7.4E-04
-35	6.5	7.1E-04	6.1E-04	4.1E-04	5.1E-04
-35	7.5	4.6E-04	3.9E-04	2.6E-04	3.3E-04
-35	8.5	2.3E-04	1.9E-04	1.3E-04	1.6E-04
-35	9.5	8.3E-05	6.4E-05	3.9E-05	5.0E-05
-35	10.5	4.8E-05	3.8E-05	2.3E-05	2.9E-05
-35	11.5	3.2E-05	2.5E-05	1.6E-05	2.0E-05
-35	12.5	6.0E-06	5.3E-06	4.0E-06	4.0E-06
-35	13.5	4.0E-06	3.5E-06	2.7E-06	2.7E-06
-35	14.5	1.9E-06	1.7E-06	1.3E-06	1.3E-06
-35	18.5	3.2E-05	2.9E-05	7.2E-05	5.4E-05
-35	24.5	3.2E-05	2.9E-05	7.2E-05	5.4E-05
-35	29.5	3.2E-05	2.9E-05	7.2E-05	5.4E-05
-35	34.5	3.2E-05	2.9E-05	7.2E-05	5.4E-05
-35	39.5	3.2E-05	2.9E-05	7.2E-05	5.4E-05
-35	44.5	3.2E-05	2.9E-05	7.2E-05	5.4E-05
-35	49.5	3.2E-05	2.9E-05	7.2E-05	5.4E-05
-45	0.5	8.6E-03	8.2E-03	6.9E-03	7.1E-03
-45	1.5	5.6E-03	5.1E-03	4.2E-03	4.5E-03
-45	2.5	3.5E-03	3.1E-03	2.4E-03	2.7E-03
-45	3.5	2.1E-03	1.8E-03	1.3E-03	1.6E-03
-45	4.5	1.4E-03	1.2E-03	8.8E-04	1.0E-03
-45	5.5	8.5E-04	7.4E-04	4.6E-04	5.7E-04
-45	6.5	5.8E-04	5.1E-04	3.1E-04	3.8E-04
-45	7.5	3.7E-04	3.2E-04	1.9E-04	2.4E-04
-45	8.5	1.8E-04	1.5E-04	8.7E-05	1.1E-04
-45	9.5	5.6E-05	4.4E-05	2.2E-05	3.0E-05
-45	10.5	3.3E-05	2.6E-05	1.3E-05	1.7E-05
-45	11.5	2.3E-05	1.8E-05	9.5E-06	1.2E-05
-45	12.5	5.3E-06	4.0E-06	2.7E-06	2.7E-06
-45	13.5	3.5E-06	2.7E-06	1.8E-06	1.8E-06
-45	14.5	1.7E-06	1.3E-06	8.4E-07	8.4E-07
-45	18.5	1.8E-05	1.8E-05	5.7E-05	4.0E-05
-45	24.5	1.8E-05	1.8E-05	5.7E-05	4.0E-05
-45	29.5	1.8E-05	1.8E-05	5.7E-05	4.0E-05

-45	34.5	1.8E-05	1.8E-05	5.7E-05	4.0E-05
-45	39.5	1.8E-05	1.8E-05	5.7E-05	4.0E-05
-45	44.5	1.8E-05	1.8E-05	5.7E-05	4.0E-05
-45	49.5	1.8E-05	1.8E-05	5.7E-05	4.0E-05
-55	0.5	6.2E-03	5.6E-03	4.6E-03	5.0E-03
-55	1.5	4.2E-03	3.6E-03	2.9E-03	3.2E-03
-55	2.5	2.7E-03	2.2E-03	1.7E-03	2.0E-03
-55	3.5	1.7E-03	1.4E-03	1.0E-03	1.2E-03
-55	4.5	1.1E-03	9.0E-04	6.4E-04	7.5E-04
-55	5.5	6.2E-04	4.9E-04	3.1E-04	3.7E-04
-55	6.5	4.2E-04	3.3E-04	2.1E-04	2.4E-04
-55	7.5	2.6E-04	2.1E-04	1.3E-04	1.5E-04
-55	8.5	1.2E-04	9.6E-05	5.7E-05	7.0E-05
-55	9.5	3.4E-05	2.5E-05	1.3E-05	1.8E-05
-55	10.5	2.1E-05	1.5E-05	8.4E-06	1.1E-05
-55	11.5	1.5E-05	1.1E-05	6.2E-06	8.2E-06
-55	12.5	4.7E-06	2.7E-06	2.0E-06	3.0E-06
-55	13.5	3.1E-06	1.8E-06	1.3E-06	2.3E-06
-55	14.5	1.5E-06	8.4E-07	6.3E-07	1.6E-06
-55	18.5	1.3E-05	1.4E-05	5.1E-05	3.2E-05
-55	24.5	1.3E-05	1.4E-05	5.1E-05	3.2E-05
-55	29.5	1.3E-05	1.4E-05	5.1E-05	3.2E-05
-55	34.5	1.3E-05	1.4E-05	5.1E-05	3.2E-05
-55	39.5	1.3E-05	1.4E-05	5.1E-05	3.2E-05
-55	44.5	1.3E-05	1.4E-05	5.1E-05	3.2E-05
-55	49.5	1.3E-05	1.4E-05	5.1E-05	3.2E-05
-65	0.5	4.3E-03	2.7E-03	1.8E-03	2.4E-03
-65	1.5	2.9E-03	1.8E-03	1.3E-03	1.7E-03
-65	2.5	1.9E-03	1.2E-03	8.9E-04	1.1E-03
-65	3.5	1.2E-03	7.9E-04	5.9E-04	7.0E-04
-65	4.5	7.9E-04	5.3E-04	3.8E-04	4.5E-04
-65	5.5	4.3E-04	2.9E-04	1.9E-04	2.3E-04
-65	6.5	2.9E-04	1.9E-04	1.3E-04	1.5E-04
-65	7.5	1.8E-04	1.2E-04	8.1E-05	9.6E-05
-65	8.5	8.6E-05	5.7E-05	3.7E-05	4.5E-05
-65	9.5	2.5E-05	1.6E-05	8.8E-06	1.3E-05
-65	10.5	1.7E-05	1.0E-05	5.6E-06	8.5E-06
-65	11.5	1.3E-05	7.7E-06	4.1E-06	6.6E-06
-65	12.5	5.3E-06	2.7E-06	1.7E-06	3.3E-06
-65	13.5	3.5E-06	1.8E-06	1.4E-06	2.9E-06
-65	14.5	1.7E-06	8.4E-07	1.2E-06	2.4E-06
-65	18.5	1.3E-05	1.3E-05	4.7E-05	2.6E-05
-65	24.5	1.3E-05	1.3E-05	4.7E-05	2.6E-05
-65	29.5	1.3E-05	1.3E-05	4.7E-05	2.6E-05
-65	34.5	1.3E-05	1.3E-05	4.7E-05	2.6E-05
-65	39.5	1.3E-05	1.3E-05	4.7E-05	2.6E-05
-65	44.5	1.3E-05	1.3E-05	4.7E-05	2.6E-05
-65	49.5	1.3E-05	1.3E-05	4.7E-05	2.6E-05
-75	0.5	2.5E-03	6.3E-04	3.9E-04	7.7E-04
-75	1.5	1.7E-03	5.2E-04	3.2E-04	5.8E-04
-75	2.5	1.1E-03	3.8E-04	2.5E-04	4.2E-04
-75	3.5	7.3E-04	2.9E-04	2.0E-04	3.1E-04
-75	4.5	5.1E-04	2.3E-04	1.6E-04	2.4E-04
-75	5.5	3.1E-04	1.8E-04	1.2E-04	1.7E-04
-75	6.5	2.1E-04	1.3E-04	8.8E-05	1.2E-04
-75	7.5	1.3E-04	8.0E-05	5.4E-05	7.4E-05
-75	8.5	6.2E-05	3.8E-05	2.5E-05	3.5E-05
-75	9.5	1.8E-05	1.1E-05	6.3E-06	9.8E-06
-75	10.5	1.4E-05	7.0E-06	4.2E-06	6.6E-06
-75	11.5	1.2E-05	5.4E-06	3.3E-06	5.1E-06
-75	12.5	6.0E-06	2.3E-06	1.3E-06	2.3E-06
-75	13.5	4.0E-06	1.9E-06	8.8E-07	1.9E-06
-75	14.5	1.9E-06	1.4E-06	4.2E-07	1.4E-06
-75	18.5	1.3E-05	1.3E-05	3.7E-05	1.8E-05
-75	24.5	1.3E-05	1.3E-05	3.7E-05	1.8E-05
-75	29.5	1.3E-05	1.3E-05	3.7E-05	1.8E-05
-75	34.5	1.3E-05	1.3E-05	3.7E-05	1.8E-05
-75	39.5	1.3E-05	1.3E-05	3.7E-05	1.8E-05
-75	44.5	1.3E-05	1.3E-05	3.7E-05	1.8E-05
-75	49.5	1.3E-05	1.3E-05	3.7E-05	1.8E-05
-85	0.5	1.6E-03	2.9E-04	1.7E-04	3.7E-04
-85	1.5	1.0E-03	1.8E-04	1.0E-04	2.2E-04
-85	2.5	7.0E-04	1.6E-04	9.2E-05	1.8E-04
-85	3.5	5.0E-04	1.4E-04	8.7E-05	1.5E-04
-85	4.5	3.6E-04	1.4E-04	8.8E-05	1.4E-04
-85	5.5	2.4E-04	1.3E-04	8.9E-05	1.2E-04
-85	6.5	1.7E-04	9.6E-05	6.4E-05	8.7E-05
-85	7.5	1.1E-04	6.1E-05	4.0E-05	5.5E-05
-85	8.5	4.9E-05	2.9E-05	1.9E-05	2.6E-05
-85	9.5	1.5E-05	9.0E-06	5.4E-06	8.1E-06
-85	10.5	1.3E-05	6.1E-06	3.8E-06	5.7E-06
-85	11.5	1.2E-05	4.8E-06	3.1E-06	4.6E-06
-85	12.5	7.3E-06	2.3E-06	1.3E-06	2.3E-06
-85	13.5	4.9E-06	1.9E-06	8.8E-07	1.9E-06
-85	14.5	2.3E-06	1.4E-06	4.2E-07	1.4E-06
-85	18.5	1.1E-05	1.2E-05	3.2E-05	1.6E-05
-85	24.5	1.1E-05	1.2E-05	3.2E-05	1.6E-05
-85	29.5	1.1E-05	1.2E-05	3.2E-05	1.6E-05
-85	34.5	1.1E-05	1.2E-05	3.2E-05	1.6E-05
-85	39.5	1.1E-05	1.2E-05	3.2E-05	1.6E-05
-85	44.5	1.1E-05	1.2E-05	3.2E-05	1.6E-05
-85	49.5	1.1E-05	1.2E-05	3.2E-05	1.6E-05

B.9 h2osea.dat

85	0.5	5.6E-04	1.1E-03	5.0E-03	1.5E-03
85	1.5	7.7E-04	1.3E-03	4.1E-03	1.4E-03
85	2.5	5.7E-04	9.3E-04	2.8E-03	1.0E-03
85	3.5	4.0E-04	6.3E-04	1.9E-03	7.0E-04
85	4.5	2.6E-04	4.0E-04	1.2E-03	4.5E-04
85	5.5	1.3E-04	2.0E-04	6.2E-04	2.3E-04

85	6.5	8.6E-05	1.3E-04	4.2E-04	1.5E-04
85	7.5	5.4E-05	8.3E-05	2.6E-04	9.3E-05
85	8.5	2.5E-05	3.9E-05	1.2E-04	4.3E-05
85	9.5	7.1E-06	1.2E-05	3.4E-05	1.1E-05
85	10.5	4.7E-06	7.5E-06	2.2E-05	7.6E-06
85	11.5	3.6E-06	5.6E-06	1.6E-05	6.1E-06
85	12.5	1.7E-06	2.0E-06	5.3E-06	2.7E-06
85	13.5	1.4E-06	1.3E-06	3.5E-06	1.8E-06
85	14.5	1.2E-06	6.3E-07	1.7E-06	8.4E-07
85	18.5	9.7E-06	1.4E-05	4.8E-05	1.4E-05
85	24.5	9.7E-06	1.4E-05	4.8E-05	1.4E-05
85	29.5	9.7E-06	1.4E-05	4.8E-05	1.4E-05
85	34.5	9.7E-06	1.4E-05	4.8E-05	1.4E-05
85	39.5	9.7E-06	1.4E-05	4.8E-05	1.4E-05
85	44.5	9.7E-06	1.4E-05	4.8E-05	1.4E-05
85	49.5	9.7E-06	1.4E-05	4.8E-05	1.4E-05
75	0.5	1.2E-03	2.0E-03	5.9E-03	3.1E-03
75	1.5	1.1E-03	1.8E-03	4.9E-03	2.2E-03
75	2.5	7.6E-04	1.2E-03	3.3E-03	1.5E-03
75	3.5	4.9E-04	7.5E-04	2.1E-03	9.7E-04
75	4.5	3.1E-04	4.7E-04	1.3E-03	6.1E-04
75	5.5	1.4E-04	2.2E-04	6.5E-04	3.0E-04
75	6.5	9.6E-05	1.5E-04	4.3E-04	2.0E-04
75	7.5	6.0E-05	9.3E-05	2.7E-04	1.2E-04
75	8.5	2.8E-05	4.4E-05	1.3E-04	5.5E-05
75	9.5	8.0E-06	1.2E-05	3.7E-05	1.3E-05
75	10.5	5.1E-06	7.9E-06	2.4E-05	8.4E-06
75	11.5	3.8E-06	5.9E-06	1.8E-05	6.2E-06
75	12.5	1.7E-06	2.0E-06	6.0E-06	2.0E-06
75	13.5	1.4E-06	1.3E-06	4.0E-06	1.3E-06
75	14.5	1.2E-06	6.3E-07	1.9E-06	6.3E-07
75	18.5	9.7E-06	1.7E-05	4.0E-05	1.6E-05
75	24.5	9.7E-06	1.7E-05	4.0E-05	1.6E-05
75	29.5	9.7E-06	1.7E-05	4.0E-05	1.6E-05
75	34.5	9.7E-06	1.7E-05	4.0E-05	1.6E-05
75	39.5	9.7E-06	1.7E-05	4.0E-05	1.6E-05
75	44.5	9.7E-06	1.7E-05	4.0E-05	1.6E-05
75	49.5	9.7E-06	1.7E-05	4.0E-05	1.6E-05
65	0.5	1.5E-03	2.9E-03	9.0E-03	4.1E-03
65	1.5	1.4E-03	2.2E-03	6.5E-03	3.0E-03
65	2.5	9.9E-04	1.5E-03	4.3E-03	2.0E-03
65	3.5	6.7E-04	9.8E-04	2.7E-03	1.3E-03
65	4.5	4.2E-04	6.2E-04	1.7E-03	8.2E-04
65	5.5	2.0E-04	3.0E-04	8.0E-04	4.0E-04
65	6.5	1.4E-04	2.0E-04	5.3E-04	2.7E-04
65	7.5	8.6E-05	1.3E-04	3.4E-04	1.7E-04
65	8.5	4.0E-05	6.0E-05	1.6E-04	7.6E-05
65	9.5	1.2E-05	1.8E-05	5.0E-05	2.0E-05
65	10.5	7.5E-06	1.1E-05	3.2E-05	1.3E-05
65	11.5	5.6E-06	8.2E-06	2.4E-05	9.7E-06
65	12.5	2.3E-06	2.7E-06	8.0E-06	3.3E-06
65	13.5	1.9E-06	1.8E-06	5.3E-06	2.2E-06
65	14.5	1.4E-06	8.4E-07	2.5E-06	1.1E-06
65	18.5	1.1E-05	2.1E-05	3.4E-05	1.7E-05
65	24.5	1.1E-05	2.1E-05	3.4E-05	1.7E-05
65	29.5	1.1E-05	2.1E-05	3.4E-05	1.7E-05
65	34.5	1.1E-05	2.1E-05	3.4E-05	1.7E-05
65	39.5	1.1E-05	2.1E-05	3.4E-05	1.7E-05
65	44.5	1.1E-05	2.1E-05	3.4E-05	1.7E-05
65	49.5	1.1E-05	2.1E-05	3.4E-05	1.7E-05
55	0.5	2.7E-03	4.9E-03	1.1E-02	6.8E-03
55	1.5	2.0E-03	3.2E-03	8.4E-03	4.5E-03
55	2.5	1.4E-03	2.1E-03	5.3E-03	2.9E-03
55	3.5	9.1E-04	1.4E-03	3.3E-03	1.8E-03
55	4.5	5.7E-04	8.7E-04	2.0E-03	1.1E-03
55	5.5	2.6E-04	4.0E-04	9.6E-04	5.3E-04
55	6.5	1.7E-04	2.6E-04	6.4E-04	3.5E-04
55	7.5	1.1E-04	1.6E-04	4.0E-04	2.2E-04
55	8.5	4.8E-05	7.6E-05	1.9E-04	1.0E-04
55	9.5	1.1E-05	1.9E-05	5.7E-05	2.7E-05
55	10.5	6.5E-06	1.2E-05	3.4E-05	1.7E-05
55	11.5	4.6E-06	8.0E-06	2.4E-05	1.3E-05
55	12.5	1.3E-06	2.0E-06	6.0E-06	4.0E-06
55	13.5	8.8E-07	1.3E-06	4.0E-06	2.7E-06
55	14.5	4.2E-07	6.3E-07	1.9E-06	1.3E-06
55	18.5	1.3E-05	2.0E-05	3.1E-05	2.0E-05
55	24.5	1.3E-05	2.0E-05	3.1E-05	2.0E-05
55	29.5	1.3E-05	2.0E-05	3.1E-05	2.0E-05
55	34.5	1.3E-05	2.0E-05	3.1E-05	2.0E-05
55	39.5	1.3E-05	2.0E-05	3.1E-05	2.0E-05
55	44.5	1.3E-05	2.0E-05	3.1E-05	2.0E-05
55	49.5	1.3E-05	2.0E-05	3.1E-05	2.0E-05
45	0.5	4.9E-03	7.8E-03	1.6E-02	1.0E-02
45	1.5	3.3E-03	5.1E-03	1.2E-02	6.6E-03
45	2.5	2.1E-03	3.2E-03	7.0E-03	4.0E-03
45	3.5	1.3E-03	1.9E-03	4.0E-03	2.4E-03
45	4.5	8.0E-04	1.2E-03	2.5E-03	1.5E-03
45	5.5	3.8E-04	5.6E-04	1.2E-03	7.2E-04
45	6.5	2.5E-04	3.7E-04	7.9E-04	4.8E-04
45	7.5	1.6E-04	2.3E-04	5.1E-04	3.1E-04
45	8.5	7.3E-05	1.1E-04	2.5E-04	1.5E-04
45	9.5	1.8E-05	3.0E-05	8.9E-05	4.8E-05
45	10.5	1.1E-05	1.7E-05	5.4E-05	3.0E-05
45	11.5	7.7E-06	1.2E-05	3.8E-05	2.1E-05
45	12.5	2.0E-06	2.7E-06	1.0E-05	6.0E-06
45	13.5	1.3E-06	1.8E-06	6.6E-06	4.0E-06
45	14.5	6.3E-07	8.4E-07	3.2E-06	1.9E-06
45	18.5	1.6E-05	1.8E-05	3.5E-05	2.7E-05
45	24.5	1.6E-05	1.8E-05	3.5E-05	2.7E-05
45	29.5	1.6E-05	1.8E-05	3.5E-05	2.7E-05
45	34.5	1.6E-05	1.8E-05	3.5E-05	2.7E-05
45	39.5	1.6E-05	1.8E-05	3.5E-05	2.7E-05

45	44.5	1.6E-05	1.8E-05	3.5E-05	2.7E-05
45	49.5	1.6E-05	1.8E-05	3.5E-05	2.7E-05
35	0.5	9.2E-03	1.3E-02	2.1E-02	1.6E-02
35	1.5	5.9E-03	7.8E-03	1.4E-02	1.0E-02
35	2.5	3.3E-03	4.6E-03	8.4E-03	5.7E-03
35	3.5	1.7E-03	2.6E-03	4.8E-03	3.0E-03
35	4.5	1.1E-03	1.7E-03	3.1E-03	2.0E-03
35	5.5	5.9E-04	8.7E-04	1.6E-03	1.0E-03
35	6.5	4.1E-04	5.9E-04	1.1E-03	6.9E-04
35	7.5	2.6E-04	3.7E-04	7.1E-04	4.5E-04
35	8.5	1.3E-04	1.8E-04	3.7E-04	2.3E-04
35	9.5	4.3E-05	5.6E-05	1.4E-04	8.4E-05
35	10.5	2.6E-05	3.3E-05	8.3E-05	5.0E-05
35	11.5	1.8E-05	2.2E-05	5.8E-05	3.5E-05
35	12.5	5.0E-06	4.7E-06	1.4E-05	9.0E-06
35	13.5	3.7E-06	3.1E-06	9.3E-06	6.3E-06
35	14.5	2.3E-06	1.5E-06	4.4E-06	3.5E-06
35	18.5	2.9E-05	3.0E-05	4.3E-05	3.8E-05
35	24.5	2.9E-05	3.0E-05	4.3E-05	3.8E-05
35	29.5	2.9E-05	3.0E-05	4.3E-05	3.8E-05
35	34.5	2.9E-05	3.0E-05	4.3E-05	3.8E-05
35	39.5	2.9E-05	3.0E-05	4.3E-05	3.8E-05
35	44.5	2.9E-05	3.0E-05	4.3E-05	3.8E-05
35	49.5	2.9E-05	3.0E-05	4.3E-05	3.8E-05
25	0.5	1.4E-02	1.8E-02	2.4E-02	2.0E-02
25	1.5	9.4E-03	1.2E-02	1.6E-02	1.3E-02
25	2.5	5.3E-03	6.8E-03	8.9E-03	7.5E-03
25	3.5	2.8E-03	3.7E-03	4.9E-03	4.0E-03
25	4.5	1.8E-03	2.4E-03	3.3E-03	2.6E-03
25	5.5	9.1E-04	1.3E-03	1.8E-03	1.4E-03
25	6.5	6.2E-04	8.7E-04	1.2E-03	9.2E-04
25	7.5	4.0E-04	5.6E-04	8.0E-04	6.0E-04
25	8.5	2.0E-04	2.8E-04	4.1E-04	3.0E-04
25	9.5	7.6E-05	9.4E-05	1.5E-04	1.1E-04
25	10.5	4.4E-05	5.5E-05	8.7E-05	6.4E-05
25	11.5	3.0E-05	3.7E-05	5.9E-05	4.4E-05
25	12.5	7.0E-06	8.3E-06	1.3E-05	1.0E-05
25	13.5	5.0E-06	5.9E-06	8.8E-06	6.6E-06
25	14.5	2.9E-06	3.3E-06	4.2E-06	3.2E-06
25	18.5	4.8E-05	5.1E-05	5.7E-05	5.4E-05
25	24.5	4.8E-05	5.1E-05	5.7E-05	5.4E-05
25	29.5	4.8E-05	5.1E-05	5.7E-05	5.4E-05
25	34.5	4.8E-05	5.1E-05	5.7E-05	5.4E-05
25	39.5	4.8E-05	5.1E-05	5.7E-05	5.4E-05
25	44.5	4.8E-05	5.1E-05	5.7E-05	5.4E-05
25	49.5	4.8E-05	5.1E-05	5.7E-05	5.4E-05
15	0.5	1.8E-02	2.0E-02	2.4E-02	2.3E-02
15	1.5	1.2E-02	1.3E-02	1.6E-02	1.5E-02
15	2.5	6.5E-03	7.6E-03	9.7E-03	8.9E-03
15	3.5	3.5E-03	4.2E-03	5.9E-03	5.3E-03
15	4.5	2.3E-03	2.8E-03	4.0E-03	3.5E-03
15	5.5	1.3E-03	1.6E-03	2.2E-03	1.9E-03
15	6.5	8.9E-04	1.1E-03	1.5E-03	1.3E-03
15	7.5	5.7E-04	6.9E-04	9.7E-04	8.3E-04
15	8.5	2.8E-04	3.3E-04	4.8E-04	4.0E-04
15	9.5	9.2E-05	1.1E-04	1.6E-04	1.3E-04
15	10.5	5.4E-05	6.1E-05	9.3E-05	7.7E-05
15	11.5	3.7E-05	4.1E-05	6.2E-05	5.2E-05
15	12.5	8.0E-06	8.6E-06	1.3E-05	1.1E-05
15	13.5	5.3E-06	5.7E-06	8.4E-06	7.5E-06
15	14.5	2.5E-06	2.7E-06	4.0E-06	3.6E-06
15	18.5	5.0E-05	5.4E-05	6.7E-05	5.7E-05
15	24.5	5.0E-05	5.4E-05	6.7E-05	5.7E-05
15	29.5	5.0E-05	5.4E-05	6.7E-05	5.7E-05
15	34.5	5.0E-05	5.4E-05	6.7E-05	5.7E-05
15	39.5	5.0E-05	5.4E-05	6.7E-05	5.7E-05
15	44.5	5.0E-05	5.4E-05	6.7E-05	5.7E-05
15	49.5	5.0E-05	5.4E-05	6.7E-05	5.7E-05
5	0.5	2.3E-02	2.5E-02	2.4E-02	2.4E-02
5	1.5	1.5E-02	1.6E-02	1.6E-02	1.6E-02
5	2.5	9.5E-03	1.1E-02	1.1E-02	1.1E-02
5	3.5	5.8E-03	6.8E-03	6.9E-03	6.8E-03
5	4.5	3.8E-03	4.5E-03	4.6E-03	4.5E-03
5	5.5	2.1E-03	2.4E-03	2.5E-03	2.5E-03
5	6.5	1.4E-03	1.6E-03	1.7E-03	1.7E-03
5	7.5	8.9E-04	1.0E-03	1.1E-03	1.1E-03
5	8.5	4.3E-04	4.9E-04	5.3E-04	5.3E-04
5	9.5	1.4E-04	1.5E-04	1.7E-04	1.7E-04
5	10.5	8.0E-05	8.7E-05	9.7E-05	1.0E-04
5	11.5	5.4E-05	5.9E-05	6.5E-05	6.7E-05
5	12.5	1.1E-05	1.2E-05	1.3E-05	1.3E-05
5	13.5	7.5E-06	8.0E-06	8.4E-06	8.8E-06
5	14.5	3.6E-06	3.8E-06	4.0E-06	4.2E-06
5	18.5	6.2E-05	6.3E-05	7.5E-05	6.7E-05
5	24.5	6.2E-05	6.3E-05	7.5E-05	6.7E-05
5	29.5	6.2E-05	6.3E-05	7.5E-05	6.7E-05
5	34.5	6.2E-05	6.3E-05	7.5E-05	6.7E-05
5	39.5	6.2E-05	6.3E-05	7.5E-05	6.7E-05
5	44.5	6.2E-05	6.3E-05	7.5E-05	6.7E-05
5	49.5	6.2E-05	6.3E-05	7.5E-05	6.7E-05
-5	0.5	2.4E-02	2.5E-02	2.1E-02	2.2E-02
-5	1.5	1.6E-02	1.6E-02	1.3E-02	1.5E-02
-5	2.5	1.0E-02	1.0E-02	8.6E-03	9.8E-03
-5	3.5	6.5E-03	6.6E-03	5.3E-03	6.4E-03
-5	4.5	4.3E-03	4.3E-03	3.4E-03	4.2E-03
-5	5.5	2.3E-03	2.3E-03	1.7E-03	2.1E-03
-5	6.5	1.6E-03	1.6E-03	1.1E-03	1.4E-03
-5	7.5	1.0E-03	1.0E-03	7.2E-04	9.2E-04
-5	8.5	5.1E-04	4.9E-04	3.6E-04	4.5E-04
-5	9.5	1.8E-04	1.5E-04	1.2E-04	1.4E-04
-5	10.5	1.0E-04	8.6E-05	6.8E-05	8.3E-05
-5	11.5	6.7E-05	5.7E-05	4.6E-05	5.5E-05

-5	12.5	1.3E-05	1.1E-05	9.3E-06	1.1E-05
-5	13.5	8.4E-06	7.1E-06	6.2E-06	7.1E-06
-5	14.5	4.0E-06	3.4E-06	3.0E-06	3.4E-06
-5	18.5	7.2E-05	7.2E-05	8.4E-05	7.8E-05
-5	24.5	7.2E-05	7.2E-05	8.4E-05	7.8E-05
-5	29.5	7.2E-05	7.2E-05	8.4E-05	7.8E-05
-5	34.5	7.2E-05	7.2E-05	8.4E-05	7.8E-05
-5	39.5	7.2E-05	7.2E-05	8.4E-05	7.8E-05
-5	44.5	7.2E-05	7.2E-05	8.4E-05	7.8E-05
-5	49.5	7.2E-05	7.2E-05	8.4E-05	7.8E-05
-15	0.5	2.2E-02	2.2E-02	1.7E-02	1.9E-02
-15	1.5	1.4E-02	1.4E-02	1.0E-02	1.2E-02
-15	2.5	8.6E-03	7.9E-03	6.0E-03	7.2E-03
-15	3.5	5.0E-03	4.4E-03	3.2E-03	4.1E-03
-15	4.5	3.3E-03	2.8E-03	2.0E-03	2.6E-03
-15	5.5	1.7E-03	1.5E-03	9.3E-04	1.3E-03
-15	6.5	1.2E-03	9.8E-04	6.3E-04	8.6E-04
-15	7.5	7.5E-04	6.2E-04	4.0E-04	5.5E-04
-15	8.5	3.7E-04	3.0E-04	2.0E-04	2.7E-04
-15	9.5	1.2E-04	9.7E-05	7.1E-05	9.1E-05
-15	10.5	6.9E-05	5.6E-05	4.2E-05	5.3E-05
-15	11.5	4.6E-05	3.8E-05	2.8E-05	3.5E-05
-15	12.5	9.3E-06	7.3E-06	6.0E-06	6.6E-06
-15	13.5	6.2E-06	4.9E-06	4.0E-06	4.4E-06
-15	14.5	3.0E-06	2.3E-06	1.9E-06	2.1E-06
-15	18.5	6.0E-05	6.2E-05	8.8E-05	7.8E-05
-15	24.5	6.0E-05	6.2E-05	8.8E-05	7.8E-05
-15	29.5	6.0E-05	6.2E-05	8.8E-05	7.8E-05
-15	34.5	6.0E-05	6.2E-05	8.8E-05	7.8E-05
-15	39.5	6.0E-05	6.2E-05	8.8E-05	7.8E-05
-15	44.5	6.0E-05	6.2E-05	8.8E-05	7.8E-05
-15	49.5	6.0E-05	6.2E-05	8.8E-05	7.8E-05
-25	0.5	2.0E-02	1.8E-02	1.3E-02	1.5E-02
-25	1.5	1.2E-02	1.1E-02	7.4E-03	8.8E-03
-25	2.5	6.6E-03	5.7E-03	3.8E-03	4.9E-03
-25	3.5	3.4E-03	2.9E-03	1.8E-03	2.5E-03
-25	4.5	2.3E-03	1.9E-03	1.2E-03	1.7E-03
-25	5.5	1.3E-03	1.0E-03	6.5E-04	9.0E-04
-25	6.5	8.7E-04	7.1E-04	4.5E-04	6.2E-04
-25	7.5	5.6E-04	4.6E-04	2.9E-04	4.0E-04
-25	8.5	2.8E-04	2.4E-04	1.5E-04	2.1E-04
-25	9.5	1.0E-04	8.8E-05	6.2E-05	7.9E-05
-25	10.5	5.8E-05	5.1E-05	3.6E-05	4.6E-05
-25	11.5	3.9E-05	3.4E-05	2.5E-05	3.1E-05
-25	12.5	7.3E-06	6.6E-06	5.3E-06	6.6E-06
-25	13.5	4.9E-06	4.4E-06	3.5E-06	4.4E-06
-25	14.5	2.3E-06	2.1E-06	1.7E-06	2.1E-06
-25	18.5	4.8E-05	5.2E-05	7.9E-05	6.6E-05
-25	24.5	4.8E-05	5.2E-05	7.9E-05	6.6E-05
-25	29.5	4.8E-05	5.2E-05	7.9E-05	6.6E-05
-25	34.5	4.8E-05	5.2E-05	7.9E-05	6.6E-05
-25	39.5	4.8E-05	5.2E-05	7.9E-05	6.6E-05
-25	44.5	4.8E-05	5.2E-05	7.9E-05	6.6E-05
-25	49.5	4.8E-05	5.2E-05	7.9E-05	6.6E-05
-35	0.5	1.4E-02	1.3E-02	1.0E-02	1.1E-02
-35	1.5	8.2E-03	7.5E-03	5.6E-03	6.1E-03
-35	2.5	4.6E-03	4.1E-03	3.0E-03	3.5E-03
-35	3.5	2.5E-03	2.1E-03	1.5E-03	1.9E-03
-35	4.5	1.7E-03	1.5E-03	1.0E-03	1.3E-03
-35	5.5	1.0E-03	8.8E-04	5.9E-04	7.4E-04
-35	6.5	7.2E-04	6.1E-04	4.1E-04	5.1E-04
-35	7.5	4.6E-04	3.9E-04	2.6E-04	3.2E-04
-35	8.5	2.4E-04	1.9E-04	1.2E-04	1.6E-04
-35	9.5	8.6E-05	6.6E-05	3.8E-05	5.0E-05
-35	10.5	5.0E-05	3.8E-05	2.3E-05	3.0E-05
-35	11.5	3.3E-05	2.6E-05	1.6E-05	2.0E-05
-35	12.5	6.6E-06	5.3E-06	4.0E-06	4.7E-06
-35	13.5	4.4E-06	3.5E-06	2.7E-06	3.1E-06
-35	14.5	2.1E-06	1.7E-06	1.3E-06	1.5E-06
-35	18.5	3.2E-05	2.9E-05	7.2E-05	5.4E-05
-35	24.5	3.2E-05	2.9E-05	7.2E-05	5.4E-05
-35	29.5	3.2E-05	2.9E-05	7.2E-05	5.4E-05
-35	34.5	3.2E-05	2.9E-05	7.2E-05	5.4E-05
-35	39.5	3.2E-05	2.9E-05	7.2E-05	5.4E-05
-35	44.5	3.2E-05	2.9E-05	7.2E-05	5.4E-05
-35	49.5	3.2E-05	2.9E-05	7.2E-05	5.4E-05
-45	0.5	8.8E-03	8.3E-03	7.0E-03	7.3E-03
-45	1.5	5.8E-03	5.2E-03	4.3E-03	4.6E-03
-45	2.5	3.6E-03	3.1E-03	2.5E-03	2.8E-03
-45	3.5	2.1E-03	1.8E-03	1.4E-03	1.6E-03
-45	4.5	1.5E-03	1.3E-03	9.1E-04	1.1E-03
-45	5.5	8.7E-04	7.5E-04	4.7E-04	5.8E-04
-45	6.5	6.0E-04	5.1E-04	3.2E-04	3.9E-04
-45	7.5	3.8E-04	3.2E-04	2.0E-04	2.4E-04
-45	8.5	1.8E-04	1.5E-04	8.9E-05	1.1E-04
-45	9.5	5.7E-05	4.4E-05	2.1E-05	3.0E-05
-45	10.5	3.4E-05	2.6E-05	1.2E-05	1.7E-05
-45	11.5	2.3E-05	1.8E-05	8.5E-06	1.2E-05
-45	12.5	5.3E-06	4.0E-06	2.0E-06	2.7E-06
-45	13.5	3.5E-06	2.7E-06	1.3E-06	1.8E-06
-45	14.5	1.7E-06	1.3E-06	6.3E-07	8.4E-07
-45	18.5	1.8E-05	1.8E-05	5.7E-05	4.0E-05
-45	24.5	1.8E-05	1.8E-05	5.7E-05	4.0E-05
-45	29.5	1.8E-05	1.8E-05	5.7E-05	4.0E-05
-45	34.5	1.8E-05	1.8E-05	5.7E-05	4.0E-05
-45	39.5	1.8E-05	1.8E-05	5.7E-05	4.0E-05
-45	44.5	1.8E-05	1.8E-05	5.7E-05	4.0E-05
-45	49.5	1.8E-05	1.8E-05	5.7E-05	4.0E-05
-55	0.5	6.1E-03	5.4E-03	4.4E-03	4.9E-03
-55	1.5	4.4E-03	3.6E-03	2.9E-03	3.3E-03
-55	2.5	2.9E-03	2.2E-03	1.7E-03	2.1E-03
-55	3.5	1.8E-03	1.4E-03	1.0E-03	1.2E-03

-55	4.5	1.2E-03	9.0E-04	6.4E-04	7.8E-04
-55	5.5	6.6E-04	4.9E-04	3.1E-04	3.8E-04
-55	6.5	4.5E-04	3.3E-04	2.0E-04	2.5E-04
-55	7.5	2.8E-04	2.1E-04	1.3E-04	1.6E-04
-55	8.5	1.3E-04	9.6E-05	5.6E-05	7.2E-05
-55	9.5	3.5E-05	2.5E-05	1.2E-05	1.8E-05
-55	10.5	2.2E-05	1.5E-05	7.4E-06	1.2E-05
-55	11.5	1.6E-05	1.1E-05	5.2E-06	8.5E-06
-55	12.5	4.7E-06	2.7E-06	1.7E-06	3.0E-06
-55	13.5	3.1E-06	1.8E-06	1.4E-06	2.3E-06
-55	14.5	1.5E-06	8.4E-07	1.2E-06	1.6E-06
-55	18.5	1.3E-05	1.4E-05	5.1E-05	3.2E-05
-55	24.5	1.3E-05	1.4E-05	5.1E-05	3.2E-05
-55	29.5	1.3E-05	1.4E-05	5.1E-05	3.2E-05
-55	34.5	1.3E-05	1.4E-05	5.1E-05	3.2E-05
-55	39.5	1.3E-05	1.4E-05	5.1E-05	3.2E-05
-55	44.5	1.3E-05	1.4E-05	5.1E-05	3.2E-05
-55	49.5	1.3E-05	1.4E-05	5.1E-05	3.2E-05
-65	0.5	4.3E-03	2.6E-03	1.6E-03	2.3E-03
-65	1.5	2.9E-03	1.7E-03	1.2E-03	1.6E-03
-65	2.5	1.9E-03	1.2E-03	8.4E-04	1.1E-03
-65	3.5	1.2E-03	7.5E-04	5.6E-04	6.9E-04
-65	4.5	7.9E-04	5.0E-04	3.6E-04	4.5E-04
-65	5.5	4.4E-04	2.8E-04	1.9E-04	2.3E-04
-65	6.5	3.0E-04	1.9E-04	1.2E-04	1.5E-04
-65	7.5	1.9E-04	1.2E-04	7.7E-05	9.5E-05
-65	8.5	8.8E-05	5.6E-05	3.5E-05	4.5E-05
-65	9.5	2.6E-05	1.6E-05	8.8E-06	1.4E-05
-65	10.5	1.7E-05	1.0E-05	5.6E-06	9.5E-06
-65	11.5	1.4E-05	7.7E-06	4.1E-06	7.6E-06
-65	12.5	5.3E-06	2.7E-06	1.7E-06	4.3E-06
-65	13.5	3.5E-06	1.8E-06	1.4E-06	3.9E-06
-65	14.5	1.7E-06	8.4E-07	1.2E-06	3.4E-06
-65	18.5	1.3E-05	1.3E-05	4.7E-05	2.6E-05
-65	24.5	1.3E-05	1.3E-05	4.7E-05	2.6E-05
-65	29.5	1.3E-05	1.3E-05	4.7E-05	2.6E-05
-65	34.5	1.3E-05	1.3E-05	4.7E-05	2.6E-05
-65	39.5	1.3E-05	1.3E-05	4.7E-05	2.6E-05
-65	44.5	1.3E-05	1.3E-05	4.7E-05	2.6E-05
-65	49.5	1.3E-05	1.3E-05	4.7E-05	2.6E-05
-75	0.5	2.5E-03	6.8E-04	3.9E-04	7.6E-04
-75	1.5	1.6E-03	5.1E-04	3.2E-04	5.5E-04
-75	2.5	1.1E-03	3.6E-04	2.3E-04	3.9E-04
-75	3.5	7.0E-04	2.6E-04	1.8E-04	2.8E-04
-75	4.5	4.9E-04	2.2E-04	1.5E-04	2.1E-04
-75	5.5	3.0E-04	1.7E-04	1.2E-04	1.6E-04
-75	6.5	2.0E-04	1.2E-04	8.4E-05	1.1E-04
-75	7.5	1.3E-04	7.6E-05	5.2E-05	6.9E-05
-75	8.5	6.1E-05	3.6E-05	2.4E-05	3.3E-05
-75	9.5	1.9E-05	1.1E-05	6.3E-06	9.8E-06
-75	10.5	1.4E-05	7.0E-06	4.2E-06	6.6E-06
-75	11.5	1.3E-05	5.4E-06	3.3E-06	5.1E-06
-75	12.5	6.6E-06	2.3E-06	1.3E-06	2.7E-06
-75	13.5	4.4E-06	1.9E-06	8.8E-07	2.4E-06
-75	14.5	2.1E-06	1.4E-06	4.2E-07	2.2E-06
-75	18.5	1.3E-05	1.3E-05	3.7E-05	1.8E-05
-75	24.5	1.3E-05	1.3E-05	3.7E-05	1.8E-05
-75	29.5	1.3E-05	1.3E-05	3.7E-05	1.8E-05
-75	34.5	1.3E-05	1.3E-05	3.7E-05	1.8E-05
-75	39.5	1.3E-05	1.3E-05	3.7E-05	1.8E-05
-75	44.5	1.3E-05	1.3E-05	3.7E-05	1.8E-05
-75	49.5	1.3E-05	1.3E-05	3.7E-05	1.8E-05
-85	0.5	1.8E-03	3.1E-04	1.7E-04	3.9E-04
-85	1.5	1.1E-03	1.9E-04	1.1E-04	2.3E-04
-85	2.5	6.9E-04	1.4E-04	7.7E-05	1.6E-04
-85	3.5	4.5E-04	1.1E-04	6.8E-05	1.3E-04
-85	4.5	3.4E-04	1.2E-04	7.8E-05	1.2E-04
-85	5.5	2.4E-04	1.3E-04	8.7E-05	1.2E-04
-85	6.5	1.7E-04	9.5E-05	6.4E-05	8.8E-05
-85	7.5	1.1E-04	6.0E-05	4.0E-05	5.6E-05
-85	8.5	5.0E-05	2.9E-05	1.9E-05	2.7E-05
-85	9.5	1.5E-05	9.0E-06	5.4E-06	8.1E-06
-85	10.5	1.4E-05	6.1E-06	3.8E-06	5.7E-06
-85	11.5	1.3E-05	4.8E-06	3.1E-06	4.6E-06
-85	12.5	8.0E-06	2.3E-06	1.3E-06	2.3E-06
-85	13.5	5.3E-06	1.9E-06	8.8E-07	1.9E-06
-85	14.5	2.5E-06	1.4E-06	4.2E-07	1.4E-06
-85	18.5	1.1E-05	1.2E-05	3.2E-05	1.6E-05
-85	24.5	1.1E-05	1.2E-05	3.2E-05	1.6E-05
-85	29.5	1.1E-05	1.2E-05	3.2E-05	1.6E-05
-85	34.5	1.1E-05	1.2E-05	3.2E-05	1.6E-05
-85	39.5	1.1E-05	1.2E-05	3.2E-05	1.6E-05
-85	44.5	1.1E-05	1.2E-05	3.2E-05	1.6E-05
-85	49.5	1.1E-05	1.2E-05	3.2E-05	1.6E-05

B.10 hno2acs.dat

310	0.0E+00
311	0.0E+00
312	2.0E-21
313	4.2E-21
314	4.6E-21
315	4.2E-21
316	3.0E-21
317	4.6E-21
318	3.6E-20
319	6.1E-20
320	2.1E-20
321	4.3E-20
322	4.0E-20
323	3.9E-20

324	4.0E-20
325	4.0E-20
326	3.1E-20
327	4.1E-20
328	7.6E-20
329	6.6E-20
330	7.3E-20
331	8.7E-20
332	1.4E-19
333	5.9E-20
334	5.9E-20
335	6.5E-20
336	5.9E-20
337	4.6E-20
338	1.9E-19
339	1.6E-19
340	1.1E-19
341	8.7E-20
342	3.4E-19
343	2.0E-19
344	1.0E-19
345	8.5E-20
346	8.3E-20
347	8.2E-20
348	7.5E-20
349	7.1E-20
350	6.8E-20
351	1.7E-19
352	1.1E-19
353	3.7E-19
354	5.0E-19
355	2.5E-19
356	1.2E-19
357	9.4E-20
358	7.8E-20
359	7.3E-20
360	6.8E-20
361	6.9E-20
362	7.3E-20
363	9.0E-20
364	1.2E-19
365	1.3E-19
366	2.1E-19
367	3.5E-19
368	4.5E-19
369	2.9E-19
370	1.2E-19
371	9.5E-20
372	8.9E-20
373	7.4E-20
374	4.8E-20
375	2.7E-20
376	1.9E-20
377	1.5E-20
378	1.9E-20
379	5.8E-20
380	7.8E-20
381	1.1E-19
382	1.4E-19
383	1.7E-19
384	2.0E-19
385	1.9E-19
386	1.2E-19
387	5.7E-20
388	3.2E-20
389	1.9E-20
390	1.2E-20
391	5.0E-21
392	0.0E+00
393	0.0E+00
394	0.0E+00
395	0.0E+00

B.11 hno3acs.dat

190	1.6E-17
195	1.1E-17
200	6.6E-18
205	2.9E-18
210	1.0E-18
215	3.6E-19
220	1.5E-19
225	8.6E-20
230	5.6E-20
235	3.7E-20
240	2.6E-20
245	2.1E-20
250	1.9E-20
255	1.9E-20
260	1.9E-20
265	1.7E-20
270	1.6E-20
275	1.3E-20
280	1.1E-20
285	8.5E-21
290	6.1E-21
295	4.1E-21
300	2.4E-21
305	1.5E-21
310	7.1E-22
315	3.2E-22

```
320  1.2E-22
325  5.0E-23
330  2.0E-23
335        0
```

B.12 hno3land.dat

```
-85  10  10  10  10
-75  10  10  10  10
-65  10  10  10  10
-55  10  10  10  10
-45  30  37  50  43
-35  75  75  75  75
-25 400 333 200 267
-15 700 567 300 433
 -5 700 600 400 500
  5 700 600 400 500
 15 400 367 300 333
 25 200 233 300 267
 35 200 333 600 467
 45 200 367 700 533
 55 100 200 400 300
 65  50 100 200 150
 75  10  23  50  37
 85  10  17  30  23
```

B.13 hno3sea.dat

```
-85  10  10  10  10
-75  10  10  10  10
-65  10  10  10  10
-55  10  10  10  10
-45  20  17  10  13
-35  25  23  20  22
-25  30  30  30  30
-15  30  32  35  33
 -5  40  43  50  47
  5  60  57  50  53
 15  70  63  50  57
 25  80  67  40  53
 35 100  80  40  60
 45  70  60  40  50
 55  50  53  60  57
 65  50  57  70  63
 75  10  23  50  37
 85  10  17  30  23
```

B.14 hno4acs.dat

```
190 1010.0e-20
195 816.0e-20
200 563.0e-20
205 367.0e-20
210 239.0e-20
215 161.0e-20
220 118.0e-20
225 93.5e-20
230 79.2e-20
235 68.2e-20
240 58.1e-20
245 48.9e-20
250 41.2e-20
255 35.0e-20
260 28.5e-20
265 23.0e-20
270 18.1e-20
275 13.4e-20
280 9.3e-20
285 6.2e-20
290 3.9e-20
295 2.4e-20
300 1.4e-20
305 0.9e-20
310 0.5e-20
315 0.3e-20
320 0.2e-20
325 0.1e-20
```

B.15 kz.dat

```
0.00E+00
1.09E+05
1.89E+05
2.88E+05
4.09E+05
5.90E+05
6.70E+05
4.48E+05
1.66E+05
1.06E+05
7.50E+04
6.04E+04
4.90E+04
3.43E+04
1.97E+04
5.00E+03
2.00E+04
4.00E+04
6.00E+04
```

```
1.00E+05
2.00E+05
3.00E+05
3.00E+05
0.00E+00
```

B.16 n2.dat

```
0.79
0.79
0.79
0.79
0.79
0.79
0.79
0.79
0.79
0.79
0.79
0.79
0.79
0.79
0.79
0.79
0.79
0.79
0.79
0.79
0.79
0.79
```

B.17 n2o5acs.dat

```
200   9.20E-18
205   8.20E-18
210   5.60E-18
215   3.70E-18
220   2.20E-18
225   1.44E-18
230   9.90E-19
235   7.70E-19
240   6.20E-19
245   5.20E-19
250   4.00E-19
255   3.20E-19
260   2.60E-19
265   2.00E-19
270   1.61E-19
275   1.30E-19
280   1.17E-19
```

B.18 no2acs.dat

```
202.02 4.15E-19  0.00E+00
204.08 4.48E-19  0.00E+00
206.19 4.45E-19  0.00E+00
208.33 4.64E-19  0.00E+00
210.53 4.87E-19  0.00E+00
212.77 4.82E-19  0.00E+00
215.06 5.02E-19  0.00E+00
217.39 4.44E-19  0.00E+00
219.78 4.71E-19  0.00E+00
222.22 3.77E-19  0.00E+00
224.72 3.93E-19  0.00E+00
227.27 2.74E-19  0.00E+00
229.89 2.78E-19  0.00E+00
232.56 1.69E-19  0.00E+00
235.29 1.62E-19  0.00E+00
238.09 8.81E-20  0.00E+00
240.96 7.47E-20  0.00E+00
243.90 3.91E-20  0.00E+00
246.91 2.75E-20  0.00E+00
250.00 2.01E-20  0.00E+00
253.17 1.97E-20  0.00E+00
256.41 2.11E-20  0.00E+00
259.74 2.36E-20  0.00E+00
263.16 2.70E-20  0.00E+00
266.67 3.25E-20  0.00E+00
270.27 3.79E-20  0.00E+00
273.97 5.03E-20  7.50E-24
277.78 5.88E-20  8.20E-24
281.69 7.00E-20 -5.30E-24
285.71 8.15E-20 -4.30E-24
289.85 9.72E-20 -3.10E-24
294.12 1.15E-19 -1.62E-23
298.51 1.34E-19 -2.84E-23
303.03 1.59E-19 -3.57E-23
307.69 1.87E-19 -5.36E-23
312.50 2.15E-19 -6.86E-23
317.50 2.48E-19 -7.86E-23
322.50 2.81E-19 -1.11E-22
327.50 3.13E-19 -1.36E-22
332.50 3.43E-19 -1.28E-22
337.50 3.80E-19 -1.61E-22
342.50 4.07E-19 -1.89E-22
347.50 4.31E-19 -1.22E-22
352.50 4.72E-19 -1.92E-22
357.50 4.83E-19 -1.10E-22
362.50 5.17E-19 -1.32E-22
367.50 5.32E-19 -1.10E-22
372.50 5.51E-19 -8.06E-23
377.50 5.64E-19 -8.67E-23
```

382.50	5.76E-19	-9.45E-23
387.50	5.93E-19	-9.23E-23
392.50	5.85E-19	-7.38E-23
397.50	6.02E-19	-5.99E-23
402.50	5.78E-19	-5.45E-23
407.50	6.00E-19	-1.13E-22
412.50	5.65E-19	1.00E-25
417.50	5.81E-19	-1.21E-22
422.50	5.81E-19	-1.21E-22

B.19 no3acs.dat

400	0.24E-19
410	0.56E-19
420	1.52E-19
430	2.22E-19
440	2.75E-19
450	3.79E-19
460	4.79E-19
470	6.35E-19
480	7.51E-19
490	10.19E-19
500	11.00E-19
510	14.43E-19
520	16.55E-19
530	20.52E-19
540	19.95E-19
550	27.04E-19
560	27.13E-19
570	27.68E-19
580	33.63E-19
590	43.02E-19
600	28.43E-19
610	18.63E-19
620	74.40E-19
630	25.54E-19
640	6.91E-19
650	9.78E-19
660	79.43E-19
670	5.40E-19
680	2.00E-19
690	0.71E-19
700	0.16E-19
710	0.00E-19
720	0.00E-19

B.20 noxland.dat

85	0.5	1.0E-10	7.3E-11	2.0E-11	4.7E-11
85	1.5	1.0E-10	7.3E-11	2.0E-11	4.7E-11
85	2.5	1.0E-10	7.3E-11	2.0E-11	4.7E-11
85	3.5	1.0E-10	7.3E-11	2.0E-11	4.7E-11
85	4.5	1.0E-10	7.3E-11	2.0E-11	4.7E-11
85	5.5	1.0E-10	7.3E-11	2.0E-11	4.7E-11
85	6.5	1.0E-10	7.3E-11	2.0E-11	4.7E-11
85	7.5	1.0E-10	7.3E-11	2.0E-11	4.7E-11
85	8.5	1.0E-10	7.3E-11	2.0E-11	4.7E-11
85	9.5	4.0E-11	4.0E-11	4.0E-11	4.0E-11
85	10.5	1.1E-10	1.1E-10	1.1E-10	1.1E-10
85	11.5	1.5E-10	1.5E-10	1.5E-10	1.5E-10
85	12.5	1.5E-10	1.5E-10	1.5E-10	1.5E-10
85	13.5	1.5E-10	1.5E-10	1.5E-10	1.5E-10
85	14.5	1.5E-10	1.5E-10	1.5E-10	1.5E-10
85	18.5	1.0E-10	1.0E-10	1.0E-10	1.0E-10
85	24.5	1.0E-09	1.0E-09	1.0E-09	1.0E-09
85	29.5	1.0E-09	1.0E-09	1.0E-09	1.0E-09
85	34.5	1.0E-08	1.0E-08	1.0E-08	1.0E-08
85	39.5	1.0E-08	1.0E-08	1.0E-08	1.0E-08
85	44.5	1.0E-08	1.0E-08	1.0E-08	1.0E-08
85	49.5	1.0E-08	1.0E-08	1.0E-08	1.0E-08
75	0.5	1.0E-10	7.3E-11	2.0E-11	4.7E-11
75	1.5	1.0E-10	7.3E-11	2.0E-11	4.7E-11
75	2.5	1.0E-10	7.3E-11	2.0E-11	4.7E-11
75	3.5	1.0E-10	7.3E-11	2.0E-11	4.7E-11
75	4.5	1.0E-10	7.3E-11	2.0E-11	4.7E-11
75	5.5	1.0E-10	7.3E-11	2.0E-11	4.7E-11
75	6.5	1.0E-10	7.3E-11	2.0E-11	4.7E-11
75	7.5	1.0E-10	7.3E-11	2.0E-11	4.7E-11
75	8.5	1.0E-10	7.3E-11	2.0E-11	4.7E-11
75	9.5	4.0E-11	4.0E-11	4.0E-11	4.0E-11
75	10.5	1.1E-10	1.1E-10	1.1E-10	1.1E-10
75	11.5	1.5E-10	1.5E-10	1.5E-10	1.5E-10
75	12.5	1.5E-10	1.5E-10	1.5E-10	1.5E-10
75	13.5	1.5E-10	1.5E-10	1.5E-10	1.5E-10
75	14.5	1.5E-10	1.5E-10	1.5E-10	1.5E-10
75	18.5	1.0E-10	1.0E-10	1.0E-10	1.0E-10
75	24.5	1.0E-09	1.0E-09	1.0E-09	1.0E-09
75	29.5	1.0E-09	1.0E-09	1.0E-09	1.0E-09
75	34.5	1.0E-08	1.0E-08	1.0E-08	1.0E-08
75	39.5	1.0E-08	1.0E-08	1.0E-08	1.0E-08
75	44.5	1.0E-08	1.0E-08	1.0E-08	1.0E-08
75	49.5	1.0E-08	1.0E-08	1.0E-08	1.0E-08
65	0.5	7.3E-10	6.1E-10	3.7E-10	4.9E-10
65	1.5	4.5E-10	3.8E-10	2.3E-10	3.1E-10
65	2.5	1.7E-10	1.4E-10	1.0E-10	1.2E-10
65	3.5	1.7E-10	1.4E-10	1.0E-10	1.2E-10
65	4.5	1.7E-10	1.4E-10	1.0E-10	1.2E-10
65	5.5	1.7E-10	1.4E-10	1.0E-10	1.2E-10
65	6.5	1.7E-10	1.4E-10	1.0E-10	1.2E-10
65	7.5	1.7E-10	1.4E-10	1.0E-10	1.2E-10
65	8.5	1.7E-10	1.4E-10	1.0E-10	1.2E-10

65	9.5	1.7E-10	1.4E-10	1.0E-10	1.2E-10
65	10.5	1.4E-10	1.3E-10	1.1E-10	1.2E-10
65	11.5	1.2E-10	1.2E-10	1.2E-10	1.2E-10
65	12.5	1.5E-10	1.5E-10	1.5E-10	1.5E-10
65	13.5	1.5E-10	1.5E-10	1.5E-10	1.5E-10
65	14.5	1.5E-10	1.5E-10	1.5E-10	1.5E-10
65	18.5	1.0E-10	1.0E-10	1.0E-10	1.0E-10
65	24.5	1.0E-09	1.0E-09	1.0E-09	1.0E-09
65	29.5	1.0E-09	1.0E-09	1.0E-09	1.0E-09
65	34.5	1.0E-08	1.0E-08	1.0E-08	1.0E-08
65	39.5	1.0E-08	1.0E-08	1.0E-08	1.0E-08
65	44.5	1.0E-08	1.0E-08	1.0E-08	1.0E-08
65	49.5	1.0E-08	1.0E-08	1.0E-08	1.0E-08
55	0.5	7.3E-10	6.1E-10	3.7E-10	4.9E-10
55	1.5	4.5E-10	3.8E-10	2.3E-10	3.1E-10
55	2.5	1.7E-10	1.4E-10	1.0E-10	1.2E-10
55	3.5	1.7E-10	1.4E-10	1.0E-10	1.2E-10
55	4.5	1.7E-10	1.4E-10	1.0E-10	1.2E-10
55	5.5	1.7E-10	1.4E-10	1.0E-10	1.2E-10
55	6.5	1.7E-10	1.4E-10	1.0E-10	1.2E-10
55	7.5	1.7E-10	1.4E-10	1.0E-10	1.2E-10
55	8.5	1.7E-10	1.4E-10	1.0E-10	1.2E-10
55	9.5	1.7E-10	1.4E-10	1.0E-10	1.2E-10
55	10.5	1.4E-10	1.3E-10	1.1E-10	1.2E-10
55	11.5	1.2E-10	1.2E-10	1.2E-10	1.2E-10
55	12.5	1.5E-10	1.5E-10	1.5E-10	1.5E-10
55	13.5	1.5E-10	1.5E-10	1.5E-10	1.5E-10
55	14.5	1.5E-10	1.5E-10	1.5E-10	1.5E-10
55	18.5	1.0E-10	1.0E-10	1.0E-10	1.0E-10
55	24.5	1.0E-09	1.0E-09	1.0E-09	1.0E-09
55	29.5	1.0E-09	1.0E-09	1.0E-09	1.0E-09
55	34.5	1.0E-08	1.0E-08	1.0E-08	1.0E-08
55	39.5	1.0E-08	1.0E-08	1.0E-08	1.0E-08
55	44.5	1.0E-08	1.0E-08	1.0E-08	1.0E-08
55	49.5	1.0E-08	1.0E-08	1.0E-08	1.0E-08
45	0.5	7.3E-10	6.1E-10	3.7E-10	4.9E-10
45	1.5	4.5E-10	3.8E-10	2.3E-10	3.1E-10
45	2.5	1.7E-10	1.4E-10	1.0E-10	1.2E-10
45	3.5	1.7E-10	1.4E-10	1.0E-10	1.2E-10
45	4.5	1.7E-10	1.4E-10	1.0E-10	1.2E-10
45	5.5	1.7E-10	1.4E-10	1.0E-10	1.2E-10
45	6.5	1.7E-10	1.4E-10	1.0E-10	1.2E-10
45	7.5	1.7E-10	1.4E-10	1.0E-10	1.2E-10
45	8.5	1.7E-10	1.4E-10	1.0E-10	1.2E-10
45	9.5	1.7E-10	1.4E-10	1.0E-10	1.2E-10
45	10.5	1.4E-10	1.3E-10	1.1E-10	1.2E-10
45	11.5	1.2E-10	1.2E-10	1.2E-10	1.2E-10
45	12.5	1.5E-10	1.5E-10	1.5E-10	1.5E-10
45	13.5	1.5E-10	1.5E-10	1.5E-10	1.5E-10
45	14.5	1.5E-10	1.5E-10	1.5E-10	1.5E-10
45	18.5	1.0E-10	1.0E-10	1.0E-10	1.0E-10
45	24.5	1.0E-09	1.0E-09	1.0E-09	1.0E-09
45	29.5	1.0E-09	1.0E-09	1.0E-09	1.0E-09
45	34.5	1.0E-08	1.0E-08	1.0E-08	1.0E-08
45	39.5	1.0E-08	1.0E-08	1.0E-08	1.0E-08
45	44.5	1.0E-08	1.0E-08	1.0E-08	1.0E-08
45	49.5	1.0E-08	1.0E-08	1.0E-08	1.0E-08
35	0.5	7.3E-10	6.1E-10	3.7E-10	4.9E-10
35	1.5	4.5E-10	3.8E-10	2.3E-10	3.1E-10
35	2.5	1.7E-10	1.4E-10	1.0E-10	1.2E-10
35	3.5	1.7E-10	1.4E-10	1.0E-10	1.2E-10
35	4.5	1.7E-10	1.4E-10	1.0E-10	1.2E-10
35	5.5	1.7E-10	1.4E-10	1.0E-10	1.2E-10
35	6.5	1.7E-10	1.4E-10	1.0E-10	1.2E-10
35	7.5	1.7E-10	1.4E-10	1.0E-10	1.2E-10
35	8.5	1.7E-10	1.4E-10	1.0E-10	1.2E-10
35	9.5	1.7E-10	1.4E-10	1.0E-10	1.2E-10
35	10.5	1.4E-10	1.3E-10	1.1E-10	1.2E-10
35	11.5	1.2E-10	1.2E-10	1.2E-10	1.2E-10
35	12.5	1.5E-10	1.5E-10	1.5E-10	1.5E-10
35	13.5	1.5E-10	1.5E-10	1.5E-10	1.5E-10
35	14.5	1.5E-10	1.5E-10	1.5E-10	1.5E-10
35	18.5	1.0E-10	1.0E-10	1.0E-10	1.0E-10
35	24.5	1.0E-09	1.0E-09	1.0E-09	1.0E-09
35	29.5	1.0E-09	1.0E-09	1.0E-09	1.0E-09
35	34.5	1.0E-08	1.0E-08	1.0E-08	1.0E-08
35	39.5	1.0E-08	1.0E-08	1.0E-08	1.0E-08
35	44.5	1.0E-08	1.0E-08	1.0E-08	1.0E-08
35	49.5	1.0E-08	1.0E-08	1.0E-08	1.0E-08
25	0.5	1.0E-10	1.0E-10	1.0E-10	1.0E-10
25	1.5	7.5E-11	7.5E-11	7.5E-11	7.5E-11
25	2.5	5.0E-11	5.0E-11	5.0E-11	5.0E-11
25	3.5	5.0E-11	5.0E-11	5.0E-11	5.0E-11
25	4.5	5.0E-11	5.0E-11	5.0E-11	5.0E-11
25	5.5	5.0E-11	5.0E-11	5.0E-11	5.0E-11
25	6.5	5.0E-11	5.0E-11	5.0E-11	5.0E-11
25	7.5	5.0E-11	5.0E-11	5.0E-11	5.0E-11
25	8.5	5.0E-11	5.0E-11	5.0E-11	5.0E-11
25	9.5	5.0E-11	5.0E-11	5.0E-11	5.0E-11
25	10.5	5.0E-11	5.0E-11	5.0E-11	5.0E-11
25	11.5	5.0E-11	5.0E-11	5.0E-11	5.0E-11
25	12.5	5.0E-11	5.0E-11	5.0E-11	5.0E-11
25	13.5	7.5E-11	7.5E-11	7.5E-11	7.5E-11
25	14.5	1.0E-10	1.0E-10	1.0E-10	1.0E-10
25	18.5	1.0E-10	1.0E-10	1.0E-10	1.0E-10
25	24.5	1.0E-09	1.0E-09	1.0E-09	1.0E-09
25	29.5	1.0E-09	1.0E-09	1.0E-09	1.0E-09
25	34.5	1.0E-08	1.0E-08	1.0E-08	1.0E-08
25	39.5	1.0E-08	1.0E-08	1.0E-08	1.0E-08
25	44.5	1.0E-08	1.0E-08	1.0E-08	1.0E-08
25	49.5	1.0E-08	1.0E-08	1.0E-08	1.0E-08
15	0.5	1.0E-10	1.0E-10	1.0E-10	1.0E-10

15	1.5	7.5E-11	7.5E-11	7.5E-11	7.5E-11
15	2.5	5.0E-11	5.0E-11	5.0E-11	5.0E-11
15	3.5	5.0E-11	5.0E-11	5.0E-11	5.0E-11
15	4.5	5.0E-11	5.0E-11	5.0E-11	5.0E-11
15	5.5	5.0E-11	5.0E-11	5.0E-11	5.0E-11
15	6.5	5.0E-11	5.0E-11	5.0E-11	5.0E-11
15	7.5	5.0E-11	5.0E-11	5.0E-11	5.0E-11
15	8.5	5.0E-11	5.0E-11	5.0E-11	5.0E-11
15	9.5	5.0E-11	5.0E-11	5.0E-11	5.0E-11
15	10.5	5.0E-11	5.0E-11	5.0E-11	5.0E-11
15	11.5	5.0E-11	5.0E-11	5.0E-11	5.0E-11
15	12.5	5.0E-11	5.0E-11	5.0E-11	5.0E-11
15	13.5	7.5E-11	7.5E-11	7.5E-11	7.5E-11
15	14.5	1.0E-10	1.0E-10	1.0E-10	1.0E-10
15	18.5	1.0E-10	1.0E-10	1.0E-10	1.0E-10
15	24.5	1.0E-09	1.0E-09	1.0E-09	1.0E-09
15	29.5	1.0E-09	1.0E-09	1.0E-09	1.0E-09
15	34.5	1.0E-08	1.0E-08	1.0E-08	1.0E-08
15	39.5	1.0E-08	1.0E-08	1.0E-08	1.0E-08
15	44.5	1.0E-08	1.0E-08	1.0E-08	1.0E-08
15	49.5	1.0E-08	1.0E-08	1.0E-08	1.0E-08
5	0.5	1.0E-10	1.0E-10	1.0E-10	1.0E-10
5	1.5	7.5E-11	7.5E-11	7.5E-11	7.5E-11
5	2.5	5.0E-11	5.0E-11	5.0E-11	5.0E-11
5	3.5	5.0E-11	5.0E-11	5.0E-11	5.0E-11
5	4.5	5.0E-11	5.0E-11	5.0E-11	5.0E-11
5	5.5	5.0E-11	5.0E-11	5.0E-11	5.0E-11
5	6.5	5.0E-11	5.0E-11	5.0E-11	5.0E-11
5	7.5	5.0E-11	5.0E-11	5.0E-11	5.0E-11
5	8.5	5.0E-11	5.0E-11	5.0E-11	5.0E-11
5	9.5	5.0E-11	5.0E-11	5.0E-11	5.0E-11
5	10.5	5.0E-11	5.0E-11	5.0E-11	5.0E-11
5	11.5	5.0E-11	5.0E-11	5.0E-11	5.0E-11
5	12.5	5.0E-11	5.0E-11	5.0E-11	5.0E-11
5	13.5	7.5E-11	7.5E-11	7.5E-11	7.5E-11
5	14.5	1.0E-10	1.0E-10	1.0E-10	1.0E-10
5	18.5	1.0E-10	1.0E-10	1.0E-10	1.0E-10
5	24.5	1.0E-09	1.0E-09	1.0E-09	1.0E-09
5	29.5	1.0E-09	1.0E-09	1.0E-09	1.0E-09
5	34.5	1.0E-08	1.0E-08	1.0E-08	1.0E-08
5	39.5	1.0E-08	1.0E-08	1.0E-08	1.0E-08
5	44.5	1.0E-08	1.0E-08	1.0E-08	1.0E-08
5	49.5	1.0E-08	1.0E-08	1.0E-08	1.0E-08
-5	0.5	1.0E-10	1.0E-10	1.0E-10	1.0E-10
-5	1.5	7.5E-11	7.5E-11	7.5E-11	7.5E-11
-5	2.5	5.0E-11	5.0E-11	5.0E-11	5.0E-11
-5	3.5	5.0E-11	5.0E-11	5.0E-11	5.0E-11
-5	4.5	5.0E-11	5.0E-11	5.0E-11	5.0E-11
-5	5.5	5.0E-11	5.0E-11	5.0E-11	5.0E-11
-5	6.5	5.0E-11	5.0E-11	5.0E-11	5.0E-11
-5	7.5	5.0E-11	5.0E-11	5.0E-11	5.0E-11
-5	8.5	5.0E-11	5.0E-11	5.0E-11	5.0E-11
-5	9.5	5.0E-11	5.0E-11	5.0E-11	5.0E-11
-5	10.5	5.0E-11	5.0E-11	5.0E-11	5.0E-11
-5	11.5	5.0E-11	5.0E-11	5.0E-11	5.0E-11
-5	12.5	5.0E-11	5.0E-11	5.0E-11	5.0E-11
-5	13.5	7.5E-11	7.5E-11	7.5E-11	7.5E-11
-5	14.5	1.0E-10	1.0E-10	1.0E-10	1.0E-10
-5	18.5	1.0E-10	1.0E-10	1.0E-10	1.0E-10
-5	24.5	1.0E-09	1.0E-09	1.0E-09	1.0E-09
-5	29.5	1.0E-09	1.0E-09	1.0E-09	1.0E-09
-5	34.5	1.0E-08	1.0E-08	1.0E-08	1.0E-08
-5	39.5	1.0E-08	1.0E-08	1.0E-08	1.0E-08
-5	44.5	1.0E-08	1.0E-08	1.0E-08	1.0E-08
-5	49.5	1.0E-08	1.0E-08	1.0E-08	1.0E-08
-15	0.5	1.0E-10	1.0E-10	1.0E-10	1.0E-10
-15	1.5	7.5E-11	7.5E-11	7.5E-11	7.5E-11
-15	2.5	5.0E-11	5.0E-11	5.0E-11	5.0E-11
-15	3.5	5.0E-11	5.0E-11	5.0E-11	5.0E-11
-15	4.5	5.0E-11	5.0E-11	5.0E-11	5.0E-11
-15	5.5	5.0E-11	5.0E-11	5.0E-11	5.0E-11
-15	6.5	5.0E-11	5.0E-11	5.0E-11	5.0E-11
-15	7.5	5.0E-11	5.0E-11	5.0E-11	5.0E-11
-15	8.5	5.0E-11	5.0E-11	5.0E-11	5.0E-11
-15	9.5	5.0E-11	5.0E-11	5.0E-11	5.0E-11
-15	10.5	5.0E-11	5.0E-11	5.0E-11	5.0E-11
-15	11.5	5.0E-11	5.0E-11	5.0E-11	5.0E-11
-15	12.5	5.0E-11	5.0E-11	5.0E-11	5.0E-11
-15	13.5	7.5E-11	7.5E-11	7.5E-11	7.5E-11
-15	14.5	1.0E-10	1.0E-10	1.0E-10	1.0E-10
-15	18.5	1.0E-10	1.0E-10	1.0E-10	1.0E-10
-15	24.5	1.0E-09	1.0E-09	1.0E-09	1.0E-09
-15	29.5	1.0E-09	1.0E-09	1.0E-09	1.0E-09
-15	34.5	1.0E-08	1.0E-08	1.0E-08	1.0E-08
-15	39.5	1.0E-08	1.0E-08	1.0E-08	1.0E-08
-15	44.5	1.0E-08	1.0E-08	1.0E-08	1.0E-08
-15	49.5	1.0E-08	1.0E-08	1.0E-08	1.0E-08
-25	0.5	7.5E-11	1.0E-10	1.5E-10	1.3E-10
-25	1.5	4.5E-11	6.0E-11	9.0E-11	7.5E-11
-25	2.5	1.5E-11	2.0E-11	3.0E-11	2.5E-11
-25	3.5	1.5E-11	2.0E-11	3.0E-11	2.5E-11
-25	4.5	1.5E-11	2.0E-11	3.0E-11	2.5E-11
-25	5.5	1.5E-11	2.0E-11	3.0E-11	2.5E-11
-25	6.5	1.5E-11	2.0E-11	3.0E-11	2.5E-11
-25	7.5	1.5E-11	2.0E-11	3.0E-11	2.5E-11
-25	8.5	1.5E-11	2.0E-11	3.0E-11	2.5E-11
-25	9.5	1.5E-11	2.0E-11	3.0E-11	2.5E-11
-25	10.5	3.3E-11	3.5E-11	4.0E-11	3.8E-11
-25	11.5	5.0E-11	5.0E-11	5.0E-11	5.0E-11
-25	12.5	5.0E-11	5.0E-11	5.0E-11	5.0E-11
-25	13.5	5.0E-11	5.0E-11	5.0E-11	5.0E-11
-25	14.5	5.0E-11	5.0E-11	5.0E-11	5.0E-11

-25	18.5	1.0E-10	1.0E-10	1.0E-10	1.0E-10
-25	24.5	1.0E-09	1.0E-09	1.0E-09	1.0E-09
-25	29.5	1.0E-09	1.0E-09	1.0E-09	1.0E-09
-25	34.5	1.0E-08	1.0E-08	1.0E-08	1.0E-08
-25	39.5	1.0E-08	1.0E-08	1.0E-08	1.0E-08
-25	44.5	1.0E-08	1.0E-08	1.0E-08	1.0E-08
-25	49.5	1.0E-08	1.0E-08	1.0E-08	1.0E-08
-35	0.5	7.5E-11	1.0E-10	1.5E-10	1.3E-10
-35	1.5	4.5E-11	6.0E-11	9.0E-11	7.5E-11
-35	2.5	1.5E-11	2.0E-11	3.0E-11	2.5E-11
-35	3.5	1.5E-11	2.0E-11	3.0E-11	2.5E-11
-35	4.5	1.5E-11	2.0E-11	3.0E-11	2.5E-11
-35	5.5	1.5E-11	2.0E-11	3.0E-11	2.5E-11
-35	6.5	1.5E-11	2.0E-11	3.0E-11	2.5E-11
-35	7.5	1.5E-11	2.0E-11	3.0E-11	2.5E-11
-35	8.5	1.5E-11	2.0E-11	3.0E-11	2.5E-11
-35	9.5	1.5E-11	2.0E-11	3.0E-11	2.5E-11
-35	10.5	3.3E-11	3.5E-11	4.0E-11	3.8E-11
-35	11.5	5.0E-11	5.0E-11	5.0E-11	5.0E-11
-35	12.5	3.4E-11	3.4E-11	3.4E-11	3.4E-11
-35	13.5	3.4E-11	3.4E-11	3.4E-11	3.4E-11
-35	14.5	3.4E-11	3.4E-11	3.4E-11	3.4E-11
-35	18.5	1.0E-10	1.0E-10	1.0E-10	1.0E-10
-35	24.5	1.0E-09	1.0E-09	1.0E-09	1.0E-09
-35	29.5	1.0E-09	1.0E-09	1.0E-09	1.0E-09
-35	34.5	1.0E-08	1.0E-08	1.0E-08	1.0E-08
-35	39.5	1.0E-08	1.0E-08	1.0E-08	1.0E-08
-35	44.5	1.0E-08	1.0E-08	1.0E-08	1.0E-08
-35	49.5	1.0E-08	1.0E-08	1.0E-08	1.0E-08
-45	0.5	7.5E-11	1.0E-10	1.5E-10	1.3E-10
-45	1.5	4.5E-11	6.0E-11	9.0E-11	7.5E-11
-45	2.5	1.5E-11	2.0E-11	3.0E-11	2.5E-11
-45	3.5	1.5E-11	2.0E-11	3.0E-11	2.5E-11
-45	4.5	1.5E-11	2.0E-11	3.0E-11	2.5E-11
-45	5.5	1.5E-11	2.0E-11	3.0E-11	2.5E-11
-45	6.5	1.5E-11	2.0E-11	3.0E-11	2.5E-11
-45	7.5	1.5E-11	2.0E-11	3.0E-11	2.5E-11
-45	8.5	1.5E-11	2.0E-11	3.0E-11	2.5E-11
-45	9.5	1.5E-11	2.0E-11	3.0E-11	2.5E-11
-45	10.5	3.3E-11	3.5E-11	4.0E-11	3.8E-11
-45	11.5	5.0E-11	5.0E-11	5.0E-11	5.0E-11
-45	12.5	2.6E-11	2.6E-11	2.6E-11	2.6E-11
-45	13.5	2.6E-11	2.6E-11	2.6E-11	2.6E-11
-45	14.5	2.6E-11	2.6E-11	2.6E-11	2.6E-11
-45	18.5	1.0E-10	1.0E-10	1.0E-10	1.0E-10
-45	24.5	1.0E-09	1.0E-09	1.0E-09	1.0E-09
-45	29.5	1.0E-09	1.0E-09	1.0E-09	1.0E-09
-45	34.5	1.0E-08	1.0E-08	1.0E-08	1.0E-08
-45	39.5	1.0E-08	1.0E-08	1.0E-08	1.0E-08
-45	44.5	1.0E-08	1.0E-08	1.0E-08	1.0E-08
-45	49.5	1.0E-08	1.0E-08	1.0E-08	1.0E-08
-55	0.5	7.5E-11	1.0E-10	1.5E-10	1.3E-10
-55	1.5	4.5E-11	6.0E-11	9.0E-11	7.5E-11
-55	2.5	1.5E-11	2.0E-11	3.0E-11	2.5E-11
-55	3.5	1.5E-11	2.0E-11	3.0E-11	2.5E-11
-55	4.5	1.5E-11	2.0E-11	3.0E-11	2.5E-11
-55	5.5	1.5E-11	2.0E-11	3.0E-11	2.5E-11
-55	6.5	1.5E-11	2.0E-11	3.0E-11	2.5E-11
-55	7.5	1.5E-11	2.0E-11	3.0E-11	2.5E-11
-55	8.5	1.5E-11	2.0E-11	3.0E-11	2.5E-11
-55	9.5	1.5E-11	2.0E-11	3.0E-11	2.5E-11
-55	10.5	3.3E-11	3.5E-11	4.0E-11	3.8E-11
-55	11.5	5.0E-11	5.0E-11	5.0E-11	5.0E-11
-55	12.5	3.4E-11	3.4E-11	3.4E-11	3.4E-11
-55	13.5	3.4E-11	3.4E-11	3.4E-11	3.4E-11
-55	14.5	3.4E-11	3.4E-11	3.4E-11	3.4E-11
-55	18.5	1.0E-10	1.0E-10	1.0E-10	1.0E-10
-55	24.5	1.0E-09	1.0E-09	1.0E-09	1.0E-09
-55	29.5	1.0E-09	1.0E-09	1.0E-09	1.0E-09
-55	34.5	1.0E-08	1.0E-08	1.0E-08	1.0E-08
-55	39.5	1.0E-08	1.0E-08	1.0E-08	1.0E-08
-55	44.5	1.0E-08	1.0E-08	1.0E-08	1.0E-08
-55	49.5	1.0E-08	1.0E-08	1.0E-08	1.0E-08
-65	0.5	7.5E-11	1.0E-10	1.5E-10	1.3E-10
-65	1.5	4.5E-11	6.0E-11	9.0E-11	7.5E-11
-65	2.5	1.5E-11	2.0E-11	3.0E-11	2.5E-11
-65	3.5	1.5E-11	2.0E-11	3.0E-11	2.5E-11
-65	4.5	1.5E-11	2.0E-11	3.0E-11	2.5E-11
-65	5.5	1.5E-11	2.0E-11	3.0E-11	2.5E-11
-65	6.5	1.5E-11	2.0E-11	3.0E-11	2.5E-11
-65	7.5	1.5E-11	2.0E-11	3.0E-11	2.5E-11
-65	8.5	1.5E-11	2.0E-11	3.0E-11	2.5E-11
-65	9.5	1.5E-11	2.0E-11	3.0E-11	2.5E-11
-65	10.5	3.3E-11	3.5E-11	4.0E-11	3.8E-11
-65	11.5	5.0E-11	5.0E-11	5.0E-11	5.0E-11
-65	12.5	2.2E-11	2.2E-11	2.2E-11	2.2E-11
-65	13.5	2.2E-11	2.2E-11	2.2E-11	2.2E-11
-65	14.5	2.2E-11	2.2E-11	2.2E-11	2.2E-11
-65	18.5	1.0E-10	1.0E-10	1.0E-10	1.0E-10
-65	24.5	1.0E-09	1.0E-09	1.0E-09	1.0E-09
-65	29.5	1.0E-09	1.0E-09	1.0E-09	1.0E-09
-65	34.5	1.0E-08	1.0E-08	1.0E-08	1.0E-08
-65	39.5	1.0E-08	1.0E-08	1.0E-08	1.0E-08
-65	44.5	1.0E-08	1.0E-08	1.0E-08	1.0E-08
-65	49.5	1.0E-08	1.0E-08	1.0E-08	1.0E-08
-75	0.5	1.0E-11	1.0E-11	1.0E-11	1.0E-11
-75	1.5	1.0E-11	1.0E-11	1.0E-11	1.0E-11
-75	2.5	1.0E-11	1.0E-11	1.0E-11	1.0E-11
-75	3.5	1.0E-11	1.0E-11	1.0E-11	1.0E-11
-75	4.5	1.0E-11	1.0E-11	1.0E-11	1.0E-11
-75	5.5	1.0E-11	1.0E-11	1.0E-11	1.0E-11
-75	6.5	1.0E-11	1.0E-11	1.0E-11	1.0E-11

```
-75  7.5 1.0E-11 1.0E-11 1.0E-11 1.0E-11
-75  8.5 1.0E-11 1.0E-11 1.0E-11 1.0E-11
-75  9.5 1.0E-11 1.0E-11 1.0E-11 1.0E-11
-75 10.5 1.8E-11 1.8E-11 1.8E-11 1.8E-11
-75 11.5 2.5E-11 2.5E-11 2.5E-11 2.5E-11
-75 12.5 2.2E-11 2.2E-11 2.2E-11 2.2E-11
-75 13.5 2.2E-11 2.2E-11 2.2E-11 2.2E-11
-75 14.5 2.2E-11 2.2E-11 2.2E-11 2.2E-11
-75 18.5 1.0E-10 1.0E-10 1.0E-10 1.0E-10
-75 24.5 1.0E-09 1.0E-09 1.0E-09 1.0E-09
-75 29.5 1.0E-09 1.0E-09 1.0E-09 1.0E-09
-75 34.5 1.0E-08 1.0E-08 1.0E-08 1.0E-08
-75 39.5 1.0E-08 1.0E-08 1.0E-08 1.0E-08
-75 44.5 1.0E-08 1.0E-08 1.0E-08 1.0E-08
-75 49.5 1.0E-08 1.0E-08 1.0E-08 1.0E-08
-85  0.5 1.0E-11 1.0E-11 1.0E-11 1.0E-11
-85  1.5 1.0E-11 1.0E-11 1.0E-11 1.0E-11
-85  2.5 1.0E-11 1.0E-11 1.0E-11 1.0E-11
-85  3.5 1.0E-11 1.0E-11 1.0E-11 1.0E-11
-85  4.5 1.0E-11 1.0E-11 1.0E-11 1.0E-11
-85  5.5 1.0E-11 1.0E-11 1.0E-11 1.0E-11
-85  6.5 1.0E-11 1.0E-11 1.0E-11 1.0E-11
-85  7.5 1.0E-11 1.0E-11 1.0E-11 1.0E-11
-85  8.5 1.0E-11 1.0E-11 1.0E-11 1.0E-11
-85  9.5 1.3E-11 1.3E-11 1.3E-11 1.3E-11
-85 10.5 1.6E-11 1.6E-11 1.6E-11 1.6E-11
-85 11.5 2.2E-11 2.2E-11 2.2E-11 2.2E-11
-85 12.5 2.2E-11 2.2E-11 2.2E-11 2.2E-11
-85 13.5 2.2E-11 2.2E-11 2.2E-11 2.2E-11
-85 14.5 2.2E-11 2.2E-11 2.2E-11 2.2E-11
-85 18.5 1.0E-10 1.0E-10 1.0E-10 1.0E-10
-85 24.5 1.0E-09 1.0E-09 1.0E-09 1.0E-09
-85 29.5 1.0E-09 1.0E-09 1.0E-09 1.0E-09
-85 34.5 1.0E-08 1.0E-08 1.0E-08 1.0E-08
-85 39.5 1.0E-08 1.0E-08 1.0E-08 1.0E-08
-85 44.5 1.0E-08 1.0E-08 1.0E-08 1.0E-08
-85 49.5 1.0E-08 1.0E-08 1.0E-08 1.0E-08
```

B.21 noxsea.dat

```
85  0.5 1.0E-10 7.3E-11 2.0E-11 4.7E-11
85  1.5 1.0E-10 7.3E-11 2.0E-11 4.7E-11
85  2.5 1.0E-10 7.3E-11 2.0E-11 4.7E-11
85  3.5 1.0E-10 7.3E-11 2.0E-11 4.7E-11
85  4.5 1.0E-10 7.3E-11 2.0E-11 4.7E-11
85  5.5 1.0E-10 7.3E-11 2.0E-11 4.7E-11
85  6.5 1.0E-10 7.3E-11 2.0E-11 4.7E-11
85  7.5 1.0E-10 7.3E-11 2.0E-11 4.7E-11
85  8.5 1.0E-10 7.3E-11 2.0E-11 4.7E-11
85  9.5 4.0E-11 4.0E-11 4.0E-11 4.0E-11
85 10.5 1.1E-10 1.1E-10 1.1E-10 1.1E-10
85 11.5 1.5E-10 1.5E-10 1.5E-10 1.5E-10
85 12.5 1.5E-10 1.5E-10 1.5E-10 1.5E-10
85 13.5 1.5E-10 1.5E-10 1.5E-10 1.5E-10
85 14.5 1.5E-10 1.5E-10 1.5E-10 1.5E-10
85 18.5 1.0E-10 1.0E-10 1.0E-10 1.0E-10
85 24.5 1.0E-09 1.0E-09 1.0E-09 1.0E-09
85 29.5 1.0E-09 1.0E-09 1.0E-09 1.0E-09
85 34.5 1.0E-08 1.0E-08 1.0E-08 1.0E-08
85 39.5 1.0E-08 1.0E-08 1.0E-08 1.0E-08
85 44.5 1.0E-08 1.0E-08 1.0E-08 1.0E-08
85 49.5 1.0E-08 1.0E-08 1.0E-08 1.0E-08
75  0.5 1.0E-10 7.3E-11 2.0E-11 4.7E-11
75  1.5 1.0E-10 7.3E-11 2.0E-11 4.7E-11
75  2.5 1.0E-10 7.3E-11 2.0E-11 4.7E-11
75  3.5 1.0E-10 7.3E-11 2.0E-11 4.7E-11
75  4.5 1.0E-10 7.3E-11 2.0E-11 4.7E-11
75  5.5 1.0E-10 7.3E-11 2.0E-11 4.7E-11
75  6.5 1.0E-10 7.3E-11 2.0E-11 4.7E-11
75  7.5 1.0E-10 7.3E-11 2.0E-11 4.7E-11
75  8.5 1.0E-10 7.3E-11 2.0E-11 4.7E-11
75  9.5 4.0E-11 4.0E-11 4.0E-11 4.0E-11
75 10.5 1.1E-10 1.1E-10 1.1E-10 1.1E-10
75 11.5 1.5E-10 1.5E-10 1.5E-10 1.5E-10
75 12.5 1.5E-10 1.5E-10 1.5E-10 1.5E-10
75 13.5 1.5E-10 1.5E-10 1.5E-10 1.5E-10
75 14.5 1.5E-10 1.5E-10 1.5E-10 1.5E-10
75 18.5 1.0E-10 1.0E-10 1.0E-10 1.0E-10
75 24.5 1.0E-09 1.0E-09 1.0E-09 1.0E-09
75 29.5 1.0E-09 1.0E-09 1.0E-09 1.0E-09
75 34.5 1.0E-08 1.0E-08 1.0E-08 1.0E-08
75 39.5 1.0E-08 1.0E-08 1.0E-08 1.0E-08
75 44.5 1.0E-08 1.0E-08 1.0E-08 1.0E-08
75 49.5 1.0E-08 1.0E-08 1.0E-08 1.0E-08
65  0.5 4.0E-11 4.0E-11 4.0E-11 4.0E-11
65  1.5 4.5E-11 4.5E-11 4.5E-11 4.5E-11
65  2.5 5.0E-11 5.0E-11 5.0E-11 5.0E-11
65  3.5 5.0E-11 5.0E-11 5.0E-11 5.0E-11
65  4.5 5.0E-11 5.0E-11 5.0E-11 5.0E-11
65  5.5 5.0E-11 5.0E-11 5.0E-11 5.0E-11
65  6.5 5.0E-11 5.0E-11 5.0E-11 5.0E-11
65  7.5 5.0E-11 5.0E-11 5.0E-11 5.0E-11
65  8.5 5.0E-11 5.0E-11 5.0E-11 5.0E-11
65  9.5 5.0E-11 5.0E-11 5.0E-11 5.0E-11
65 10.5 7.5E-11 7.5E-11 7.5E-11 7.5E-11
65 11.5 1.0E-10 1.0E-10 1.0E-10 1.0E-10
65 12.5 1.5E-10 1.5E-10 1.5E-10 1.5E-10
65 13.5 1.5E-10 1.5E-10 1.5E-10 1.5E-10
65 14.5 1.5E-10 1.5E-10 1.5E-10 1.5E-10
65 18.5 1.0E-10 1.0E-10 1.0E-10 1.0E-10
65 24.5 1.0E-09 1.0E-09 1.0E-09 1.0E-09
```

65	29.5	1.0E-09	1.0E-09	1.0E-09	1.0E-09
65	34.5	1.0E-08	1.0E-08	1.0E-08	1.0E-08
65	39.5	1.0E-08	1.0E-08	1.0E-08	1.0E-08
65	44.5	1.0E-08	1.0E-08	1.0E-08	1.0E-08
65	49.5	1.0E-08	1.0E-08	1.0E-08	1.0E-08
55	0.5	4.0E-11	4.0E-11	4.0E-11	4.0E-11
55	1.5	4.5E-11	4.5E-11	4.5E-11	4.5E-11
55	2.5	5.0E-11	5.0E-11	5.0E-11	5.0E-11
55	3.5	5.0E-11	5.0E-11	5.0E-11	5.0E-11
55	4.5	5.0E-11	5.0E-11	5.0E-11	5.0E-11
55	5.5	5.0E-11	5.0E-11	5.0E-11	5.0E-11
55	6.5	5.0E-11	5.0E-11	5.0E-11	5.0E-11
55	7.5	5.0E-11	5.0E-11	5.0E-11	5.0E-11
55	8.5	5.0E-11	5.0E-11	5.0E-11	5.0E-11
55	9.5	5.0E-11	5.0E-11	5.0E-11	5.0E-11
55	10.5	7.5E-11	7.5E-11	7.5E-11	7.5E-11
55	11.5	1.0E-10	1.0E-10	1.0E-10	1.0E-10
55	12.5	1.5E-10	1.5E-10	1.5E-10	1.5E-10
55	13.5	1.5E-10	1.5E-10	1.5E-10	1.5E-10
55	14.5	1.5E-10	1.5E-10	1.5E-10	1.5E-10
55	18.5	1.0E-10	1.0E-10	1.0E-10	1.0E-10
55	24.5	1.0E-09	1.0E-09	1.0E-09	1.0E-09
55	29.5	1.0E-09	1.0E-09	1.0E-09	1.0E-09
55	34.5	1.0E-08	1.0E-08	1.0E-08	1.0E-08
55	39.5	1.0E-08	1.0E-08	1.0E-08	1.0E-08
55	44.5	1.0E-08	1.0E-08	1.0E-08	1.0E-08
55	49.5	1.0E-08	1.0E-08	1.0E-08	1.0E-08
45	0.5	4.0E-11	4.0E-11	4.0E-11	4.0E-11
45	1.5	4.5E-11	4.5E-11	4.5E-11	4.5E-11
45	2.5	5.0E-11	5.0E-11	5.0E-11	5.0E-11
45	3.5	5.0E-11	5.0E-11	5.0E-11	5.0E-11
45	4.5	5.0E-11	5.0E-11	5.0E-11	5.0E-11
45	5.5	5.0E-11	5.0E-11	5.0E-11	5.0E-11
45	6.5	5.0E-11	5.0E-11	5.0E-11	5.0E-11
45	7.5	5.0E-11	5.0E-11	5.0E-11	5.0E-11
45	8.5	5.0E-11	5.0E-11	5.0E-11	5.0E-11
45	9.5	5.0E-11	5.0E-11	5.0E-11	5.0E-11
45	10.5	7.5E-11	7.5E-11	7.5E-11	7.5E-11
45	11.5	1.0E-10	1.0E-10	1.0E-10	1.0E-10
45	12.5	1.5E-10	1.5E-10	1.5E-10	1.5E-10
45	13.5	1.5E-10	1.5E-10	1.5E-10	1.5E-10
45	14.5	1.5E-10	1.5E-10	1.5E-10	1.5E-10
45	18.5	1.0E-10	1.0E-10	1.0E-10	1.0E-10
45	24.5	1.0E-09	1.0E-09	1.0E-09	1.0E-09
45	29.5	1.0E-09	1.0E-09	1.0E-09	1.0E-09
45	34.5	1.0E-08	1.0E-08	1.0E-08	1.0E-08
45	39.5	1.0E-08	1.0E-08	1.0E-08	1.0E-08
45	44.5	1.0E-08	1.0E-08	1.0E-08	1.0E-08
45	49.5	1.0E-08	1.0E-08	1.0E-08	1.0E-08
35	0.5	4.0E-11	4.0E-11	4.0E-11	4.0E-11
35	1.5	4.5E-11	4.5E-11	4.5E-11	4.5E-11
35	2.5	5.0E-11	5.0E-11	5.0E-11	5.0E-11
35	3.5	5.0E-11	5.0E-11	5.0E-11	5.0E-11
35	4.5	5.0E-11	5.0E-11	5.0E-11	5.0E-11
35	5.5	5.0E-11	5.0E-11	5.0E-11	5.0E-11
35	6.5	5.0E-11	5.0E-11	5.0E-11	5.0E-11
35	7.5	5.0E-11	5.0E-11	5.0E-11	5.0E-11
35	8.5	5.0E-11	5.0E-11	5.0E-11	5.0E-11
35	9.5	5.0E-11	5.0E-11	5.0E-11	5.0E-11
35	10.5	7.5E-11	7.5E-11	7.5E-11	7.5E-11
35	11.5	1.0E-10	1.0E-10	1.0E-10	1.0E-10
35	12.5	1.5E-10	1.5E-10	1.5E-10	1.5E-10
35	13.5	1.5E-10	1.5E-10	1.5E-10	1.5E-10
35	14.5	1.5E-10	1.5E-10	1.5E-10	1.5E-10
35	18.5	1.0E-10	1.0E-10	1.0E-10	1.0E-10
35	24.5	1.0E-09	1.0E-09	1.0E-09	1.0E-09
35	29.5	1.0E-09	1.0E-09	1.0E-09	1.0E-09
35	34.5	1.0E-08	1.0E-08	1.0E-08	1.0E-08
35	39.5	1.0E-08	1.0E-08	1.0E-08	1.0E-08
35	44.5	1.0E-08	1.0E-08	1.0E-08	1.0E-08
35	49.5	1.0E-08	1.0E-08	1.0E-08	1.0E-08
25	0.5	4.0E-11	4.0E-11	4.0E-11	4.0E-11
25	1.5	4.5E-11	4.5E-11	4.5E-11	4.5E-11
25	2.5	5.0E-11	5.0E-11	5.0E-11	5.0E-11
25	3.5	5.0E-11	5.0E-11	5.0E-11	5.0E-11
25	4.5	5.0E-11	5.0E-11	5.0E-11	5.0E-11
25	5.5	5.0E-11	5.0E-11	5.0E-11	5.0E-11
25	6.5	5.0E-11	5.0E-11	5.0E-11	5.0E-11
25	7.5	5.0E-11	5.0E-11	5.0E-11	5.0E-11
25	8.5	5.0E-11	5.0E-11	5.0E-11	5.0E-11
25	9.5	5.0E-11	5.0E-11	5.0E-11	5.0E-11
25	10.5	5.0E-11	5.0E-11	5.0E-11	5.0E-11
25	11.5	5.0E-11	5.0E-11	5.0E-11	5.0E-11
25	12.5	5.0E-11	5.0E-11	5.0E-11	5.0E-11
25	13.5	7.5E-11	7.5E-11	7.5E-11	7.5E-11
25	14.5	1.0E-10	1.0E-10	1.0E-10	1.0E-10
25	18.5	1.0E-10	1.0E-10	1.0E-10	1.0E-10
25	24.5	1.0E-09	1.0E-09	1.0E-09	1.0E-09
25	29.5	1.0E-09	1.0E-09	1.0E-09	1.0E-09
25	34.5	1.0E-08	1.0E-08	1.0E-08	1.0E-08
25	39.5	1.0E-08	1.0E-08	1.0E-08	1.0E-08
25	44.5	1.0E-08	1.0E-08	1.0E-08	1.0E-08
25	49.5	1.0E-08	1.0E-08	1.0E-08	1.0E-08
15	0.5	4.0E-11	4.0E-11	4.0E-11	4.0E-11
15	1.5	4.5E-11	4.5E-11	4.5E-11	4.5E-11
15	2.5	5.0E-11	5.0E-11	5.0E-11	5.0E-11
15	3.5	5.0E-11	5.0E-11	5.0E-11	5.0E-11
15	4.5	5.0E-11	5.0E-11	5.0E-11	5.0E-11
15	5.5	5.0E-11	5.0E-11	5.0E-11	5.0E-11
15	6.5	5.0E-11	5.0E-11	5.0E-11	5.0E-11
15	7.5	5.0E-11	5.0E-11	5.0E-11	5.0E-11
15	8.5	5.0E-11	5.0E-11	5.0E-11	5.0E-11

15	9.5	5.0E-11	5.0E-11	5.0E-11	5.0E-11
15	10.5	5.0E-11	5.0E-11	5.0E-11	5.0E-11
15	11.5	5.0E-11	5.0E-11	5.0E-11	5.0E-11
15	12.5	5.0E-11	5.0E-11	5.0E-11	5.0E-11
15	13.5	7.5E-11	7.5E-11	7.5E-11	7.5E-11
15	14.5	1.0E-10	1.0E-10	1.0E-10	1.0E-10
15	18.5	1.0E-10	1.0E-10	1.0E-10	1.0E-10
15	24.5	1.0E-09	1.0E-09	1.0E-09	1.0E-09
15	29.5	1.0E-09	1.0E-09	1.0E-09	1.0E-09
15	34.5	1.0E-08	1.0E-08	1.0E-08	1.0E-08
15	39.5	1.0E-08	1.0E-08	1.0E-08	1.0E-08
15	44.5	1.0E-08	1.0E-08	1.0E-08	1.0E-08
15	49.5	1.0E-08	1.0E-08	1.0E-08	1.0E-08
5	0.5	4.0E-11	4.0E-11	4.0E-11	4.0E-11
5	1.5	4.5E-11	4.5E-11	4.5E-11	4.5E-11
5	2.5	5.0E-11	5.0E-11	5.0E-11	5.0E-11
5	3.5	5.0E-11	5.0E-11	5.0E-11	5.0E-11
5	4.5	5.0E-11	5.0E-11	5.0E-11	5.0E-11
5	5.5	5.0E-11	5.0E-11	5.0E-11	5.0E-11
5	6.5	5.0E-11	5.0E-11	5.0E-11	5.0E-11
5	7.5	5.0E-11	5.0E-11	5.0E-11	5.0E-11
5	8.5	5.0E-11	5.0E-11	5.0E-11	5.0E-11
5	9.5	5.0E-11	5.0E-11	5.0E-11	5.0E-11
5	10.5	5.0E-11	5.0E-11	5.0E-11	5.0E-11
5	11.5	5.0E-11	5.0E-11	5.0E-11	5.0E-11
5	12.5	5.0E-11	5.0E-11	5.0E-11	5.0E-11
5	13.5	7.5E-11	7.5E-11	7.5E-11	7.5E-11
5	14.5	1.0E-10	1.0E-10	1.0E-10	1.0E-10
5	18.5	1.0E-10	1.0E-10	1.0E-10	1.0E-10
5	24.5	1.0E-09	1.0E-09	1.0E-09	1.0E-09
5	29.5	1.0E-09	1.0E-09	1.0E-09	1.0E-09
5	34.5	1.0E-08	1.0E-08	1.0E-08	1.0E-08
5	39.5	1.0E-08	1.0E-08	1.0E-08	1.0E-08
5	44.5	1.0E-08	1.0E-08	1.0E-08	1.0E-08
5	49.5	1.0E-08	1.0E-08	1.0E-08	1.0E-08
-5	0.5	4.0E-11	4.0E-11	4.0E-11	4.0E-11
-5	1.5	4.5E-11	4.5E-11	4.5E-11	4.5E-11
-5	2.5	5.0E-11	5.0E-11	5.0E-11	5.0E-11
-5	3.5	5.0E-11	5.0E-11	5.0E-11	5.0E-11
-5	4.5	5.0E-11	5.0E-11	5.0E-11	5.0E-11
-5	5.5	5.0E-11	5.0E-11	5.0E-11	5.0E-11
-5	6.5	5.0E-11	5.0E-11	5.0E-11	5.0E-11
-5	7.5	5.0E-11	5.0E-11	5.0E-11	5.0E-11
-5	8.5	5.0E-11	5.0E-11	5.0E-11	5.0E-11
-5	9.5	5.0E-11	5.0E-11	5.0E-11	5.0E-11
-5	10.5	5.0E-11	5.0E-11	5.0E-11	5.0E-11
-5	11.5	5.0E-11	5.0E-11	5.0E-11	5.0E-11
-5	12.5	5.0E-11	5.0E-11	5.0E-11	5.0E-11
-5	13.5	7.5E-11	7.5E-11	7.5E-11	7.5E-11
-5	14.5	1.0E-10	1.0E-10	1.0E-10	1.0E-10
-5	18.5	1.0E-10	1.0E-10	1.0E-10	1.0E-10
-5	24.5	1.0E-09	1.0E-09	1.0E-09	1.0E-09
-5	29.5	1.0E-09	1.0E-09	1.0E-09	1.0E-09
-5	34.5	1.0E-08	1.0E-08	1.0E-08	1.0E-08
-5	39.5	1.0E-08	1.0E-08	1.0E-08	1.0E-08
-5	44.5	1.0E-08	1.0E-08	1.0E-08	1.0E-08
-5	49.5	1.0E-08	1.0E-08	1.0E-08	1.0E-08
-15	0.5	4.0E-11	4.0E-11	4.0E-11	4.0E-11
-15	1.5	4.5E-11	4.5E-11	4.5E-11	4.5E-11
-15	2.5	5.0E-11	5.0E-11	5.0E-11	5.0E-11
-15	3.5	5.0E-11	5.0E-11	5.0E-11	5.0E-11
-15	4.5	5.0E-11	5.0E-11	5.0E-11	5.0E-11
-15	5.5	5.0E-11	5.0E-11	5.0E-11	5.0E-11
-15	6.5	5.0E-11	5.0E-11	5.0E-11	5.0E-11
-15	7.5	5.0E-11	5.0E-11	5.0E-11	5.0E-11
-15	8.5	5.0E-11	5.0E-11	5.0E-11	5.0E-11
-15	9.5	5.0E-11	5.0E-11	5.0E-11	5.0E-11
-15	10.5	5.0E-11	5.0E-11	5.0E-11	5.0E-11
-15	11.5	5.0E-11	5.0E-11	5.0E-11	5.0E-11
-15	12.5	5.0E-11	5.0E-11	5.0E-11	5.0E-11
-15	13.5	7.5E-11	7.5E-11	7.5E-11	7.5E-11
-15	14.5	1.0E-10	1.0E-10	1.0E-10	1.0E-10
-15	18.5	1.0E-10	1.0E-10	1.0E-10	1.0E-10
-15	24.5	1.0E-09	1.0E-09	1.0E-09	1.0E-09
-15	29.5	1.0E-09	1.0E-09	1.0E-09	1.0E-09
-15	34.5	1.0E-08	1.0E-08	1.0E-08	1.0E-08
-15	39.5	1.0E-08	1.0E-08	1.0E-08	1.0E-08
-15	44.5	1.0E-08	1.0E-08	1.0E-08	1.0E-08
-15	49.5	1.0E-08	1.0E-08	1.0E-08	1.0E-08
-25	0.5	1.0E-11	1.0E-11	1.0E-11	1.0E-11
-25	1.5	1.0E-11	1.0E-11	1.0E-11	1.0E-11
-25	2.5	1.0E-11	1.0E-11	1.0E-11	1.0E-11
-25	3.5	1.0E-11	1.0E-11	1.0E-11	1.0E-11
-25	4.5	1.0E-11	1.0E-11	1.0E-11	1.0E-11
-25	5.5	1.0E-11	1.0E-11	1.0E-11	1.0E-11
-25	6.5	1.0E-11	1.0E-11	1.0E-11	1.0E-11
-25	7.5	1.0E-11	1.0E-11	1.0E-11	1.0E-11
-25	8.5	1.0E-11	1.0E-11	1.0E-11	1.0E-11
-25	9.5	1.0E-11	1.0E-11	1.0E-11	1.0E-11
-25	10.5	1.8E-11	1.8E-11	1.8E-11	1.8E-11
-25	11.5	2.5E-11	2.5E-11	2.5E-11	2.5E-11
-25	12.5	2.5E-11	2.5E-11	2.5E-11	2.5E-11
-25	13.5	2.5E-11	2.5E-11	2.5E-11	2.5E-11
-25	14.5	2.5E-11	2.5E-11	2.5E-11	2.5E-11
-25	18.5	1.0E-10	1.0E-10	1.0E-10	1.0E-10
-25	24.5	1.0E-09	1.0E-09	1.0E-09	1.0E-09
-25	29.5	1.0E-09	1.0E-09	1.0E-09	1.0E-09
-25	34.5	1.0E-08	1.0E-08	1.0E-08	1.0E-08
-25	39.5	1.0E-08	1.0E-08	1.0E-08	1.0E-08
-25	44.5	1.0E-08	1.0E-08	1.0E-08	1.0E-08
-25	49.5	1.0E-08	1.0E-08	1.0E-08	1.0E-08
-35	0.5	1.0E-11	1.0E-11	1.0E-11	1.0E-11

-35	1.5	1.0E-11	1.0E-11	1.0E-11	1.0E-11
-35	2.5	1.0E-11	1.0E-11	1.0E-11	1.0E-11
-35	3.5	1.0E-11	1.0E-11	1.0E-11	1.0E-11
-35	4.5	1.0E-11	1.0E-11	1.0E-11	1.0E-11
-35	5.5	1.0E-11	1.0E-11	1.0E-11	1.0E-11
-35	6.5	1.0E-11	1.0E-11	1.0E-11	1.0E-11
-35	7.5	1.0E-11	1.0E-11	1.0E-11	1.0E-11
-35	8.5	1.0E-11	1.0E-11	1.0E-11	1.0E-11
-35	9.5	1.0E-11	1.0E-11	1.0E-11	1.0E-11
-35	10.5	1.8E-11	1.8E-11	1.8E-11	1.8E-11
-35	11.5	2.5E-11	2.5E-11	2.5E-11	2.5E-11
-35	12.5	3.4E-11	3.4E-11	3.4E-11	3.4E-11
-35	13.5	3.4E-11	3.4E-11	3.4E-11	3.4E-11
-35	14.5	3.4E-11	3.4E-11	3.4E-11	3.4E-11
-35	18.5	1.0E-10	1.0E-10	1.0E-10	1.0E-10
-35	24.5	1.0E-09	1.0E-09	1.0E-09	1.0E-09
-35	29.5	1.0E-09	1.0E-09	1.0E-09	1.0E-09
-35	34.5	1.0E-08	1.0E-08	1.0E-08	1.0E-08
-35	39.5	1.0E-08	1.0E-08	1.0E-08	1.0E-08
-35	44.5	1.0E-08	1.0E-08	1.0E-08	1.0E-08
-35	49.5	1.0E-08	1.0E-08	1.0E-08	1.0E-08
-45	0.5	1.0E-11	1.0E-11	1.0E-11	1.0E-11
-45	1.5	1.0E-11	1.0E-11	1.0E-11	1.0E-11
-45	2.5	1.0E-11	1.0E-11	1.0E-11	1.0E-11
-45	3.5	1.0E-11	1.0E-11	1.0E-11	1.0E-11
-45	4.5	1.0E-11	1.0E-11	1.0E-11	1.0E-11
-45	5.5	1.0E-11	1.0E-11	1.0E-11	1.0E-11
-45	6.5	1.0E-11	1.0E-11	1.0E-11	1.0E-11
-45	7.5	1.0E-11	1.0E-11	1.0E-11	1.0E-11
-45	8.5	1.0E-11	1.0E-11	1.0E-11	1.0E-11
-45	9.5	1.0E-11	1.0E-11	1.0E-11	1.0E-11
-45	10.5	1.8E-11	1.8E-11	1.8E-11	1.8E-11
-45	11.5	2.5E-11	2.5E-11	2.5E-11	2.5E-11
-45	12.5	2.6E-11	2.6E-11	2.6E-11	2.6E-11
-45	13.5	2.6E-11	2.6E-11	2.6E-11	2.6E-11
-45	14.5	2.6E-11	2.6E-11	2.6E-11	2.6E-11
-45	18.5	1.0E-10	1.0E-10	1.0E-10	1.0E-10
-45	24.5	1.0E-09	1.0E-09	1.0E-09	1.0E-09
-45	29.5	1.0E-09	1.0E-09	1.0E-09	1.0E-09
-45	34.5	1.0E-08	1.0E-08	1.0E-08	1.0E-08
-45	39.5	1.0E-08	1.0E-08	1.0E-08	1.0E-08
-45	44.5	1.0E-08	1.0E-08	1.0E-08	1.0E-08
-45	49.5	1.0E-08	1.0E-08	1.0E-08	1.0E-08
-55	0.5	1.0E-11	1.0E-11	1.0E-11	1.0E-11
-55	1.5	1.0E-11	1.0E-11	1.0E-11	1.0E-11
-55	2.5	1.0E-11	1.0E-11	1.0E-11	1.0E-11
-55	3.5	1.0E-11	1.0E-11	1.0E-11	1.0E-11
-55	4.5	1.0E-11	1.0E-11	1.0E-11	1.0E-11
-55	5.5	1.0E-11	1.0E-11	1.0E-11	1.0E-11
-55	6.5	1.0E-11	1.0E-11	1.0E-11	1.0E-11
-55	7.5	1.0E-11	1.0E-11	1.0E-11	1.0E-11
-55	8.5	1.0E-11	1.0E-11	1.0E-11	1.0E-11
-55	9.5	1.0E-11	1.0E-11	1.0E-11	1.0E-11
-55	10.5	1.8E-11	1.8E-11	1.8E-11	1.8E-11
-55	11.5	2.5E-11	2.5E-11	2.5E-11	2.5E-11
-55	12.5	3.4E-11	3.4E-11	3.4E-11	3.4E-11
-55	13.5	3.4E-11	3.4E-11	3.4E-11	3.4E-11
-55	14.5	3.4E-11	3.4E-11	3.4E-11	3.4E-11
-55	18.5	1.0E-10	1.0E-10	1.0E-10	1.0E-10
-55	24.5	1.0E-09	1.0E-09	1.0E-09	1.0E-09
-55	29.5	1.0E-09	1.0E-09	1.0E-09	1.0E-09
-55	34.5	1.0E-08	1.0E-08	1.0E-08	1.0E-08
-55	39.5	1.0E-08	1.0E-08	1.0E-08	1.0E-08
-55	44.5	1.0E-08	1.0E-08	1.0E-08	1.0E-08
-55	49.5	1.0E-08	1.0E-08	1.0E-08	1.0E-08
-65	0.5	1.0E-11	1.0E-11	1.0E-11	1.0E-11
-65	1.5	1.0E-11	1.0E-11	1.0E-11	1.0E-11
-65	2.5	1.0E-11	1.0E-11	1.0E-11	1.0E-11
-65	3.5	1.0E-11	1.0E-11	1.0E-11	1.0E-11
-65	4.5	1.0E-11	1.0E-11	1.0E-11	1.0E-11
-65	5.5	1.0E-11	1.0E-11	1.0E-11	1.0E-11
-65	6.5	1.0E-11	1.0E-11	1.0E-11	1.0E-11
-65	7.5	1.0E-11	1.0E-11	1.0E-11	1.0E-11
-65	8.5	1.0E-11	1.0E-11	1.0E-11	1.0E-11
-65	9.5	1.0E-11	1.0E-11	1.0E-11	1.0E-11
-65	10.5	1.8E-11	1.8E-11	1.8E-11	1.8E-11
-65	11.5	2.5E-11	2.5E-11	2.5E-11	2.5E-11
-65	12.5	2.2E-11	2.2E-11	2.2E-11	2.2E-11
-65	13.5	2.2E-11	2.2E-11	2.2E-11	2.2E-11
-65	14.5	2.2E-11	2.2E-11	2.2E-11	2.2E-11
-65	18.5	1.0E-10	1.0E-10	1.0E-10	1.0E-10
-65	24.5	1.0E-09	1.0E-09	1.0E-09	1.0E-09
-65	29.5	1.0E-09	1.0E-09	1.0E-09	1.0E-09
-65	34.5	1.0E-08	1.0E-08	1.0E-08	1.0E-08
-65	39.5	1.0E-08	1.0E-08	1.0E-08	1.0E-08
-65	44.5	1.0E-08	1.0E-08	1.0E-08	1.0E-08
-65	49.5	1.0E-08	1.0E-08	1.0E-08	1.0E-08
-75	0.5	1.0E-11	1.0E-11	1.0E-11	1.0E-11
-75	1.5	1.0E-11	1.0E-11	1.0E-11	1.0E-11
-75	2.5	1.0E-11	1.0E-11	1.0E-11	1.0E-11
-75	3.5	1.0E-11	1.0E-11	1.0E-11	1.0E-11
-75	4.5	1.0E-11	1.0E-11	1.0E-11	1.0E-11
-75	5.5	1.0E-11	1.0E-11	1.0E-11	1.0E-11
-75	6.5	1.0E-11	1.0E-11	1.0E-11	1.0E-11
-75	7.5	1.0E-11	1.0E-11	1.0E-11	1.0E-11
-75	8.5	1.0E-11	1.0E-11	1.0E-11	1.0E-11
-75	9.5	1.3E-11	1.3E-11	1.3E-11	1.3E-11
-75	10.5	1.6E-11	1.6E-11	1.6E-11	1.6E-11
-75	11.5	2.2E-11	2.2E-11	2.2E-11	2.2E-11
-75	12.5	2.2E-11	2.2E-11	2.2E-11	2.2E-11
-75	13.5	2.2E-11	2.2E-11	2.2E-11	2.2E-11
-75	14.5	2.2E-11	2.2E-11	2.2E-11	2.2E-11

```
-75 18.5 1.0E-10 1.0E-10 1.0E-10 1.0E-10
-75 24.5 1.0E-09 1.0E-09 1.0E-09 1.0E-09
-75 29.5 1.0E-09 1.0E-09 1.0E-09 1.0E-09
-75 34.5 1.0E-08 1.0E-08 1.0E-08 1.0E-08
-75 39.5 1.0E-08 1.0E-08 1.0E-08 1.0E-08
-75 44.5 1.0E-08 1.0E-08 1.0E-08 1.0E-08
-75 49.5 1.0E-08 1.0E-08 1.0E-08 1.0E-08
-85  0.5 1.0E-11 1.0E-11 1.0E-11 1.0E-11
-85  1.5 1.0E-11 1.0E-11 1.0E-11 1.0E-11
-85  2.5 1.0E-11 1.0E-11 1.0E-11 1.0E-11
-85  3.5 1.0E-11 1.0E-11 1.0E-11 1.0E-11
-85  4.5 1.0E-11 1.0E-11 1.0E-11 1.0E-11
-85  5.5 1.0E-11 1.0E-11 1.0E-11 1.0E-11
-85  6.5 1.0E-11 1.0E-11 1.0E-11 1.0E-11
-85  7.5 1.0E-11 1.0E-11 1.0E-11 1.0E-11
-85  8.5 1.0E-11 1.0E-11 1.0E-11 1.0E-11
-85  9.5 1.3E-11 1.3E-11 1.3E-11 1.3E-11
-85 10.5 1.6E-11 1.6E-11 1.6E-11 1.6E-11
-85 11.5 2.2E-11 2.2E-11 2.2E-11 2.2E-11
-85 12.5 2.2E-11 2.2E-11 2.2E-11 2.2E-11
-85 13.5 2.2E-11 2.2E-11 2.2E-11 2.2E-11
-85 14.5 2.2E-11 2.2E-11 2.2E-11 2.2E-11
-85 18.5 1.0E-10 1.0E-10 1.0E-10 1.0E-10
-85 24.5 1.0E-09 1.0E-09 1.0E-09 1.0E-09
-85 29.5 1.0E-09 1.0E-09 1.0E-09 1.0E-09
-85 34.5 1.0E-08 1.0E-08 1.0E-08 1.0E-08
-85 39.5 1.0E-08 1.0E-08 1.0E-08 1.0E-08
-85 44.5 1.0E-08 1.0E-08 1.0E-08 1.0E-08
-85 49.5 1.0E-08 1.0E-08 1.0E-08 1.0E-08
```

B.22 o2.dat

```
0.2
0.2
0.2
0.2
0.2
0.2
0.2
0.2
0.2
0.2
0.2
0.2
0.2
0.2
0.2
0.2
0.2
0.2
0.2
0.2
0.2
0.2
```

B.23 o3acs.dat

```
175.439   81.1E-20
176.991   79.9E-20
178.571   78.6E-20
180.180   76.3E-20
181.818   72.9E-20
183.486   68.8E-20
185.185   62.2E-20
186.916   57.6E-20
188.679   52.6E-20
190.476   47.6E-20
192.308   42.8E-20
194.175   38.3E-20
196.078   34.7E-20
198.020   32.3E-20
200.000   31.4E-20
202.020   32.6E-20
204.082   36.4E-20
206.186   43.4E-20
208.333   54.2E-20
210.526   69.9E-20
212.766   92.1E-20
215.054    119.0E-20
217.391    155.0E-20
219.780    199.0E-20
222.222    256.0E-20
224.719    323.0E-20
227.293    400.0E-20
229.885    483.0E-20
232.558    579.0E-20
235.294    686.0E-20
239.095    797.0E-20
240.964    900.0E-20
243.902   1000.0E-20
246.914   1080.0E-20
250.000   1130.0E-20
253.165   1150.0E-20
256.410   1120.0E-20
259.740   1060.0E-20
263.158    965.0E-20
266.667    834.0E-20
270.270    692.0E-20
273.973    542.0E-20
277.778    402.0E-20
```

```
281.690        277.0E-20
285.714        179.0E-20
289.855        109.0E-20
294.118       62.4E-20
298.25 5.10E-19
300.0 4.00E-19
302.2 2.85E-19
303.7 2.36E-19
305.1 2.00E-19
306.5 1.65E-19
307.9 1.38E-19
309.3 1.15E-19
310.0 1.05E-19
310.7 9.30E-20
312.8 7.00E-20
315.6 5.00E-20
318.5 3.50E-20
320.0 2.91E-20
330.0 7.78E-21
340.0 1.71E-21
350.0 2.66E-22
360.0 5.49E-23
370.0 0.00
380.0 0.00
390.0 0.00
400.0 0.00
410.0 2.91E-23
420.0 3.99E-23
430.0 6.83E-23
445.0 1.49E-22
465.0 3.68E-22
485.0 8.43E-22
505.0 1.66E-21
525.0 2.07E-21
545.0 3.07E-21
565.0 4.32E-21
585.0 4.33E-21
605.0 4.85E-21
625.0 3.60E-21
645.0 2.61E-21
665.0 1.85E-21
685.0 1.25E-21
705.0 8.41E-22
725.0 5.69E-22
```

B.24 o3land.dat

```
85  0.5 8.5E+11 4.9E+11 6.7E+11 8.5E+11
85  1.5 7.7E+11 4.4E+11 6.1E+11 7.7E+11
85  2.5 1.0E+12 1.0E+12 1.0E+12 1.0E+12
85  3.5 9.0E+11 9.0E+11 9.0E+11 9.0E+11
85  4.5 8.1E+11 8.1E+11 8.1E+11 8.1E+11
85  5.5 7.3E+11 7.3E+11 7.3E+11 7.3E+11
85  6.5 6.5E+11 6.5E+11 6.5E+11 6.5E+11
85  7.5 7.3E+11 8.7E+11 8.0E+11 7.3E+11
85  8.5 7.7E+11 1.0E+12 9.0E+11 7.7E+11
85  9.5 1.6E+12 1.6E+12 1.4E+12 1.2E+12
85 10.5 2.0E+12 2.0E+12 1.5E+12 1.3E+12
85 11.5 2.5E+12 3.2E+12 1.7E+12 1.5E+12
85 12.5 3.4E+12 4.1E+12 1.8E+12 1.7E+12
85 13.5 4.2E+12 5.0E+12 1.9E+12 1.9E+12
85 14.5 5.1E+12 5.9E+12 2.0E+12 2.1E+12
85 18.5 8.2E+12 8.4E+12 4.9E+12 5.1E+12
85 24.5 6.5E+12 5.3E+12 3.8E+12 5.0E+12
85 29.5 3.5E+12 3.0E+12 2.7E+12 3.4E+12
85 34.5 1.2E+12 1.3E+12 1.3E+12 1.5E+12
85 39.5 4.3E+11 4.2E+11 4.9E+11 6.0E+11
85 44.5 1.8E+11 1.5E+11 1.6E+11 2.2E+11
85 49.5 7.0E+10 5.9E+10 5.1E+10 8.0E+10
75  0.5 8.5E+11 4.9E+11 6.7E+11 8.5E+11
75  1.5 7.7E+11 4.4E+11 6.1E+11 7.7E+11
75  2.5 1.0E+12 1.0E+12 1.0E+12 1.0E+12
75  3.5 9.0E+11 9.0E+11 9.0E+11 9.0E+11
75  4.5 8.1E+11 8.1E+11 8.1E+11 8.1E+11
75  5.5 7.3E+11 7.3E+11 7.3E+11 7.3E+11
75  6.5 6.5E+11 6.5E+11 6.5E+11 6.5E+11
75  7.5 7.3E+11 8.7E+11 8.0E+11 7.3E+11
75  8.5 7.7E+11 1.0E+12 9.0E+11 7.7E+11
75  9.5 1.7E+12 1.7E+12 1.6E+12 1.3E+12
75 10.5 2.1E+12 2.3E+12 1.7E+12 1.4E+12
75 11.5 2.7E+12 3.4E+12 1.7E+12 1.4E+12
75 12.5 3.5E+12 4.3E+12 1.8E+12 1.6E+12
75 13.5 4.4E+12 5.3E+12 1.8E+12 1.9E+12
75 14.5 5.2E+12 6.2E+12 1.9E+12 2.1E+12
75 18.5 8.2E+12 8.5E+12 5.0E+12 5.1E+12
75 24.5 6.6E+12 5.2E+12 3.9E+12 4.9E+12
75 29.5 3.4E+12 3.0E+12 2.6E+12 3.2E+12
75 34.5 1.2E+12 1.3E+12 1.3E+12 1.5E+12
75 39.5 4.2E+11 4.6E+11 4.7E+11 5.7E+11
75 44.5 1.8E+11 1.7E+11 1.7E+11 2.3E+11
75 49.5 7.6E+10 5.9E+10 5.4E+10 8.3E+10
65  0.5 9.7E+11 9.7E+11 1.2E+12 9.7E+11
65  1.5 8.8E+11 8.8E+11 1.1E+12 8.8E+11
65  2.5 8.0E+11 1.0E+12 1.4E+12 8.0E+11
65  3.5 7.2E+11 9.0E+11 1.3E+12 7.2E+11
65  4.5 6.5E+11 8.1E+11 1.1E+12 6.5E+11
65  5.5 5.8E+11 7.3E+11 1.0E+12 5.8E+11
65  6.5 5.2E+11 6.5E+11 9.1E+11 5.2E+11
65  7.5 4.6E+11 5.8E+11 8.1E+11 4.6E+11
65  8.5 4.1E+11 5.2E+11 7.2E+11 4.1E+11
65  9.5 3.7E+11 4.6E+11 6.4E+11 3.7E+11
```

65	10.5	4.0E+11	5.2E+11	6.9E+11	4.0E+11
65	11.5	4.2E+11	5.6E+11	7.0E+11	4.2E+11
65	12.5	3.0E+12	3.7E+12	1.6E+12	1.4E+12
65	13.5	3.8E+12	4.5E+12	1.7E+12	1.7E+12
65	14.5	4.6E+12	5.3E+12	1.8E+12	1.9E+12
65	18.5	7.5E+12	8.1E+12	4.8E+12	4.7E+12
65	24.5	6.1E+12	5.3E+12	4.2E+12	4.8E+12
65	29.5	3.4E+12	3.2E+12	3.0E+12	3.4E+12
65	34.5	1.2E+12	1.5E+12	1.4E+12	1.6E+12
65	39.5	4.4E+11	5.3E+11	5.2E+11	6.9E+11
65	44.5	1.9E+11	1.8E+11	1.7E+11	2.6E+11
65	49.5	8.2E+10	5.9E+10	5.8E+10	8.3E+10
55	0.5	9.7E+11	9.7E+11	1.2E+12	9.7E+11
55	1.5	8.8E+11	8.8E+11	1.1E+12	8.8E+11
55	2.5	8.0E+11	1.0E+12	1.4E+12	8.0E+11
55	3.5	7.2E+11	9.0E+11	1.3E+12	7.2E+11
55	4.5	6.5E+11	8.1E+11	1.1E+12	6.5E+11
55	5.5	5.8E+11	7.3E+11	1.0E+12	5.8E+11
55	6.5	5.2E+11	6.5E+11	9.1E+11	5.2E+11
55	7.5	4.6E+11	5.8E+11	8.1E+11	4.6E+11
55	8.5	4.1E+11	5.2E+11	7.2E+11	4.1E+11
55	9.5	3.7E+11	4.6E+11	6.4E+11	3.7E+11
55	10.5	4.0E+11	5.2E+11	6.9E+11	4.0E+11
55	11.5	4.2E+11	5.6E+11	7.0E+11	4.2E+11
55	12.5	2.2E+12	2.6E+12	1.5E+12	1.3E+12
55	13.5	2.7E+12	3.2E+12	1.6E+12	1.4E+12
55	14.5	3.3E+12	3.7E+12	1.7E+12	1.6E+12
55	18.5	6.2E+12	6.9E+12	4.7E+12	4.4E+12
55	24.5	5.7E+12	5.3E+12	4.8E+12	4.8E+12
55	29.5	3.5E+12	3.6E+12	3.5E+12	3.6E+12
55	34.5	1.4E+12	1.7E+12	1.7E+12	1.9E+12
55	39.5	5.6E+11	5.8E+11	5.8E+11	7.8E+11
55	44.5	2.3E+11	1.9E+11	1.8E+11	2.6E+11
55	49.5	8.4E+10	6.0E+10	6.1E+10	8.0E+10
45	0.5	9.7E+11	9.7E+11	1.2E+12	9.7E+11
45	1.5	8.8E+11	8.8E+11	1.1E+12	8.8E+11
45	2.5	8.0E+11	1.0E+12	1.4E+12	8.0E+11
45	3.5	7.2E+11	9.0E+11	1.3E+12	7.2E+11
45	4.5	6.5E+11	8.1E+11	1.1E+12	6.5E+11
45	5.5	5.8E+11	7.3E+11	1.0E+12	5.8E+11
45	6.5	5.2E+11	6.5E+11	9.1E+11	5.2E+11
45	7.5	4.6E+11	5.8E+11	8.1E+11	4.6E+11
45	8.5	4.1E+11	5.2E+11	7.2E+11	4.1E+11
45	9.5	3.7E+11	4.6E+11	6.4E+11	3.7E+11
45	10.5	4.0E+11	5.2E+11	6.9E+11	4.0E+11
45	11.5	4.2E+11	5.6E+11	7.0E+11	4.2E+11
45	12.5	1.5E+12	1.8E+12	1.3E+12	1.0E+12
45	13.5	1.7E+12	2.1E+12	1.4E+12	1.2E+12
45	14.5	2.0E+12	2.4E+12	1.5E+12	1.3E+12
45	18.5	5.1E+12	5.6E+12	4.5E+12	4.0E+12
45	24.5	5.3E+12	5.3E+12	5.1E+12	4.8E+12
45	29.5	3.6E+12	3.9E+12	4.1E+12	3.9E+12
45	34.5	1.6E+12	1.9E+12	1.9E+12	2.0E+12
45	39.5	6.5E+11	6.1E+11	6.3E+11	8.1E+11
45	44.5	2.4E+11	1.9E+11	1.9E+11	2.5E+11
45	49.5	7.6E+10	6.0E+10	6.4E+10	7.4E+10
35	0.5	9.7E+11	9.7E+11	1.2E+12	9.7E+11
35	1.5	8.8E+11	8.8E+11	1.1E+12	8.8E+11
35	2.5	8.0E+11	1.0E+12	1.4E+12	8.0E+11
35	3.5	7.2E+11	9.0E+11	1.3E+12	7.2E+11
35	4.5	6.5E+11	8.1E+11	1.1E+12	6.5E+11
35	5.5	5.8E+11	7.3E+11	1.0E+12	5.8E+11
35	6.5	5.2E+11	6.5E+11	9.1E+11	5.2E+11
35	7.5	4.6E+11	5.8E+11	8.1E+11	4.6E+11
35	8.5	4.1E+11	5.2E+11	7.2E+11	4.1E+11
35	9.5	3.7E+11	4.6E+11	6.4E+11	3.7E+11
35	10.5	4.0E+11	5.2E+11	6.9E+11	4.0E+11
35	11.5	4.2E+11	5.6E+11	7.0E+11	4.2E+11
35	12.5	1.1E+12	1.3E+12	9.8E+11	7.8E+11
35	13.5	1.2E+12	1.5E+12	1.1E+12	8.9E+11
35	14.5	1.4E+12	1.7E+12	1.2E+12	1.0E+12
35	18.5	4.4E+12	4.7E+12	4.1E+12	3.7E+12
35	24.5	5.1E+12	5.2E+12	5.2E+12	4.8E+12
35	29.5	3.7E+12	4.2E+12	4.4E+12	4.1E+12
35	34.5	1.8E+12	2.0E+12	2.1E+12	2.1E+12
35	39.5	6.7E+11	6.4E+11	7.0E+11	7.9E+11
35	44.5	2.2E+11	1.9E+11	2.1E+11	2.3E+11
35	49.5	7.0E+10	6.2E+10	6.7E+10	6.9E+10
25	0.5	7.3E+11	1.0E+12	1.0E+12	7.3E+11
25	1.5	6.6E+11	9.4E+11	9.1E+11	6.6E+11
25	2.5	7.9E+11	9.5E+11	1.1E+12	7.9E+11
25	3.5	7.1E+11	8.5E+11	1.0E+12	7.1E+11
25	4.5	6.4E+11	7.7E+11	9.1E+11	6.4E+11
25	5.5	5.7E+11	6.9E+11	8.1E+11	5.7E+11
25	6.5	5.1E+11	6.2E+11	7.3E+11	5.1E+11
25	7.5	4.6E+11	5.5E+11	6.5E+11	4.6E+11
25	8.5	4.1E+11	4.9E+11	5.8E+11	4.1E+11
25	9.5	3.6E+11	4.4E+11	5.1E+11	3.6E+11
25	10.5	3.6E+11	4.5E+11	5.1E+11	3.6E+11
25	11.5	3.5E+11	4.4E+11	5.0E+11	3.5E+11
25	12.5	7.3E+11	8.0E+11	6.5E+11	5.7E+11
25	13.5	8.3E+11	9.0E+11	7.4E+11	6.7E+11
25	14.5	9.6E+11	1.0E+12	8.1E+11	7.6E+11
25	18.5	3.6E+12	3.8E+12	3.5E+12	3.1E+12
25	24.5	4.7E+12	4.9E+12	5.0E+12	4.6E+12
25	29.5	4.0E+12	4.5E+12	4.6E+12	4.4E+12
25	34.5	2.0E+12	2.1E+12	2.2E+12	2.2E+12
25	39.5	6.8E+11	6.7E+11	7.6E+11	7.6E+11
25	44.5	2.1E+11	2.0E+11	2.3E+11	2.2E+11
25	49.5	6.7E+10	6.3E+10	6.8E+10	6.8E+10
15	0.5	4.9E+11	1.1E+12	8.0E+11	4.9E+11
15	1.5	4.4E+11	1.0E+12	7.2E+11	4.4E+11

15	2.5	7.8E+11	9.1E+11	8.4E+11	7.8E+11
15	3.5	7.0E+11	8.1E+11	7.6E+11	7.0E+11
15	4.5	6.3E+11	7.4E+11	6.8E+11	6.3E+11
15	5.5	5.7E+11	6.6E+11	6.1E+11	5.7E+11
15	6.5	5.1E+11	5.9E+11	5.5E+11	5.1E+11
15	7.5	4.5E+11	5.3E+11	4.9E+11	4.5E+11
15	8.5	4.0E+11	4.7E+11	4.4E+11	4.0E+11
15	9.5	3.6E+11	4.2E+11	3.9E+11	3.6E+11
15	10.5	3.1E+11	3.7E+11	3.4E+11	3.1E+11
15	11.5	2.7E+11	3.2E+11	3.0E+11	2.7E+11
15	12.5	3.7E+11	2.9E+11	3.3E+11	3.7E+11
15	13.5	4.6E+11	3.0E+11	3.8E+11	4.6E+11
15	14.5	5.3E+11	3.0E+11	4.2E+11	5.3E+11
15	18.5	2.6E+12	2.7E+12	2.7E+12	2.4E+12
15	24.5	4.2E+12	4.5E+12	4.6E+12	4.4E+12
15	29.5	4.4E+12	4.7E+12	4.7E+12	4.6E+12
15	34.5	2.2E+12	2.2E+12	2.3E+12	2.2E+12
15	39.5	7.1E+11	6.9E+11	7.8E+11	7.4E+11
15	44.5	2.2E+11	2.1E+11	2.4E+11	2.2E+11
15	49.5	6.5E+10	6.4E+10	6.9E+10	6.7E+10
5	0.5	4.9E+11	1.1E+12	8.0E+11	4.9E+11
5	1.5	4.4E+11	1.0E+12	7.2E+11	4.4E+11
5	2.5	7.8E+11	9.1E+11	8.4E+11	7.8E+11
5	3.5	7.0E+11	8.1E+11	7.6E+11	7.0E+11
5	4.5	6.3E+11	7.4E+11	6.8E+11	6.3E+11
5	5.5	5.7E+11	6.6E+11	6.1E+11	5.7E+11
5	6.5	5.1E+11	5.9E+11	5.5E+11	5.1E+11
5	7.5	4.5E+11	5.3E+11	4.9E+11	4.5E+11
5	8.5	4.0E+11	4.7E+11	4.4E+11	4.0E+11
5	9.5	3.6E+11	4.2E+11	3.9E+11	3.6E+11
5	10.5	3.1E+11	3.7E+11	3.4E+11	3.1E+11
5	11.5	2.7E+11	3.2E+11	3.0E+11	2.7E+11
5	12.5	3.7E+11	2.9E+11	3.3E+11	3.7E+11
5	13.5	4.6E+11	3.0E+11	3.8E+11	4.6E+11
5	14.5	5.3E+11	3.0E+11	4.2E+11	5.3E+11
5	18.5	1.9E+12	1.9E+12	2.0E+12	2.0E+12
5	24.5	4.0E+12	4.1E+12	4.2E+12	4.2E+12
5	29.5	4.6E+12	4.8E+12	4.7E+12	4.8E+12
5	34.5	2.4E+12	2.3E+12	2.3E+12	2.2E+12
5	39.5	7.5E+11	6.9E+11	7.6E+11	7.2E+11
5	44.5	2.3E+11	2.1E+11	2.3E+11	2.2E+11
5	49.5	6.6E+10	6.5E+10	7.0E+10	6.7E+10
-5	0.5	4.9E+11	4.9E+11	5.5E+11	6.1E+11
-5	1.5	4.4E+11	4.4E+11	5.0E+11	5.5E+11
-5	2.5	6.0E+11	6.0E+11	9.0E+11	1.2E+12
-5	3.5	5.4E+11	5.4E+11	8.1E+11	1.1E+12
-5	4.5	4.9E+11	4.9E+11	7.3E+11	9.7E+11
-5	5.5	4.4E+11	4.4E+11	6.5E+11	8.7E+11
-5	6.5	3.9E+11	3.9E+11	5.9E+11	7.8E+11
-5	7.5	3.5E+11	3.5E+11	5.2E+11	7.0E+11
-5	8.5	3.1E+11	3.1E+11	4.6E+11	6.2E+11
-5	9.5	2.7E+11	2.7E+11	4.1E+11	5.5E+11
-5	10.5	2.4E+11	2.4E+11	3.6E+11	4.8E+11
-5	11.5	2.1E+11	2.1E+11	3.2E+11	4.2E+11
-5	12.5	2.6E+11	2.6E+11	3.0E+11	3.3E+11
-5	13.5	2.3E+11	2.3E+11	2.7E+11	3.1E+11
-5	14.5	2.0E+11	2.0E+11	2.4E+11	2.8E+11
-5	18.5	2.0E+12	2.2E+12	2.1E+12	1.9E+12
-5	24.5	4.1E+12	4.3E+12	4.2E+12	4.1E+12
-5	29.5	4.6E+12	4.8E+12	4.6E+12	4.7E+12
-5	34.5	2.2E+12	2.2E+12	2.4E+12	2.2E+12
-5	39.5	7.4E+11	6.9E+11	7.6E+11	7.1E+11
-5	44.5	2.2E+11	2.2E+11	2.3E+11	2.1E+11
-5	49.5	6.8E+10	6.6E+10	6.7E+10	6.5E+10
-15	0.5	4.9E+11	4.9E+11	5.5E+11	6.1E+11
-15	1.5	4.4E+11	4.4E+11	5.0E+11	5.5E+11
-15	2.5	6.0E+11	6.0E+11	9.0E+11	1.2E+12
-15	3.5	5.4E+11	5.4E+11	8.1E+11	1.1E+12
-15	4.5	4.9E+11	4.9E+11	7.3E+11	9.7E+11
-15	5.5	4.4E+11	4.4E+11	6.5E+11	8.7E+11
-15	6.5	3.9E+11	3.9E+11	5.9E+11	7.8E+11
-15	7.5	3.5E+11	3.5E+11	5.2E+11	7.0E+11
-15	8.5	3.1E+11	3.1E+11	4.6E+11	6.2E+11
-15	9.5	2.7E+11	2.7E+11	4.1E+11	5.5E+11
-15	10.5	2.4E+11	2.4E+11	3.6E+11	4.8E+11
-15	11.5	2.1E+11	2.1E+11	3.2E+11	4.2E+11
-15	12.5	2.6E+11	2.6E+11	3.0E+11	3.3E+11
-15	13.5	2.3E+11	2.3E+11	2.7E+11	3.1E+11
-15	14.5	2.0E+11	2.0E+11	2.4E+11	2.8E+11
-15	18.5	2.7E+12	3.0E+12	2.6E+12	2.4E+12
-15	24.5	4.5E+12	4.7E+12	4.5E+12	4.4E+12
-15	29.5	4.3E+12	4.7E+12	4.7E+12	4.6E+12
-15	34.5	2.1E+12	2.2E+12	2.3E+12	2.2E+12
-15	39.5	7.1E+11	6.9E+11	7.5E+11	7.1E+11
-15	44.5	2.2E+11	2.1E+11	2.2E+11	2.1E+11
-15	49.5	6.7E+10	6.5E+10	6.6E+10	6.6E+10
-25	0.5	4.9E+11	4.9E+11	5.5E+11	6.1E+11
-25	1.5	4.4E+11	4.4E+11	5.0E+11	5.5E+11
-25	2.5	6.0E+11	6.0E+11	9.0E+11	1.2E+12
-25	3.5	5.4E+11	5.4E+11	8.1E+11	1.1E+12
-25	4.5	4.9E+11	4.9E+11	7.3E+11	9.7E+11
-25	5.5	4.4E+11	4.4E+11	6.5E+11	8.7E+11
-25	6.5	3.9E+11	3.9E+11	5.9E+11	7.8E+11
-25	7.5	3.5E+11	3.5E+11	5.2E+11	7.0E+11
-25	8.5	3.1E+11	3.1E+11	4.6E+11	6.2E+11
-25	9.5	2.7E+11	2.7E+11	4.1E+11	5.5E+11
-25	10.5	2.4E+11	2.4E+11	3.6E+11	4.8E+11
-25	11.5	2.1E+11	2.1E+11	3.2E+11	4.2E+11
-25	12.5	2.6E+11	2.6E+11	3.0E+11	3.3E+11
-25	13.5	2.3E+11	2.3E+11	2.7E+11	3.1E+11
-25	14.5	2.0E+11	2.0E+11	2.4E+11	2.8E+11
-25	18.5	3.5E+12	4.1E+12	3.3E+12	3.0E+12

-25	24.5	4.8E+12	5.2E+12	4.8E+12	4.6E+12
-25	29.5	4.0E+12	4.4E+12	4.5E+12	4.4E+12
-25	34.5	1.9E+12	2.1E+12	2.2E+12	2.1E+12
-25	39.5	7.3E+11	6.8E+11	7.0E+11	7.4E+11
-25	44.5	2.2E+11	2.0E+11	2.1E+11	2.2E+11
-25	49.5	6.9E+10	6.4E+10	6.5E+10	6.8E+10
-35	0.5	3.6E+11	2.4E+11	3.6E+11	4.9E+11
-35	1.5	3.3E+11	2.2E+11	3.3E+11	4.4E+11
-35	2.5	9.0E+11	8.0E+11	9.0E+11	1.0E+12
-35	3.5	8.1E+11	7.2E+11	8.1E+11	9.0E+11
-35	4.5	7.3E+11	6.5E+11	7.3E+11	8.1E+11
-35	5.5	6.5E+11	5.8E+11	6.5E+11	7.3E+11
-35	6.5	5.9E+11	5.2E+11	5.9E+11	6.5E+11
-35	7.5	5.2E+11	4.6E+11	5.2E+11	5.8E+11
-35	8.5	4.6E+11	4.1E+11	4.6E+11	5.2E+11
-35	9.5	4.1E+11	3.7E+11	4.1E+11	4.6E+11
-35	10.5	7.3E+11	5.3E+11	5.6E+11	9.3E+11
-35	11.5	1.1E+12	7.0E+11	7.0E+11	1.4E+12
-35	12.5	4.2E+11	4.9E+11	3.5E+11	3.5E+11
-35	13.5	5.3E+11	6.7E+11	3.8E+11	3.8E+11
-35	14.5	6.1E+11	8.1E+11	4.0E+11	4.0E+11
-35	18.5	4.2E+12	5.0E+12	3.9E+12	3.5E+12
-35	24.5	5.0E+12	5.3E+12	5.0E+12	4.6E+12
-35	29.5	3.8E+12	4.1E+12	4.3E+12	4.1E+12
-35	34.5	1.8E+12	2.0E+12	2.0E+12	2.1E+12
-35	39.5	7.5E+11	6.6E+11	6.4E+11	7.8E+11
-35	44.5	2.4E+11	2.0E+11	1.9E+11	2.4E+11
-35	49.5	7.4E+10	6.4E+10	6.3E+10	7.1E+10
-45	0.5	3.6E+11	2.4E+11	3.6E+11	4.9E+11
-45	1.5	3.3E+11	2.2E+11	3.3E+11	4.4E+11
-45	2.5	9.0E+11	8.0E+11	9.0E+11	1.0E+12
-45	3.5	8.1E+11	7.2E+11	8.1E+11	9.0E+11
-45	4.5	7.3E+11	6.5E+11	7.3E+11	8.1E+11
-45	5.5	6.5E+11	5.8E+11	6.5E+11	7.3E+11
-45	6.5	5.9E+11	5.2E+11	5.9E+11	6.5E+11
-45	7.5	5.2E+11	4.6E+11	5.2E+11	5.8E+11
-45	8.5	4.6E+11	4.1E+11	4.6E+11	5.2E+11
-45	9.5	4.1E+11	3.7E+11	4.1E+11	4.6E+11
-45	10.5	7.3E+11	5.3E+11	5.6E+11	9.3E+11
-45	11.5	1.1E+12	7.0E+11	7.0E+11	1.4E+12
-45	12.5	4.2E+11	4.9E+11	3.5E+11	3.5E+11
-45	13.5	5.3E+11	6.7E+11	3.8E+11	3.8E+11
-45	14.5	6.1E+11	8.1E+11	4.0E+11	4.0E+11
-45	18.5	5.0E+12	5.8E+12	4.3E+12	3.9E+12
-45	24.5	5.2E+12	5.2E+12	4.8E+12	4.6E+12
-45	29.5	3.5E+12	3.7E+12	3.9E+12	3.8E+12
-45	34.5	1.6E+12	1.9E+12	1.7E+12	2.0E+12
-45	39.5	7.0E+11	6.2E+11	5.8E+11	8.2E+11
-45	44.5	2.5E+11	2.0E+11	1.8E+11	2.6E+11
-45	49.5	7.9E+10	6.3E+10	6.0E+10	7.7E+10
-55	0.5	3.6E+11	2.4E+11	3.6E+11	4.9E+11
-55	1.5	3.3E+11	2.2E+11	3.3E+11	4.4E+11
-55	2.5	9.0E+11	8.0E+11	9.0E+11	1.0E+12
-55	3.5	8.1E+11	7.2E+11	8.1E+11	9.0E+11
-55	4.5	7.3E+11	6.5E+11	7.3E+11	8.1E+11
-55	5.5	6.5E+11	5.8E+11	6.5E+11	7.3E+11
-55	6.5	5.9E+11	5.2E+11	5.9E+11	6.5E+11
-55	7.5	5.2E+11	4.6E+11	5.2E+11	5.8E+11
-55	8.5	4.6E+11	4.1E+11	4.6E+11	5.2E+11
-55	9.5	4.1E+11	3.7E+11	4.1E+11	4.6E+11
-55	10.5	7.3E+11	5.3E+11	5.6E+11	9.3E+11
-55	11.5	1.1E+12	7.0E+11	7.0E+11	1.4E+12
-55	12.5	4.2E+11	4.9E+11	3.5E+11	3.5E+11
-55	13.5	5.3E+11	6.7E+11	3.8E+11	3.8E+11
-55	14.5	6.1E+11	8.1E+11	4.0E+11	4.0E+11
-55	18.5	6.0E+12	6.3E+12	4.8E+12	4.5E+12
-55	24.5	5.5E+12	5.0E+12	4.4E+12	4.6E+12
-55	29.5	3.3E+12	3.2E+12	3.4E+12	3.5E+12
-55	34.5	1.3E+12	1.6E+12	1.5E+12	1.9E+12
-55	39.5	5.4E+11	5.6E+11	5.4E+11	7.9E+11
-55	44.5	2.1E+11	1.9E+11	1.7E+11	2.8E+11
-55	49.5	7.9E+10	6.2E+10	5.8E+10	8.2E+10
-65	0.5	3.6E+11	2.4E+11	4.9E+11	4.9E+11
-65	1.5	3.3E+11	2.2E+11	4.4E+11	4.4E+11
-65	2.5	6.0E+11	5.0E+11	7.0E+11	7.0E+11
-65	3.5	5.4E+11	4.5E+11	6.3E+11	6.3E+11
-65	4.5	4.9E+11	4.0E+11	5.7E+11	5.7E+11
-65	5.5	4.4E+11	3.6E+11	5.1E+11	5.1E+11
-65	6.5	3.9E+11	3.3E+11	4.6E+11	4.6E+11
-65	7.5	3.5E+11	2.9E+11	4.1E+11	4.1E+11
-65	8.5	3.1E+11	2.6E+11	3.6E+11	3.6E+11
-65	9.5	1.2E+12	9.9E+11	6.0E+11	7.9E+11
-65	10.5	1.4E+12	1.1E+12	7.4E+11	9.8E+11
-65	11.5	1.6E+12	1.2E+12	9.9E+11	1.3E+12
-65	12.5	2.2E+12	1.8E+12	1.4E+12	1.7E+12
-65	13.5	2.7E+12	2.4E+12	1.9E+12	2.1E+12
-65	14.5	3.3E+12	3.0E+12	2.3E+12	2.5E+12
-65	18.5	6.8E+12	6.7E+12	4.9E+12	5.1E+12
-65	24.5	5.9E+12	4.9E+12	4.0E+12	4.7E+12
-65	29.5	3.3E+12	2.5E+12	2.8E+12	3.2E+12
-65	34.5	1.1E+12	1.2E+12	1.3E+12	1.5E+12
-65	39.5	3.8E+11	4.5E+11	4.9E+11	6.6E+11
-65	44.5	1.7E+11	1.7E+11	1.6E+11	2.5E+11
-65	49.5	7.2E+10	5.8E+10	5.5E+10	8.3E+10
-75	0.5	3.6E+11	2.4E+11	4.9E+11	4.9E+11
-75	1.5	3.3E+11	2.2E+11	4.4E+11	4.4E+11
-75	2.5	6.0E+11	5.0E+11	7.0E+11	7.0E+11
-75	3.5	5.4E+11	4.5E+11	6.3E+11	6.3E+11
-75	4.5	4.9E+11	4.0E+11	5.7E+11	5.7E+11
-75	5.5	4.4E+11	3.6E+11	5.1E+11	5.1E+11
-75	6.5	3.9E+11	3.3E+11	4.6E+11	4.6E+11
-75	7.5	3.5E+11	2.9E+11	4.1E+11	4.1E+11

-75	8.5	3.1E+11	2.6E+11	3.6E+11	3.6E+11
-75	9.5	1.4E+12	1.1E+12	6.4E+11	9.4E+11
-75	10.5	1.6E+12	1.3E+12	8.0E+11	1.2E+12
-75	11.5	1.9E+12	1.4E+12	1.1E+12	1.6E+12
-75	12.5	2.6E+12	2.0E+12	1.6E+12	2.0E+12
-75	13.5	3.2E+12	2.7E+12	2.0E+12	2.5E+12
-75	14.5	3.9E+12	3.3E+12	2.5E+12	2.9E+12
-75	18.5	7.4E+12	7.0E+12	4.9E+12	5.4E+12
-75	24.5	6.2E+12	4.9E+12	3.7E+12	4.8E+12
-75	29.5	3.5E+12	2.2E+12	2.5E+12	3.0E+12
-75	34.5	1.1E+12	8.8E+11	1.1E+12	1.3E+12
-75	39.5	3.6E+11	3.6E+11	4.5E+11	5.5E+11
-75	44.5	1.6E+11	1.4E+11	1.6E+11	2.2E+11
-75	49.5	6.5E+10	5.4E+10	5.2E+10	8.0E+10
-85	0.5	3.6E+11	2.4E+11	4.9E+11	4.9E+11
-85	1.5	3.3E+11	2.2E+11	4.4E+11	4.4E+11
-85	2.5	6.0E+11	5.0E+11	7.0E+11	7.0E+11
-85	3.5	5.4E+11	4.5E+11	6.3E+11	6.3E+11
-85	4.5	4.9E+11	4.0E+11	5.7E+11	5.7E+11
-85	5.5	4.4E+11	3.6E+11	5.1E+11	5.1E+11
-85	6.5	3.9E+11	3.3E+11	4.6E+11	4.6E+11
-85	7.5	3.5E+11	2.9E+11	4.1E+11	4.1E+11
-85	8.5	3.1E+11	2.6E+11	3.6E+11	3.6E+11
-85	9.5	1.4E+12	1.2E+12	6.4E+11	9.5E+11
-85	10.5	1.7E+12	1.4E+12	8.0E+11	1.2E+12
-85	11.5	2.0E+12	1.5E+12	1.1E+12	1.6E+12
-85	12.5	2.7E+12	2.1E+12	1.6E+12	2.1E+12
-85	13.5	3.3E+12	2.8E+12	2.0E+12	2.5E+12
-85	14.5	4.0E+12	3.4E+12	2.5E+12	3.0E+12
-85	18.5	7.5E+12	7.0E+12	4.9E+12	5.5E+12
-85	24.5	6.4E+12	4.9E+12	3.6E+12	4.8E+12
-85	29.5	3.6E+12	2.2E+12	2.4E+12	3.0E+12
-85	34.5	1.1E+12	8.2E+11	1.1E+12	1.3E+12
-85	39.5	3.6E+11	3.2E+11	4.5E+11	5.3E+11
-85	44.5	1.6E+11	1.3E+11	1.6E+11	2.0E+11
-85	49.5	6.2E+10	5.2E+10	5.0E+10	7.8E+10

B.25 o3sea.dat

85	0.5	8.5E+11	4.9E+11	6.7E+11	8.5E+11
85	1.5	7.7E+11	4.4E+11	6.1E+11	7.7E+11
85	2.5	1.0E+12	1.0E+12	1.0E+12	1.0E+12
85	3.5	9.0E+11	9.0E+11	9.0E+11	9.0E+11
85	4.5	8.1E+11	8.1E+11	8.1E+11	8.1E+11
85	5.5	7.3E+11	7.3E+11	7.3E+11	7.3E+11
85	6.5	6.5E+11	6.5E+11	6.5E+11	6.5E+11
85	7.5	7.3E+11	8.7E+11	8.0E+11	7.3E+11
85	8.5	7.7E+11	1.0E+12	9.0E+11	7.7E+11
85	9.5	1.6E+12	1.6E+12	1.4E+12	1.2E+12
85	10.5	2.0E+12	2.0E+12	1.5E+12	1.3E+12
85	11.5	2.5E+12	3.2E+12	1.7E+12	1.5E+12
85	12.5	3.4E+12	4.1E+12	1.8E+12	1.7E+12
85	13.5	4.2E+12	5.0E+12	1.9E+12	1.9E+12
85	14.5	5.1E+12	5.9E+12	2.0E+12	2.1E+12
85	18.5	8.2E+12	8.4E+12	4.9E+12	5.1E+12
85	24.5	6.5E+12	5.3E+12	3.8E+12	5.0E+12
85	29.5	3.5E+12	3.0E+12	2.7E+12	3.4E+12
85	34.5	1.2E+12	1.3E+12	1.3E+12	1.5E+12
85	39.5	4.3E+11	4.2E+11	4.9E+11	6.0E+11
85	44.5	1.8E+11	1.5E+11	1.6E+11	2.2E+11
85	49.5	7.0E+10	5.9E+10	5.1E+10	8.0E+10
75	0.5	8.5E+11	4.9E+11	6.7E+11	8.5E+11
75	1.5	7.7E+11	4.4E+11	6.1E+11	7.7E+11
75	2.5	1.0E+12	1.0E+12	1.0E+12	1.0E+12
75	3.5	9.0E+11	9.0E+11	9.0E+11	9.0E+11
75	4.5	8.1E+11	8.1E+11	8.1E+11	8.1E+11
75	5.5	7.3E+11	7.3E+11	7.3E+11	7.3E+11
75	6.5	6.5E+11	6.5E+11	6.5E+11	6.5E+11
75	7.5	7.3E+11	8.7E+11	8.0E+11	7.3E+11
75	8.5	7.7E+11	1.0E+12	9.0E+11	7.7E+11
75	9.5	1.7E+12	1.7E+12	1.6E+12	1.3E+12
75	10.5	2.1E+12	2.3E+12	1.7E+12	1.4E+12
75	11.5	2.7E+12	3.4E+12	1.7E+12	1.4E+12
75	12.5	3.5E+12	4.3E+12	1.8E+12	1.6E+12
75	13.5	4.4E+12	5.3E+12	1.8E+12	1.9E+12
75	14.5	5.2E+12	6.2E+12	1.9E+12	2.1E+12
75	18.5	8.2E+12	8.5E+12	5.0E+12	5.1E+12
75	24.5	6.6E+12	5.2E+12	3.9E+12	4.9E+12
75	29.5	3.4E+12	3.0E+12	2.6E+12	3.2E+12
75	34.5	1.2E+12	1.3E+12	1.3E+12	1.5E+12
75	39.5	4.2E+11	4.6E+11	4.7E+11	5.7E+11
75	44.5	1.8E+11	1.7E+11	1.7E+11	2.3E+11
75	49.5	7.6E+10	5.9E+10	5.4E+10	8.3E+10
65	0.5	7.3E+11	9.7E+11	1.2E+12	7.3E+11
65	1.5	6.6E+11	8.8E+11	1.1E+12	6.6E+11
65	2.5	1.0E+12	1.2E+12	1.5E+12	1.0E+12
65	3.5	9.0E+11	1.1E+12	1.3E+12	9.0E+11
65	4.5	8.1E+11	1.0E+12	1.2E+12	8.1E+11
65	5.5	7.3E+11	9.1E+11	1.1E+12	7.3E+11
65	6.5	6.5E+11	8.1E+11	9.8E+11	6.5E+11
65	7.5	5.8E+11	7.3E+11	8.7E+11	5.8E+11
65	8.5	5.2E+11	6.4E+11	7.7E+11	5.2E+11
65	9.5	4.6E+11	5.7E+11	6.8E+11	4.6E+11
65	10.5	4.4E+11	5.7E+11	7.1E+11	4.4E+11
65	11.5	4.2E+11	5.6E+11	7.0E+11	4.2E+11
65	12.5	3.0E+12	3.7E+12	1.6E+12	1.4E+12
65	13.5	3.8E+12	4.5E+12	1.7E+12	1.7E+12
65	14.5	4.6E+12	5.3E+12	1.8E+12	1.9E+12
65	18.5	7.5E+12	8.1E+12	4.8E+12	4.7E+12
65	24.5	6.1E+12	5.3E+12	4.2E+12	4.8E+12
65	29.5	3.4E+12	3.2E+12	3.0E+12	3.4E+12

65	34.5	1.2E+12	1.5E+12	1.4E+12	1.6E+12
65	39.5	4.4E+11	5.3E+11	5.2E+11	6.9E+11
65	44.5	1.9E+11	1.8E+11	1.7E+11	2.6E+11
65	49.5	8.2E+10	5.9E+10	5.8E+10	8.3E+10
55	0.5	7.3E+11	9.7E+11	1.2E+12	7.3E+11
55	1.5	6.6E+11	8.8E+11	1.1E+12	6.6E+11
55	2.5	1.0E+12	1.2E+12	1.5E+12	1.0E+12
55	3.5	9.0E+11	1.1E+12	1.3E+12	9.0E+11
55	4.5	8.1E+11	1.0E+12	1.2E+12	8.1E+11
55	5.5	7.3E+11	9.1E+11	1.1E+12	7.3E+11
55	6.5	6.5E+11	8.1E+11	9.8E+11	6.5E+11
55	7.5	5.8E+11	7.3E+11	8.7E+11	5.8E+11
55	8.5	5.2E+11	6.4E+11	7.7E+11	5.2E+11
55	9.5	4.6E+11	5.7E+11	6.8E+11	4.6E+11
55	10.5	4.4E+11	5.7E+11	7.1E+11	4.4E+11
55	11.5	4.2E+11	5.6E+11	7.0E+11	4.2E+11
55	12.5	2.2E+12	2.6E+12	1.5E+12	1.3E+12
55	13.5	2.7E+12	3.2E+12	1.6E+12	1.4E+12
55	14.5	3.3E+12	3.7E+12	1.7E+12	1.6E+12
55	18.5	6.2E+12	6.9E+12	4.7E+12	4.4E+12
55	24.5	5.7E+12	5.3E+12	4.8E+12	4.8E+12
55	29.5	3.5E+12	3.6E+12	3.5E+12	3.6E+12
55	34.5	1.4E+12	1.7E+12	1.7E+12	1.9E+12
55	39.5	5.6E+11	5.8E+11	5.8E+11	7.8E+11
55	44.5	2.3E+11	1.9E+11	1.8E+11	2.6E+11
55	49.5	8.4E+10	6.0E+10	6.1E+10	8.0E+10
45	0.5	7.3E+11	9.7E+11	1.2E+12	7.3E+11
45	1.5	6.6E+11	8.8E+11	1.1E+12	6.6E+11
45	2.5	1.0E+12	1.2E+12	1.5E+12	1.0E+12
45	3.5	9.0E+11	1.1E+12	1.3E+12	9.0E+11
45	4.5	8.1E+11	1.0E+12	1.2E+12	8.1E+11
45	5.5	7.3E+11	9.1E+11	1.1E+12	7.3E+11
45	6.5	6.5E+11	8.1E+11	9.8E+11	6.5E+11
45	7.5	5.8E+11	7.3E+11	8.7E+11	5.8E+11
45	8.5	5.2E+11	6.4E+11	7.7E+11	5.2E+11
45	9.5	4.6E+11	5.7E+11	6.8E+11	4.6E+11
45	10.5	4.4E+11	5.7E+11	7.1E+11	4.4E+11
45	11.5	4.2E+11	5.6E+11	7.0E+11	4.2E+11
45	12.5	1.5E+12	1.8E+12	1.3E+12	1.0E+12
45	13.5	1.7E+12	2.1E+12	1.4E+12	1.2E+12
45	14.5	2.0E+12	2.4E+12	1.5E+12	1.3E+12
45	18.5	5.1E+12	5.6E+12	4.5E+12	4.0E+12
45	24.5	5.3E+12	5.3E+12	5.1E+12	4.8E+12
45	29.5	3.6E+12	3.9E+12	4.1E+12	3.9E+12
45	34.5	1.6E+12	1.9E+12	1.9E+12	2.0E+12
45	39.5	6.5E+11	6.1E+11	6.3E+11	8.1E+11
45	44.5	2.4E+11	1.9E+11	1.9E+11	2.5E+11
45	49.5	7.6E+10	6.0E+10	6.4E+10	7.4E+10
35	0.5	7.3E+11	9.7E+11	1.2E+12	7.3E+11
35	1.5	6.6E+11	8.8E+11	1.1E+12	6.6E+11
35	2.5	1.0E+12	1.2E+12	1.5E+12	1.0E+12
35	3.5	9.0E+11	1.1E+12	1.3E+12	9.0E+11
35	4.5	8.1E+11	1.0E+12	1.2E+12	8.1E+11
35	5.5	7.3E+11	9.1E+11	1.1E+12	7.3E+11
35	6.5	6.5E+11	8.1E+11	9.8E+11	6.5E+11
35	7.5	5.8E+11	7.3E+11	8.7E+11	5.8E+11
35	8.5	5.2E+11	6.4E+11	7.7E+11	5.2E+11
35	9.5	4.6E+11	5.7E+11	6.8E+11	4.6E+11
35	10.5	4.4E+11	5.7E+11	7.1E+11	4.4E+11
35	11.5	4.2E+11	5.6E+11	7.0E+11	4.2E+11
35	12.5	1.1E+12	1.3E+12	9.8E+11	7.8E+11
35	13.5	1.2E+12	1.5E+12	1.1E+12	8.9E+11
35	14.5	1.4E+12	1.7E+12	1.2E+12	1.0E+12
35	18.5	4.4E+12	4.7E+12	4.1E+12	3.7E+12
35	24.5	5.1E+12	5.2E+12	5.2E+12	4.8E+12
35	29.5	3.7E+12	4.2E+12	4.4E+12	4.1E+12
35	34.5	1.8E+12	2.0E+12	2.1E+12	2.1E+12
35	39.5	6.7E+11	6.4E+11	7.0E+11	7.9E+11
35	44.5	2.2E+11	1.9E+11	2.1E+11	2.3E+11
35	49.5	7.0E+10	6.2E+10	6.7E+10	6.9E+10
25	0.5	6.1E+11	9.1E+11	9.4E+11	6.1E+11
25	1.5	5.5E+11	8.3E+11	8.5E+11	5.5E+11
25	2.5	8.0E+11	9.7E+11	1.1E+12	8.0E+11
25	3.5	7.2E+11	8.7E+11	9.6E+11	7.2E+11
25	4.5	6.5E+11	7.9E+11	8.7E+11	6.5E+11
25	5.5	5.8E+11	7.1E+11	7.8E+11	5.8E+11
25	6.5	5.2E+11	6.3E+11	7.0E+11	5.2E+11
25	7.5	4.6E+11	5.7E+11	6.2E+11	4.6E+11
25	8.5	4.1E+11	5.0E+11	5.5E+11	4.1E+11
25	9.5	3.7E+11	4.5E+11	4.9E+11	3.7E+11
25	10.5	3.4E+11	4.3E+11	4.8E+11	3.4E+11
25	11.5	3.2E+11	4.0E+11	4.6E+11	3.2E+11
25	12.5	6.6E+11	7.6E+11	6.0E+11	5.0E+11
25	13.5	7.3E+11	8.5E+11	6.7E+11	5.8E+11
25	14.5	8.5E+11	9.5E+11	7.3E+11	6.5E+11
25	18.5	3.6E+12	3.8E+12	3.5E+12	3.1E+12
25	24.5	4.7E+12	4.9E+12	5.0E+12	4.6E+12
25	29.5	4.0E+12	4.5E+12	4.6E+12	4.4E+12
25	34.5	2.0E+12	2.1E+12	2.2E+12	2.2E+12
25	39.5	6.8E+11	6.7E+11	7.6E+11	7.6E+11
25	44.5	2.1E+11	2.0E+11	2.3E+11	2.2E+11
25	49.5	6.7E+10	6.3E+10	6.8E+10	6.8E+10
15	0.5	4.9E+11	8.5E+11	6.7E+11	4.9E+11
15	1.5	4.4E+11	7.7E+11	6.1E+11	4.4E+11
15	2.5	6.0E+11	7.0E+11	6.5E+11	6.0E+11
15	3.5	5.4E+11	6.3E+11	5.8E+11	5.4E+11
15	4.5	4.9E+11	5.7E+11	5.3E+11	4.9E+11
15	5.5	4.3E+11	5.1E+11	4.7E+11	4.3E+11
15	6.5	3.9E+11	4.6E+11	4.2E+11	3.9E+11
15	7.5	3.5E+11	4.1E+11	3.8E+11	3.5E+11
15	8.5	3.1E+11	3.6E+11	3.3E+11	3.1E+11
15	9.5	2.7E+11	3.2E+11	3.0E+11	2.7E+11

15	10.5	2.4E+11	2.8E+11	2.6E+11	2.4E+11
15	11.5	2.1E+11	2.5E+11	2.3E+11	2.1E+11
15	12.5	2.2E+11	2.1E+11	2.2E+11	2.2E+11
15	13.5	2.7E+11	2.1E+11	2.4E+11	2.7E+11
15	14.5	3.0E+11	2.0E+11	2.5E+11	3.0E+11
15	18.5	2.6E+12	2.7E+12	2.7E+12	2.4E+12
15	24.5	4.2E+12	4.5E+12	4.6E+12	4.4E+12
15	29.5	4.4E+12	4.7E+12	4.7E+12	4.6E+12
15	34.5	2.2E+12	2.2E+12	2.3E+12	2.2E+12
15	39.5	7.1E+11	6.9E+11	7.8E+11	7.4E+11
15	44.5	2.2E+11	2.1E+11	2.4E+11	2.2E+11
15	49.5	6.5E+10	6.4E+10	6.9E+10	6.7E+10
5	0.5	4.9E+11	8.5E+11	6.7E+11	4.9E+11
5	1.5	4.4E+11	7.7E+11	6.1E+11	4.4E+11
5	2.5	6.0E+11	7.0E+11	6.5E+11	6.0E+11
5	3.5	5.4E+11	6.3E+11	5.8E+11	5.4E+11
5	4.5	4.9E+11	5.7E+11	5.3E+11	4.9E+11
5	5.5	4.3E+11	5.1E+11	4.7E+11	4.3E+11
5	6.5	3.9E+11	4.6E+11	4.2E+11	3.9E+11
5	7.5	3.5E+11	4.1E+11	3.8E+11	3.5E+11
5	8.5	3.1E+11	3.6E+11	3.3E+11	3.1E+11
5	9.5	2.7E+11	3.2E+11	3.0E+11	2.7E+11
5	10.5	2.4E+11	2.8E+11	2.6E+11	2.4E+11
5	11.5	2.1E+11	2.5E+11	2.3E+11	2.1E+11
5	12.5	2.2E+11	2.1E+11	2.2E+11	2.2E+11
5	13.5	2.7E+11	2.1E+11	2.4E+11	2.7E+11
5	14.5	3.0E+11	2.0E+11	2.5E+11	3.0E+11
5	18.5	1.9E+12	1.9E+12	2.0E+12	2.0E+12
5	24.5	4.0E+12	4.1E+12	4.2E+12	4.2E+12
5	29.5	4.6E+12	4.8E+12	4.7E+12	4.8E+12
5	34.5	2.4E+12	2.3E+12	2.3E+12	2.2E+12
5	39.5	7.5E+11	6.9E+11	7.6E+11	7.2E+11
5	44.5	2.3E+11	2.1E+11	2.3E+11	2.2E+11
5	49.5	6.6E+10	6.5E+10	7.0E+10	6.7E+10
-5	0.5	3.6E+11	3.6E+11	3.6E+11	4.9E+11
-5	1.5	3.3E+11	3.3E+11	3.3E+11	4.4E+11
-5	2.5	7.0E+11	6.0E+11	7.0E+11	9.0E+11
-5	3.5	6.3E+11	5.4E+11	6.3E+11	8.1E+11
-5	4.5	5.7E+11	4.9E+11	5.7E+11	7.3E+11
-5	5.5	5.1E+11	4.3E+11	5.1E+11	6.5E+11
-5	6.5	4.6E+11	3.9E+11	4.6E+11	5.9E+11
-5	7.5	4.1E+11	3.5E+11	4.1E+11	5.2E+11
-5	8.5	3.6E+11	3.1E+11	3.6E+11	4.6E+11
-5	9.5	3.2E+11	2.7E+11	3.2E+11	4.1E+11
-5	10.5	2.8E+11	2.4E+11	2.8E+11	3.6E+11
-5	11.5	2.5E+11	2.1E+11	2.5E+11	3.2E+11
-5	12.5	1.8E+11	1.7E+11	2.1E+11	2.4E+11
-5	13.5	1.6E+11	3.1E+11	2.1E+11	2.1E+11
-5	14.5	1.4E+11	1.6E+11	2.0E+11	1.8E+11
-5	18.5	2.0E+12	2.2E+12	2.1E+12	1.9E+12
-5	24.5	4.1E+12	4.3E+12	4.2E+12	4.1E+12
-5	29.5	4.6E+12	4.8E+12	4.6E+12	4.7E+12
-5	34.5	2.2E+12	2.2E+12	2.4E+12	2.2E+12
-5	39.5	7.4E+11	6.9E+11	7.6E+11	7.1E+11
-5	44.5	2.2E+11	2.2E+11	2.3E+11	2.1E+11
-5	49.5	6.8E+10	6.6E+10	6.7E+10	6.5E+10
-15	0.5	3.6E+11	3.6E+11	3.6E+11	4.9E+11
-15	1.5	3.3E+11	3.3E+11	3.3E+11	4.4E+11
-15	2.5	7.0E+11	6.0E+11	7.0E+11	9.0E+11
-15	3.5	6.3E+11	5.4E+11	6.3E+11	8.1E+11
-15	4.5	5.7E+11	4.9E+11	5.7E+11	7.3E+11
-15	5.5	5.1E+11	4.3E+11	5.1E+11	6.5E+11
-15	6.5	4.6E+11	3.9E+11	4.6E+11	5.9E+11
-15	7.5	4.1E+11	3.5E+11	4.1E+11	5.2E+11
-15	8.5	3.6E+11	3.1E+11	3.6E+11	4.6E+11
-15	9.5	3.2E+11	2.7E+11	3.2E+11	4.1E+11
-15	10.5	2.8E+11	2.4E+11	2.8E+11	3.6E+11
-15	11.5	2.5E+11	2.1E+11	2.5E+11	3.2E+11
-15	12.5	1.8E+11	1.7E+11	2.1E+11	2.4E+11
-15	13.5	1.6E+11	3.1E+11	2.1E+11	2.1E+11
-15	14.5	1.4E+11	1.6E+11	2.0E+11	1.8E+11
-15	18.5	2.7E+12	3.0E+12	2.6E+12	2.4E+12
-15	24.5	4.5E+12	4.7E+12	4.5E+12	4.4E+12
-15	29.5	4.3E+12	4.7E+12	4.7E+12	4.6E+12
-15	34.5	2.1E+12	2.2E+12	2.3E+12	2.2E+12
-15	39.5	7.1E+11	6.9E+11	7.5E+11	7.1E+11
-15	44.5	2.2E+11	2.1E+11	2.2E+11	2.1E+11
-15	49.5	6.7E+10	6.5E+10	6.6E+10	6.6E+10
-25	0.5	3.6E+11	3.6E+11	3.6E+11	4.9E+11
-25	1.5	3.3E+11	3.3E+11	3.3E+11	4.4E+11
-25	2.5	7.0E+11	6.0E+11	7.0E+11	9.0E+11
-25	3.5	6.3E+11	5.4E+11	6.3E+11	8.1E+11
-25	4.5	5.7E+11	4.9E+11	5.7E+11	7.3E+11
-25	5.5	5.1E+11	4.3E+11	5.1E+11	6.5E+11
-25	6.5	4.6E+11	3.9E+11	4.6E+11	5.9E+11
-25	7.5	4.1E+11	3.5E+11	4.1E+11	5.2E+11
-25	8.5	3.6E+11	3.1E+11	3.6E+11	4.6E+11
-25	9.5	3.2E+11	2.7E+11	3.2E+11	4.1E+11
-25	10.5	2.8E+11	2.4E+11	2.8E+11	3.6E+11
-25	11.5	2.5E+11	2.1E+11	2.5E+11	3.2E+11
-25	12.5	1.8E+11	1.7E+11	2.1E+11	2.4E+11
-25	13.5	1.6E+11	3.1E+11	2.1E+11	2.1E+11
-25	14.5	1.4E+11	1.6E+11	2.0E+11	1.8E+11
-25	18.5	3.5E+12	4.1E+12	3.3E+12	3.0E+12
-25	24.5	4.8E+12	5.2E+12	4.8E+12	4.6E+12
-25	29.5	4.0E+12	4.4E+12	4.5E+12	4.4E+12
-25	34.5	1.9E+12	2.1E+12	2.2E+12	2.1E+12
-25	39.5	7.3E+11	6.8E+11	7.0E+11	7.4E+11
-25	44.5	2.2E+11	2.0E+11	2.1E+11	2.2E+11
-25	49.5	6.9E+10	6.4E+10	6.5E+10	6.8E+10
-35	0.5	3.6E+11	2.4E+11	4.3E+11	6.1E+11
-35	1.5	3.3E+11	2.2E+11	3.9E+11	5.5E+11

-35	2.5	9.0E+11	8.0E+11	9.0E+11	1.0E+12
-35	3.5	8.1E+11	7.2E+11	8.1E+11	9.0E+11
-35	4.5	7.3E+11	6.5E+11	7.3E+11	8.1E+11
-35	5.5	6.5E+11	5.8E+11	6.5E+11	7.3E+11
-35	6.5	5.9E+11	5.2E+11	5.9E+11	6.5E+11
-35	7.5	5.2E+11	4.6E+11	5.2E+11	5.8E+11
-35	8.5	4.6E+11	4.1E+11	4.6E+11	5.2E+11
-35	9.5	4.1E+11	3.7E+11	4.1E+11	4.6E+11
-35	10.5	7.3E+11	5.3E+11	5.6E+11	9.3E+11
-35	11.5	1.1E+12	7.0E+11	7.0E+11	1.4E+12
-35	12.5	4.2E+11	4.9E+11	3.5E+11	3.5E+11
-35	13.5	5.3E+11	6.7E+11	3.8E+11	3.8E+11
-35	14.5	6.1E+11	8.1E+11	4.0E+11	4.0E+11
-35	18.5	4.2E+12	5.0E+12	3.9E+12	3.5E+12
-35	24.5	5.0E+12	5.3E+12	5.0E+12	4.6E+12
-35	29.5	3.8E+12	4.1E+12	4.3E+12	4.1E+12
-35	34.5	1.8E+12	2.0E+12	2.0E+12	2.1E+12
-35	39.5	7.5E+11	6.6E+11	6.4E+11	7.8E+11
-35	44.5	2.4E+11	2.0E+11	1.9E+11	2.4E+11
-35	49.5	7.4E+10	6.4E+10	6.3E+10	7.1E+10
-45	0.5	3.6E+11	2.4E+11	4.3E+11	6.1E+11
-45	1.5	3.3E+11	2.2E+11	3.9E+11	5.5E+11
-45	2.5	9.0E+11	8.0E+11	9.0E+11	1.0E+12
-45	3.5	8.1E+11	7.2E+11	8.1E+11	9.0E+11
-45	4.5	7.3E+11	6.5E+11	7.3E+11	8.1E+11
-45	5.5	6.5E+11	5.8E+11	6.5E+11	7.3E+11
-45	6.5	5.9E+11	5.2E+11	5.9E+11	6.5E+11
-45	7.5	5.2E+11	4.6E+11	5.2E+11	5.8E+11
-45	8.5	4.6E+11	4.1E+11	4.6E+11	5.2E+11
-45	9.5	4.1E+11	3.7E+11	4.1E+11	4.6E+11
-45	10.5	7.3E+11	5.3E+11	5.6E+11	9.3E+11
-45	11.5	1.1E+12	7.0E+11	7.0E+11	1.4E+12
-45	12.5	4.2E+11	4.9E+11	3.5E+11	3.5E+11
-45	13.5	5.3E+11	6.7E+11	3.8E+11	3.8E+11
-45	14.5	6.1E+11	8.1E+11	4.0E+11	4.0E+11
-45	18.5	5.0E+12	5.8E+12	4.3E+12	3.9E+12
-45	24.5	5.2E+12	5.2E+12	4.8E+12	4.6E+12
-45	29.5	3.5E+12	3.7E+12	3.9E+12	3.8E+12
-45	34.5	1.6E+12	1.9E+12	1.7E+12	2.0E+12
-45	39.5	7.0E+11	6.2E+11	5.8E+11	8.2E+11
-45	44.5	2.5E+11	2.0E+11	1.8E+11	2.6E+11
-45	49.5	7.9E+10	6.3E+10	6.0E+10	7.7E+10
-55	0.5	3.6E+11	2.4E+11	4.3E+11	6.1E+11
-55	1.5	3.3E+11	2.2E+11	3.9E+11	5.5E+11
-55	2.5	9.0E+11	8.0E+11	9.0E+11	1.0E+12
-55	3.5	8.1E+11	7.2E+11	8.1E+11	9.0E+11
-55	4.5	7.3E+11	6.5E+11	7.3E+11	8.1E+11
-55	5.5	6.5E+11	5.8E+11	6.5E+11	7.3E+11
-55	6.5	5.9E+11	5.2E+11	5.9E+11	6.5E+11
-55	7.5	5.2E+11	4.6E+11	5.2E+11	5.8E+11
-55	8.5	4.6E+11	4.1E+11	4.6E+11	5.2E+11
-55	9.5	4.1E+11	3.7E+11	4.1E+11	4.6E+11
-55	10.5	7.3E+11	5.3E+11	5.6E+11	9.3E+11
-55	11.5	1.1E+12	7.0E+11	7.0E+11	1.4E+12
-55	12.5	4.2E+11	4.9E+11	3.5E+11	3.5E+11
-55	13.5	5.3E+11	6.7E+11	3.8E+11	3.8E+11
-55	14.5	6.1E+11	8.1E+11	4.0E+11	4.0E+11
-55	18.5	6.0E+12	6.3E+12	4.8E+12	4.5E+12
-55	24.5	5.5E+12	5.0E+12	4.4E+12	4.6E+12
-55	29.5	3.3E+12	3.2E+12	3.4E+12	3.5E+12
-55	34.5	1.3E+12	1.6E+12	1.5E+12	1.9E+12
-55	39.5	5.4E+11	5.6E+11	5.4E+11	7.9E+11
-55	44.5	2.1E+11	1.9E+11	1.7E+11	2.8E+11
-55	49.5	7.9E+10	6.2E+10	5.8E+10	8.2E+10
-65	0.5	3.6E+11	2.4E+11	4.9E+11	4.9E+11
-65	1.5	3.3E+11	2.2E+11	4.4E+11	4.4E+11
-65	2.5	6.0E+11	5.0E+11	7.0E+11	7.0E+11
-65	3.5	5.4E+11	4.5E+11	6.3E+11	6.3E+11
-65	4.5	4.9E+11	4.0E+11	5.7E+11	5.7E+11
-65	5.5	4.4E+11	3.6E+11	5.1E+11	5.1E+11
-65	6.5	3.9E+11	3.3E+11	4.6E+11	4.6E+11
-65	7.5	3.5E+11	2.9E+11	4.1E+11	4.1E+11
-65	8.5	3.1E+11	2.6E+11	3.6E+11	3.6E+11
-65	9.5	1.2E+12	9.9E+11	6.0E+11	7.9E+11
-65	10.5	1.4E+12	1.1E+12	7.4E+11	9.8E+11
-65	11.5	1.6E+12	1.2E+12	9.9E+11	1.3E+12
-65	12.5	2.2E+12	1.8E+12	1.4E+12	1.7E+12
-65	13.5	2.7E+12	2.4E+12	1.9E+12	2.1E+12
-65	14.5	3.3E+12	3.0E+12	2.3E+12	2.5E+12
-65	18.5	6.8E+12	6.7E+12	4.9E+12	5.1E+12
-65	24.5	5.9E+12	4.9E+12	4.0E+12	4.7E+12
-65	29.5	3.3E+12	2.5E+12	2.8E+12	3.2E+12
-65	34.5	1.1E+12	1.2E+12	1.3E+12	1.5E+12
-65	39.5	3.8E+11	4.5E+11	4.9E+11	6.6E+11
-65	44.5	1.7E+11	1.7E+11	1.6E+11	2.5E+11
-65	49.5	7.2E+10	5.8E+10	5.5E+10	8.3E+10
-75	0.5	3.6E+11	2.4E+11	4.9E+11	4.9E+11
-75	1.5	3.3E+11	2.2E+11	4.4E+11	4.4E+11
-75	2.5	6.0E+11	5.0E+11	7.0E+11	7.0E+11
-75	3.5	5.4E+11	4.5E+11	6.3E+11	6.3E+11
-75	4.5	4.9E+11	4.0E+11	5.7E+11	5.7E+11
-75	5.5	4.4E+11	3.6E+11	5.1E+11	5.1E+11
-75	6.5	3.9E+11	3.3E+11	4.6E+11	4.6E+11
-75	7.5	3.5E+11	2.9E+11	4.1E+11	4.1E+11
-75	8.5	3.1E+11	2.6E+11	3.6E+11	3.6E+11
-75	9.5	1.4E+12	1.1E+12	6.4E+11	9.4E+11
-75	10.5	1.6E+12	1.3E+12	8.0E+11	1.2E+12
-75	11.5	1.9E+12	1.4E+12	1.1E+12	1.6E+12
-75	12.5	2.6E+12	2.0E+12	1.6E+12	2.0E+12
-75	13.5	3.2E+12	2.7E+12	2.0E+12	2.5E+12
-75	14.5	3.9E+12	3.3E+12	2.5E+12	2.9E+12
-75	18.5	7.4E+12	7.0E+12	4.9E+12	5.4E+12

```
-75 24.5 6.2E+12 4.9E+12 3.7E+12 4.8E+12
-75 29.5 3.5E+12 2.2E+12 2.5E+12 3.0E+12
-75 34.5 1.1E+12 8.8E+11 1.1E+12 1.3E+12
-75 39.5 3.6E+11 3.6E+11 4.5E+11 5.5E+11
-75 44.5 1.6E+11 1.4E+11 1.6E+11 2.2E+11
-75 49.5 6.5E+10 5.4E+10 5.2E+10 8.0E+10
-85  0.5 3.6E+11 2.4E+11 4.9E+11 4.9E+11
-85  1.5 3.3E+11 2.2E+11 4.4E+11 4.4E+11
-85  2.5 6.0E+11 5.0E+11 7.0E+11 7.0E+11
-85  3.5 5.4E+11 4.5E+11 6.3E+11 6.3E+11
-85  4.5 4.9E+11 4.0E+11 5.7E+11 5.7E+11
-85  5.5 4.4E+11 3.6E+11 5.1E+11 5.1E+11
-85  6.5 3.9E+11 3.3E+11 4.6E+11 4.6E+11
-85  7.5 3.5E+11 2.9E+11 4.1E+11 4.1E+11
-85  8.5 3.1E+11 2.6E+11 3.6E+11 3.6E+11
-85  9.5 1.4E+12 1.2E+12 6.4E+11 9.5E+11
-85 10.5 1.7E+12 1.4E+12 8.0E+11 1.2E+12
-85 11.5 2.0E+12 1.5E+12 1.1E+12 1.6E+12
-85 12.5 2.7E+12 2.1E+12 1.6E+12 2.1E+12
-85 13.5 3.3E+12 2.8E+12 2.0E+12 2.5E+12
-85 14.5 4.0E+12 3.4E+12 2.5E+12 3.0E+12
-85 18.5 7.5E+12 7.0E+12 4.9E+12 5.5E+12
-85 24.5 6.4E+12 4.9E+12 3.6E+12 4.8E+12
-85 29.5 3.6E+12 2.2E+12 2.4E+12 3.0E+12
-85 34.5 1.1E+12 8.2E+11 1.1E+12 1.3E+12
-85 39.5 3.6E+11 3.2E+11 4.5E+11 5.3E+11
-85 44.5 1.6E+11 1.3E+11 1.6E+11 2.0E+11
-85 49.5 6.2E+10 5.2E+10 5.0E+10 7.8E+10
```

B.26 par.dat

```
#
# Parameter file for acm.
#
# This first row of numbers indicates
# whether a particular gas will
# be solved for (1=yes, -1=no)
#
1 1 1 1 1 1 1 1 1 1 1 1 1 1 1 1 1 1 1 1
#
# This number indicates what type of
# output the user wishes:
#
# 0 none
# 1 time (diurnal)
# 2 height
# 3 diurnally averaged height
# 4 total column (time)
3
# The next line indicates whether a
# particular gas concentration will
# be output (-1 means no output, any
# other number is taken as the height
# or time grid point depending upon the
# second line variable above).
#
1 1 1 1 1 1 1 1 1 1 1 1 1 1 1 1 1 1 1 1
#
# The concentrations are given in the
# following order:
#
# 1. O1D
# 2. O
# 3. OH
# 4. H
# 5. HO2
# 6. H2O2
# 7. NO
# 8. HNO2
# 9. NO2
# 10. HO2NO2
# 11. NO3
# 12. N2O5
# 13. CH3
# 14. CH3O2
# 15. CH3OOH
# 16. CH3O
# 17. H2CO
# 18. HCO
# 19. CH4
# 20. HNO3
#
# Convergence criterion
0.01
```

B.27 solarflx.dat

```
201.00 7.00E+11 0.00030915
203.05 8.05E+11 0.00030915
205.15 9.86E+11 0.00030915
207.25 1.20E+12 0.00030915
209.40 1.91E+12 0.00030915
211.65 3.14E+12 0.00030915
213.90 3.54E+12 0.00030915
216.20 3.52E+12 0.00030915
218.60 4.37E+12 0.00030915
221.00 4.96E+12 0.00030915
223.45 6.04E+12 0.00030915
226.00 5.12E+12 0.00030915
```

228.60	5.04E+12	0.00030915
231.25	5.59E+12	0.00030915
233.95	4.89E+12	0.00030915
236.70	5.36E+12	0.00030915
239.55	4.62E+12	0.00030915
242.45	6.97E+12	0.00030915
245.40	6.07E+12	0.00030915
248.45	6.06E+12	0.00030915
251.60	5.72E+12	0.00030915
254.80	7.03E+12	0.00030915
258.05	1.41E+13	0.00030915
261.45	1.27E+13	0.00030915
264.95	3.06E+13	0.00030915
268.50	3.28E+13	0.00030915
272.15	2.92E+13	0.00030915
275.90	2.74E+13	0.00030915
279.75	1.93E+13	0.00030915
283.70	3.70E+13	0.00030915
287.80	5.17E+13	0.00030915
292.00	8.24E+13	0.00030915
296.30	7.70E+13	0.00030756
300.75	7.20E+13	0.00030756
306.50	6.29E+13	0.00030616
312.50	9.90E+13	0.00030616
317.50	1.17E+14	0.00030490
322.50	1.24E+14	0.00030490
327.50	1.39E+14	0.00030377
332.50	1.72E+14	0.00030377
337.50	1.63E+14	0.00030275
342.50	1.79E+14	0.00030275
347.50	1.69E+14	0.00030182
352.50	1.74E+14	0.00030182
357.50	1.83E+14	0.00030098
362.50	1.65E+14	0.00030098
367.50	2.14E+14	0.00030022
372.50	2.16E+14	0.00030022
377.50	1.94E+14	0.00029951
382.50	2.22E+14	0.00029951
387.50	1.80E+14	0.00029887
392.50	2.36E+14	0.00029887
397.50	1.87E+14	0.00029828
402.50	3.38E+14	0.00029828
407.50	3.40E+14	0.00029773
412.50	3.68E+14	0.00029773
417.50	3.94E+14	0.00029723
422.50	3.90E+14	0.00029723
427.50	3.62E+14	0.00029676
432.50	3.34E+14	0.00029676
437.50	3.96E+14	0.00029633
442.50	4.04E+14	0.00029633
447.50	4.36E+14	0.00029592
452.50	4.72E+14	0.00029592
457.50	4.62E+14	0.00029555
462.50	4.78E+14	0.00029555
467.50	4.76E+14	0.00029520
472.50	4.78E+14	0.00029520
477.50	4.88E+14	0.00029487
482.50	5.02E+14	0.00029487
487.50	4.60E+14	0.00029457
492.50	4.78E+14	0.00029457
497.50	4.96E+14	0.00029428
502.50	4.80E+14	0.00029428
507.50	4.92E+14	0.000294024
512.50	4.98E+14	0.000294024
517.50	4.64E+14	0.000293768
522.50	4.78E+14	0.000293768
527.50	4.84E+14	0.000293528
532.50	5.10E+14	0.000293528
537.50	5.02E+14	0.000293304
542.50	4.98E+14	0.000293304
547.50	5.10E+14	0.00029308
552.50	5.06E+14	0.00029308
557.50	5.08E+14	0.000292888
562.50	5.00E+14	0.000292888
567.50	5.14E+14	0.000292696
572.50	5.16E+14	0.000292696
577.50	5.34E+14	0.000292516
582.50	5.34E+14	0.000292516
587.50	5.40E+14	0.000292348
592.50	5.24E+14	0.000292348
597.50	5.38E+14	0.00029218
602.50	5.26E+14	0.00029218
607.50	5.36E+14	0.000292032
612.50	5.32E+14	0.000292032
617.50	5.18E+14	0.000291884
622.50	5.38E+14	0.000291884
627.50	5.22E+14	0.000291744
632.50	5.24E+14	0.000291744
637.50	5.24E+14	0.000291612
642.50	5.26E+14	0.000291612
647.50	5.20E+14	0.00029148
652.50	5.10E+14	0.00029148
657.50	4.96E+14	0.00029136
662.50	5.14E+14	0.00029136
667.50	5.22E+14	0.00029124
672.50	5.22E+14	0.00029124
677.50	5.24E+14	0.00029113
682.50	5.24E+14	0.00029113
687.50	5.14E+14	0.00029103
692.50	5.04E+14	0.00029103
697.50	5.20E+14	0.00029093
702.50	5.16E+14	0.00029093

707.50	5.04E+14	0.000290842
712.50	5.02E+14	0.000290842
717.50	4.96E+14	0.000290754
722.50	4.90E+14	0.000290754
727.50	4.96E+14	0.000290666
732.50	4.89E+14	0.000290666
737.50	4.88E+14	0.000290666
742.50	4.78E+14	0.000290666
747.50	4.80E+14	0.000290666
752.50	4.82E+14	0.000290666
757.50	4.80E+14	0.000290666
762.50	4.76E+14	0.000290666
767.50	4.68E+14	0.000290666
772.50	4.64E+14	0.000290666
777.50	4.60E+14	0.000290666
782.50	4.66E+14	0.000290666
787.50	4.68E+14	0.000290666
792.50	4.58E+14	0.000290666
797.50	4.58E+14	0.000290666
802.50	4.54E+14	0.000290666
807.50	4.54E+14	0.000290666
812.50	4.40E+14	0.000290666
817.50	4.44E+14	0.000290666
822.50	4.36E+14	0.000290666
827.50	4.40E+14	0.000290666
832.50	4.28E+14	0.000290666
837.50	4.28E+14	0.000290666
842.50	4.26E+14	0.000290666
847.50	4.18E+14	0.000290666
852.50	4.10E+14	0.000290666

B.28 stdatm.dat

5.00E+04	1E+05	284.90	9.55E+04	2.4E+19
1.50E+05	1E+05	278.40	8.46E+04	2.2E+19
2.50E+05	1E+05	271.90	7.47E+04	2.0E+19
3.50E+05	1E+05	265.40	6.58E+04	1.8E+19
4.50E+05	1E+05	258.90	5.77E+04	1.6E+19
5.50E+05	1E+05	252.40	5.05E+04	1.5E+19
6.50E+05	1E+05	245.90	4.40E+04	1.3E+19
7.50E+05	1E+05	239.40	3.83E+04	1.2E+19
8.50E+05	1E+05	232.90	3.31E+04	1.0E+19
9.50E+05	1E+05	226.40	2.85E+04	9.1E+18
1.05E+06	1E+05	219.90	2.45E+04	8.1E+18
1.15E+06	1E+05	216.65	2.26E+04	7.0E+18
1.25E+06	1E+05	216.65	1.66E+04	5.3E+18
1.35E+06	1E+05	216.65	1.44E+04	4.6E+18
1.45E+06	1E+05	216.65	1.21E+04	4.1E+18
1.85E+06	7E+05	216.65	5.53E+03	1.9E+18
2.45E+06	5E+05	220.65	2.55E+03	8.4E+17
2.95E+06	5E+05	225.55	1.20E+03	3.8E+17
3.45E+06	5E+05	235.51	5.75E+02	1.8E+17
3.95E+06	5E+05	248.51	2.87E+02	8.4E+16
4.45E+06	5E+05	262.35	1.49E+02	4.1E+16
4.95E+06	5E+05	269.16	7.98E+01	2.2E+16

B.29 templand.dat

85	0.5	246.9	254.0	272.2	257.4
85	1.5	251.2	256.8	271.3	257.1
85	2.5	248.3	253.7	266.9	253.9
85	3.5	244.0	249.2	261.7	249.4
85	4.5	238.6	243.5	255.8	243.8
85	5.5	233.6	238.3	250.4	238.7
85	6.5	228.0	232.8	243.5	233.0
85	7.5	222.8	227.9	237.1	227.8
85	8.5	218.2	223.5	231.5	223.2
85	9.5	215.1	221.3	228.4	220.7
85	10.5	214.5	222.5	229.5	221.7
85	11.5	214.2	223.1	229.9	222.1
85	12.5	212.7	224.3	230.3	221.8
85	13.5	212.1	224.5	230.0	221.2
85	14.5	211.4	224.7	229.8	220.6
85	18.5	233.3	215.9	192.1	198.8
85	24.5	238.4	218.7	192.0	200.4
85	29.5	243.9	223.9	197.0	206.1
85	34.5	249.8	231.5	207.1	215.7
85	39.5	256.1	241.6	222.2	229.2
85	44.5	262.8	254.1	242.5	246.8
85	49.5	269.9	269.0	267.8	268.3
75	0.5	252.6	259.4	275.4	264.3
75	1.5	254.0	259.7	273.7	262.1
75	2.5	250.3	255.7	269.1	258.1
75	3.5	245.6	250.8	263.7	253.1
75	4.5	240.1	244.9	257.6	247.3
75	5.5	235.0	239.7	252.2	242.1
75	6.5	229.1	233.9	244.6	235.4
75	7.5	223.6	228.6	237.7	229.3
75	8.5	218.8	223.9	231.5	223.8
75	9.5	215.6	221.4	227.7	220.6
75	10.5	214.9	222.3	227.8	220.7
75	11.5	214.6	222.8	227.8	220.7
75	12.5	213.3	223.5	227.6	220.2
75	13.5	212.8	223.6	227.5	219.9
75	14.5	212.2	223.7	227.4	219.5
75	18.5	231.8	217.4	194.5	201.1
75	24.5	236.3	219.5	194.4	202.5
75	29.5	241.4	224.2	199.2	207.9
75	34.5	247.4	231.5	209.0	217.2
75	39.5	254.1	241.4	223.7	230.3

75	44.5	261.6	253.9	243.4	247.4
75	49.5	269.8	269.0	267.9	268.3
65	0.5	251.4	265.0	284.8	267.7
65	1.5	254.1	263.5	279.3	264.9
65	2.5	250.6	258.4	273.4	260.5
65	3.5	246.1	252.9	267.3	255.3
65	4.5	240.7	247.1	261.1	249.5
65	5.5	235.8	241.9	255.6	244.3
65	6.5	229.6	235.3	247.5	237.1
65	7.5	223.9	229.3	240.0	230.5
65	8.5	218.8	224.0	233.3	224.7
65	9.5	215.4	220.8	228.5	220.8
65	10.5	214.6	220.8	226.3	220.0
65	11.5	214.2	220.8	225.3	219.6
65	12.5	213.5	221.2	223.8	218.7
65	13.5	213.4	221.4	223.7	218.6
65	14.5	213.3	221.7	223.6	218.4
65	18.5	229.6	219.9	201.7	208.4
65	24.5	233.2	222.0	202.7	210.8
65	29.5	237.9	226.5	207.7	216.3
65	34.5	244.0	233.5	216.8	224.8
65	39.5	251.2	242.9	229.9	236.4
65	44.5	259.8	254.8	247.1	251.0
65	49.5	269.6	269.1	268.3	268.7
55	0.5	256.4	268.2	283.1	273.5
55	1.5	256.5	267.1	279.0	269.9
55	2.5	253.3	262.7	273.7	265.4
55	3.5	249.0	257.7	268.0	260.4
55	4.5	243.7	252.2	262.1	254.8
55	5.5	239.0	247.2	256.7	249.8
55	6.5	233.1	240.2	248.6	242.6
55	7.5	227.7	233.7	241.2	235.9
55	8.5	222.9	228.0	234.5	229.9
55	9.5	220.2	224.1	229.5	225.6
55	10.5	220.5	222.9	226.7	223.8
55	11.5	220.7	222.3	225.4	222.9
55	12.5	220.3	221.4	222.7	220.8
55	13.5	219.9	221.3	222.1	220.2
55	14.5	219.5	221.2	221.4	219.6
55	18.5	224.9	219.7	211.4	216.5
55	24.5	227.3	222.0	213.9	219.5
55	29.5	231.7	226.6	219.2	224.8
55	34.5	238.1	233.7	227.3	232.4
55	39.5	246.5	243.1	238.3	242.3
55	44.5	256.9	254.9	252.1	254.5
55	49.5	269.3	269.1	268.8	269.1
45	0.5	269.3	277.0	288.0	281.7
45	1.5	265.8	274.4	285.1	277.5
45	2.5	261.9	269.6	279.7	273.2
45	3.5	257.1	264.1	274.1	268.0
45	4.5	251.5	258.2	268.1	262.2
45	5.5	246.4	252.8	262.8	256.9
45	6.5	239.7	244.9	254.5	249.0
45	7.5	233.6	237.6	246.7	241.8
45	8.5	228.1	231.1	239.9	235.3
45	9.5	224.2	225.9	233.3	229.5
45	10.5	222.6	222.3	226.7	224.4
45	11.5	221.9	220.7	223.7	222.1
45	12.5	219.6	217.8	217.3	216.6
45	13.5	218.8	217.3	215.9	215.2
45	14.5	217.9	216.9	214.5	213.8
45	18.5	216.6	215.7	216.1	217.9
45	24.5	217.6	217.4	218.5	220.0
45	29.5	221.8	222.1	223.5	224.7
45	34.5	228.9	229.5	231.0	232.0
45	39.5	239.2	239.8	241.1	241.8
45	44.5	252.5	252.9	253.8	254.1
45	49.5	268.9	268.9	269.0	269.0
35	0.5	282.5	286.0	294.2	290.8
35	1.5	276.7	281.5	290.0	285.2
35	2.5	272.5	276.4	284.5	280.5
35	3.5	267.4	270.8	278.7	275.0
35	4.5	261.5	264.6	272.6	268.9
35	5.5	256.2	259.0	267.2	263.3
35	6.5	248.6	250.6	258.8	255.1
35	7.5	241.5	242.9	251.1	247.4
35	8.5	235.3	236.0	244.2	240.6
35	9.5	229.7	229.7	237.0	233.8
35	10.5	224.8	223.7	228.6	226.5
35	11.5	222.5	220.9	224.8	223.2
35	12.5	215.4	214.3	214.6	213.6
35	13.5	212.8	212.5	211.4	210.4
35	14.5	210.0	210.6	208.1	207.0
35	18.5	206.7	208.5	212.6	212.3
35	24.5	204.2	207.2	212.5	211.7
35	29.5	206.7	210.3	216.1	215.2
35	34.5	214.4	218.0	223.5	222.6
35	39.5	227.2	230.3	234.7	233.9
35	44.5	245.1	247.0	249.7	249.2
35	49.5	268.1	268.3	268.6	268.5
25	0.5	290.1	294.1	299.2	296.4
25	1.5	284.6	288.7	293.4	290.3
25	2.5	280.8	283.3	287.3	285.1
25	3.5	276.0	277.4	280.9	279.3
25	4.5	270.1	271.0	274.4	273.1
25	5.5	264.9	265.2	268.6	267.5
25	6.5	256.6	256.9	260.3	259.0
25	7.5	249.0	249.1	252.6	251.2
25	8.5	242.2	242.2	245.8	244.3
25	9.5	235.4	235.2	238.5	237.0
25	10.5	227.7	227.4	229.8	228.5
25	11.5	224.2	223.8	225.8	224.7

25	12.5	212.1	212.3	213.0	211.9
25	13.5	207.4	208.0	208.3	207.1
25	14.5	202.5	203.5	203.4	202.1
25	18.5	197.7	198.9	202.7	202.2
25	24.5	190.3	192.3	197.7	197.0
25	29.5	190.6	192.9	199.0	198.3
25	34.5	198.4	200.7	206.6	206.0
25	39.5	213.7	215.7	220.6	220.1
25	44.5	236.7	237.9	240.9	240.6
25	49.5	267.2	267.3	267.6	267.6
15	0.5	296.1	298.8	299.9	299.0
15	1.5	290.1	292.7	293.7	292.8
15	2.5	285.3	286.8	287.2	286.7
15	3.5	279.8	280.5	280.7	280.4
15	4.5	273.7	274.0	274.1	274.0
15	5.5	268.1	268.2	268.2	268.3
15	6.5	259.6	259.8	259.9	260.0
15	7.5	251.8	252.1	252.3	252.3
15	8.5	244.8	245.3	245.5	245.4
15	9.5	237.5	238.0	238.2	238.1
15	10.5	228.8	229.3	229.3	229.1
15	11.5	224.9	225.3	225.3	225.1
15	12.5	210.9	211.2	211.7	211.0
15	13.5	205.4	205.6	206.6	205.4
15	14.5	199.7	199.8	201.2	199.7
15	18.5	191.5	191.5	194.3	193.5
15	24.5	181.0	180.9	185.3	184.3
15	29.5	179.7	179.5	184.8	183.6
15	34.5	187.6	187.4	192.6	191.5
15	39.5	204.8	204.5	209.0	208.0
15	44.5	231.1	230.9	233.7	233.1
15	49.5	266.6	266.6	266.9	266.8
5	0.5	297.8	298.6	297.8	298.0
5	1.5	291.6	292.4	291.6	291.9
5	2.5	285.6	286.2	285.5	285.9
5	3.5	279.7	280.2	279.4	279.8
5	4.5	273.9	274.2	273.5	273.8
5	5.5	268.7	268.8	268.1	268.4
5	6.5	260.4	260.6	259.9	260.2
5	7.5	252.7	253.0	252.2	252.6
5	8.5	245.9	246.3	245.4	245.9
5	9.5	238.5	239.0	238.1	238.5
5	10.5	229.5	230.0	229.2	229.5
5	11.5	225.5	225.9	225.2	225.4
5	12.5	210.6	211.0	211.5	210.8
5	13.5	204.6	204.9	206.3	205.0
5	14.5	198.4	198.6	200.9	199.0
5	18.5	189.2	188.9	192.1	190.4
5	24.5	177.5	176.9	181.9	179.4
5	29.5	175.7	174.8	180.7	177.9
5	34.5	183.6	182.7	188.6	185.9
5	39.5	201.4	200.6	205.6	203.3
5	44.5	229.0	228.5	231.6	230.2
5	49.5	266.4	266.3	266.7	266.5
-5	0.5	297.6	297.7	296.7	297.8
-5	1.5	291.5	291.6	291.0	292.1
-5	2.5	285.7	286.0	285.2	285.9
-5	3.5	279.8	280.2	279.4	279.9
-5	4.5	273.9	274.2	273.6	273.9
-5	5.5	268.7	268.9	268.4	268.5
-5	6.5	260.4	260.6	260.0	260.2
-5	7.5	252.8	253.1	252.2	252.6
-5	8.5	246.0	246.3	245.2	245.7
-5	9.5	238.6	239.0	237.8	238.3
-5	10.5	229.6	230.0	229.0	229.3
-5	11.5	225.5	225.9	224.9	225.2
-5	12.5	210.6	211.0	211.5	210.9
-5	13.5	204.7	205.0	206.4	205.2
-5	14.5	198.5	198.8	201.1	199.4
-5	18.5	189.1	188.9	191.8	189.9
-5	24.5	177.4	176.8	181.5	178.6
-5	29.5	175.5	174.7	180.2	177.0
-5	34.5	183.5	182.6	188.1	184.9
-5	39.5	201.3	200.5	205.1	202.5
-5	44.5	228.9	228.4	231.3	229.7
-5	49.5	266.4	266.3	266.6	266.4
-15	0.5	296.4	296.2	293.6	295.2
-15	1.5	291.1	290.5	288.4	290.7
-15	2.5	285.9	285.6	284.0	285.4
-15	3.5	280.2	280.0	278.8	279.6
-15	4.5	274.3	274.0	273.0	273.4
-15	5.5	268.9	268.6	267.7	267.8
-15	6.5	260.5	260.1	259.2	259.3
-15	7.5	252.6	252.3	251.4	251.4
-15	8.5	245.7	245.4	244.4	244.3
-15	9.5	238.3	238.1	237.1	237.0
-15	10.5	229.4	229.4	228.6	228.5
-15	11.5	225.4	225.5	224.8	224.6
-15	12.5	211.2	211.5	212.1	211.6
-15	13.5	205.6	206.0	207.3	206.7
-15	14.5	199.8	200.3	202.3	201.6
-15	18.5	191.0	191.0	192.3	190.7
-15	24.5	180.4	180.2	181.9	179.9
-15	29.5	179.0	178.7	180.7	178.4
-15	34.5	187.0	186.6	188.6	186.4
-15	39.5	204.2	203.9	205.5	203.7
-15	44.5	230.8	230.5	231.5	230.4
-15	49.5	266.6	266.5	266.6	266.5
-25	0.5	294.2	293.1	289.2	290.5
-25	1.5	289.3	287.5	283.8	285.8
-25	2.5	284.4	282.9	279.7	281.5
-25	3.5	278.8	277.3	274.4	276.0

-25	4.5	272.5	270.9	268.0	269.5
-25	5.5	266.9	265.2	262.2	263.6
-25	6.5	258.2	256.5	254.1	255.1
-25	7.5	250.2	248.6	246.6	247.2
-25	8.5	243.0	241.5	239.9	240.2
-25	9.5	235.8	234.5	233.5	233.5
-25	10.5	227.8	227.1	226.9	226.6
-25	11.5	224.1	223.7	223.9	223.4
-25	12.5	212.6	213.0	214.5	213.8
-25	13.5	208.4	209.1	211.1	210.5
-25	14.5	204.0	205.1	207.5	207.0
-25	18.5	196.8	198.1	196.2	195.4
-25	24.5	189.1	191.2	187.6	187.0
-25	29.5	189.1	191.8	187.2	186.8
-25	34.5	197.0	199.6	194.9	194.7
-25	39.5	212.6	214.8	210.8	210.7
-25	44.5	236.0	237.4	234.8	234.8
-25	49.5	267.1	267.3	267.0	267.0
-35	0.5	287.9	286.7	283.5	283.7
-35	1.5	284.0	281.8	278.1	279.3
-35	2.5	279.8	277.6	273.3	274.9
-35	3.5	274.5	272.2	267.5	269.4
-35	4.5	268.2	265.7	260.8	262.9
-35	5.5	262.6	259.9	254.8	257.1
-35	6.5	253.9	251.3	246.7	248.8
-35	7.5	245.8	243.2	239.2	241.2
-35	8.5	238.6	236.1	232.6	234.4
-35	9.5	231.8	229.6	227.1	228.6
-35	10.5	225.1	223.6	223.1	224.0
-35	11.5	222.1	220.9	221.2	221.8
-35	12.5	214.4	214.4	216.6	216.7
-35	13.5	212.2	212.7	215.3	215.4
-35	14.5	210.0	210.9	213.9	213.9
-35	18.5	207.3	208.4	202.8	203.1
-35	24.5	204.9	207.4	197.1	198.9
-35	29.5	207.5	210.8	198.1	200.6
-35	34.5	215.1	218.6	205.6	208.4
-35	39.5	227.8	230.8	219.7	222.2
-35	44.5	245.4	247.3	240.3	241.9
-35	49.5	268.1	268.3	267.6	267.7
-45	0.5	280.5	279.7	277.3	277.6
-45	1.5	277.2	275.5	272.2	273.4
-45	2.5	272.7	271.2	267.0	268.5
-45	3.5	267.4	265.8	261.0	262.8
-45	4.5	261.4	259.6	254.4	256.5
-45	5.5	256.0	254.0	248.4	250.8
-45	6.5	247.9	245.8	240.6	243.1
-45	7.5	240.5	238.2	233.5	236.0
-45	8.5	233.8	231.5	227.1	229.7
-45	9.5	228.3	226.0	222.3	224.9
-45	10.5	224.4	222.1	219.7	222.1

-45	11.5	222.6	220.3	218.6	220.9
-45	12.5	219.0	217.0	216.5	218.7
-45	13.5	218.3	216.5	216.2	218.4
-45	14.5	217.6	216.0	215.9	218.1
-45	18.5	216.0	216.3	212.3	211.9
-45	24.5	217.7	218.4	211.1	211.8
-45	29.5	222.3	223.2	214.1	215.5
-45	34.5	229.7	230.6	221.4	223.1
-45	39.5	239.9	240.7	232.9	234.4
-45	44.5	253.0	253.5	248.5	249.6
-45	49.5	268.9	269.0	268.4	268.5
-55	0.5	274.5	273.4	271.0	271.8
-55	1.5	270.5	268.6	265.8	267.0
-55	2.5	265.5	263.9	260.6	261.8
-55	3.5	260.2	258.6	254.8	256.2
-55	4.5	254.5	252.7	248.5	250.0
-55	5.5	249.5	247.5	242.8	244.5
-55	6.5	242.4	240.2	235.3	237.3
-55	7.5	236.0	233.6	228.4	230.7
-55	8.5	230.2	227.6	222.3	224.8
-55	9.5	226.5	223.5	217.7	220.5
-55	10.5	225.8	222.0	215.3	218.5
-55	11.5	225.5	221.4	214.2	217.6
-55	12.5	225.0	220.1	212.1	216.4
-55	13.5	225.0	219.9	211.8	216.5
-55	14.5	225.0	219.7	211.5	216.6
-55	18.5	218.3	220.6	219.9	217.6
-55	24.5	221.2	223.4	221.4	219.3
-55	29.5	226.4	228.3	225.6	223.8
-55	34.5	233.8	235.4	232.4	231.0
-55	39.5	243.3	244.5	241.9	240.9
-55	44.5	255.1	255.8	254.1	253.6
-55	49.5	269.1	269.2	269.0	269.0
-65	0.5	270.2	264.6	259.5	262.9
-65	1.5	266.0	260.7	257.3	259.7
-65	2.5	261.0	256.4	253.4	255.3
-65	3.5	255.7	251.7	248.6	250.3
-65	4.5	250.4	246.4	243.0	244.7
-65	5.5	245.6	241.7	238.0	239.7
-65	6.5	239.2	235.2	230.8	232.7
-65	7.5	233.3	229.3	224.1	226.2
-65	8.5	228.0	224.0	218.2	220.4
-65	9.5	225.2	220.9	213.4	216.0
-65	10.5	226.2	220.9	210.3	213.4
-65	11.5	226.6	221.0	208.9	212.2
-65	12.5	227.9	220.7	205.3	210.1
-65	13.5	228.4	220.4	204.3	209.8
-65	14.5	228.9	220.2	203.3	209.6
-65	18.5	216.0	223.1	224.2	219.6
-65	24.5	218.7	226.1	226.5	221.8
-65	29.5	223.9	230.9	230.8	226.4

-65	34.5	231.5	237.6	237.2	233.4
-65	39.5	241.6	246.3	245.8	242.9
-65	44.5	254.1	256.8	256.5	254.8
-65	49.5	269.0	269.3	269.3	269.1
-75	0.5	263.3	249.3	244.5	251.0
-75	1.5	259.4	247.8	243.4	248.7
-75	2.5	254.7	244.6	240.7	245.2
-75	3.5	250.2	241.7	238.2	241.9
-75	4.5	245.9	239.1	235.8	238.8
-75	5.5	242.0	236.9	233.7	236.0
-75	6.5	236.1	231.0	226.9	229.1
-75	7.5	230.7	225.5	220.4	222.7
-75	8.5	225.8	220.5	214.7	216.9
-75	9.5	223.5	217.7	209.9	212.1
-75	10.5	225.0	218.0	206.1	208.5
-75	11.5	225.7	218.2	204.4	206.9
-75	12.5	228.0	218.0	199.6	203.2
-75	13.5	228.9	217.7	198.0	202.3
-75	14.5	229.8	217.4	196.4	201.4
-75	18.5	212.4	224.6	227.5	219.7
-75	24.5	214.3	227.4	229.5	221.7
-75	29.5	219.1	232.1	233.6	226.1
-75	34.5	227.0	238.7	239.5	233.1
-75	39.5	237.9	247.1	247.5	242.5
-75	44.5	251.9	257.3	257.4	254.5
-75	49.5	268.8	269.3	269.4	269.1
-85	0.5	258.1	241.5	236.8	243.5
-85	1.5	253.0	237.4	232.7	239.1
-85	2.5	249.5	236.3	231.8	237.4
-85	3.5	246.1	235.4	231.2	235.8
-85	4.5	242.7	234.6	231.0	234.6
-85	5.5	239.6	234.0	230.8	233.4
-85	6.5	234.3	228.5	224.4	226.9
-85	7.5	229.4	223.3	218.3	220.8
-85	8.5	225.0	218.6	212.8	215.2
-85	9.5	223.1	215.8	208.1	210.5
-85	10.5	224.8	215.9	204.2	206.7
-85	11.5	225.6	215.9	202.5	205.0
-85	12.5	228.5	215.8	197.5	201.1
-85	13.5	229.6	215.7	195.9	200.2
-85	14.5	230.8	215.6	194.2	199.3
-85	18.5	210.5	225.1	229.5	219.7
-85	24.5	212.0	228.1	231.2	220.9
-85	29.5	216.8	232.9	234.8	224.8
-85	34.5	224.8	239.4	240.4	231.6
-85	39.5	236.2	247.7	248.1	241.2
-85	44.5	250.8	257.7	257.7	253.7
-85	49.5	268.7	269.4	269.4	269.0

B.30 tempsea.dat

85	0.5	246.9	254.0	272.2	257.4
85	1.5	251.2	256.8	271.3	257.1
85	2.5	248.3	253.7	266.9	253.9
85	3.5	244.0	249.2	261.7	249.4
85	4.5	238.6	243.5	255.8	243.8
85	5.5	233.6	238.3	250.4	238.7
85	6.5	228.0	232.8	243.5	233.0
85	7.5	222.8	227.9	237.1	227.8
85	8.5	218.2	223.5	231.5	223.2
85	9.5	215.1	221.3	228.4	220.7
85	10.5	214.5	222.5	229.5	221.7
85	11.5	214.2	223.1	229.9	222.1
85	12.5	212.7	224.3	230.3	221.8
85	13.5	212.1	224.5	230.0	221.2
85	14.5	211.4	224.7	229.8	220.6
85	18.5	233.3	215.91	192.09	198.75
85	24.5	238.39	218.66	191.99	200.42
85	29.5	243.88	223.86	196.98	206.06
85	34.5	249.78	231.49	207.06	215.66
85	39.5	256.08	241.56	222.23	229.24
85	44.5	262.8	254.07	242.49	246.78
85	49.5	269.92	269.02	267.84	268.28
75	0.5	256.0	262.0	275.5	266.5
75	1.5	256.0	261.5	274.4	263.5
75	2.5	251.9	257.2	269.7	259.3
75	3.5	246.9	252.0	264.3	254.2
75	4.5	241.0	246.0	258.2	248.2
75	5.5	235.8	240.6	252.7	242.9
75	6.5	229.6	234.5	245.1	236.0
75	7.5	223.9	229.0	238.1	229.7
75	8.5	218.8	224.0	231.9	224.1
75	9.5	215.4	221.3	228.0	220.7
75	10.5	214.5	222.1	227.9	220.5
75	11.5	214.1	222.4	227.8	220.4
75	12.5	212.7	223.0	227.6	219.6
75	13.5	212.1	223.1	227.4	219.3
75	14.5	211.6	223.2	227.3	218.8
75	18.5	231.83	217.43	194.46	201.07
75	24.5	236.25	219.52	194.38	202.54
75	29.5	241.43	224.22	199.23	207.91
75	34.5	247.38	231.51	209.01	217.17
75	39.5	254.08	241.41	223.72	230.33
75	44.5	261.55	253.9	243.36	247.38
75	49.5	269.78	269	267.92	268.34
65	0.5	258.1	267.1	283.2	270.6
65	1.5	258.6	265.2	278.5	267.2
65	2.5	254.6	260.2	272.8	262.6
65	3.5	249.7	254.7	266.8	257.3
65	4.5	243.9	248.8	260.6	251.3

65	5.5	238.7	243.4	255.1	245.9
65	6.5	232.2	236.7	247.0	238.7
65	7.5	226.3	230.6	239.4	232.1
65	8.5	221.0	225.1	232.8	226.2
65	9.5	217.5	221.9	228.1	222.3
65	10.5	216.8	221.9	226.3	221.3
65	11.5	216.5	221.9	225.5	220.9
65	12.5	215.9	222.2	224.3	219.9
65	13.5	215.8	222.3	224.2	219.7
65	14.5	215.7	222.5	224.1	219.5
65	18.5	229.64	219.85	201.71	208.41
65	24.5	233.15	221.96	202.68	210.83
65	29.5	237.92	226.5	207.71	216.31
65	34.5	243.96	233.48	216.79	224.83
65	39.5	251.24	242.91	229.91	236.41
65	44.5	259.79	254.78	247.08	251.04
65	49.5	269.6	269.08	268.31	268.71
55	0.5	265.7	273.7	285.7	276.9
55	1.5	263.5	270.3	281.7	272.3
55	2.5	259.1	265.0	276.1	267.5
55	3.5	253.9	259.2	270.1	262.1
55	4.5	247.9	253.1	263.9	256.0
55	5.5	242.6	247.6	258.3	250.6
55	6.5	235.7	240.1	249.9	243.0
55	7.5	229.4	233.3	242.1	235.9
55	8.5	223.8	227.1	235.2	229.7
55	9.5	220.1	223.0	229.7	225.0
55	10.5	219.0	221.6	226.1	222.4
55	11.5	218.6	221.0	224.4	221.2
55	12.5	218.0	220.2	221.3	218.9
55	13.5	218.0	220.2	220.9	218.4
55	14.5	218.0	220.2	220.4	218.0
55	18.5	224.86	219.69	211.43	216.49
55	24.5	227.28	221.97	213.86	219.49
55	29.5	231.7	226.64	219.15	224.8
55	34.5	238.11	233.68	227.29	232.41
55	39.5	246.51	243.11	238.28	242.32
55	44.5	256.91	254.91	252.13	254.54
55	49.5	269.3	269.1	268.82	269.07
45	0.5	273.9	280.5	290.9	284.2
45	1.5	269.5	276.2	287.0	279.2
45	2.5	265.2	270.9	281.2	274.3
45	3.5	259.9	265.0	275.0	268.7
45	4.5	253.7	258.5	268.5	262.4
45	5.5	248.2	252.8	262.6	256.7
45	6.5	240.7	244.6	254.2	248.5
45	7.5	233.8	237.1	246.3	241.0
45	8.5	227.6	230.4	239.4	234.2
45	9.5	223.1	225.1	233.0	228.4
45	10.5	220.7	221.6	227.0	223.4
45	11.5	219.7	220.0	224.2	221.1

45	12.5	217.4	217.2	217.9	216.0
45	13.5	217.0	216.9	216.3	214.8
45	14.5	216.5	216.5	214.6	213.5
45	18.5	216.56	215.67	216.08	217.89
45	24.5	217.62	217.44	218.49	220.03
45	29.5	221.75	222.05	223.46	224.73
45	34.5	228.93	229.5	231	231.97
45	39.5	239.18	239.79	241.1	241.77
45	44.5	252.48	252.92	253.76	254.12
45	49.5	268.85	268.9	268.99	269.02
35	0.5	283.5	288.1	295.7	291.6
35	1.5	278.0	283.2	291.2	286.1
35	2.5	273.2	277.6	285.4	280.8
35	3.5	267.7	271.5	279.2	274.9
35	4.5	261.4	264.9	272.6	268.4
35	5.5	255.7	258.9	266.8	262.6
35	6.5	247.7	250.3	258.4	254.1
35	7.5	240.3	242.4	250.7	246.3
35	8.5	233.7	235.3	243.8	239.3
35	9.5	228.0	228.9	236.8	232.6
35	10.5	223.2	222.9	228.9	225.5
35	11.5	221.1	220.2	225.3	222.3
35	12.5	214.7	213.9	214.9	213.4
35	13.5	212.6	212.2	211.4	210.4
35	14.5	210.3	210.6	207.8	207.4
35	18.5	206.74	208.5	212.64	212.26
35	24.5	204.16	207.15	212.45	211.73
35	29.5	206.7	210.32	216.07	215.16
35	34.5	214.37	218.03	223.49	222.56
35	39.5	227.15	230.25	234.71	233.91
35	44.5	245.05	247	249.73	249.23
35	49.5	268.07	268.27	268.56	268.5
25	0.5	290.9	295.6	300.0	296.9
25	1.5	285.4	290.1	294.4	291.0
25	2.5	281.0	284.0	287.8	285.2
25	3.5	275.7	277.6	281.2	279.1
25	4.5	269.5	270.8	274.5	272.7
25	5.5	263.9	264.8	268.6	267.0
25	6.5	255.5	256.2	260.3	258.5
25	7.5	247.9	248.3	252.7	250.7
25	8.5	241.0	241.3	245.9	243.7
25	9.5	234.2	234.4	238.7	236.5
25	10.5	226.9	226.8	230.0	228.1
25	11.5	223.6	223.4	226.1	224.3
25	12.5	212.3	212.4	213.1	211.9
25	13.5	207.9	208.3	208.3	207.2
25	14.5	203.5	204.1	203.2	202.4
25	18.5	197.67	198.91	202.74	202.15
25	24.5	190.33	192.3	197.67	197
25	29.5	190.57	192.9	198.95	198.27
25	34.5	198.37	200.7	206.59	205.96

25	39.5	213.74	215.7	220.58	220.09
25	44.5	236.68	237.91	240.93	240.63
25	49.5	267.18	267.31	267.63	267.6
15	0.5	296.1	298.5	299.1	298.5
15	1.5	290.2	292.6	293.1	292.2
15	2.5	285.3	286.6	286.9	286.3
15	3.5	279.7	280.4	280.7	280.2
15	4.5	273.6	274.0	274.4	274.1
15	5.5	268.0	268.3	268.7	268.6
15	6.5	259.6	259.9	260.4	260.3
15	7.5	251.7	252.2	252.8	252.5
15	8.5	244.7	245.3	246.1	245.6
15	9.5	237.4	238.0	238.8	238.2
15	10.5	228.8	229.4	229.8	229.3
15	11.5	224.9	225.4	225.8	225.3
15	12.5	211.0	211.4	211.9	211.1
15	13.5	205.6	205.8	206.5	205.5
15	14.5	199.9	200.0	200.9	199.7
15	18.5	191.53	191.48	194.29	193.54
15	24.5	181.03	180.86	185.31	184.25
15	29.5	179.74	179.5	184.76	183.56
15	34.5	187.64	187.39	192.64	191.47
15	39.5	204.76	204.53	208.95	207.99
15	44.5	231.07	230.93	233.69	233.1
15	49.5	266.59	266.58	266.87	266.81
5	0.5	296.9	297.7	296.7	296.8
5	1.5	290.8	291.4	290.8	290.8
5	2.5	285.6	286.1	285.5	285.6
5	3.5	280.0	280.4	279.9	280.0
5	4.5	273.9	274.3	273.9	274.0
5	5.5	268.5	268.8	268.5	268.6
5	6.5	260.2	260.5	260.1	260.3
5	7.5	252.5	252.9	252.4	252.6
5	8.5	245.6	246.1	245.5	245.7
5	9.5	238.3	238.8	238.1	238.3
5	10.5	229.4	229.9	229.2	229.3
5	11.5	225.3	225.9	225.2	225.3
5	12.5	210.7	211.0	211.4	210.8
5	13.5	204.7	204.9	206.0	205.1
5	14.5	198.6	198.6	200.5	199.1
5	18.5	189.21	188.94	192.07	190.43
5	24.5	177.53	176.87	181.88	179.44
5	29.5	175.66	174.79	180.74	177.92
5	34.5	183.61	182.69	188.64	185.87
5	39.5	201.38	200.58	205.6	203.28
5	44.5	228.97	228.46	231.6	230.16
5	49.5	266.37	266.31	266.65	266.5
-5	0.5	296.7	297.2	295.8	296.2
-5	1.5	290.7	291.0	290.2	290.7
-5	2.5	285.7	286.1	285.5	285.7
-5	3.5	280.1	280.6	280.1	280.2
-5	4.5	274.1	274.5	274.2	274.2
-5	5.5	268.7	269.0	268.9	268.8
-5	6.5	260.3	260.7	260.4	260.4
-5	7.5	252.6	253.1	252.5	252.6
-5	8.5	245.7	246.3	245.5	245.6
-5	9.5	238.4	238.9	238.0	238.2
-5	10.5	229.5	230.0	229.2	229.3
-5	11.5	225.5	226.0	225.1	225.3
-5	12.5	210.8	211.0	211.4	210.9
-5	13.5	204.8	205.0	206.1	205.3
-5	14.5	198.7	198.7	200.6	199.4
-5	18.5	189.08	188.88	191.84	189.9
-5	24.5	177.37	176.8	181.45	178.62
-5	29.5	175.5	174.7	180.2	176.96
-5	34.5	183.47	182.61	188.09	184.91
-5	39.5	201.26	200.51	205.12	202.47
-5	44.5	228.9	228.41	231.3	229.65
-5	49.5	266.36	266.31	266.62	266.44
-15	0.5	296.3	296.0	293.3	295.0
-15	1.5	290.6	290.2	287.9	289.9
-15	2.5	285.5	285.3	283.8	284.8
-15	3.5	279.9	279.9	278.8	279.2
-15	4.5	273.9	273.8	272.9	273.2
-15	5.5	268.5	268.4	267.6	267.7
-15	6.5	260.0	259.9	259.1	259.2
-15	7.5	252.2	252.1	251.2	251.3
-15	8.5	245.2	245.1	244.2	244.3
-15	9.5	237.8	237.8	236.9	236.9
-15	10.5	229.1	229.2	228.5	228.4
-15	11.5	225.1	225.3	224.6	224.6
-15	12.5	211.2	211.4	211.8	211.5
-15	13.5	205.7	205.8	206.9	206.5
-15	14.5	200.0	200.1	201.9	201.2
-15	18.5	190.98	191.03	192.28	190.72
-15	24.5	180.37	180.18	181.94	179.88
-15	29.5	179.04	178.71	180.7	178.44
-15	34.5	186.99	186.61	188.55	186.38
-15	39.5	204.23	203.88	205.49	203.71
-15	44.5	230.75	230.52	231.52	230.42
-15	49.5	266.56	266.53	266.64	266.52
-25	0.5	295.3	293.2	288.7	291.3
-25	1.5	289.9	287.6	283.4	286.3
-25	2.5	284.5	282.6	279.2	281.3
-25	3.5	278.6	277.0	273.8	275.6
-25	4.5	272.3	270.6	267.4	269.1
-25	5.5	266.6	265.0	261.7	263.3
-25	6.5	258.1	256.4	253.7	254.9
-25	7.5	250.2	248.5	246.2	247.1
-25	8.5	243.2	241.5	239.6	240.2
-25	9.5	236.0	234.5	233.2	233.5
-25	10.5	228.0	227.1	226.7	226.7

-25	11.5	224.4	223.7	223.7	223.5
-25	12.5	212.6	212.9	214.4	213.9
-25	13.5	208.3	209.0	211.1	210.5
-25	14.5	203.7	205.0	207.7	207.0
-25	18.5	196.75	198.07	196.24	195.37
-25	24.5	189.06	191.24	187.63	187.04
-25	29.5	189.14	191.76	187.18	186.82
-25	34.5	196.98	199.62	194.89	194.7
-25	39.5	212.59	214.83	210.76	210.69
-25	44.5	235.96	237.37	234.79	234.78
-25	49.5	267.11	267.26	266.98	266.98
-35	0.5	288.6	287.3	283.7	284.6
-35	1.5	284.6	282.2	278.1	279.9
-35	2.5	280.0	277.7	273.2	275.1
-35	3.5	274.6	272.2	267.4	269.4
-35	4.5	268.3	265.7	260.6	262.9
-35	5.5	262.7	259.9	254.6	257.0
-35	6.5	254.0	251.3	246.4	248.8
-35	7.5	246.0	243.3	238.9	241.2
-35	8.5	238.9	236.2	232.3	234.4
-35	9.5	232.2	229.8	226.8	228.7
-35	10.5	225.6	223.9	223.0	224.3
-35	11.5	222.6	221.2	221.2	222.3
-35	12.5	214.9	214.7	216.9	217.4
-35	13.5	212.6	213.0	215.7	216.0
-35	14.5	210.2	211.3	214.5	214.6
-35	18.5	207.3	208.43	202.76	203.13
-35	24.5	204.88	207.41	197.13	198.87
-35	29.5	207.49	210.8	198.07	200.63
-35	34.5	215.11	218.58	205.58	208.39
-35	39.5	227.76	230.75	219.67	222.16
-35	44.5	245.42	247.33	240.33	241.94
-35	49.5	268.11	268.31	267.57	267.74
-45	0.5	280.8	280.0	277.6	278.0
-45	1.5	277.7	275.8	272.5	273.9
-45	2.5	273.1	271.4	267.4	268.9
-45	3.5	267.7	266.0	261.4	263.1
-45	4.5	261.7	259.8	254.8	256.8
-45	5.5	256.3	254.1	248.8	251.0
-45	6.5	248.2	245.9	240.8	243.3
-45	7.5	240.7	238.3	233.5	236.1
-45	8.5	234.0	231.6	226.9	229.7
-45	9.5	228.5	226.1	222.0	224.9
-45	10.5	224.5	222.1	219.3	222.2
-45	11.5	222.7	220.3	218.1	221.0
-45	12.5	219.2	217.1	216.1	219.0
-45	13.5	218.5	216.7	216.0	218.9
-45	14.5	217.9	216.2	215.9	218.7
-45	18.5	216.01	216.33	212.29	211.87
-45	24.5	217.74	218.43	211.1	211.79
-45	29.5	222.3	223.2	214.13	215.52

-45	34.5	229.7	230.63	221.38	223.06
-45	39.5	239.93	240.74	232.85	234.42
-45	44.5	253	253.51	248.53	249.57
-45	49.5	268.9	268.96	268.43	268.54
-55	0.5	274.4	273.1	270.4	271.5
-55	1.5	271.1	268.6	265.7	267.4
-55	2.5	266.2	263.9	260.6	262.3
-55	3.5	260.9	258.6	254.8	256.6
-55	4.5	255.2	252.8	248.5	250.4
-55	5.5	250.1	247.5	242.7	244.8
-55	6.5	243.0	240.3	235.2	237.5
-55	7.5	236.4	233.6	228.3	230.9
-55	8.5	230.5	227.7	222.2	224.9
-55	9.5	226.6	223.6	217.6	220.6
-55	10.5	225.7	222.1	215.1	218.6
-55	11.5	225.3	221.4	214.0	217.7
-55	12.5	224.7	220.2	212.0	216.5
-55	13.5	224.8	220.0	211.7	216.7
-55	14.5	224.8	219.8	211.5	216.8
-55	18.5	218.31	220.55	219.87	217.56
-55	24.5	221.24	223.37	221.38	219.3
-55	29.5	226.39	228.31	225.56	223.77
-55	34.5	233.76	235.36	232.42	230.97
-55	39.5	243.33	244.52	241.94	240.9
-55	44.5	255.12	255.8	254.14	253.57
-55	49.5	269.13	269.19	269.02	268.96
-65	0.5	270.0	264.1	258.7	262.5
-65	1.5	265.9	259.9	256.5	259.4
-65	2.5	261.0	255.8	252.7	255.2
-65	3.5	255.8	251.2	248.0	250.2
-65	4.5	250.5	246.0	242.5	244.6
-65	5.5	245.7	241.3	237.6	239.6
-65	6.5	239.3	235.0	230.5	232.7
-65	7.5	233.4	229.1	223.9	226.3
-65	8.5	228.2	223.9	218.1	220.6
-65	9.5	225.4	220.8	213.5	216.4
-65	10.5	226.3	221.0	210.6	214.1
-65	11.5	226.8	221.1	209.2	213.1
-65	12.5	228.1	220.9	205.9	211.6
-65	13.5	228.5	220.7	205.0	211.6
-65	14.5	229.0	220.5	204.0	211.5
-65	18.5	215.99	223.12	224.23	219.59
-65	24.5	218.71	226.05	226.45	221.78
-65	29.5	223.88	230.89	230.79	226.39
-65	34.5	231.49	237.63	237.24	233.43
-65	39.5	241.55	246.28	245.8	242.89
-65	44.5	254.06	256.84	256.47	254.77
-65	49.5	269.02	269.3	269.26	269.09
-75	0.5	263.4	250.0	244.6	250.7
-75	1.5	259.2	247.7	243.2	248.1
-75	2.5	254.2	243.9	239.9	244.2

-75	3.5	249.7	240.9	237.2	240.8
-75	4.5	245.4	238.5	235.1	237.9
-75	5.5	241.6	236.4	233.2	235.2
-75	6.5	235.9	230.6	226.5	228.6
-75	7.5	230.6	225.2	220.1	222.3
-75	8.5	225.9	220.4	214.5	216.8
-75	9.5	223.6	217.7	209.7	212.2
-75	10.5	225.3	218.2	206.2	208.8
-75	11.5	226.0	218.4	204.5	207.3
-75	12.5	228.3	218.2	199.8	203.8
-75	13.5	229.2	217.9	198.2	202.8
-75	14.5	230.0	217.6	196.6	201.9
-75	18.5	212.43	224.55	227.51	219.74
-75	24.5	214.27	227.42	229.54	221.65
-75	29.5	219.14	232.12	233.55	226.09
-75	34.5	227.03	238.66	239.54	233.05
-75	39.5	237.93	247.05	247.5	242.53
-75	44.5	251.85	257.28	257.43	254.53
-75	49.5	268.79	269.34	269.35	269.06
-85	0.5	259.1	242.2	237.2	244.2
-85	1.5	253.8	237.8	233.0	239.6
-85	2.5	249.1	234.5	229.8	235.9
-85	3.5	245.3	233.1	228.9	234.1
-85	4.5	242.3	233.5	229.8	233.7
-85	5.5	239.7	233.8	230.7	233.5
-85	6.5	234.4	228.4	224.4	227.1
-85	7.5	229.5	223.2	218.2	220.9
-85	8.5	225.1	218.5	212.7	215.3
-85	9.5	223.2	215.7	208.0	210.6
-85	10.5	225.1	215.9	204.3	206.9
-85	11.5	226.0	216.0	202.6	205.2
-85	12.5	229.0	216.0	197.7	201.5
-85	13.5	230.1	215.9	196.1	200.6
-85	14.5	231.2	215.8	194.4	199.8
-85	18.5	210.51	225.1	229.52	219.73
-85	24.5	212	228.13	231.16	220.86
-85	29.5	216.78	232.9	234.8	224.83
-85	34.5	224.84	239.41	240.44	231.62
-85	39.5	236.17	247.66	248.09	241.24
-85	44.5	250.79	257.65	257.73	253.69
-85	49.5	268.68	269.38	269.38	268.97

Appendix C

GCRC-ACM User's Guide

C.1 Name

acm — Remote Atmospheric Chemistry Modeling Tool by F. Moraes and M.A.K. Khalil (copyright 1993, 1994, 1995)

C.2 Syntax

acm *latitude season half* [*cloud-height cloud-optical depth*]

C.3 Description

Acm is a general purpose tool for modeling the chemistry of the remote (unpolluted) troposphere. It is a one-dimensional model spanning the region from the surface of the earth to the top of the stratosphere. It currently includes 20 reactive species including: $O(^1D)$, HO, HO_2, H, H_2O_2, NO, and NO_2 as well as 6 non-reactive or source gases, CH_4, CO, O_3, H_2, NO_x, and H_2O. The model includes detailed calculations of the actinic flux for clear as well as cloudy sky conditions. The model is well suited to the study of cloud effects on trace gas concentrations and the feedbacks in the complex atmospheric chemistry system.

C.4 Conventions

The *acm* is controllable by the user through the use of two mechanisms: a parameter file and command-line arguments. The parameter file is used to set information needed by the program which will probably not change from model run to model run. This information includes the chemical species to be solved for, the type of output the user wishes, and which species to output data about. Details on the parameter file is given below in the parameter file section.

The command-line arguments are used for setting information which will likely change from run to run. This includes the latitude at which to run the model, the season in which the model runs, and up to three sets of cloud layers. Details on the command line interface to *acm* is given below in the command-line arguments section.

C.5 Command-Line Arguments.

latitude is the latitude at which the model will be run. This number is given in degrees running from 90 at the north pole to -90 at the south.

season is the season in which the model will be run. This number is 0 for winter, 1 for spring, 2 for summer, and 3 for fall.

half is the half-dimension of either land or sea. The value is either 0, for land areas, or 1, for oceanic areas.

cloud-height is the height of the top of a cloud layer in model grid points. A cloud-height value given on the command line must always be followed by a cloud-optical-depth value.

cloud-optical-depth is the optical depth of the cloud whose height was given just preceding it on the command line.

There may be a total of three cloud height/optical-depth pairs. Any more will be ignored by the program.

C.6 Parameter File

Acm looks in the user's current directory for the file par.dat. If it does not find this file it will use the file in acm/dat/par.dat for the parameter file. This file consists of three pieces of information. The first is a row with a number for each reactive species in the program (see the section on bugs below) which tells the program if that species should be used in the model or not. If the number is '1' it will be used and if the number is '0' it will not.

The second piece of information tells the program what kind of output the user would like. It is a single number with the following information

0 Don't output any information.

1 Output the diurnal cycle for a given atmospheric layer.

2 Output the atmospheric layers for a given time of day.

3 Output the diurnally averaged values for each atmospheric layer.

4 Output the diurnally and spatially averaged values.

The third piece of information is similar to the first in that it consists of a row of numbers, one for each reactive gas in the model. But here the number indicates whether to output information on the gas concentration and if so where. A value of -1 indicates that the gas concentration should not be output. For the type 0 above this information in not used; for type 1 it tells which layer to output; for type 2 it tells which time to output; and for types 3 and 4 it tells only whether to output or not.

C.7 Availability

The GRCR-ACM is available to any interested party by writing to the address below and providing your name and shipping address.

Global Change Research Center
Oregon Graduate Institute
20000 NW Walker Road
Beaverton, OR 97006

Biographical Note

Francis Moraes was born in California in 1964. He received his B.S. in applied physics from Sonoma State University in 1990 and his M.S. in Atmospheric Physics from Oregon Graduate Institute in 1992 with a thesis entitled "Methane From Destabilized Permafrost in a Warmer World". He has had 4 papers listed in *Current Contents* since 1990, co-authored a book chapter in *Atmospheric Methane: Sources, Sinks, and Role in Global Change*, and given numerous talks at scientific meetings. He has been on the staff in the Global Change Research Center at OGI since 1994.

He has been married since 1990 to Amanda Tunison and lives in Woodland, WA. His interests include the writing of short fiction, chess, playing music, close-up conjuring, and a recent odd fascination with cooking.